Catching metastasizing cells in the act

Frank Coumans

Catching metastasizing cells in the act

Frank Annie Willie Coumans

Samenstelling promotiecommissie:

Prof. dr.	G. van der Steenhoven	Universiteit Twente (voorzitter)
Prof. dr.	L.W.M.M. Terstappen MD	Universiteit Twente (promotor)
Prof. dr.	J. Greve	Universiteit Twente
Prof. dr.	J.L. Herek	Universiteit Twente
Prof. dr.	M.J. Ijzerman	Universiteit Twente
Prof. dr. ir.	J. den Toonder	Technische Universiteit Eindhoven
Prof. dr.	S. Sleijfer MD	Erasumus Universiteit
Dr.	G. Attard MD	Institute for Cancer Research, UK

This work was financially
supported by Veridex LLC.

ISBN 978-90-365-3444-4
DOI 10.3990/1.9789036534444

Catching metastasizing cells in the act

Proefschrift

ter verkrijging van
de graad van doctor aan de Universiteit Twente,
op gezag van de rector magnificus,
prof. dr. H. Brinksma,
volgens besluit van het College voor Promoties
in het openbaar te verdedigen
op woensdag 10 oktober 2012 om 12:45 uur

door

Frank Annie Willie Coumans

geboren op 5 mei 1978
te Sittard

Dit proefschrift is goedgekeurd door:

Prof. dr. L.W.M.M. Terstappen MD (promotor)

Table of contents

Introduction 3 - 5

Chapter 1 7 - 43
Technology requirements for detection of residual disease in cancer patients. F.A.W. Coumans , S. Siesling, L.W.M.M Terstappen. Submitted for publication.

Chapter 2 45 - 62
Detection and characterization of Circulating Tumor Cells by the Cell Search approach. F.A.W. Coumans , L.W.M.M Terstappen. Circulating Tumour Cells - Methods in Molecular Biology. Humana Press, USA. In press.

Chapter 3 63 - 84
Circulating Tumor Cell - Trapping Devices. F.A.W. Coumans *, S.T. Ligthart *, J. Swennenhuis , L.W.M.M. Terstappen. Biofunctional Surface Engineering in Medicine "Nanobiotechnology" series by Pan Stanford Publishing. Edited by Prof. Dr. Martin Scholz. In press.

Chapter 4 85 - 101
F.A.W. Coumans , C.J.M. Doggen, G. Attard, J.S. de Bono, L.W.M.M. Terstappen. All circulating EpCAM+CD45-CK+ but not EpCAM+CD45+CK+ objects predict overall survival in castration-resistant prostate cancer. Annals of Oncology 21, 1851-1857, 2010.

Chapter 5 103 - 122
Unbiased and Automated Identification of a Circulating Tumour Cell Definition That Associates with Overall Survival. S.T. Ligthart, F.A.W. Coumans, G. Attard, A.M. Cassidy, J.S. de Bono, L.W.M.M. Terstappen. Plos One, doi:10.1371/journal.pone.0027419, 2011.

Chapter 6 123 - 140
Interpretation of changes in Circulating Tumor Cell counts. S.T. Ligthart*, F.A.W. Coumans*, L.W.M.M. Terstappen. Translational Oncology, in press, 2012.

Chapter 7 141 - 162
Challenges in the Enumeration and Phenotyping of CTC. F.A.W. Coumans, S.T. Ligthart, J. Uhr, L.W.M.M. Terstappen. Clinical Cancer Research, doi:10.1158/1078-0432.CCR-12-1585, 2012.

Chapter 8 163 - 182
Factors influencing filtration of tumor cells from whole blood. F.A.W. Coumans*, G. van Dalum*, M. Beck, L.W.M.M. Terstappen. Submitted for publication.

Chapter 9 183 - 206
Filter requirements for circulating tumor cell enrichment and detection. F.A.W. Coumans*, G. van Dalum*, M. Beck, L.W.M.M. Terstappen. Submitted for publication.

Chapter 10 207 - 223
Enrichment of circulating tumor cells from large sample volumes by means of filtration. F.A.W. Coumans, L.W.M.M. Terstappen.

Chapter 11 225 - 248
Flat-top illumination profile in an epi-fluorescence microscope by dual micro lens arrays. F.A.W. Coumans, E. van der Pol, L.W.M.M. Terstappen. Cytometry Part A, 81A, p 324–331, doi: 10.1002/cyto.a.22029, 2012.

* authors contributed equally

Summary 249
Samenvatting 251
Outlook 253
Publications 261
Biography 265
Acknowledgements 267

Chapter 12 269 - 276
De bloederige ontmaskering van de circulerende tumor cel. Jasmijn Coumans-Rijcken and Frank Coumans.

Introduction

Thesis motivation

Cancer incidence in Europe in 2006 was reported to be nearly 2.3 million people , with a cancer mortality of 1.2 million [1]. In the Netherlands cancer has become the leading cause of mortality. Total cancer incidence is still increasing and so is the social and economical impact of cancer. The per patient cost of cancer treatment is high and will become an enormous economic burden if the efficiency of cancer therapy is not improved. Robust diagnostic tests for the diagnosis of cancer, monitoring of its therapy and selection of the most appropriate therapy will become increasingly important to improve the quality of life and restrain healthcare costs. The need for improved diagnostic tests for cancer is exemplified in the case study depicted below and is the subject of this thesis. The figure on page 4 depicts the case of a 38 year old woman who finds a lump in her breast. A mammogram confirms the presence of a suspicious mass and a subsequent biopsy shows evidence for an invasive ductal carcinoma. The tumor is removed by breast conserving surgery. Fortunately the tumor is small (T_1) with no evidence of lymph node involvement (N_0) or distant metastasis (M_0). Immunohistochemistry shows that the tumor expresses the estrogen receptor (ER^+) and progesterone receptor (PR^+). After reconstructive surgery of the breast the woman has regular check-ups. Four years after the tumor has been removed the woman presents with pain in her thigh. X-ray followed by a bone scan showed a suspicious mass in her femur (thighbone), which is confirmed to be malignant breast cancer by biopsy. Computed tomography (CT) scan of liver, lung and brain shows no evidence of other metastatic sites. The femur is treated with radiation therapy and the woman receives hormonal therapy as immunohistochemistry of the original tumor suggested sensitivity of the tumor for hormonal therapy (ER^+, PR^+). A year later a CT scan showed evidence of liver metastasis and a first line of chemotherapy is started. After several lines of therapy her quality of life rapidly deteriorates and she dies.

[1] Ferlay, J., Autier, P. et al. "Estimates of the cancer incidence and mortality in Europe in 2006. Ann Oncol 18(3): 581-592, 2007

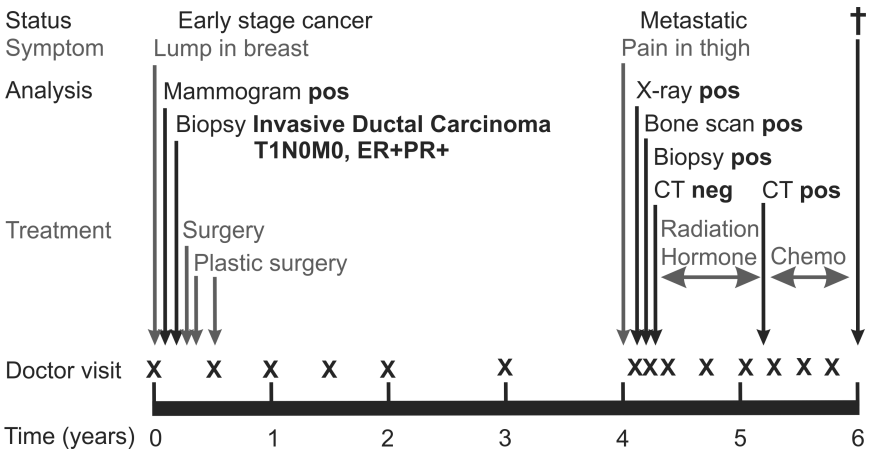

Case study of 38 year old woman with breast cancer

In this case, there are three time points when better diagnostic tools could improve treatment. First, at the time of diagnosis the tumor had already spread to other organs given by the fact that the disease recurred after surgery with curative intent. Removal of the tumor before it has spread to distant organs is the most effective way to treat cancer. Better screening tools for cancer may have resulted in an earlier diagnosis before the spread of the tumor to distant sites. Second at the time of diagnosis no evidence of distant metastases were found. Better diagnostic tools could have detected that this tumor had already spread to other organs. Beside surgery, (neo)adjuvant therapy could have eradicated the tumor cells at the distant sites and reduced or eliminated the possibility for disease recurrence. Third, once a patient has recurred, the selection of therapies is typically based on tissue that was collected at the time of surgery. In the years between surgery and recurrence, the cancer has evolved, possibly no longer responding to the drugs that the primary tumor would have responded to. Diagnostic tools that can provide the current state of the tumor would improve the selection and monitoring of treatments. Diagnostic tools that can shorten the time needed to confirm that the cancer is responding to treatment would improve the patient's wellbeing. Formation of a distant metastasis from a primary tumor requires that cells pass through the blood. While in the blood, these cells are called circulating tumor cells (CTC). The detection of CTC for improvement of cancer diagnostics is the topic of this thesis.

Thesis contents

The contents of this thesis are as follows: In chapter 1 we investigate at what size a tumor starts to seed and relate this size to the sensitivity required for detection of the primary tumor by both mammography and CTC enumeration before the primary has metastasized. Chapter 2 gives a detailed description of the CellSearch method for CTC enumeration, which is the only method that has been extensively validated in clinical trials. In chapter 3 a broader overview of the field is given. In addition, we investigate whether the sample that is enriched in the CellSearch AutoPrep can be further purified on an immuno-functionalized column for better molecular diagnostics on the CTC.

Counting circulating tumor cells requires defining a tumor cell, preferably in such a way that all tumor cells are counted, while no other cells are included in the count. Due to technological limitations this is not possible; the trade-off between the goal of detecting all CTC and the goal of not counting any other cells is extensively evaluated in chapters 4 to 6. First by human inspection of all cells in chapter 4, and later by means of an automated CTC identification algorithm, which is described and validated for prostate cancer in chapter 5. In chapter 6 we also investigate how to use the CellSearch method for CTC enumeration to determine whether a treatment is working.

To determine what treatment to give a patient based on CTC characteristics, it is a minimum requirement that at least one CTC is found in the patient. Because in 20–50% of patients with metastatic carcinoma no CTC are found using the CellSearch method, we investigate whether this absence of CTC can be explained by assay limitations in chapter 7. We find that a large sample volume is needed, too expensive to process by CellSearch. In recent years, several alternatives to the CellSearch approach have been proposed. One promising alternative is enrichment by means of filtration, which does not require antibodies for enrichment and thus may allow for a large increase in sample volume. The mechanism of enrichment by means of filtration is described in chapter 8 and the optimal filter for such filtration evaluated in chapter 9. One way to increase the number of CTC found, is to increase the blood volume sampled, which we study in chapter 10. Once the CTC are found, quantification of the presence of treatment targets can be improved by a modification of the CellSearch Analyzer II, and is described in chapter 11.

CHAPTER 1

Technology requirements for detection of residual disease in cancer patients

Frank A.W. Coumans, Sabine Siesling and Leon W.M.M. Terstappen

Abstract

The formation of distant metastasis (DM) requires that cells disseminate from the primary tumor and overcome a series of obstacles before formation of metastasis. The aim of this study was to develop a model for this metastatic cascade to estimate when a metastasis is formed and the technology requirements to detect the primary tumor before this time. The model for DM was developed using data and relationships described in literature. The model was calibrated using primary tumor size, probability of DM and time to DM of 38715 patients with surgically removed $T_xN_xM_0$ breast cancer from the Netherlands Cancer Registry. In the metastatic cascade model, both metastatic efficiency and dissemination rate contribute equally to the probability of developing a metastasis. The number of circulating tumor cells (CTC) is directly related to, but not equal to, the dissemination rate. To reduce the 5-year risk of DM for $T_xN_xM_0$ from 9.2% to 1%, the primary tumor needs to be detected and removed before it reaches a diameter of 2.7 ± 1.6 mm. At this size, the model predicts that there will be 9 ± 6 CTC/ L blood. To reduce the rate of DM in surgically treated $T_xN_xM_0$ breast cancer to 1% imaging technology will need to be able to detect lesions of 2.7 mm in diameter or smaller. Before CTC detection can be applied in the early disease setting, sensitivity will need to be improved by at least 15-fold and combined with technology that minimizes false positives.

1.1 Introduction

The majority of deaths from cancer are due to distant disseminated disease rather than the primary tumor [1]. While metastases are often discovered years after surgical removal of the primary tumor, probably at least one metastasis was already present at the time of surgery. Understanding of the formation of distant metastasis (DM) is crucial for the improvement of patient care. For the successful colonization of a secondary site a cancer cell must complete a series of steps to become a clinically detectable lesion, baptized the metastatic cascade [2, 3, 4, 5]. This cascade is an inefficient process, generating metastasis by sending large numbers of malignant cells into the circulation [6, 7]. The number of cells disseminated and the efficiency of metastasis formation contribute to the probability that a metastasis has formed. Assays for enumeration of circulating tumor cells (CTC) in blood [8] provide access to the number of disseminated cells. The CTC are the new seeds of a tumor, and as such provide an opportunity to estimate the metastatic efficiency. Due to metastatic inefficiency, the presence of CTC does not imply that metastases already exist. Identification and enumeration of CTC at or before the diagnosis of the primary tumor may allow estimation of the probability of DM being present and thus help identify patients who will benefit from more intensive monitoring or therapy after surgical removal of the primary lesion. Here we developed a model for the metastatic cascade and estimated the sensitivity needed for imaging and CTC detection to detect a primary tumor before it has formed DM.

1.2 Materials and methods

1.2.1 Distant Metastasis statistics

The probability of DM and time to DM was determined based on patients selected from the population based Netherlands Cancer Registry (NCR, www.iknl.nl). Based on pathological notification specially trained registrars gather data directly from the patient files on patient, tumor characteristics and treatment for all malignancies in all hospitals in the Netherlands. Women with pathological stage $T_{1A}N_xM_0$-$T_2N_xM_0$ invasive breast cancer, being 25 years or older at time of diagnosis, who had had mastectomy or breast conserving surgery and were diagnosed between 2003 to 2006 were selected. Patients were excluded if any evidence of residual tumor was found after surgery. Patients were followed until at least five years after diagnosis and both occurrence and date of DM were registered. Time between diagnosis and occurrence of DM is summarized with mean and standard deviation. Probability of a DM within the five years of follow-up and the 95% confidence interval of DM was determined by Poisson statistics.

1.2.2 Parameter fitting

A model for the development and detection of DM was developed and tested in Matlab 2009a (Mathworks, Natick, MA). The model requires determination whether a disseminated tumor cell has successfully formed a metastasis. The probability that metastases were formed was determined by applying the Poisson limit theorem to the binomial distribution of the number of seeds per time interval and the probability of a successful seed. The resulting cumulative distribution function was compared to a pseudo random number generated by Matlab. The product of dissemination rate and metastatic efficiency was fit to the probability of DM for stage T_{1B} patients, running 10,000 iterations and randomizing doubling time for each iteration. After fitting the data we compared predicted and actual probability of DM for the other T-stages of the primary tumor. The time to DM in the model was defined as the time between removal of the primary tumor and the time when the first DM reaches 8 mm in diameter (T_{1B}). Doubling time mean and standard deviation was determined from the time to DM. CTC concentration was fit to available literature values; patients with metastatic disease have 3.0 CTC/ mL (5–95 percentile: 0.02–417) [9, 10, 11, 12], and patients with early stage breast cancer have CTC at a concentration of 0.03 CTC/ mL (range of estimates 0.01–0.05) [13, 14, 15, 16]. We further assumed a cardiac output of 5 L/minute.

1.3 Results

1.3.1 Model for formation of distant metastasis

The steps in the metastatic cascade are summarized in figure 1.1. A tumor grows locally (1). Cells disseminate from the primary tumor (2). The tumor cells that survive in the circulation (3) ultimately arrest in the microcirculation of an organ and may extravasate into the surrounding tissue (4). Extravasated cells can either; survive as a singular dormant cell (5A), form a micro metastasis (5B), or grow into a macro metastasis (5C). While it is unknown what triggers a primary tumor to start shedding cells into the blood stream, this shedding starts well before the primary tumor is detectable by current imaging techniques [17, 18, 19]. A model for the formation of metastasis is described using relationships described in literature. Because we are looking for a small detection limit, we fit the model to the probability of DM and time to DM for a T_{1B} tumor, which is the smallest frequently discovered tumor. It is typically discovered when it reaches a diameter of 8 mm. We tested the fit of the model against the T_{1A}, T_{1C} and T_2 stage DM data. Further model assumptions are listed in paragraph 1.5.1. The formation of distant metastasis is described with functions for the steps, depicted in figure 1.1, see paragraph 1.5.2 for a more elaborate derivation:

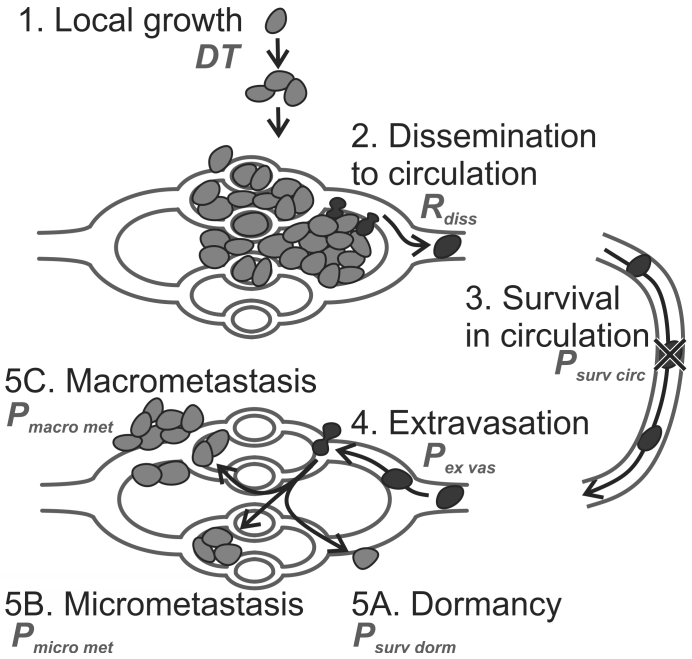

Figure 1.1: Steps in the metastatic cascade. *Relevant parameters are shown near the description of each step. Cells in tissue are indicated in light gray, cells in blood or in transition between blood vessel and tissue are indicated in black. Local growth (step 1/equation 1.1) is needed to provide sufficient disseminated cells. Steps 2-5 are typically referred to as the metastatic cascade (equations 1.8-1.10, and 1.13). Step 5 has multiple outcomes, with cells surviving, but not replicating (5A), briefly or slowly replicating (5B) or rapidly replicating (5C).*

1. Local growth: In a comparison of functions typically used to describe tumor growth (exponential, Gompertz or logistic), the logistic function fit best [20], equation 1.1:

$$\begin{aligned} N_{mass}(t) =& \frac{N_{max}}{[1+(N_{max}^{1/4}-1)e^{-ln(2)t/4DT}]^4} \\ \approx& \frac{N_{max}}{[1+(N_{max}e^{-ln(2)t/DT})^{1/4}]^4} \end{aligned} \tag{1.1}$$

Gompertz and logistic functions have a slowing growth rate as the tumor reaches a maximum size N_{max} (N = number of tumor cells) at a certain time (t). N_{max} is typically chosen at 10^{12} cells / 1 kilogram. We assume metastases grow according to equation 1.1. Changes in growth rate as

a function of supply of nutrition, due to occurrence of growth enhancing mutations or due to chemo or hormonal therapy are not considered in any of the growth models.
2. Dissemination to circulation: The relationship between tumor diameter (D_{mass}) and the number of disseminated cells (N_{diss}) is assumed linear and is derived from murine data comparing CTC counts to the diameter of the primary tumor [21, 22, 23, 24]. To derive the diameter of the lesion from the number of cells (N_{mass}), we assumed a spherical lesion. Once the primary tumor reaches a critical size (N_{crit}), it starts to disseminate cells into the bloodstream at a rate (R_{diss}):

$$R_{diss} = \begin{cases} C_{diss} \cdot D_{mass} & \text{if } N_{mass} > N_{crit} \\ 0 & \text{if } N_{mass} \leq N_{crit} \end{cases} \tag{1.2}$$

3,4,5C. Formation of a metastasis: The relationship between the number of cells injected into the circulation and the number of macroscopic metastases is linear [25, 26, 27], with slope $\gamma_{metastatic}$ the metastatic efficiency. We now find the total number of metastases:

$$N_{total\ macro\ met} = \gamma_{metastatic} \cdot C_{diss} \int D_{mass}\, dt \tag{1.3}$$

In this equation, the number of metastases formed is equal to the metastatic efficiency times the total number of cells disseminated from the tumor. The rate of cell dissemination (R_{diss}) is measurable by detecting the number of CTC, while the metastatic efficiency ($\gamma_{metastatic}$) may be measurable either by genotyping these CTC or the primary tissue.

1.3.2 Model for circulating tumor cell concentration

The concentration of CTC is determined by the dissemination rate and the number of passages through circulation that the typical CTC makes, illustrated in a schematic diagram in figure 1.2. In this diagram, the CTC concentration in several veins is shown. Each passage through the microvasculature of an organ takes a fraction η of cells out of circulation, with $\eta = 1$ meaning capture of all CTC by the microvascular bed of an organ and $\eta = 0$ meaning no CTC are captured. A breast tumor disseminates CTC into the efferent vein, which is diluted in the vena cava. Passage through the lung (η_{lung}) and arm (η_{arm}) are required to end up in the cubital vein were the blood is drawn. Derivation of the CTC concentration in the cubital vein ($[CTC]_{cubital}$), equation 1.4, is derived in paragraph 1.5.3.

$$[CTC]_{cubital} = \frac{R_{diss}}{Q_{total} \cdot \eta_{circulation}} (1 - \eta_{lung})(1 - \eta_{arm}) \tag{1.4}$$

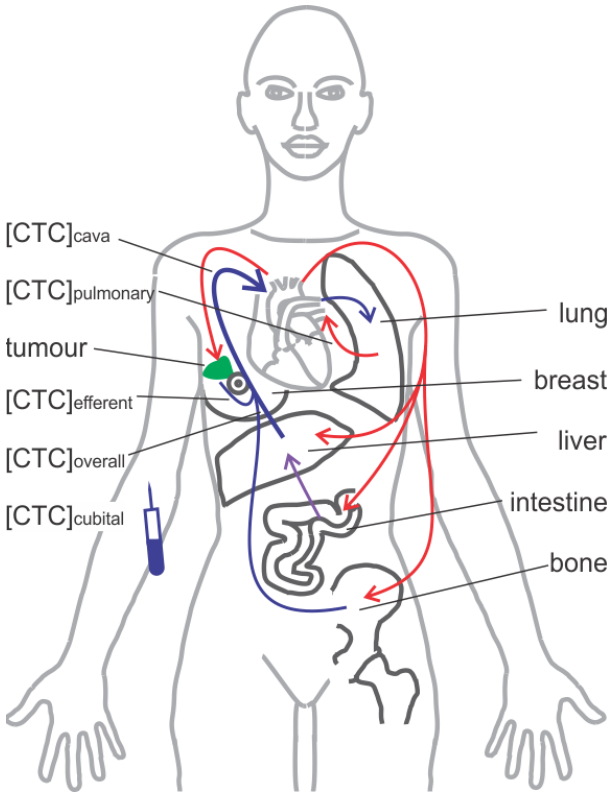

Figure 1.2: Schematic diagram for CTC concentration model. *The different CTC concentrations from equations 1.16–1.23 are shown on the left and some organs are shown on the right. CTC are always sampled from the veins. Deoxygentated blood is shown in blue, oxygenated blood in red. Part of the blood supply to the liver passes through the intestine first. Some of the organs from equation 1.21 are shown in the figure. The liver receives blood directly as well as through the intestine, the contribution through the liver is counted separately where the fraction of CTC that pass both the intestine and liver,* $1-\eta$*, equals:* $(1-\eta_{intestine})(1-\eta_{liver})$*.*

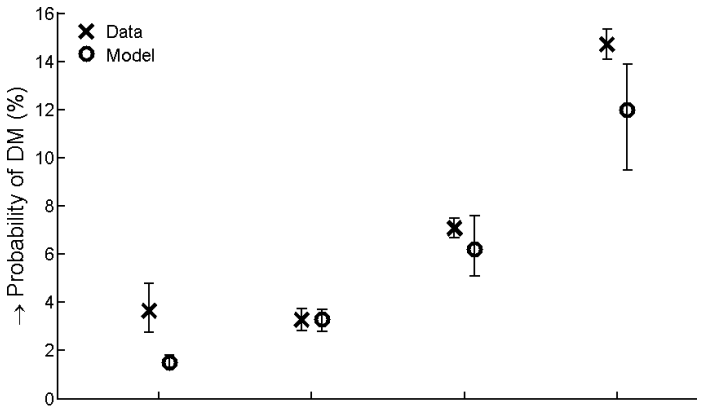

Tn	T1A	T1B	T1C	T2
Diamet. (mm)	4	8.5	15	26
N Total	1447	5959	17151	14158
N with DM	53	196	1216	2085
Time to DM (months)				
Mean	35.1	34.6	34.6	30.2
SD	19.2	17.5	16.9	17.0

Figure 1.3: Probability of distant metastasis by T-stage for patients who are N_xM_0. *Total n=38715, number of DM n=3550. Whiskers indicate 95% confidence intervals determined using Poisson statistics. Below the T-stage further statistics are shown, including median diameter in mm, number of patients included, number of patients with a DM as well as mean and standard deviation of time to DM.*

Q_{total} represents the cardiac output, Q_i the blood flow to an organ and η_i the capture efficiency of an organ, summed over all organs:

$$\begin{aligned}(1-\eta_{circulation}) =& (1-\eta_{lung})(1-\eta_{systemic}) \\ =& (1-\eta_{lung})\sum \frac{Q_i \cdot (1-\eta_i)}{Q_{total}}\end{aligned} \tag{1.5}$$

The CTC concentration detected in the cubital vein is measured to determine the dissemination rate, however it should be noted that while $[CTC]_{cubital}$ is proportional to the number of cells disseminated from the tumor it is not equal to R_{diss}/Q_{total}. From this equation it is easily seen that the impact of low $\eta_{circulation}$ is to increase the CTC concentration and that for η_{lung} or $\eta_{arm} = 1$ no CTC are detectable in the cubital vein.

1.3.3 Distant metastasis statistics

Of 42318 patients matching our search criteria, 38715 (91%) patients were included, see figure 1.5 for details. The probability of DM after surgery and the time to DM from stage T_{1A}–T_2 invasive breast carcinoma patients, without known metastases at time of diagnosis (N_xM_0) was determined and shown in figure 1.3. Three thousand five hundred and fifty patients developed DM within five years after surgery. The overall probability of DM was 9.2%, with a time to DM of 32.0 ± 17.2 months. Variation in mean time to DM between different T-stages is small (range 30.2–35.1 months). 95% of detected primary tumors are 5 mm or larger (median 17 mm). Information of both T-stage and diameter of the primary was available for the majority of patients in our database. Median diameter was determined on the 33876 patients (88% of total) who had both T-stage and the diameter of the tumor available. Probability of DM, time to DM and median size by stage was used to fit the model (equations 1.3 and 1.4) to the clinical data and compare the result with values reported in the literature for both human and murine studies. Summary data are found in table 1.1, with more detailed information in supplemental tables.

1.3.4 Tumor doubling time

From the time to DM of the 38715 breast cancer patients, we determined a doubling time (DT) of 1.7 ± 0.9 months. Human values for DT are estimated by fitting a growth model to imaging data reported in the literature, see table 1.4. Their median DT estimate is 5.7 months (range 2.0 to 11.2 months). We did not consider doubling times in murine models because they are not comparable.

1.3.5 Organ trapping of CTC

The CTC concentration can be used to determine the rate of tumor cell dissemination. The CTC concentration in the cubital vein is equal to the rate of CTC dissemination times the number of times a CTC circulates, minus the number of CTC captured indefinitely in the microvasculatures or lung and arm, equation 1.4. Capture efficiency is defined as the percentage of CTC that is captured indefinitely in the microvasculature of an organ. The number of times a CTC circulates is inversely proportional to the weighted capture efficiency of all organs, equation 1.5. A circulation capture efficiency of 50% means the average CTC makes two passages through circulation before it is trapped or destroyed. To estimate the dissemination rate from the CTC concentration, we need estimates of the capture efficiencies of each organ. Two human studies have determined the CTC concentration simultaneously from two different sampling sites, table 1.5. This allows estimation of the capture efficiency of the organs between these two sampling

Table 1.1: Metastatic cascade parameter estimates from our model, human and murine studies. *Literature values are the median of all estimates with the range of estimates in parenthesis. Detailed data for each publication is given in supplementary tables indicated in the right hand column*

parameter	symbol [a]	model	human	murine	table
doubling time (mo)	DT	1.7 ± 0.9	5.7 (2.0–11.2)		1.4
dissemination rate (CTC/h·g)	R_{diss}	$0.3{\cdot}10^3$–$130{\cdot}10^3$ [b]	$3.1{\cdot}10^3$ (90–$78{\cdot}10^3$)	$1.0{\cdot}10^5$ ($1.5{\cdot}10^{-1}$–$8.7{\cdot}10^6$)	1.8,1.9
critical size (g)	N_{crit}	< 1		0.4 (0.2–0.8)	1.9
survival in circulation	$P_{surv\ circ}$		$< 80\%$	90% (70–95%)	1.11
extravasation	$P_{ex\ vas}$			65% (20–96%)	1.11
dormant survival	$P_{surv\ dorm}$			36% (35–50%)	1.10
formation of micro met	$P_{micro\ met}$			6% (1–80%)	1.10
formation of macro met	$P_{macro\ met}$			0.01% (0.016–6%)	1.10
metastatic efficiency	$\gamma_{metastatic}$	$3.6{\cdot}10^{-11}$–$1.5{\cdot}10^{-8}$ [b]		0.007% (0.0001–0.6%)	1.10
capture efficiency					1.5,1.6
high affinity	$\eta_{high\ aff}$		31% (24–44%)	95% (28–100%)	
low affinity	$\eta_{low\ aff}$			25% (1–29%)	
circulation	$\eta_{circulation}$			70% (43–95%)	
CTC decay time (h)			2.4	0.7 (0.2–1.4)	1.7

[a] See results for further descriptions, [b] see table 1.3.

Table 1.2: Incidence of metastases versus blood flow. *Blood flow to different organ systems [31] and % of breast cancer patients ($N = 432$) with distant metastases in these organs at time of death [32]. Included in the table are all organs which receive at least 5% of cardiac output, or in which metastases were found in at least 4% of patients.*

organ	cardiac output (%)	Px w/ mets (%) [b]	% Px w mets/ % cardiac output
adrenal gl.	< 1	9	> 9
pleura	< 1	9	> 9
bone	5	12	2.40
skin	9	7	0.78
liver	27 [a]	13	0.48
brain	13	2	0.15
lung	100	13	0.13
kidney	20	2	0.10
muscle	15	0	0
other	10	< 3	< 0.3

[a] 21% via portal vein, 6% direct, [b] patients with metastasis.

sites. If we assume that the capture efficiency of all organs is equal, we find estimates from 24–44%. Murine models allow determination of capture efficiency from data in several publications, table 1.6. From these studies we conclude that some organs have high capture efficiency of 95% (range 28–100%), while others have low efficiency of 25% (range 1–29%), leading to estimates for the capture efficiency of the circulation of 42% to 95%, or 1.1–2.4 passages through circulation per CTC. This suggests that the number of CTC detected rapidly reduces after the source of new CTC is removed. In contrast in murine models, the half life of CTC in circulation after injection of a tumor cell line with in vivo flowcytometry is 0.7 (range 0.2–1.4) hours, table 1.7. The half life of CTC after surgical removal of the primary breast tumor in humans is reported as 2.4 hours [28]. This apparent discrepancy may be explained by a slow passage of CTC through the microvasculature due to severe deformation needed to squeeze through a capillary [29, 30]. For a CTC to extravasate it needs to be captured first, therefore capture efficiency of an organ directly affects metastatic efficiency of that organ. The incidence of metastases relative to the blood flow to an organ suggests that the metastatic efficiency is different for different organs [31, 32]. Table 1.2 shows that bone, skin, liver, pleura and adrenal gland have a high incidence of metastases relative to the blood flow, lung and brain a medium incidence and other organs a low incidence of metastasis.

Since we found a wide range of estimates, we considered three organ CTC capture efficiencies; (1) all organs take 90% of CTC per pass through

Table 1.3: Metastatic efficiency and dissemination rates for different capture efficiencies. *Mean with range of estimates in parenthesis*

capture efficiency [a]				metastatic efficiency [b]	dissemination rate [c]
$\eta_{high\ aff}$	$\eta_{med\ aff}$	$\eta_{low\ aff}$	η_{circ}		
90%	90%	90%	99%	$3.6{\cdot}10^{-11}$ ($3.0{\cdot}10^{-11}$–$4.1{\cdot}10^{-11}$)	$130{\cdot}10^{3}$ ($40{\cdot}10^{3}$–$210{\cdot}10^{3}$)
10%	10%	10%	19%	$1.5{\cdot}10^{-8}$ ($1.2{\cdot}10^{-8}$–$1.7{\cdot}10^{-8}$)	310 (110–520)
95%	25%	5%	54%	$2.3{\cdot}10^{-9}$ ($2.0{\cdot}10^{-9}$–$2.7{\cdot}10^{-9}$)	990 (330–1,660)

[a] aff = affinity, circ = circulation, [b] range of estimates from 95% CI of probability of recurrence of 2.8–3.7% for T_{1B} tumors, [c] determined for primary tumor at mass of 6 g, range of estimates from range of 0.01–0.05 CTC/ mL before surgery.

the microcirculation, (2) all organs take 10%, or (3) 95% is taken out by high incidence of metastasis organs, 25% by medium incidence organs, and 5% by all others.

1.3.6 Formation of metastases and dissemination rate

The probability of forming a metastasis is primarily determined by (1) the number of cells entering the circulation and (2) the probability that each of these cells forms a metastasis ($\gamma_{metastatic}$). The number of cells entering the circulation is a function of the dissemination rate (R_{diss}) and the elapsed time, which is affected by the tumor doubling time (DT). For a given DT, the probability of forming a metastasis before surgery is determined by the product of $\gamma_{metastatic}$ and R_{diss}. This product was split into R_{diss} and $\gamma_{metastatic}$ using equation 1.4, to match the CTC concentration reported for breast cancer before surgery of 0.03 CTC/ mL (range 0.01–0.05 [13, 14, 15, 16]. With the three capture efficiencies described earlier, we find a dissemination rate for an 8 mm tumor of 310–130,000 CTC/h·g tumor and a metastatic efficiency of $3.6 \cdot 10^{-11} - 1.5 \cdot 10^{-8}$ metastases formed per disseminated cell, table 1.3. CTC in a metastatic patient are present at a concentration of 3 CTC/ mL of blood [12], however a 100-fold lower concentration is detected in patients before surgery. While in our model the total tumor mass of all lesions is larger for a metastatic patient, the difference is not sufficient to cause such a high change in CTC concentration. To achieve the higher CTC concentration post surgery, we increased the dissemination rate by 25-fold for all metastatic lesions. We could also achieve this CTC concentration in metastatic patients by increasing the metastatic efficiency 10,000-fold. Either scenario, or a combination, is conceivable, since a cell that has completed the metastatic cascade may be genetically predisposed towards formation of metastasis and/or dissemination into the circulation.

The dissemination rate can be estimated from two human studies which determined the CTC concentration in the efferent vein of colorectal and renal cancer, table 1.8, where we found a median of 3,100 CTC/h·g tumor, and a range of estimates of 90–78,000 CTC/h·g, which is similar to our model estimates of 310–130,000 CTC/h·g tumor. In murine models both dissemination rate and the metastatic efficiency have been extensively studied as summarized in table 1.1. The dissemination rate determined by various techniques spans a wide range of nearly 7 orders of magnitude, table 1.9. The median estimate is $1.0 \cdot 10^5$ CTC/h·g (range 0.15 to $8.7 \cdot 10^6$ CTC/h·g). Metastatic efficiency has been determined either from the number of macro metastases formed from injection of a known number of malignant cells, or by observing the individual probabilities in the metastatic cascade by means of intra-vital video microscopy (IVM, [33]). Methods, which determined the metastatic efficiency from injection of a known number of cells, estimated $\gamma_{metastatic}$ at 0.005% (range 0.0001–6%), table 1.10. From the IVM studies we find a comparable $\gamma_{metastatic}$ of 0.011%, primarily caused by the low probability of extravasated cells to form a macro metastasis, paragraph 1.5.4.
It was not possible to estimate the size at which the tumor starts disseminating (N_{crit}) from the tumor size and DM data from the breast cancer patients. When we changed N_{crit} after fitting the model, we found that the probability of forming a first metastasis is unaffected by any value of N_{crit} below 1 g tumor. From clinical evidence [17, 18, 19], we expect that N_{crit} is substantially smaller than 1 g (2.7 mm diameter). While no study determines N_{crit} directly, several detect CTC concentration as a function of tumor size, table 1.9. This allows estimation of an upper limit of N_{crit} at < 0.4 g (range < 0.2–< 0.8 g), with the understanding that lower N_{crit} was possible, but could not be detected due to limited assay sensitivity.

1.3.7 Sensitivity needed for radiographic imaging and CTC detection to detect a tumor before it gives rise to metastasis

The model was used to predict the technology needs for detection of tumors before metastasis can occur. The values used for the model are provided in table 1.1. In figure 1.4 an example is shown of a T_{1B} breast tumor. Panel A shows the development of the total tumor mass and the tumor cell number per equation 1.1. The black line represents the case for which the tumor is surgically removed and the gray line the case for which the tumor is not removed. In panel B, the solid black line shows the maximum diameter of the tumor. This diameter is important for detection of a tumor by an imaging method. In this case, the T_{1B} tumor is detected when it reaches 8 mm, 3.4 years after its inception, and is surgically removed. If an imaging system is employed to detect all lesions in a patient, it must be capable

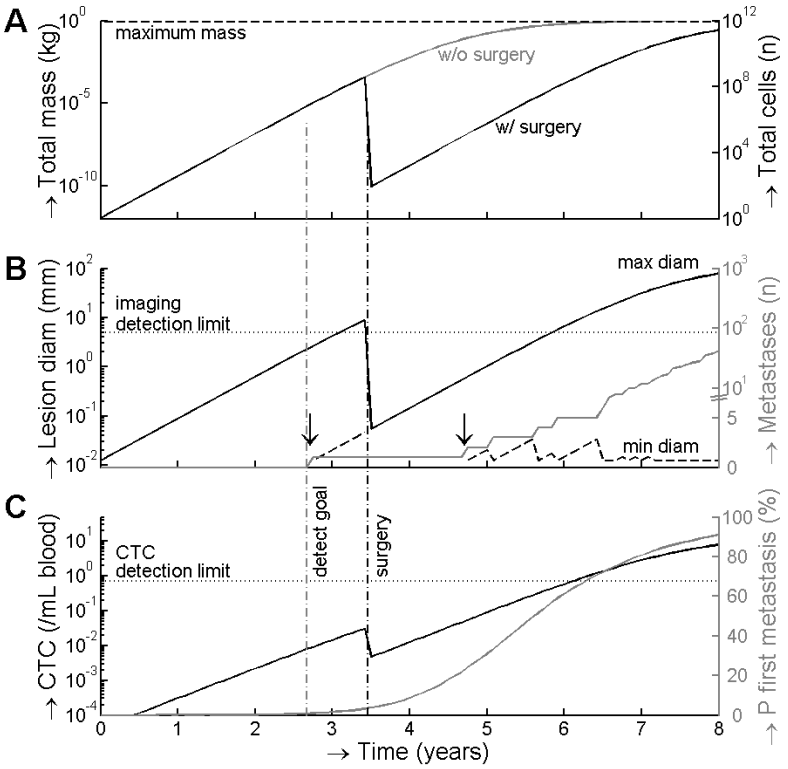

Figure 1.4: Application of the model to estimate the technology requirements for radiographic imaging and CTC detection to reduce the probability of distant metastasis to below 1%. *Panel A shows the time needed to develop a tumor mass and the number of tumor cells for a stage T_{1B} tumor removed by surgery (black line) or not removed by surgery (gray line). Panel B shows the maximum (black solid line) and minimum size (black dashed line) of the primary tumor and/or metastasis and the number of metastasis in gray. Minimum size is only shown when 2 or more lesions exist; the formation of the second lesion before and after surgery are indicated with a vertical black arrow. Panel C shows the development of the CTC concentration in black, and the cumulative probability that a first metastasis has occurred in gray. The black vertical dashed line indicates the time at which the primary tumor is surgically removed in our model. The cumulative probability is used to determine the detection goal (vertical dashed gray line); the time when the primary tumor needs to be removed to reduce 5 year recurrence from 9% (from all $T_xN_xM_0$) to 1%. This line intercepts with a CTC concentration of 9 CTC/L of whole blood and a lesion size of 2.7 mm, and represent the required sensitivities for radiographic imaging and CTC detection.*

of identifying the smallest lesions. The dashed line in panel B shows the diameter of the smallest lesion at times multiple lesions exist. In figure 1.4, the tumor has seeded a metastasis 2.8 years after initiation of the tumor. At the time of surgery this lesion has a diameter of 70 µm; undetectable by imaging. The total number of metastases is shown in a solid gray line on the secondary y-axis. The number of metastases is relatively stable from 3.4 years (surgery) to ≈5.5 years, but rapidly increases after 6 years because the metastasis has become sufficiently large to make formation of new metastases probable again. Panel C shows the CTC concentration in solid black and the probability of forming the first DM is solid gray on the secondary y-axis. To reduce the probability of DM from 9.2% in the patients included in our study to 1%, the tumor needs to be detected by the time it reaches 2.7 ± 1.6 mm or when the CTC concentration is 9 ± 6 CTC/L of whole blood.

1.4 Discussion

The most effective therapy to treat breast cancer is to surgically remove the primary tumor before it has formed a distant metastasis (DM). The probability that a DM has been formed prior to surgery can be modeled by estimation of the probabilities of each of the steps required for the formation of metastasis. Three key components of this probability are the rate of tumor cell dissemination (R_{diss}), the tumor doubling time (DT) and the probability of successful completion of the metastatic cascade ($\gamma_{metastatic}$). R_{diss} can be determined from the CTC concentration if the fraction of CTC removed in each passage through the circulation is known. The number of DM formed per disseminated tumor cell, $\gamma_{metastatic}$, may be estimated by genotyping the CTC or the primary tissue. Here we combined literature values with clinical data from the NCR to obtain estimates for DT, R_{diss} and $\gamma_{metastatic}$ for patients. Using this model, we predicted the sensitivity needed of radiographic imaging and CTC enumeration for detection of a primary tumor before DM formation has occurred.
Data from the NCR was used to determine the probability for breast cancer DM by T-stage and the time between surgical intervention and DM. To obtain a patient group with a minimal risk of DM, we included only patients with complete removal of the tumor after surgical resection, relatively small tumors (T_1,T_2) and no detectable metastasis (M_0). The NCR recorded data for DM five years after surgical intervention. From the time to DM of 32 ± 18 months, we determined a DT of 1.7 ± 0.9 months for DM; threefold faster than the DT of 5.7 months determined from primary tumor imaging data. A DM with a DT of 5.7 months would lead to discovery of a DM 9.5 years after initiation of the DM; the 5-year (60 month) observation window is too short to observe tumors with a DT of 5.7 months, it is likely that our estimate of 1.7 months represents tumors with aggressive growth rates. In

addition, the DT of 5.7 months is determined on primary tumors, while the DT of 1.7 months is determined on the DM. The DM may have a different DT than the primary lesion in the same patient. Differences in DT of DM and primary may be attributable to natural selection in the metastatic cascade, different micro environment or accumulation of growth enhancing mutations.

Determination of the number of cells disseminated from the tumor can be derived from the CTC concentration if we know the number of CTC removed from circulation by each passage through the microcirculation. We approximated this, by assuming that each organ captures a fraction (η) of the CTC delivered by the flow of blood (Q) to each organ, see equation 1.4. Two effects are apparent from this equation; (1) if the microcirculation does not allow any CTC to pass, no CTC are detectable when sampling the cubital vein and (2) low capture efficiency increases the CTC concentration because CTC make multiple passages ($1/\eta$) in the circulation. When CTC were detected at two sites simultaneously, typical capture efficiency per organ was approximately 30% in human studies, table 1.5. At least one of the organs between these two sampling sites was an organ with high incidence of metastases, such as liver and lung for colorectal cancer. Murine literature values suggest that capture efficiencies can vary greatly by organ (1–100%). Several murine studies injected a colorectal cell line in the portal vein and determined the capture of cells in the liver (a metastatic site for colorectal cancer) and report capture efficiencies of 97–100%, table 1.6. One proposed mechanism for capture is mechanical entrapment [33]. Mechanical entrapment may be less effective for human CTC, as they are smaller than tumor cell lines [34]. In addition, selective blocking of surface antibodies in the vasculature or on the cell lines can reduce the capture efficiency by 2-3 fold [35, 36, 37]. A possible consequence is that some organs have high capture efficiency, while others have low efficiency due to differences in expression of proteins or microvasculature geometry. The distribution of capture efficiencies may affect the cell dissemination rate by two orders of magnitude for the same number of CTC.

If a very high fraction of cells is trapped in the first capillary bed encountered, then breast cancer should metastasize primarily to the lungs. Breast cancer metastasizes to multiple distant organs, primarily the lungs (13% of patients), bones (12%) and liver (13%) [32], table 1.2. If η_{lung} is 90%, the probability that a cell forms a lung metastasis needs to be 200-fold lower than the probability of a bone metastasis, since the supply of (CTC depleted) blood to the bones is 20-fold lower than to the lung.

We tested three scenarios; (1) all organs have η of 90%, (2) all organs have η of 10% and (3) η varies between high ($\eta = 95\%$), medium ($\eta = 25\%$) and low ($\eta = 5\%$) for different organs depending on incidence of metastases relative to blood supply (table 1.2). Considering these three scenarios, the rate at which CTC disseminate from the primary lesion varies by 400-fold for the same detected CTC concentration, table 1.3. From murine studies,

we conclude that dissemination rate is linearly dependent on the diameter of a lesion. For a diameter of 8 mm (typical T_{1B}) we find dissemination rates of 310–130,000 CTC/h·g tumor when we fit the clinical data to our model. This is surprisingly close to dissemination rates determined from the tumor efferent vein in human studies of 90–78,000 CTC/h·g tumor. Dissemination rates determined in murine models span a very wide range of 7 orders of magnitude (0.15–8,700,000 CTC/h·g tumor), table 1.9. While this variation may be caused by differences in the detection methods used or differences between cell lines, the variation between murine estimates makes comparison with our model futile. While it is possible that a tumor needs a minimum size before dissemination starts it is not an important factor in our model, as this size has no influence on the probability of metastasis until a tumor is at least 3 mm in diameter.

Metastatic efficiency in our model is estimated at 1 metastasis per 70 million to 28 billion disseminated tumor cells. This is substantially less likely than the murine model median estimate of 1 in 14,000 disseminated cells (range 1 in 170 to 1 in 1 million). The large difference of metastatic efficiency between murine model and human model may be attributed to many factors, including use of cell lines with high metastatic efficiency, the 2,000-fold difference in size between human and mouse and the immunodeficiency of most mouse models. Murine models suggest that disseminated cells have high survival in circulation and are efficient at extravasation, table 1.11. Survival of extravasated cells beyond 2 weeks is estimated between 4% and 50%, if these continue to survive this would leave a substantial number of dormant, but malignant, cells scattered throughout the body, up to a billion cells in our model, paragraph 1.5.4. These cells may constitute a malignant time-bomb, since dormant cells may be reactivated at a later time [38]. In the shorter term, metastatic efficiency is limited primarily by the ability of a disseminated cell to grow in a new site, table 1.2.

The model as described above does not consider evolution over time of the metastatic properties of primary tumor or metastatic lesions [17]. However, to obtain a match between the CTC concentration in early stage disease and CTC in metastatic disease, we applied a single increase in the dissemination rate of 25-fold, or an increase in the metastatic efficiency of 10,000-fold. Our rationale was that the metastatic cell has become efficient at disseminating and/or metastasizing due to natural selection by the metastatic cascade and has thus become genetically more prone to formation of new metastases [39, 40]. We recognize that it is equally feasible that such evolution occurs more gradually.

To determine the probability of metastases in a patient, three parameters are relevant, the dissemination rate, the growth rate and the metastatic efficiency. The dissemination rate can be determined from the CTC concentration, the growth rate and metastatic efficiency can be estimated from the primary tumor or, alternatively, by genotyping captured CTC. This is supported by the observation that both CTC concentration and hormone

receptor status from primary tissue information are independent prognostic data in multivariate analyses [41, 42].
Applying the model allows for estimation of the probability of metastases as a function of primary tumor size. Figure 1.3 illustrates that the model reasonably predicts the probability of DM for stages T_{1B} to T_2. The probability of DM grows slightly faster in the data than in the model, which may be caused by a slow increase in dissemination rate or metastatic efficiency over time. With current imaging technology, 94% of detected lesions have a size of 6 mm or more, with a specificity of 40% [43]. From the data of the NCR, we conclude that current clinical practice in the Netherlands has similar detection characteristics, with 95% of the tumors detected when the tumor is 5 mm or larger, with a median size of 17 mm. The larger probability of DM for T_{1A} than T_{1B} in the NCR data is unexpected and raises the question whether these small tumors are truly more aggressive, or whether the difficulty to detect tumors smaller than 5 mm has caused a sampling bias in the T_{1A} sample. Dividing all patients into breast cancer subgroups based on the gene signature [44, 45, 46, 47] could resolve this question, as there are marked differences between subgroups, and it is feasible that these subgroups have different metastatic efficiency and dissemination rates.

In our model we find that to reduce the overall probability of DM from 9.2% to 1% the tumor needs to be detected by the time it reaches 2.7 ± 1.6 mm. This requires an improvement in imaging technology, but without further reducing the specificity. Alternatively, to achieve probability of DM of 1%, a tumor would need to be detected when the CTC concentration is 9 ± 6 CTC/ L of whole blood. This requires at least a 15-fold improvement in the CTC detection limit. Possible approaches for this improvement are discussed elsewhere [48]. To implement CTC as a screening tool, the improved CTC detection will need to have a minimal impact on the screened patient and to have similar specificity to radiological imaging. We note that by definition, CTC enumeration will not detect benign lesions. On the other hand, CTC detection could have excellent sensitivity and specificity for malignant lesions if the malignancy of detected CTC is confirmed with whole genome comparative genome hybridization [49, 50].

1.5 Supplemental information

1.5.1 Model assumptions

For the model we assumed the following:

- a single malignant breast cell with an approximate size of 10^{-6} mm^3, starts to grow. Once the malignant mass has reached a minimum size, tumor cells shed into the blood.

- each of the disseminated cells has a probability of forming a metastasis.
- after the primary tumor reaches a certain diameter, it is discovered and surgically removed.
- in case of DM at least one metastasis was formed prior to surgery.
- probability of DM is defined as the probability that at least one metastasis was present at the time of surgery, continues to grow and is discovered once it has reached a size of 8 mm.
- for fitting of the model, the primary is detected when it reaches a size of 8 mm (stage T_{1B}).
- for testing the model, the primary is detected when it reaches the median size representative of each T_x stage.
- the probability that a cell in captured in the microvasculature of an organ is independent of the microvasculatures it may already have passed through.

1.5.2 Metastatic cascade Model derivation

The steps in the metastatic cascade are summarized in figure 1.1. A tumor grows locally (1). Cells disseminate from the primary tumor (2). The tumor cells that survive in the circulation (3) ultimately arrest in the microcirculation of an organ and may extravasate into the surrounding tissue (4). Extravasated cells can either; survive as a singular dormant cell (5A), form a micro-metastasis (5B), or grow into a macro-metastasis (5C).

1: Local growth: Functions described for tumor growth are exponential [51, 52, 53, 54, 55, 56, 20, 57], Gompertz [58, 20] or logistic function [20, 59, 60]. Gompertz and logistic functions have a slowing growth rate as the tumor reaches a maximum size N_{max} (N = number of tumor cells) at a certain time (t). N_{max} is typically chosen at 10^{12} cells / 1 kilogram. Based on a comparison of possible functions across a wide range of breast tumor sizes [20] we use the logistic equation:

$$\begin{aligned} N_{mass}(t) =& \frac{N_{max}}{[1 + (N_{max}^{1/4} - 1)e^{-ln2t/4DT}]^4} \\ \approx& \frac{N_{max}}{[1 + (N_{max}e^{-ln2t/DT})^{1/4}]^4} \end{aligned} \tag{1.6}$$

The time needed for a tumor to double in size, the doubling time (DT), changes as the tumor grows. In equation 1.6 DT at time t (DT_t) is related to DT at time 0 [60]:

$$DT_t = -\frac{4DT}{ln\,2} ln\left(\frac{\sqrt[4]{\frac{N_{max}}{2N_{mass}(t)} - 1}}{\sqrt[4]{\frac{N_{max}}{N_{mass}(t)} - 1}}\right) \tag{1.7}$$

In a model with growth slowing over time DT is typically determined for a tumor size of 12 mm (table 1.4, at this size DT is 23% longer compared to the DT at the start of growth, and at a size of 8 mm DT is 16% longer. We assume macro-metastases grow according to equation 1.6 and have the same doubling time as the primary. Changes in growth rate as a function of supply of nutrition, due to occurrence of growth enhancing mutations or due to chemo or hormonal therapy are not considered in any of the growth models.

2. Dissemination to circulation: The relationship between tumor diameter (D_{mass}) and the number of disseminated cells (N_{diss}) is assumed linear with coefficient C_{diss} and is derived from murine data comparing CTC counts to the diameter of the primary tumor [21, 22, 23, 24]. To derive the diameter of the lesion from the number of cells (N_{mass}), we assumed a spherical lesion. Once the primary tumor reaches a critical size (N_{crit}), it starts to disseminate cells into the bloodstream at a certain rate (R_{diss}) as described in equation 1.8:

$$R_{diss} = \begin{cases} C_{diss} \cdot D_{mass} & \text{if } N_{mass} > N_{crit} \\ 0 & \text{if } N_{mass} \leq N_{crit} \end{cases} \tag{1.8}$$

3. Survival in circulation: Disseminated cells (N_{diss}) will have a probability that they can survive in circulation ($P_{surv\ circ}$) a precondition to form distant metastasis. The number of surviving cells ($N_{surv\ circ}$) is defined as:

$$N_{surv\ circ} = R_{diss} \cdot P_{surv\ circ} \tag{1.9}$$

4. Extravasation: The ability to extravasate is also a condition for formation of a distant metastasis. The number of tumor cells that extravasate into the tissue ($N_{ex\ vas}$) can be defined as:

$$N_{ex\ vas} = N_{surv\ circ} \cdot P_{ex\ vas} \tag{1.10}$$

$P_{ex\ vas}$ in this equation is the probability that a tumor cell extravasates. The fate of a tumor cell once it has extravasated is death, dormancy, or growth into a micro- or macro-metastatic site depicted as step 5 in figure 1.1.

5A. Dormancy: An extravasated cell may survive in the new micro environment, but cease to grow; the number of dormant cells (N_{dorm}) is defined as:

$$N_{dorm} = N_{ex\ vas} \cdot P_{surv\ dorm} \tag{1.11}$$

$P_{surv\ dorm}$ in this equation is the probability that a tumor cell remains dormant.

5B. Micro-metastasis: An extravasated cell may replicate briefly or very slowly to form a micro-metastasis the number of tumor cells that form a micro-metastasis ($N_{micro\ met}$) are defined as:

$$N_{micro\ met} = N_{ex\ vas} \cdot P_{micro\ met} \tag{1.12}$$

$P_{micro\ met}$ in this equation is the probability that a tumor cell forms a micro-metastasis.

5C. Macro-metastasis: An extravasated cell may continue to replicate rapidly and form a macro-metastasis. The number of tumor cells that form a macro-metastasis ($N_{macro\ met}$) are defined as:

$$N_{macro\ met} = N_{ex\ vas} \cdot P_{macro\ met} \tag{1.13}$$

$P_{macro\ met}$ is the probability that a tumor cell forms a macro-metastasis. The macro-metastases are the most unfavorable outcome, posing the most immediate threat to survival of the patient. The total number of macro-metastases is found by integrating over time:

$$\begin{aligned} N_{total\ macro\ met} &= \int R_{diss} \cdot P_{surv\ circ} \cdot P_{ex\ vas} \cdot P_{macro\ met}\ dt \\ &= \gamma_{metastatic} \cdot C_{diss} \int D_{mass}\ dt \end{aligned} \tag{1.14}$$

With:

$$\gamma_{metastatic} = P_{surv\ circ} \cdot P_{ex\ vas} \cdot P_{macro\ met} \tag{1.15}$$

Equations 1.8–1.10, 1.13, and 1.14 provide a linear relationship between the number of cells injected into the circulation and the number of macro-metastases, as suggested in literature [25, 26, 27]. The number of metastases formed, equation 1.3/1.14, is equal to the total number of cells disseminated from the tumor, times the product of probabilities that this cell survives in the circulation, extravasates, progresses to a macro-metastasis. The metastatic efficiency of the tumor ($\gamma_{metastatic}$) is the probability that a cell that entered the circulation forms a distant metastasis. The number of disseminated cells (N_{diss}) is measurable by detecting the number of CTC, while the metastatic efficiency ($\gamma_{metastatic}$) may be measurable either by genotyping these CTC or the primary tissue.

1.5.3 CTC concentration and capture of CTC by the microvasculature

The concentration of CTC is determined by the dissemination rate and the number of passages through circulation that the typical CTC makes. Assum-

ing a fraction of CTC are lost in every passage through the microvasculature, the concentration of CTC is different in various places in the circulation, see figure 1.2. The CTC concentration in the cephalic vein resulting from a primary tumor in the breast is derived. First the concentration of CTC from the tumor efferent vein ($[CTC]_{efferent}$) is given, with the number of CTC disseminated (R_{diss}) independent of the local flow rate [61]:

$$[CTC]_{efferent} = \frac{R_{diss}}{Q_{total}} \tag{1.16}$$

The flow from the efferent vein ($Q_{efferent}$) is mixed with the whole blood volume in the vena cava and the concentration at the end of the vena cava is:

$$\begin{aligned}[CTC]_{cava} =& \frac{R_{diss}}{Q_{efferent}} \frac{Q_{efferent}}{Q_{total}} + [CTC]_{residual} \\ =& \frac{R_{diss}}{Q_{total}} + [CTC]_{residual}\end{aligned} \tag{1.17}$$

With $[CTC]_{residual}$ the concentration of CTC that have made at least one passage through the circulation. The concentration of CTC in the pulmonary vein is now derived assuming that the lungs capture a fraction of CTC ($0 \leq \eta_{lung} \leq 1$):

$$[CTC]_{pulmonary} = [CTC]_{cava}(1 - \eta_{lung}) \tag{1.18}$$

This immediately leads to the concentration of CTC that is detected in the cubital vein:

$$[CTC]_{cubital} = [CTC]_{cava}(1 - \eta_{lung})(1 - \eta_{arm}) \tag{1.19}$$

The contribution to $[CTC]_{residual}$ from CTC that have made k passages can be described as follows, with η_i the capture efficiency (ranging from 0 to 1) and Q_i the blood flow of all organs in the systemic circulation in equation 1.21:

$$\begin{aligned}[CTC]_{residual,k\ passages} =& \frac{R_{diss}}{Q_{total}}(1 - \eta_{lung})^k \left(\sum \frac{Q_i(1 - \eta_i)}{Q_{total}} \right)^k \\ =& \frac{R_{diss}}{Q_{total}}(1 - \eta_{lung})^k (1 - \eta_{systemic})^k\end{aligned} \tag{1.20}$$

$$1 - \eta_{systemic} = \sum \frac{Q_i(1 - \eta_i)}{Q_{total}} \tag{1.21}$$

This equation is a hybrid model attributing distribution of tumor cells to organs both to the blood supply to each organ [62] as well as organ specific

factors [63] as suggested elsewhere [7]. After summing over an infinite number of passages, equation 1.20 and 1.21 together lead to equation 1.22, which in turn leads to a more general form of the CTC concentration in cubital vein in equation eqs. (1.4) and (1.23), with $(1 - \eta_{circulation}) = (1 - \eta_{lung})(1 - \eta_{systemic})$:

$$\begin{aligned}[CTC]_{cava} =& \frac{R_{diss}}{Q_{total}} \left(1 + \sum_{k=1}^{\infty} (1 - \eta_{circulation})^k\right) \\ =& \frac{R_{diss}}{Q_{total}} \frac{1}{\eta_{circulation}} \end{aligned} \tag{1.22}$$

$$[CTC]_{cubital} = \frac{R_{diss}}{Q_{total} \cdot \eta_{circulation}} (1 - \eta_{lung})(1 - \eta_{arm}) \tag{1.23}$$

From this equation it is easily seen that the impact of low $\eta_{circulation}$ is to increase the CTC concentration and the impact of high η_{lung} is to reduce the number of CTC detected in the cubital vein. This equation can be derived analogously for all other carcinoma, yielding the same result, except for colorectal carcinoma (equation 1.24) and lung carcinoma (equation 1.25).

Colorectal carcinoma:

$$[CTC]_{cubital} = \frac{R_{diss}}{Q_{total} \cdot \eta_{circulation}} (1 - \eta_{liver})(1 - \eta_{lung})(1 - \eta_{arm}) \tag{1.24}$$

Lung carcinoma:

$$[CTC]_{cubital} = \frac{R_{diss}}{Q_{total} \cdot \eta_{circulation}} (1 - \eta_{arm}) \tag{1.25}$$

1.5.4 Individual probabilities in the metastatic cascade

The metastatic efficiency is defined as the product of the probability of survival in circulation, the probability of extravasation, and the probability of growth into a macro-metastasis. Human studies for probabilities in the metastatic cascade are quite limited; we only found values for survival in circulation from studies that determined that 23–80% of CTC had caspase cleaved cytokeratin (M30-positive) and were thus undergoing apoptosis [64, 65], therefore survival in circulation was less than 80%. Considering that cytokeratin cleavage occurs late in apoptosis and the % necrotic cells was not determined, true survival in circulation is most likely lower. To dissect the individual probabilities in the metastatic efficiency, intra-vital video microscopy (IVM) [33, 66] has been used extensively. Using IVM, The median estimate for probability of extravasation is 65%, table 1.11. Due to limitations in the time that a single animal can be observed, most studies monitored a time window of 24 hours. A single study [67] monitored the

process up to 72 hours, which found that while 55% of cells arrested in the microvasculature had extravasated by 24 hours, 96% had extravasated by 72 hours. It is therefore likely that the estimate of 65% is too low because the process takes longer than the typical observation window of up to 24 hours. Probability of extravasation was determined in organs with high incidence of metastases for all studies and may be lower in other organs. The probability of surviving in the circulation was derived together with the probability of extravasation, table 1.11, precluding direct determination of the probability of survival. The product of probabilities found ranges from 43% to 89% with a median at 80%. Using the estimate of 65% for extravasation, the probability of surviving in circulation is at least 70%. An extravasated cell can die, become dormant, form a micro-metastasis or continue to grow into a macro-metastasis. IVM studies that compared tumor cell distribution in an organ after injection and 2–3 weeks later found that the probability of surviving as a single cell (dormant) was 36% (range 4–50%, table 1.10. If we assume that 36% of extravasated cells continue to survive over the years, $3 \cdot 10^6$–$1 \cdot 10^9$ dormant malignant cells have scattered throughout the body by the time of surgery. The probability of forming micro-metastases is estimated at 6% (range 1–80%), table 1.10. The probability that an extravasated cell forms a macro-metastasis was estimated by IVM at 0.025% (range 0.001–6%), table 1.10.
The metastatic efficiency is the probability that a disseminated cell grows in a new site. The product of the probability of survival in circulation, extravasation and growth to a macro-metastasis is the metastatic efficiency. When we combine the IVM estimates for each probability together in equation 1.15, we find $\gamma_{metastatic}$ of 0.011%. Other methods which determined the metastatic efficiency from injection of a known number of cells estimated $\gamma_{metastatic}$ at a comparable value of 0.005% (range 0.0001–6%) [25, 26, 27, 68, 69, 70, 71].

This metastatic efficiency is limited primarily by the ability of a disseminated cell to grow in a new site. The reasons for the limited ability to grow in a new organ is still under investigation, potential causes include genetic predisposition of the disseminated cell, proximity to other tumor cells, and local microenvironment (growth factors, nutrients, space). Proximity of other cells is suggested from two experiments; (1) when clumps of 4–7 cells are injected versus the same total number of individual cells from the same population, the probability of forming a macro-metastasis is increased 3–10 fold [25, 72] and (2) migration to preferred sites of growth is observed after extravasation [67, 33], bringing tumor cells closer together. Genetic predisposition is suggested by a relatively high metastatic efficiency of tumor cells harvested from metastases of other tumors [27, 71]. In one study, the metastases from MDA-435 cells were collected and seeded to new animals. These cells were more likely to metastasize to the same organ again, indicating that de genetic makeup of a cell is important in determining where metastases form [70].

1.5.5 Supplemental figures and tables

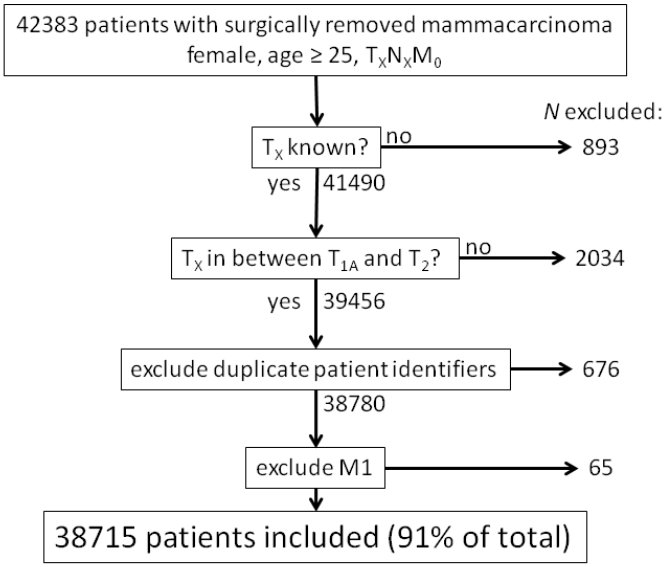

N by T_X: 1447 (4%) T_{1A}, 5959 (15%) T_{1B}, 17151 (44%) T_{1C}, 14158 (37%) T_2
N by N_X: 23979 (62%) N_0, 10320 (27%) N_1, 2552 (7%) N_2, 1157 (3%) N_3, 707 (2%) N_X
Therapy after surgery: 15943 (41%) hormone-, and/or 1149 (3%) immuno-,
and/or 13354 (35%) chemo-therapy, 17709 (46%) no therapy

Figure 1.5: Exclusion diagram. *Of 42383 patients included by the initial search criteria, 3668 (9%) were excluded for the reasons detailed in the diagram. The distribution of patients by T-stage, node (N) status and therapy after surgery are shown for the 38715 included patients.*

Table 1.4: Human breast cancer values for doubling time

publication	N	tumor [a] size (mm)	doubling time (months) median	range	
Lundgren 1977 [51]	13	N/A	6.9	1.4-13.0	[b]
Heuser 1979 [52]	32	14	10.6 [c]	3.6-31.0	[b]
Von Fournier 1980 [58]	100	17	6.6 [c]	2.1-20.6	[d]
Galante 1981 [53]	196	N/A	2.0	N/A	
Tabbane 1989 [54]	75	N/A	3.8	0.5-25.3	[b]
Kuroishi 1990 [55]	142	N/A	5.7 [c]	0.4-42.4	[b]
Spratt 1993 [20]	448	9	8.5	5.0-15.7	[c]
Peer 1993 [56]	236	>10	5.0	1.5-17.1	[e]
Tilanus-Linthorst 2005 [57]	47	12	2.0 [c]	0.4-18.6	[b]
Weedon-Felkjaer 2008 [59]	969	15	3.1	1.0-9.6	[f]
Millet 2011 [60]	37	9	11.2 [c]	-222.9-146.6	[b]

[a] N/A = not available, [b] minimum-maximum, [c] mean, [d] 2.5-97.5 percentile, [e] 68% confidence interval, [f] 25-75 percentile.

Table 1.5: Capture efficiency in human studies. *Determined from difference between CTC in efferent and cubital vein*

publication	cancer	N	efferent vein	CTC efferent	CTC cubital	fold red. [a]	dilution factor [b]	$\eta(\%)$ [c]
Planz 1997 [73]	prost [d]	15	vesical plexus	19	1.5	12.6	>20	31
Wind 2009 [74] [e]	colo [f]	13	portal	0.05–0.08	0.01–0.03	2–6	4.8	24–32
Wind 2009 [74] [g]	colo [f]	18	portal	0.50	0.04	13	4.8	44

[a] reduction, [b] determined from distribution of cardiac output at rest, [c] estimated according to equation 1.23, with $(1-\eta)^2 = (1-\eta_{lung})(1-\eta_{arm})$ for prostate and $(1-\eta)^3 = (1-\eta_{liver})(1-\eta_{lung})(1-\eta_{arm})$ for colorectal, [d] prostate, [e] laparoscopic surgery, [f] colorectal, [g] open surgery.

Table 1.6: Capture efficiency in murine studies

publication	method [a]	detection organ	cell line	injection site	capture efficiency (%) [b]
Mizuno 1998 [75]	radio-label	liver, lung, kidney, spleen small intestine large intestine	KM12-HX (colon)	portal, left heart, femoral	$\eta_{liver} = 99$ $\eta_{lung} = 92$ $\eta_{smintest} = 52$ [c] $\eta_{lgintest} = 27$ [c] $\eta_{kidney} = 28$ $\eta_{spleen} = 25$ $\eta_{other} = 18$ $\eta_{circulation} = 95$
Steinbauer 2003 [76]	IVM	liver	CT-26 (colon)	mesentery	$\eta_{liver} = 97$
Mook 2003 [77]	IVM	liver	CC531s (murine colon)	portal	$\eta_{liver} = 100$
Schlutter 2006 [78]	IVM	liver, lung, skin, kidney, muscle, mesenteric	HT-29LMM (colon)	left heart	$\eta_{lung} = 0.29 \cdot \eta_{liver}$ $\eta_{other} < 0.13 \cdot \eta_{liver}$ $\eta_{circulation} < 47$ [d]
Kimura 2010 [79]	IVM	lung	HT1080 / MMT (murine breast)	tail	$\eta_{lungHT1080} = 0.75 \cdot \eta_{lungMMT}$
Rhim 2012 [80]	FCS	left and right heart	spontaneous panctreatic carcinoma	N/A	$\eta_{lung} = 69$

[a] *IVM: Intra vital microscopy, FCS: flow cytometry,* [b] *estimated from data in paper using equation 1.23,*
[c] *large/small intestine,* [d] *because* $\eta_{liver} \leq 100\%$.

Table 1.7: Decay time as observed with in vivo flow cytometry. *Cells were injected in tail vein, detected in the mouse ear over periods of 1.5–50 hours. Decay time determined assuming exponential decay.*

publication	cell line	decay time (h)
Georgakoudi 2004 [81]	LNCaP (prostate)	1.4
	MLL (murine prostate)	0.6
Galanzha 2009 [82]	MDA-MB-231 (breast)	0.8
Galanzha 2009 [24]	B16-F10 (melanoma)	0.2

Table 1.8: Human values for dissemination rate.

publication	cancer	N	diameter (mm)	disseminated cells [a]	C_{diss} (CTC/h·g) [b]
Glaves 1988 [83]	Renal	15	5 –10	890	$78 \cdot 10^3$
Wind 2009 [74] [c]	Colon	13	4.1 ±1.4	0.05	90
Wind 2009 [74] [d]	Colon	18	5.0 ±2.3	3.2	$3.1 \cdot 10^3$

[a] mean CTC/ mL tumor efferent blood, [b] for spherical tumor, [c] laparoscopic surgery, [d] open surgery.

Table 1.9: Murine tumor size and CTC dissemination rate.

publication	method [a]	cell line	tumor size (g)	CTC/ mL blood	CTC/h·g tumor	N_{crit}(g)
Liotta 1974 [21]	M/Eff	T241 (fibrosarcoma)	0.5–3.6	2-21	$0.1 \cdot 10^3$–$1.7 \cdot 10^3$	0.4
Butler 1975 [84]	FM/Eff	MTW9 (murine breast)	2.6–3.7	$17 \cdot 10^3$–$20 \cdot 10^3$	$1.3 \cdot 10^5$–$1.7 \cdot 10^5$	-
Swartz 1999 [61]	FCM/Eff	LS174T (colon)	0.5		$2.6 \cdot 10^5$	-
		LS LiM 6 (colon)	0.5		$1.0 \cdot 10^5$	-
Schmidt 1999 [23]	FCM/Tot	MDA-435-HAL-GFP (breast)	0.4–3.1	3250–7000	$1.5 \cdot 10^6$–$15.8 \cdot 10^6$	0.4
Wyckoff 2000 [85]	Cul/Tot	MTLn3-GFP	31.0	5.7	$1.2 \cdot 10^3$	-
		MTC-GFP (murine breast)	44.5	0.06	0.15	-
Eliane 2008 [86]	FM/Tot	MDA-231	0.2–4.4	106–975	4.810^4–$1.7 \cdot 10^6$	0.2
		SUM-159	0.7–6.1	0–335	0–$7.2 \cdot 10^4$	0.8
		SKBR-3 (all breast)	0.1–3.3	0–121	0–$1.5 \cdot 10^5$	0.3
Goodale 2009 [87]	FCM/Tot	MDA-435-HAL	1.73	7790	$4.3 \cdot 10^6$	-

[a] *FCM: flow cytometry, FM: fluorescence microscopy, M: microscopy, Cul: culture of blood cells, Eff: measurement performed by directly perfusing the tumor bearing organ and collecting venous output, Tot: measurement performed by detecting CTC concentration in right heart, converted to shed rate by multiplying with cardiac output of animal (mouse 16 mL/min [88], rat 110 mL/min [89]). Assumes negligible number of cells make second pass through circulation.*

Table 1.10: Cell fate after extravasation. *All probabilities in %*

publication	method [a]	cell line	P_{dorm} [b]	$P_{micro\ met}$	$P_{macro\ met}$
Schaeffer 1973 [26]	histology	C3HBA (murine breast)			0.005 [c]
Fidler 1973 [25]	histology	B16 (melanoma)			0.6 [c]
Milas 1974 [27]	autopsy	mammary carcinoma [d]			0.03 [c]
Mayhew 1984 [68]	histology	B16F10 (melanoma)			0.6
		Lewis (lung)			0.002 [c]
Price 1989 [69]	histology	HT-29 (colon)			>0.0001 [c]
Price 1990 [70]	autopsy	MDA-MB-435			0.007 [c]
Morris 1994 [67]	IVM	D2A1		< 1	
		D2.OR (murine breast)		< 1	
Chambers 1995 [33]	IVM	various	50		
Luzzi 1998 [90]	IVM	B16F1 (melanoma)	36	2	0.025
Naumov 1999 [91]	IVM	CHO-K1-GFP (hamster ovary)		80	
Cameron 2000 [92]	IVM	B16F10	3.5		6
Steinbauer 2003 [76]	IVM	CT-26 (colon)		6	
Mook 2003 [77]	IVM	CC531s (murine colon)			0.001
Podsypanina 2008 [71]	BL	spontaneous carcinoma [d]			0.014 [c]

[a] *IVM: intra vital fluorescence microscopy, BL: Bioluminescence,* [b] *survival as single cell > 2 weeks,* [c] *probability to form macro-metastasis from number of injected cells,* [d] *induced in one animal by feeding of a carcinogen, and then minced to inoculate another animal.*

Table 1.11: Survival in circulation and extravasation probability as observed with intra-vital video microscopy *All probabilities in %*

publication	cell line	injection site	observation organ	time (h)[a]	$P_{ex\ vas}$	$P_{surv} \cdot P_{ex\ vas}$
Morris 1994 [67]	D2A1/D2.OR	mesentery	liver	24	55	
	(murine breast)			72	96	
Koop 1995 [93]	B16F10 (melanoma)	chick embryo		24		> 80
Chambers 1995 [33]	various [b]	various	various			89
Steinbauer 2003 [76]	CT-26 (colon)	mesentery	liver	48		43
Schlutter 2006 [78]	HT-29LMM (colon)	left heart	liver	0.5	29	
Martin 2010 [94]	R221A-GFP (breast)	spleen	liver	24	50	
		tail	lung	24	20	

[a] *observation time,* [b] *review of other publications.*

1.6 References

[1] A. Minn and J. Massague, *Devita, Hellman & RosenbergŠs Cancer: principles & practice of oncology*, ch. Invasion and metastasis, pp. 118–133. Lippincott-Raven, Philadelphia, PA, 8th ed. ed., 2008.

[2] E. Woodhouse, R. Chuaqui, and L. Liotta, "General mechanisms of metastasis," *Cancer*, vol. 80, no. S8, pp. 1529–1537, 1997.

[3] I. Fidler, "Critical determinants of cancer metastasis: rationale for therapy," *Cancer chemotherapy and pharmacology*, vol. 43, no. 7, pp. 3–10, 1999.

[4] K. Pantel and R. Brakenhoff, "Dissecting the metastatic cascade," *Nature Reviews Cancer*, vol. 4, no. 6, pp. 448–456, 2004.

[5] C. Klein, "The metastasis cascade," *Science*, vol. 321, no. 5897, pp. 1785–1787, 2008.

[6] L. Weiss *et al.*, "Random and nonrandom processes in metastasis, and metastatic inefficiency.," *Invasion & metastasis*, vol. 3, no. 4, p. 193, 1983.

[7] A. Chambers, A. Groom, I. MacDonald, *et al.*, "Dissemination and growth of cancer cells in metastatic sites," *Nature Reviews Cancer*, vol. 2, pp. 563–572, 2002.

[8] K. Pantel and C. Alix-Panabières, "Circulating tumour cells in cancer patients: challenges and perspectives," *Trends in molecular medicine*, vol. 16, no. 9, pp. 398–406, 2010.

[9] M. Cristofanilli, G. T. Budd, M. J. Ellis, A. Stopeck, J. Matera, M. C. Miller, J. M. Reuben, G. V. Doyle, W. J. Allard, L. W. Terstappen, and D. F. Hayes, "Circulating tumor cells, disease progression, and survival in metastatic breast cancer," *N. Engl. J. Med.*, vol. 351, pp. 781–791, Aug 2004.

[10] S. J. Cohen, C. J. Punt, N. Iannotti, B. H. Saidman, K. D. Sabbath, N. Y. Gabrail, J. Picus, M. Morse, E. Mitchell, M. C. Miller, G. V. Doyle, H. Tissing, L. W. Terstappen, and N. J. Meropol, "Relationship of circulating tumor cells to tumor response, progression-free survival, and overall survival in patients with metastatic colorectal cancer," *J. Clin. Oncol.*, vol. 26, pp. 3213–3221, Jul 2008.

[11] J. S. de Bono, H. I. Scher, R. B. Montgomery, C. Parker, M. C. Miller, H. Tissing, G. V. Doyle, L. W. Terstappen, K. J. Pienta, and D. Raghavan, "Circulating tumor cells predict survival benefit from treatment in metastatic castration-resistant prostate cancer," *Clin. Cancer Res.*, vol. 14, pp. 6302–6309, Oct 2008.

[12] F. Coumans, S. T. Ligthart, and L. W. M. Terstappen, "Challenges in the enumeration and phenotyping of CTC," *Clinical Cancer Research*, 2012.

[13] B. Rack, C. Schindlbeck, U. Andergassen, R. Lorenz, T. Zwingers, A. Schneeweiss, W. Lichtenegger, M. Beckmann, H. Sommer, K. Pantel, *et al.*, "Prognostic relevance of circulating tumor cells in the peripheral blood of primary breast cancer patients," *Cancer Res*, vol. 70, no. 24 Suppl, p. 93s, 2010.

[14] B. Franken, M. De Groot, L. Terstappen, W. Mastboom, J. Van der Palen, and A. Tibbe, "Circulating tumor cells, disease recurrence and survival in newly diagnosed breast cancer," in *Proceedings of San Antonio Breast Cancer conference*, 2011.

[15] J. Pierga, D. Hajage, T. Bachelot, S. Delaloge, E. Brain, M. Campone, V. Diéras, E. Rolland, L. Mignot, C. Mathiot, *et al.*, "High independent prognostic and predictive value of circulating tumor cells compared with serum tumor markers in a large prospective trial in first-line chemotherapy for metastatic breast cancer patients," *Annals of Oncology*, vol. 23, no. 3, pp. 618–624, 2011.

[16] A. Lucci, C. Hall, A. Lodhi, A. Bhattacharyya, A. Anderson, L. Xiao, I. Bedrosian, H. Kuerer, and S. Krishnamurthy, "Circulating tumour cells in non-metastatic breast cancer: a prospective study," *The Lancet Oncology*, 2012.

[17] J. Gray, "Evidence emerges for early metastasis and parallel evolution of primary and metastatic tumors," *Cancer Cell*, vol. 4, no. 1, pp. 4–6, 2003.

[18] C. Klein, "The systemic progression of human cancer: a focus on the individual disseminated cancer cell-the unit of selection," *Advances in cancer research*, vol. 89, pp. 35–67, 2003.

[19] O. Schmidt-Kittler, T. Ragg, A. Daskalakis, M. Granzow, A. Ahr, T. Blankenstein, M. Kaufmann, J. Diebold, H. Arnholdt, P. Müller, *et al.*, "From latent disseminated cells to overt metastasis: genetic analysis of systemic breast cancer progression," *Proceedings of the National Academy of Sciences*, vol. 100, no. 13, p. 7737, 2003.

[20] J. Spratt, D. Von Fournier, J. Spratt, and E. Weber, "Decelerating growth and human breast cancer," *Cancer*, vol. 71, no. 6, pp. 2013–2019, 1993.

[21] L. Liotta, J. Kleinerman, and G. Saidel, "Quantitative relationships of intravascular tumor cells, tumor vessels, and pulmonary metastases following tumor implantation," *Cancer research*, vol. 34, no. 5, p. 997, 1974.

[22] D. Glaves, "Correlation between circulating cancer cells and incidence of metastases.," *British journal of cancer*, vol. 48, no. 5, p. 665, 1983.

[23] C. Schmidt, S. Settle, J. Keene, W. Westlin, G. Nickols, and D. Griggs, "Characterization of spontaneous metastasis in an aggressive breast carcinoma model using flow cytometry," *Clinical and Experimental Metastasis*, vol. 17, no. 6, pp. 537–544, 1999.

[24] E. Galanzha, E. Shashkov, P. Spring, J. Suen, and V. Zharov, "In vivo, noninvasive, label-free detection and eradication of circulating metastatic melanoma cells using two-color photoacoustic flow cytometry with a diode laser," *Cancer research*, vol. 69, no. 20, p. 7926, 2009.

[25] I. Fidler, "The relationship of embolic homogeneity, number, size and viability to the incidence of experimental metastasis," *European Journal of Cancer (1965)*, vol. 9, no. 3, pp. 223–227, 1973.

[26] J. Shaeffer, A. El-Mahdi, and W. Constable, "Radiation control of microscopic pulmonary metastases in C3H mice," *Cancer*, vol. 32, no. 2, pp. 346–351, 1973.

[27] L. Milas, N. Hunter, and H. Withers, "Corynebacterium granulosum-induced protection against artificial pulmonary metastases of a syngeneic fibrosarcoma in mice," *Cancer research*, vol. 34, no. 3, pp. 613–620, 1974.

[28] S. Meng, D. Tripathy, E. Frenkel, S. Shete, E. Naftalis, J. Huth, P. Beitsch, M. Leitch, S. Hoover, D. Euhus, *et al.*, "Circulating tumor cells in patients with breast cancer dormancy," *Clinical cancer research*, vol. 10, no. 24, pp. 8152–8162, 2004.

[29] V. Morris, I. MacDonald, S. Koop, E. Schmidt, A. Chambers, and A. Groom, "Early interactions of cancer cells with the microvasculature in mouse liver and muscle during hematogenous metastasis: videomicroscopic analysis," *Clinical and Experimental Metastasis*, vol. 11, no. 5, pp. 377–390, 1993.

[30] K. Yamauchi, M. Yang, P. Jiang, N. Yamamoto, M. Xu, Y. Amoh, K. Tsuji, M. Bouvet, H. Tsuchiya, K. Tomita, *et al.*, "Real-time in vivo dual-color imaging of intracapillary cancer cell and nucleus deformation and migration," *Cancer research*, vol. 65, no. 10, p. 4246, 2005.

[31] L. Sherwood, *Human physiology: from cells to systems*. Wadsworth, Belmont, CA, 1997.

[32] G. Disibio and S. W. French, "Metastatic patterns of cancers - results from a large autopsy study," *Archives of Pathology & Laboratory Medicine*, vol. 132, pp. 931–939, 2008.

[33] A. Chambers, I. MacDonald, E. Schmidt, S. Koop, V. Morris, R. Khokha, and A. Groom, "Steps in tumor metastasis: new concepts from intravital videomicroscopy," *Cancer and Metastasis Reviews*, vol. 14, no. 4, pp. 279–301, 1995.

[34] F. Coumans, G. van Dalum, M. Beck, and L. Terstappen, "Filter requirements for circulating tumor cell enrichment and detection," *submitted*, 2012.

[35] L. Ding, M. Sunamura, T. Kodama, J. Yamauchi, D. Duda, H. Shimamura, K. Shibuya, K. Takeda, and S. Matsuno, "In vivo evaluation of the early events associated with liver metastasis of circulating cancer cells," *British journal of cancer*, vol. 85, no. 3, p. 431, 2001.

[36] P. Gassmann, A. Hemping-Bovenkerk, S. Mees, and J. Haier, "Metastatic tumor cell arrest in the liver–lumen occlusion and specific adhesion are not exclusive," *International journal of colorectal disease*, vol. 24, no. 7, pp. 851–858, 2009.

[37] P. Gassmann, M. Kang, S. Mees, and J. Haier, "In vivo tumor cell adhesion in the pulmonary microvasculature is exclusively mediated by tumor cell-endothelial cell interaction," *BMC cancer*, vol. 10, no. 1, p. 177, 2010.

[38] J. Uhr and K. Pantel, "Controversies in clinical cancer dormancy," *Proceedings of the National Academy of Sciences*, vol. 108, no. 30, p. 12396, 2011.

[39] F. Al-Mulla, W. Keith, I. Pickford, J. Going, and G. Birnie, "Comparative genomic hybridization analysis of primary colorectal carcinomas and their synchronous metastases," *Genes, Chromosomes and Cancer*, vol. 24, no. 4, pp. 306–314, 1999.

[40] S. Ramaswamy, K. Ross, E. Lander, and T. Golub, "A molecular signature of metastasis in primary solid tumors," *Nature genetics*, vol. 33, no. 1, pp. 49–54, 2002.

[41] T. Molloy, A. Bosma, L. Baumbusch, M. Synnestvedt, E. Borgen, H. Russnes, E. Schlichting, L. Van't Veer, B. Naume, *et al.*, "The prognostic significance of tumor cell detection in the peripheral blood versus the bone marrow in 733 early-stage breast cancer patients," *Breast Cancer Res*, vol. 13, p. R61, 2011.

[42] E. Saloustros, M. Perraki, S. Apostolaki, G. Kallergi, A. Xyrafas, K. Kalbakis, S. Agelaki, A. Kalykaki, V. Georgoulias, D. Mavroudis, *et al.*, "Cytokeratin-19 mrna-positive circulating tumor cells during follow-up of patients with operable breast cancer: prognostic relevance for late relapse," *Breast Cancer Research*, vol. 13, no. 3, p. R60, 2011.

[43] K. Kelly, J. Dean, W. Comulada, and S. Lee, "Breast cancer detection using automated whole breast ultrasound and mammography in radiographically dense breasts," *European radiology*, vol. 20, no. 3, pp. 734–742, 2010.

[44] T. Sørlie, R. Tibshirani, J. Parker, T. Hastie, J. Marron, A. Nobel, S. Deng, H. Johnsen, R. Pesich, S. Geisler, *et al.*, "Repeated observation of breast tumor subtypes in independent gene expression data sets," *Proceedings of the National Academy of Sciences*, vol. 100, no. 14, p. 8418, 2003.

[45] Y. Wang, J. Klijn, Y. Zhang, A. Sieuwerts, M. Look, F. Yang, D. Talantov, M. Timmermans, M. Meijer-van Gelder, J. Yu, *et al.*, "Gene-expression profiles to predict distant metastasis of lymph-node-negative primary breast cancer," *The Lancet*, vol. 365, no. 9460, pp. 671–679, 2005.

[46] L. Van't Veer and R. Bernards, "Enabling personalized cancer medicine through analysis of gene-expression patterns," *Nature*, vol. 452, no. 7187, pp. 564–570, 2008.

[47] C. Curtis, S. Shah, S. Chin, G. Turashvili, O. Rueda, M. Dunning, D. Speed, A. Lynch, S. Samarajiwa, Y. Yuan, *et al.*, "The genomic and transcriptomic architecture of 2,000 breast tumours reveals novel subgroups," *Nature*, vol. 486, no. 7403, pp. 346–352, 2012.

[48] F. Coumans and L. W. M. Terstappen, "Filtration of circulating tumor cells from large sample volumes," *submitted*, 2012.

[49] C. Klein, S. Seidl, K. Petat-Dutter, S. Offner, J. Geigl, O. Schmidt-Kittler, N. Wendler, B. Passlick, R. Huber, G. Schlimok, *et al.*, "Combined transcriptome and genome analysis of single micrometastatic cells," *Nature biotechnology*, vol. 20, no. 4, pp. 387–392, 2002.

[50] N. Stoecklein, S. Hosch, M. Bezler, F. Stern, C. Hartmann, C. Vay, A. Siegmund, P. Scheunemann, P. Schurr, W. Knoefel, *et al.*, "Direct genetic analysis of single disseminated cancer cells for prediction of outcome and therapy selection in esophageal cancer," *Cancer Cell*, vol. 13, no. 5, pp. 441–453, 2008.

[51] B. Lundgren, "Observations on growth rate of breast carcinomas and its possible implications for lead time," *Cancer*, vol. 40, no. 4, pp. 1722–1725, 1977.

[52] L. Heuser, J. Spratt, and H. Polk Jr, "Growth rates of primary breast cancers," *Cancer*, vol. 43, no. 5, pp. 1888–1894, 1979.

[53] E. Galante, A. Guzzon, G. Gallus, M. Mauri, A. Bono, A. De Carli, M. Merson, and S. Di Pietro, "Prognostic significance of the growth rate of breast cancer: preliminary evaluation on the follow-up of 196 breast cancers.," *Tumori*, vol. 67, no. 4, p. 333, 1981.

[54] F. Tabbane, J. Bahi, K. Rahal, A. May, M. Riahi, M. Cammoun, M. Hechiche, M. Jaziri, and N. Mourali, "Inflammatory symptoms in breast cancer. correlations with growth rate, clinicopathologic variables, and evolution," *Cancer*, vol. 64, no. 10, pp. 2081–2089, 1989.

[55] T. Kuroishi, S. Tominaga, T. Morimoto, H. Tashiro, S. Itoh, H. Watanabe, M. Fukuda, J. Ota, T. Horino, T. Ishida, *et al.*, "Tumor growth rate and prognosis of breast cancer mainly detected by mass screening," *Cancer Science*, vol. 81, no. 5, pp. 454–462, 1990.

[56] P. Peer, J. Van Dijck, A. Verbeek, J. Hendriks, and R. Holland, "Age-dependent growth rate of primary breast cancer," *Cancer*, vol. 71, no. 11, pp. 3547–3551, 1993.

[57] M. Tilanus-Linthorst, M. Kriege, C. Boetes, W. Hop, I. Obdeijn, J. Oosterwijk, H. Peterse, H. Zonderland, S. Meijer, A. Eggermont, *et al.*, "Hereditary breast cancer growth rates and its impact on screening policy," *European Journal of Cancer*, vol. 41, no. 11, pp. 1610–1617, 2005.

[58] D. Fournier, E. Weber, W. Hoeffken, M. Bauer, F. Kubli, and V. Barth, "Growth rate of 147 mammary carcinomas," *Cancer*, vol. 45, no. 8, pp. 2198–2207, 1980.

[59] H. Weedon-Fekjær, B. Lindqvist, L. Vatten, O. Aalen, S. Tretli, *et al.*, "Breast cancer tumor growth estimated through mammography screening data," *Breast Cancer Res*, vol. 10, no. 3, p. R41, 2008.

[60] I. Millet, E. Bouic-Pages, D. Hoa, D. Azria, and P. Taourel, "Growth of breast cancer recurrences assessed by consecutive MRI," *BMC cancer*, vol. 11, no. 1, p. 155, 2011.

[61] M. Swartz, C. Kristensen, R. Melder, S. Roberge, E. Calautti, D. Fukumura, and R. Jain, "Cells shed from tumours show reduced clonogenicity, resistance to apoptosis, and in vivo tumorigenicity," *British journal of cancer*, vol. 81, no. 5, p. 756, 1999.

[62] J. Ewing, "Neoplastic diseases. a treatise on tumors," *The American Journal of the Medical Sciences*, vol. 176, no. 2, p. 278, 1928.

[63] S. Paget, "The distribution of secondary growths in cancer of the breast. 1889.," *Cancer metastasis reviews*, vol. 8, no. 2, p. 98, 1889.

[64] J. F. Swennenhuis, A. G. Tibbe, R. Levink, R. C. Sipkema, and L. W. Terstappen, "Characterization of circulating tumor cells by fluorescence in situ hybridization," *Cytometry A*, vol. 75, pp. 520–527, Jun 2009.

[65] E. Rossi, U. Basso, R. Celadin, F. Zilio, S. Pucciarelli, M. Aieta, C. Barile, T. Sava, G. Bonciarelli, S. Tumolo, *et al.*, "M30 neoepitope expression in epithelial cancer: quantification of apoptosis in circulating tumor cells by cellsearch analysis," *Clinical Cancer Research*, vol. 16, no. 21, pp. 5233–5243, 2010.

[66] E. Beerling, L. Ritsma, N. Vrisekoop, P. Derksen, and J. van Rheenen, "Intravital microscopy: new insights into metastasis of tumors," *Journal of Cell Science*, vol. 124, no. 3, pp. 299–310, 2011.

[67] V. Morris, S. Koop, I. MacDonald, E. Schmidt, M. Grattan, D. Percy, A. Chambers, and A. Groom, "Mammary carcinoma cell lines of high and low metastatic potential differ not in extravasation but in subsequent migration and growth," *Clinical and Experimental Metastasis*, vol. 12, no. 6, pp. 357–367, 1994.

[68] E. Mayhew and D. Glaves, "Quantitation of tumorigenic disseminating and arrested cancer cells.," *British journal of cancer*, vol. 50, no. 2, p. 159, 1984.

[69] J. Price, L. Daniels, D. Campbell, and R. Giavazzi, "Organ distribution of experimental metastases of a human colorectal carcinoma injected in nude mice," *Clinical and Experimental Metastasis*, vol. 7, no. 1, pp. 55–68, 1989.

[70] J. Price, A. Polyzos, R. Dan Zhang, and L. Daniels, "Tumorigenicity and metastasis of human breast carcinoma cell lines in nude mice," *Cancer research*, vol. 50, no. 3, p. 717, 1990.

[71] K. Podsypanina, Y. Du, M. Jechlinger, L. Beverly, D. Hambardzumyan, and H. Varmus, "Seeding and propagation of untransformed mouse mammary cells in the lung," *Science's STKE*, vol. 321, no. 5897, p. 1841, 2008.

[72] L. Liotta, J. Kleinerman, and G. Saldel, "The significance of hematogenous tumor cell clumps in the metastatic process," *Cancer research*, vol. 36, no. 3, pp. 889–894, 1976.

[73] B. Planz, P. Szyska, M. Valdor, W. Boeckmann, L. Füzesi, and G. Jakse, "Detection of circulating prostatic cells during radical prostatectomy," *Urological research*, vol. 25, no. 6, pp. 385–389, 1997.

[74] J. Wind, J. Tuynman, A. Tibbe, J. Swennenhuis, D. Richel, M. van Berge Henegouwen, and W. Bemelman, "Circulating tumour cells during laparoscopic and open surgery for primary colonic cancer in portal and peripheral blood," *European Journal of Surgical Oncology (EJSO)*, vol. 35, no. 9, pp. 942–950, 2009.

[75] N. Mizuno, Y. Kato, K. Shirota, Y. Izumi, T. Irimura, H. Harashima, H. Kiwada, N. Motoji, A. Shigematsu, and Y. Sugiyama, "Mechanism of initial distribution of blood-borne colon carcinoma cells in the liver," *Journal of hepatology*, vol. 28, no. 5, pp. 878–885, 1998.

[76] M. Steinbauer, M. Guba, G. Cernaianu, G. Köhl, M. Cetto, L. Kunz-Schughart, E. Geissler, W. Falk, and K. Jauch, "Gfp-transfected tumor cells are useful in examining early metastasis in vivo, but immune reaction precludes long-term tumor development studies in immunocompetent mice," *Clinical and Experimental Metastasis*, vol. 20, no. 2, pp. 135–141, 2003.

[77] O. Mook, J. Van Marle, H. Vreeling-Sindelárová, R. Jonges, W. Frederiks, and C. Van Noorden, "Visualization of early events in tumor formation of egfp-transfected rat colon cancer cells in liver," *Hepatology*, vol. 38, no. 2, pp. 295–304, 2003.

[78] K. Schlüter, P. Gassmann, A. Enns, T. Korb, A. Hemping-Bovenkerk, J. Hölzen, and J. Haier, "Organ-specific metastatic tumor cell adhesion and extravasation of colon carcinoma cells with different metastatic potential," *The American journal of pathology*, vol. 169, no. 3, pp. 1064–1073, 2006.

[79] H. Kimura, K. Hayashi, K. Yamauchi, N. Yamamoto, H. Tsuchiya, K. Tomita, H. Kishimoto, M. Bouvet, and R. Hoffman, "Real-time imaging of single cancer-cell dynamics of lung metastasis," *Journal of cellular biochemistry*, vol. 109, no. 1, pp. 58–64, 2010.

[80] A. Rhim, E. Mirek, N. Aiello, A. Maitra, J. Bailey, F. McAllister, M. Reichert, G. Beatty, A. Rustgi, R. Vonderheide, *et al.*, "Emt and dissemination precede pancreatic tumor formation," *Cell*, vol. 148, no. 1, pp. 349–361, 2012.

[81] I. Georgakoudi, N. Solban, J. Novak, W. Rice, X. Wei, T. Hasan, and C. Lin, "In vivo flow cytometry: a new method for enumerating circulating cancer cells.," *Cancer research*, vol. 64, no. 15, p. 5044, 2004.

[82] E. I. Galanzha, E. V. Shashkov, T. Kelly, J. W. Kim, L. L. Yang, and V. P. Zharov, "In vivo magnetic enrichment and multiplex photoacoustic detection of circulating tumour cells," *Nature Nanotechnology*, vol. 4, pp. 855–860, 2009.

[83] D. Glaves, R. Huben, and L. Weiss, "Haematogenous dissemination of cells from human renal adenocarcinomas.," *British journal of cancer*, vol. 57, no. 1, p. 32, 1988.

[84] T. Butler and P. Gullino, "Quantitation of cell shedding into efferent blood of mammary adenocarcinoma," *Cancer Research*, vol. 35, no. 3, p. 512, 1975.

[85] J. Wyckoff, J. Jones, J. Condeelis, and J. Segall, "A critical step in metastasis: in vivo analysis of intravasation at the primary tumor," *Cancer research*, vol. 60, no. 9, p. 2504, 2000.

[86] J. Eliane, M. Repollet, K. Luker, M. Brown, J. Rae, G. Dontu, A. Schott, M. Wicha, G. Doyle, D. Hayes, *et al.*, "Monitoring serial changes in circulating human breast cancer cells in murine xenograft models," *Cancer research*, vol. 68, no. 14, p. 5529, 2008.

[87] D. Goodale, C. Phay, C. Postenka, M. Keeney, and A. Allan, "Characterization of tumor cell dissemination patterns in preclinical models of cancer metastasis using flow cytometry and laser scanning cytometry," *Cytometry Part A*, vol. 75, no. 4, pp. 344–355, 2009.

[88] B. Janssen, J. Debets, P. Leenders, and J. Smits, "Chronic measurement of cardiac output in conscious mice," *American Journal of Physiology-Regulatory, Integrative and Comparative Physiology*, vol. 282, no. 3, pp. R928–R935, 2002.

[89] M. Delp, M. Evans, and C. Duan, "Effects of aging on cardiac output, regional blood flow, and body composition in fischer-344 rats," *Journal of Applied Physiology*, vol. 85, no. 5, pp. 1813–1822, 1998.

[90] K. Luzzi, I. MacDonald, E. Schmidt, N. Kerkvliet, V. Morris, A. Chambers, and A. Groom, "Multistep nature of metastatic inefficiency: dormancy of solitary cells after successful extravasation and limited survival of early micrometastases," *The American journal of pathology*, vol. 153, no. 3, pp. 865–873, 1998.

[91] G. Naumov, S. Wilson, I. MacDonald, E. Schmidt, V. Morris, A. Groom, R. Hoffman, and A. Chambers, "Cellular expression of green fluorescent protein, coupled with high-resolution in vivo videomicroscopy, to monitor steps in tumor metastasis," *Journal of cell science*, vol. 112, no. 12, pp. 1835–1842, 1999.

[92] M. Cameron, E. Schmidt, N. Kerkvliet, K. Nadkarni, V. Morris, A. Groom, A. Chambers, and I. MacDonald, "Temporal progression of metastasis in lung: cell survival, dormancy, and location dependence of metastatic inefficiency," *Cancer research*, vol. 60, no. 9, p. 2541, 2000.

[93] S. Koop, I. MacDonald, K. Luzzi, E. Schmidt, V. Morris, M. Grattan, R. Khokha, A. Chambers, and A. Groom, "Fate of melanoma cells entering the microcirculation: over 80% survive and extravasate," *Cancer research*, vol. 55, no. 12, p. 2520, 1995.

[94] M. Martin, G. Kremers, K. Short, J. Rocheleau, L. Xu, D. Piston, L. Matrisian, and D. Gorden, "Rapid extravasation and establishment of breast cancer micrometastases in the liver microenvironment," *Molecular Cancer Research*, vol. 8, no. 10, pp. 1319–1327, 2010.

CHAPTER 2

Detection and characterization of Circulating Tumor Cells by the CellSearch approach

F.A.W. Coumans and L.W.M.M. Terstappen
Chapter in book "Circulating Tumour Cells", from the series "Methods in Molecular Biology", Humana Press, New York, NY, USA, in press, expected 2012

Abstract

Cancer metastasis occurs when cells shed from a primary or metastatic tumor, enter the circulation, and begin to grow in distant locations of the body. With current techniques it is possible to measure the presence of a few circulating tumor cells (CTC) in a blood sample. Detection of even the presence of a very small number (one or more) of these CTC in a 7.5 mL blood sample with the CellSearch system is associated with a significant decrease in survival of patients with metastatic carcinomas. The techniques and definitions used for the detection and enumeration of CTC with the CellSearch system were validated in a series of preclinical and prospective multicenter studies. In this chapter we will describe in detail the sample acquisition, sample preparation, data acquisition and assignment of CTC used in the CellSearch system.

2.1 Introduction

Carcinomas are derived from epithelial cells that are not normally found in circulation. Detection of CTC with the CellSearch® system is based on this premise and uses ferrofluid coupled to monoclonal antibodies specific for the Epithelial Cell Adhesion Molecule (EpCAM) that are expressed on cells of epithelial origin to immunomagnetically enrich CTC from 7.5 mL of blood. The enriched cells are stained with Phycoerthrin (PE) conjugated monoclonal antibodies directed against cytokeratins 8, 18, 19 (CK) also expressed on cells of epithelial origin, Allophycocyanin (APC) conjugated monoclonal antibodies identifying CD45 expressed on leukocytes and the nucleic acid dye 4',6-diamidino-2-phenylindole, dihydrochloride (DAPI). A computer controlled fluorescence microscope is used to present all the objects that stain with both DAPI and PE to the operator that classifies the events as a tumor cell when it's larger than 4 x 4 μm^2, its morphological features are consistent with that of a tumor cell and it exhibits the phenotype EpCAM+, CK+, DAPI+ and CD45-. The definition of a CTC in the CellSearch system was set in as series of preclinical studies [1, 2, 3, 4, 5, 6, 7, 8, 9] and was used in the system validation study [10], as well as the prospective multicenter studies [11, 12, 13, 14]. In a recent study data from the CellSearch metastatic prostate cancer study were reanalyzed using a variety of CTC definitions and it was shown that fragments of tumor cells or tumor micro particles (< 4 µm) are present at a much larger frequency and their presence also indicates a worse prognosis [15]. In this chapter, we will describe the methods underlying the identification and enumeration of Circulating Tumor cells by the CellSearch system.

2.2 Materials

1. CellSave Preservative Tubes
2. CellTracks® AutoPrep® System
3. MagNest® cell presentation device
4. CellTracks Analyzer II®
5. CellTracks AutoPrep Instrument Buffer
6. Swing bucket centrifuge capable of 800 x g
7. Test tube racks
8. Calibrated micro-pipettors and tips
9. Vortex mixer

10. CellSearch Circulating Tumor Cell Kit. This kit contains supplies to process sixteen 7.5 mL blood samples:
    - 3.0 mL of a suspension of ferromagnetic nanoparticles conjugated to a mouse monoclonal antibody specific for the cell surface marker EpCAM (clone VU1D9) present on epithelial cells in a buffer containing bovine serum albumin (BSA) and ProClin 300 as a preservative.
    - 3.0 mL of mouse monoclonal antibodies specific to cytokeratins 8, 18 (clone C11), cytokeratin 19 (clone A53-B/A2) conjugated to PE and mouse anti-CD45 monoclonal antibody (clone HI30) conjugated to APC in a buffer containing bovine serum albumin (BSA) and sodium azide as a preservative.
    - 3.0 mL of the nucleic acid dye DAPI and ProClin 300 as a preservative.
    - 3.0 mL of a capture enhancement reagent for controlled ferrofluid aggregation in a buffer containing BSA, and sodium azide as a preservative.
    - 3.0 mL of a buffer containing reagents to permeabilize the cell membrane to permit the staining of cytokeratins reagent and sodium azide as a preservative.
    - 3.0 mL of a cell fixative in a buffer containing BSA, and sodium azide as a preservative.
    - Two 110 mL bottles of dilution buffer containing sodium azide as a preservative.
    - Sixteen 15 mL conical centrifuge tubes and caps.
    - Sixteen cell presentation cartridges and plugs.

The materials needed for the enumeration of CTC by the CellSearch system can be obtained from Veridex LLC, Raritan, NJ, USA.

2.3 Methods

2.3.1 Blood Collection

1. Collect whole blood aseptically by venipuncture or from a venous port into a CellSave Preservative Tube.
2. The tube should be filled until the blood flow stops to ensure the correct ratio of sample to anticoagulant and preservative. Immediately mix by gently inverting the tube eight times.
3. Blood samples may be stored or transported in CellSave Preservative Tube. Samples should not be refrigerated.

2.3.2 Blood sample preparation for processing with the CellTracks AutoPrep System

1. Transfer 7.5 mL of blood from the CellSave Preservative Tube into a 15 mL conical tube.
2. Add 6.5 mL of dilution buffer.
3. After capping of the tube it should be mixed by inversion.
4. Place the tube in the centrifuge for 10 minutes at 800 x g with the brake off.
5. Place the sample on the CellTracks AutoPrep System within one hour of centrifugation.

2.3.3 CTC enrichment and fluorescent labeling by the CellTracks AutoPrep System

The CellTracks AutoPrep is a fully automated sample preparation system that can process 8 blood samples at a time. The system contains nine stations each performing a specific task. Samples are passed consecutively along these stations with fixed intervals of 14 minutes. Each of the stations is depicted in figure 2.1 and the tasks performed at each station are described below:

- Station 1: The interface between red cells and the diluted plasma is detected and the plasma is aspirated and discarded. Next 150 µL EpCAM ferrofluid, 150 µL capture enhancement reagent (6), 3 mL of dilution buffer and 3 mL of system buffer is added. The sample volume is now 9-10 mL. The probe that adds the buffers also mixes the sample.
- Station 2: A magnet assembly that consists of three magnets is moved towards the sample tube such that three sides of the tube are in contact with the magnets. Movement of the magnet assembly back and forth is used to move the ferrofluid through the sample, increasing the number of collisions between cells and ferrofluid.
- Station 3: magnetic incubation identical to station 2.
- Station 4: Two side by side magnets with opposite polarization are placed against the tube. The opposite polarization generates a high magnetic field gradient at the interface between the magnets. The magnet is also tilted slightly such that it is closest to the tube at the bottom. The magnetic cells and free ferrofluid accumulate at the highest gradient, which is found at the interface between the magnets in horizontal direction and near the bottom of the tube in vertical

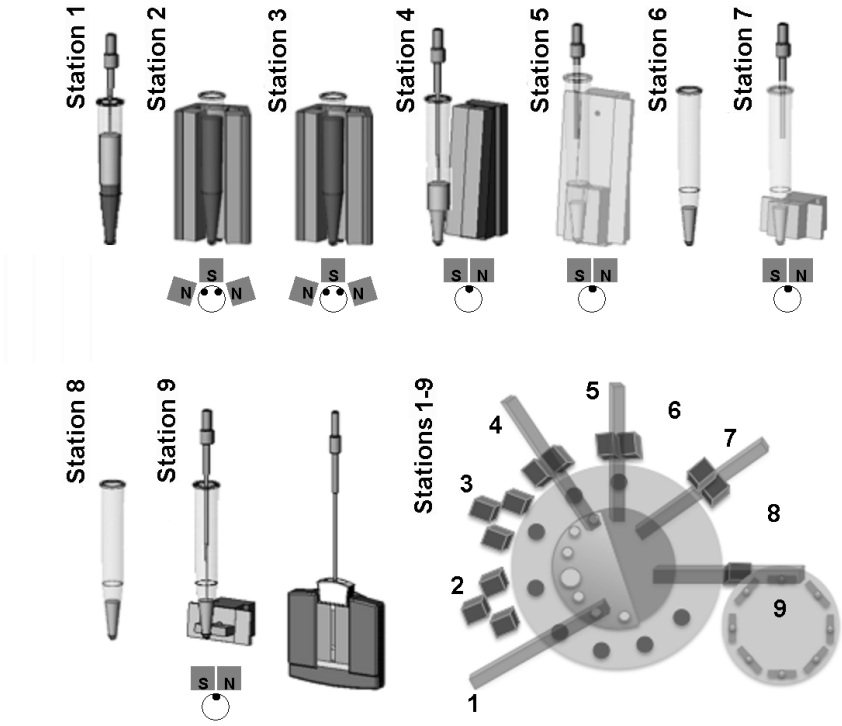

Figure 2.1: CellTracks AutoPrep layout. *A diagram for each station is shown, with the polarization of magnets in a diagram below. The place where magnetic cells accumulate in the sample tube is indicated with a dot in the magnetic diagram. The top view of nine stations as they are positioned in the CellTracks Autoprep and the carousel holding eight MagNests with the sample cartridges is shown in the right bottom corner.*

direction. Once the cells have accumulated, the blood is aspirated and discarded. The magnet is moved away from the tube and the sample is resuspended by addition of 1.5 mL of dilution buffer followed by 1.5 mL of system buffer. The sample volume is now 3 mL.

- Station 5: Two slightly tilted magnets with opposite polarization are placed against the tube. Again, the magnetically labeled cells and the free ferrofluid will accumulate at the interface between the two magnets and near the bottom of the tube where the distance to the magnet is shortest. The buffer is aspirated and discarded. The magnet is moved away from the tube and the sample is resuspended by addition of 200 µL of dilution buffer followed by 200 µL of system buffer. The system now adds 150 µL permeabilization reagent, 150

µL DAPI and 150 µL fluorescently labeled antibodies. The sample is mixed and the volume has now been reduced to 850 µL.

- Station 6: Incubation of the sample.
- Station 7: 500 µL of system buffer and 500 µL of dilution buffer are added to the sample after mixing. Two slightly tilted short magnets with opposite polarization are placed against the tube. Magnetically labeled cells and free ferrofluid will accumulate near the interface of the two magnets. The fluid is aspirated and discarded. The magnets are moved away from the tube and the sample is resuspended by addition of 400 µL of dilution buffer followed by 500 µL of system buffer.
- Station 8: The sample is not touched to permit the cells to settle.
- Station 9: The top 300 µL is aspirated to remove excess free ferrofluid and discarded and a small magnet is placed against the tube. After magnetic separation the fluid is aspirated. After moving the magnets away from the tube the cells and free ferrofluid are resuspended by addition of 150 µL of a cell fixative and 125 µL of system buffer. The sample is transferred to the analysis cartridge that is contained within the MagNest cell presentation device. The sample tube is washed with 75 µL of system buffer which is subsequently used to top off the analysis cartridge.

2.3.4 Principles of the MagNest cell presentation device

The use of cytospins for microscopic examination of cells is accompanied with variable cell losses. For rare event detection all cells present in the sample need to be examined. For optical examination of the cells in the sample a device was constructed that permitted an even distribution of the cells on an analysis surface. The device consists of two magnets that are held together by an iron yoke and an analysis cartridge with an optically transparent cover slip that is placed between the two magnets. The configuration of the magnets and the analysis cartridge needed to be such that vertical gradient inside the cartridge is large enough to move the magnetically labeled cells to the upper surface in a reasonable time with no gradient that moves the cells in the sideways direction. The latter would lead to accumulation of cells on the sides or center of the cover slip.

Figure 2.2 shows the position of the two magnets with the North (N) and South (S) pole. The magnetic field created by the particular shape and position of the magnets are calculated with a simulation program and the derived trajectory of magnetically labeled cells are illustrated by dotted lines in the figure. Dimensioning of the cartridge relative to the magnets is such that all magnetically labeled cells will move vertically with no movement

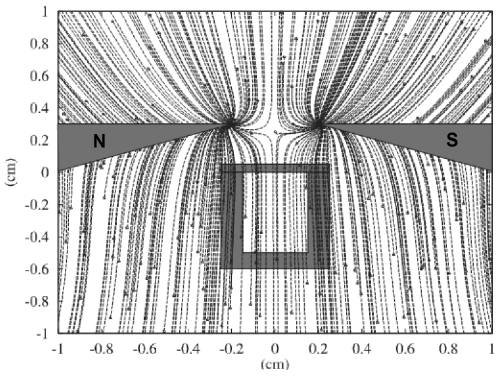

Figure 2.2: Cell presentation with MagNest device. *The North (N) and south (S) pole of the magnets in the cross section of a MagNest are shown. The position of the sample cartridge with the cover slip on top is shown between the two magnets. The dotted lines are simulated with a computer program and represent the trajectories that magnetically labeled cells follow.*

in the horizontal direction. Different placement or shape of cartridge or magnets may alter the distribution of cells on the cover slip dramatically [16].

2.3.5 Image acquisition with the CellTracks Analyzer II

The sample cartridge inside the MagNest is imaged on the CellTracks Analyzer II, a computer controlled epi-fluorescence microscope with a mercury light source and a NA 0.45 10X objective. Before imaging, the exact location of the cover slip on the sample cartridge is determined in xyz dimensions. The system determines the locations to be imaged, such that the combined image covers the entire surface of the cover slip with 10 pixels overlap between adjacent images, typically resulting in 175 locations. The images are taken with a high sensitivity monochrome 12-bit CCD camera. Each pixel represents a 650 x 650 nm^2 area of the sample. At each location images are taken with each of the four filter cubes. The filter cubes used to acquire the fluorescent images are designed to minimize cross talk between the fluorochromes DAPI, FITC, PE and APC, while maximizing the light intensity from the mercury bulb. Filter specifications are given as center wavelength (CWL) with full width half maximum (FWHM) for band pass filters (BP CWL/FWHM) and cut on (CO) wavelength for long pass filters (LP CO). DAPI: excitation BP 365/20, emission LP 400, FITC/DiOC: excitation BP 475/20, emission 510/20, PE: excitation BP 547/12, emission 578/25, APC: excitation 620/30, emission BP 580/55. The FITC cube was

originally optimized for the detection of 3,3'-dihexadecyloxacarbocyanine perchlorate (DiOC) staining and is sometimes called the DiOC cube. Once imaging is complete, the image analysis algorithm is started automatically to select events of high contrast that appear in both the PE and DAPI channels.

2.3.6 Image analysis algorithm

The image analysis algorithm looks at the images from each of the 175 locations to identify possible CTC events:

1. For a location it takes the DAPI, FITC, PE and APC images and reduces each 12-bit image to 8-bits. This is achieved by remapping each pixel to a scale from 0 to 255, with 255 equal to the 7th brightest and 0 equal to the 7th dimmest pixel in the image. The 4 remapped images are stored as a 4 layer Lempel-Ziv-Welch (LZW) compressed tiff image.

2. The DAPI image is divided into segments of 10 x 10 pixels. Each segment is rescaled once again to the brightest (255) and dimmest pixel (0) found in an environment of 50 x 50 pixels around the 10 x 10 pixel segment. If at least 10% of pixels in the 10 x 10 segment are found to be above 100, the 10 x 10 segment contains a positive event.

3. Once all segments have been analyzed, the coordinates of all positive segments are stored, with adjacent segments combined into larger squares. The stored squares encompass objects.

4. Steps 2 and 3 are repeated for the PE image.

5. The coordinates of positive PE and DAPI segments are compared to identify events, which are positive in both channels. Positive in both channels means that a positive square in the DAPI channel partially overlaps or touches a positive square in the PE channel.

6. After all locations are completed, events on the border of an image which touch an event on the adjacent image are combined into single objects to prevent double counting of CTC.

7. For each event a thumbnail image is generated for review by the operator. Each thumbnail consists of a false color overlay image showing PE (green) and DAPI (purple) signals, as well as monochrome images of APC, FITC, PE and DAPI signals. All images are scaled from minimum to maximum before presentation.

2.3.7 CTC assignment in CellSearch

In CellSearch samples from healthy individuals or patients with no known malignant disease the DAPI positive PE positive events presented to the operator for review typically range from 6-937 (mean 74, median 46, n=67) events. In samples from cancer patients the number of events can be higher. For example in the prospective multicenter study enrolling patients with metastatic castration resistant prostate cancer 0-24087 (mean 580, median 128, n=1535) events positive in DAPI and PE were found. After review of all the events from this study by trained operators, an average of 7% of the found events was considered CTC by the CellSearch CTC definition. CellSearch defines a CTC as an object with cell like morphology, a nucleus, cytokeratin 8, 18 and /or 19 and no CD45.

A flow diagram of the review process is shown in figure 2.3. Examples of objects that are assigned as CTC are shown in figure 2.4 and examples of objects that are not assigned as CTC are shown in figure 2.5.

Rules for reviewing a CTC: In some samples the ferrofluid forms very thick opaque lines that mask part of the cell image (figure 2.5, panel A) and the reviewer needs to guess what is obstructed by the ferrofluid lines. In the CellTracks Analyzer II ferrofluid lines will always run vertically on the thumbnail images. In cases were multiple objects are shown in one thumbnail and two or more are considered a CTC, it is counted as one CTC (figure 2.4, panel B).

1. **Does the object have the morphology of a cell?** Diffuse staining in the PE image may be identified by the algorithm as a potential CTC (figure 2.5, panel B). For example part of a large region of PE positive material is occasionally selected (figure 2.5, panel C). An object in the PE channel which looks like two or more concentric rings is most likely an air bubble in the sample (figure 2.5, panel D). Sometimes these bubbles appear near or on a nucleus of a white blood cell. All objects represented in figure 2.5, panels B-D do not have morphology consistent with a cell.

2. **Do all images contain the same shape?** If all the images have the same shape, the object is an artifact (figure 2.5, panel C). Occasionally, one of the images does not contain any signal, but the other images do contain the same shape (figure 2.5, panel E) and is also considered an artifact.

3. **Is the object FITC negative?** Any object positive in FITC is an artifact.

4. **Is the object DAPI positive?** Objects without a nucleus are not cells.

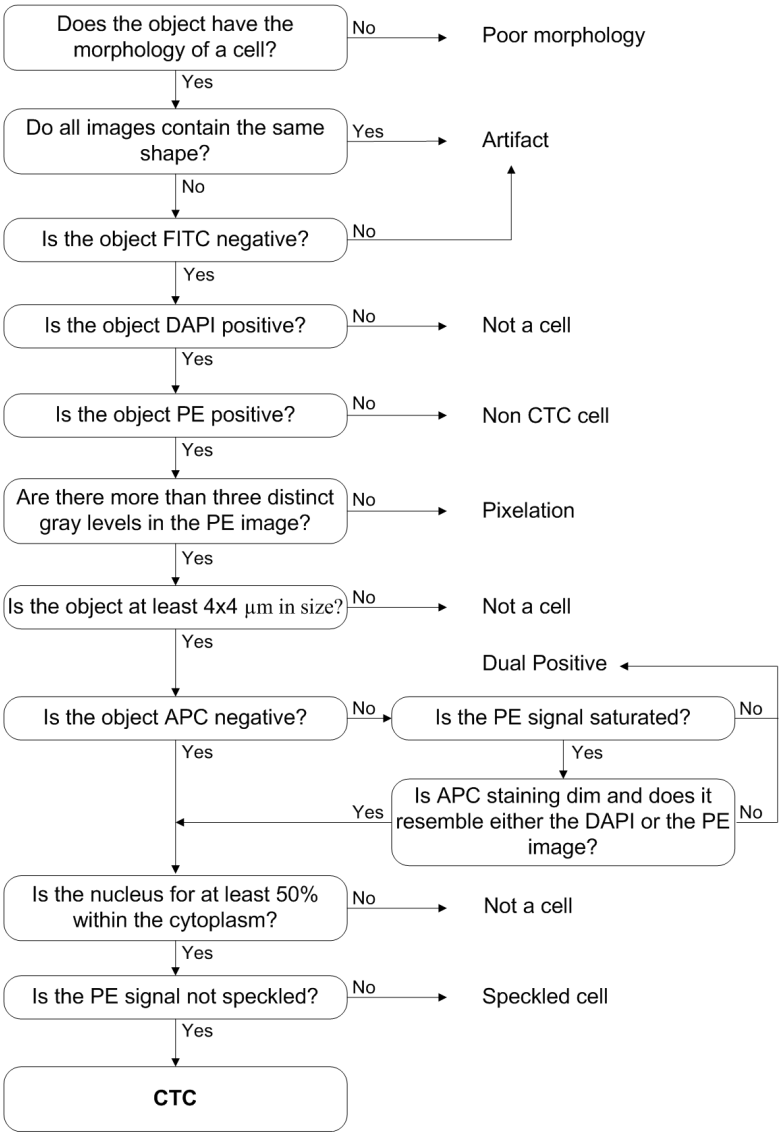

Figure 2.3: Flow diagram for CTC evaluation.

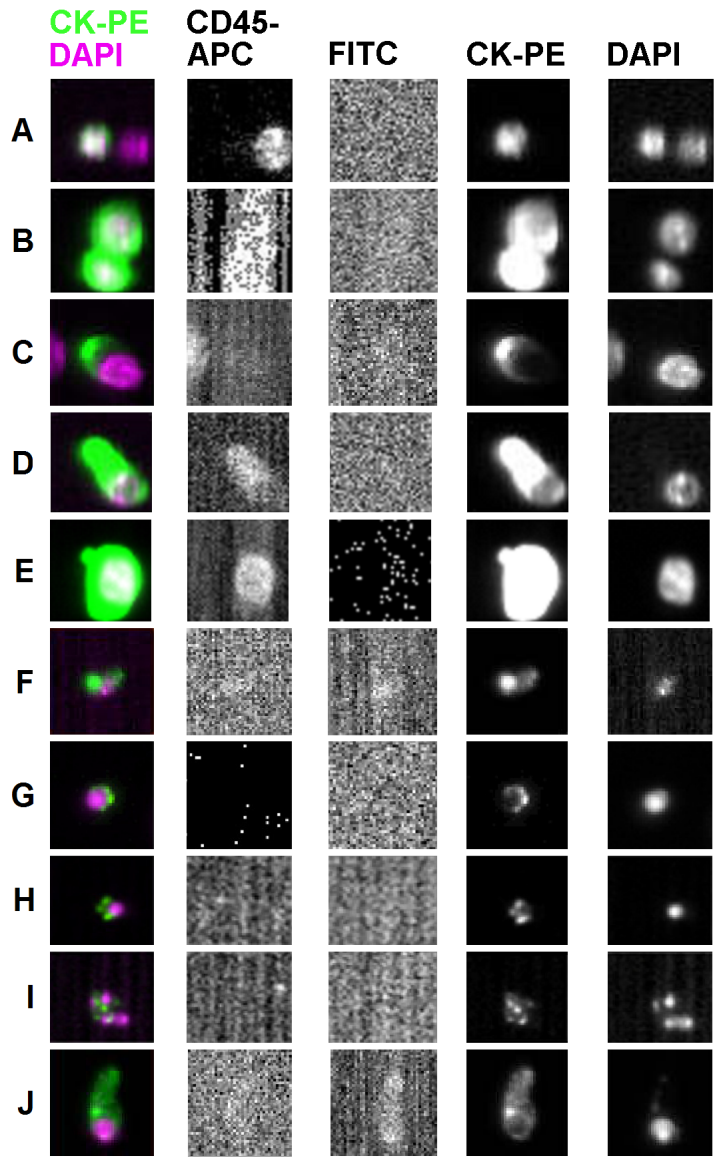

Figure 2.4: Examples of objects counted as CTC. Panels A-E *show obvious CTC and* ***panels F-J*** *show challenging cases.* ***A:*** *CTC next to a white blood cell;* ***B:*** *two CTC counted as one;* ***C:*** *CTC with partial nucleus of another cell;* ***D/E:*** *CTC with crosstalk into APC channel;* ***F/G:*** *CTC with difficult to judge cytoplasm boundary and small nucleus;* ***H/I:*** *CTC with speckles, but continuous low intensity cytoplasm staining;* ***J:*** *CTC which just meets 50% rule.*

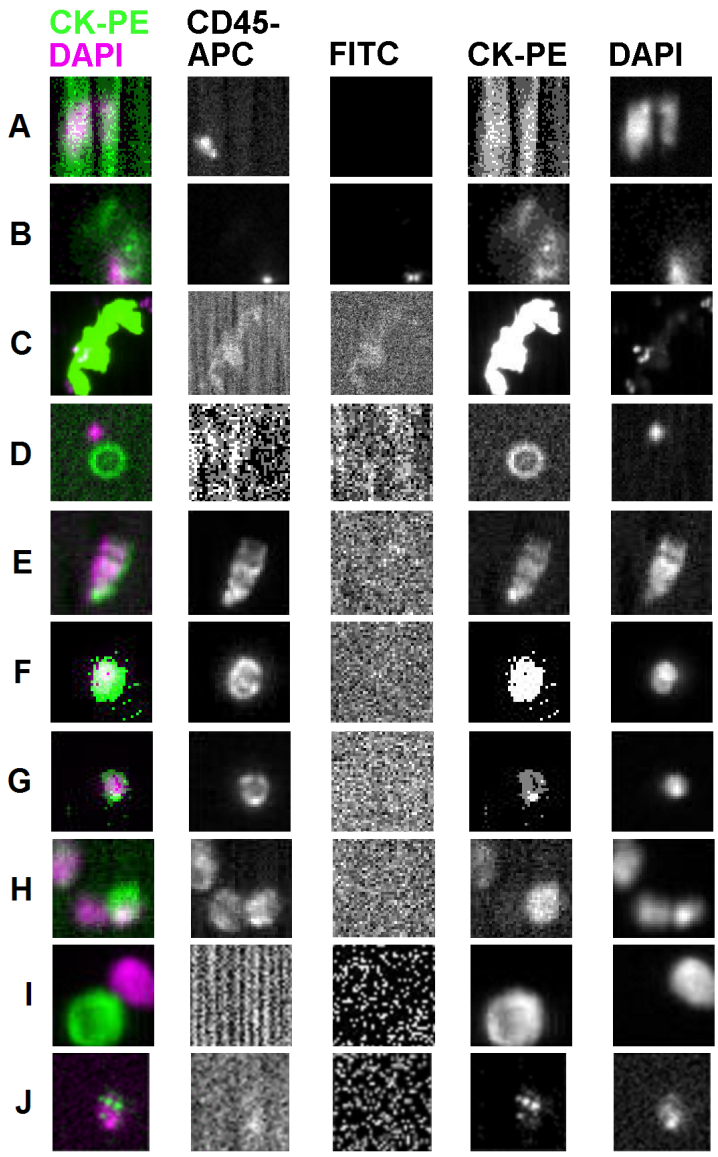

Figure 2.5: Examples of objects not counted as CTC. Panels; A: *Ferrofluid obstructing image in DAPI channel;* ***B-D:*** *Poor morphology objects;* ***E:*** *Artifact;* ***F/G:*** *Pixelation;* ***H:*** *Two dual positive cells and one white blood cell;* ***I:*** *Cytoplasm without nucleus;* ***J:*** *Speckled cell*

5. **Is the object PE positive?** Objects without cytokeratin 8, 18 and/or 19 are not considered a CTC.

6. **Are there more than three distinct gray levels in the PE image?** Occasionally very little signal appears like a real shape due to successive scaling steps in the image processing. If such an artifact occurred, there are very few distinct gray levels in the image, which is called pixelation. The examples in figure 2.5, panels F and G have two and three gray levels respectively. They should not be confused with the cell in figure 2.4, panel E, which is not pixelated, but saturated due to high intensity PE signal.

7. **Is the object at least 4 x 4 µm^2 in size?** The CellTracks review software provides a 4×4 µm^2 size box. Objects that are smaller are not considered a cell even if they contain nuclear material as well as cytoplasm. The examples in figure 2.4, panels G and H are slightly larger than 4×4 µm^2.

8. **Is the object APC negative?** CD45-APC positive objects are cells of hematopoietic origin. The only exception can occur due to cross talk. When cross talk occurred, the PE signal is saturated, the APC staining is dim and resembles either DAPI or PE staining. Examples of such CTC are illustrated in figure 2.4, panels D and E. If any of these conditions is not met, the cell is dual positive and not considered a CTC (figure 2.5, panel H). When many dual positives are found in a sample, and a cell without APC staining is found that has similar size and appearance in DAPI/PE to the dual positive cells, it is assumed that this cell is also a dual positive.

9. **Is the nucleus for at least 50% within the cytoplasm?** Also called the 50% rule. If there is any doubt as to whether the object in the PE signal and the object in the DAPI signal actually belong to each other, the object should not be counted as a CTC (figure 2.5, panel I). The CellSearch method excludes any events for which less than 50% of the nucleus is within the cytoplasm.

10. **Is the PE signal not speckled?** Occasionally a nucleus is seen with a few small dots of PE on the nucleus. If there is no continuous PE staining (even very dim) the object is a speckled cell, and not counted as a CTC (figure 2.5, panel J). Cells that are considered CTC, because there is continuous PE staining with some high intensity spots are shown in figure 2.4, panels H and I.

11. The cells that meet all criteria are called CTC and examples are shown in figure 2.4.

2.4 Notes

2.4.1 Blood Collection

1. Draw initial samples prior to initiation of a therapy regimen. Subsequent samples can be drawn after the start of a therapy regimen, usually at 3 to 4 week intervals, to follow CTC levels during therapy.

2. Maintain the samples at room temperature before processing. Refrigeration of the sample can result in uneven distribution of the ferrofluid in the analysis chamber and can obscure the cells from the viewing plane.

2.4.2 CTC enrichment and fluorescent labeling by the CellTracks AutoPrep System

3. The addition of buffer to the whole blood and centrifugation of the sample before placement of the sample on the CellTracks Autoprep is performed because in the plasma of some donors contains a factor that aggregates the ferrofluid, thereby reducing the ability to capture the target cells. Aggregation also gives rise to an uneven distribution of the ferrofluid and magnetically labeled cells over the analysis surface of the cartridge. Although the partial removal of the plasma significantly reduces the chance of ferrofluid aggregation in some instances one still can notice an uneven distribution of the ferrofluid over the analysis surface. This can also be observed as thicker lines of the ferrofluid.

4. Visual inspection of the analysis surface of the cartridge while in the Magnest after processing on the CellTracks Autoprep can help with the assessment of the quality of the sample after processing. An even brownish color should be seen across the entire surface and when inspected under a bright field microscope one can observe evenly distributed thin lines that run between the magnets. Little back dots, thick black lines and empty regions suggest that there are issues either with the starting blood sample or with the reagents used by the system.

2.4.3 Image acquisition with the CellTracks Analyzer II

5. The spectrum of the mercury arc lamp in the CellTracks Analyzer II does not permit a good excitation of APC. In case very bright PE objects are present in the sample the APC filter cube can pass some of the PE fluorescence and could result in a true CTC being rejected

on account of apparent CD45-APC staining, which in reality is cross talk of the CK-PE signal. Granulocytes that are non-specifically carried over through the procedure express significantly less CD45 as compared to lymphocytes and frequently appear as CD45 negative. Poor APC sensitivity of the CellTracks Analyzer II complicates review of CTC samples.

6. The CellSearch Circulating Tumor Cell Control Kit checks the overall system performance, including instrument, reagents and operator technique. The control cells in this kit are derived from the breast cancer tumor cell-line SKBR-3. The cells are stabilized and labeled with fluorescent membrane dyes. In the kit cells are present at a low and high concentration. The cells at a high concentration are labeled with DiOC16 [3] and are detected by the FITC filter cube. This filter cube is used for three purposes: 1.) to detect high control cells to check overall performance of the system when using the Circulating Tumor Cell Control Kit, 2.) to discard artifacts when using the Circulating Tumor Cell Kit and 3.) to detect the presence or absence of FITC on CTC when using the Circulating Tumor Cell Kit in combination with marker reagents such as Her2 FITC and EGFR FITC.

7. The CellTracks Analyzer II is a fluorescence microscope equipped with a mercury arc lamp as light source. The illumination is not equal over the field of view, as a result fluorescence signal intensity is reduced in areas with lower illumination intensity. The ferrofluid lines cover parts of the cells and thus reduce the signal intensity from these cells. Because thickness of ferrofluid lines is variable they contribute to variation in signal intensity. Both phenomena increase variation in signal intensity, complicating attempts to quantify density of (immuno)fluorescent targets on the cells.

2.4.4 Image analysis algorithm

8. The choice for contrast based segmentation and the frequent remapping of pixels to cover the maximum range provides robustness against variation in reagent and sample quality and allows for a great variety of targets to be used without changing any algorithm parameters. The disadvantage is excessive sensitivity for very low contrast objects and loss of intensity information. One of the consequences of the latter is the appearance of pixelated objects (figure 2.5, panels F/G) and difficulty in judging boundaries of cytoplasm for the 50% rule (figure 2.4, panel G) and speckled cells (figure 2.4, panels H/I, figure 2.5 J).

9. The repeated scaling of the images destroys all intensity information. It is feasible that the intensity of the PE, DAPI and APC signal is of

value in determining whether an event is truly a CTC. Representation of the monochrome thumbnails on a color bar scale instead of a gray scale may allow reviewers to consider both morphology and intensity of the object, but would require extensive retraining.

2.4.5 CTC assignment in CellSearch

10. Squamous epithelial cells can occasionally be seen among the images. They have a typical morphology (small nucleus, large cytoplasma) that can be easily discriminated from CTC . These cells are either introduced by the needle stick or exfoliated from the skin and accidently found their way into the blood sample.

11. If there is a very bright clump of CK-PE in the image of a cell, the rest of the PE image will appear to be dimmer. This may make it look like the cytoplasm does not surround the nucleus, while it in fact does.

12. Judging whether signal in the CD45-APC channel is due to crosstalk or due to presence of CD45-APC is occasionally difficult and subjective.

13. Events with a clear nucleus that do not stain with cytokeratin nor with CD45 are occasionally presented among the DAPI positive, PE positive objects. This is caused by an object in the proximity of this event that does fit the criteria. These cells with obvious morphology of a cell may well represent CTC that do not express the cytokeratins. Review of the actual images can reveal more of these cells.

14. If it is obvious that part of the object is not shown in the thumbnail, the thumbnail may need to be expanded. Sometimes another thumbnail contains the other object. The CellTracks Analyzer II software allows the user to expand the thumbnail and to determine whether the object is also shown in another thumbnail.

15. The 50% rule is subjective. The operator lacks adequate tools in the CellTracks Analyzer II software to assess whether the requirement is met. Shift of the nucleus from the cytoplasm can be caused by problems during scanning. In the case of stage issues, the nucleus is offset from the cytokeratin in the same direction and magnitude for all events found in the sample.

16. A recent study demonstrated that objects as shown in figure 2.5, panels I and J are also prognostic for survival in hormone refractory prostate cancer patients [15]. This suggests that the rules for identifying CTCs can be simplified which will lead to a reduction of operator to operator variability.

17. Parts of the review process are subjective and intra as well as inter operator variability are the main source of error in CTC enumeration. Statistical modeling suggested that reduction of the operator review error to zero, would reduce the cutoff from 5 CTC to 1 CTC [17].

Acknowledgements

Figure 2.3 was modified from a bachelor thesis by Edzo Klawer.

2.5 References

[1] L. W. Terstappen, C. Rao, S. Gross, V. Kotelnikov, E. Racilla, J. Uhr, and A. Weiss, "Flow cytometry–principles and feasibility in transfusion medicine. Enumeration of epithelial derived tumor cells in peripheral blood," *Vox Sang.*, vol. 74 Suppl 2, pp. 269–274, 1998.

[2] E. Racila, D. Euhus, A. J. Weiss, C. Rao, J. McConnell, L. W. Terstappen, and J. W. Uhr, "Detection and characterization of carcinoma cells in the blood," *Proc. Natl. Acad. Sci. U.S.A.*, vol. 95, pp. 4589–4594, Apr 1998.

[3] L. W. Terstappen, C. Rao, S. Gross, and A. J. Weiss, "Peripheral blood tumor cell load reflects the clinical activity of the disease in patients with carcinoma of the breast," *Int. J. Oncol.*, vol. 17, pp. 573–578, Sep 2000.

[4] J. G. Moreno, S. M. O'Hara, S. Gross, G. Doyle, H. Fritsche, L. G. Gomella, and L. W. Terstappen, "Changes in circulating carcinoma cells in patients with metastatic prostate cancer correlate with disease status," *Urology*, vol. 58, pp. 386–392, Sep 2001.

[5] D. F. Hayes, T. M. Walker, B. Singh, E. S. Vitetta, J. W. Uhr, S. Gross, C. Rao, G. V. Doyle, and L. W. Terstappen, "Monitoring expression of HER-2 on circulating epithelial cells in patients with advanced breast cancer," *Int. J. Oncol.*, vol. 21, pp. 1111–1117, Nov 2002.

[6] P. Liberti, C. Rao, and L. Terstappen, "Optimization of ferrofluids and protocols for the enrichment of breast tumor cells in blood," *J Magnetism and Magnetic Materials*, vol. 225, pp. 301–307, 2001.

[7] M. Kagan, D. Howard, T. Bendele, J. Mayes, J. Silvia, M. Repollet, J. Doyle, J. Allard, N. Tu, T. Bui, T. Russell, C. Rao, M. Hermann, H. Rutner, and L. Terstappen, "A sample preparation and analysis system for identification of circulating tumor cells," *J Clinical Ligand Assay*, vol. 25, pp. 104–50, 2002.

[8] C. G. Rao, D. Chianese, G. V. Doyle, M. C. Miller, T. Russell, R. A. Sanders, and L. W. Terstappen, "Expression of epithelial cell adhesion molecule in carcinoma cells present in blood and primary and metastatic tumors," *Int. J. Oncol.*, vol. 27, pp. 49–57, Jul 2005.

[9] C. J. Larson, J. G. Moreno, K. J. Pienta, S. Gross, M. Repollet, S. M. O'hara, T. Russell, and L. W. Terstappen, "Apoptosis of circulating tumor cells in prostate cancer patients," *Cytometry A*, vol. 62, pp. 46–53, Nov 2004.

[10] W. J. Allard, J. Matera, M. C. Miller, M. Repollet, M. C. Connelly, C. Rao, A. G. Tibbe, J. W. Uhr, and L. W. Terstappen, "Tumor cells circulate in the peripheral blood of all major carcinomas but not in healthy subjects or patients with nonmalignant diseases," *Clin. Cancer Res.*, vol. 10, pp. 6897–6904, Oct 2004.

[11] M. Cristofanilli, G. T. Budd, M. J. Ellis, A. Stopeck, J. Matera, M. C. Miller, J. M. Reuben, G. V. Doyle, W. J. Allard, L. W. Terstappen, and D. F. Hayes, "Circulating tumor cells, disease progression, and survival in metastatic breast cancer," *N. Engl. J. Med.*, vol. 351, pp. 781–791, Aug 2004.

[12] S. J. Cohen, C. J. Punt, N. Iannotti, B. H. Saidman, K. D. Sabbath, N. Y. Gabrail, J. Picus, M. Morse, E. Mitchell, M. C. Miller, G. V. Doyle, H. Tissing, L. W. Terstappen, and N. J. Meropol, "Relationship of circulating tumor cells to tumor response, progression-free survival, and overall survival in patients with metastatic colorectal cancer," *J. Clin. Oncol.*, vol. 26, pp. 3213–3221, Jul 2008.

[13] J. S. de Bono, H. I. Scher, R. B. Montgomery, C. Parker, M. C. Miller, H. Tissing, G. V. Doyle, L. W. Terstappen, K. J. Pienta, and D. Raghavan, "Circulating tumor cells predict survival benefit from treatment in metastatic castration-resistant prostate cancer," *Clin. Cancer Res.*, vol. 14, pp. 6302–6309, Oct 2008.

[14] M. Miller, G. Doyle, and L. Terstappen, "Significance of circulating tumor cells detected by the CellSearch® system in patients with metastatic breast colorectal and prostate cancer," *Cancer. J Oncology*, vol. Article ID 617421, pp. 1–8, 2009.

[15] F. A. Coumans, C. J. Doggen, G. Attard, J. S. de Bono, and L. W. Terstappen, "All circulating EpCAM+CK+CD45- objects predict overall survival in castration-resistant prostate cancer," *Ann. Oncol.*, vol. 21, pp. 1851–1857, Sep 2010.

[16] A. G. Tibbe, B. G. de Grooth, J. Greve, G. J. Dolan, C. Rao, and L. W. Terstappen, "Magnetic field design for selecting and aligning immunomagnetic labeled cells," *Cytometry*, vol. 47, pp. 163–172, Mar 2002.

[17] A. G. Tibbe, M. C. Miller, and L. W. Terstappen, "Statistical considerations for enumeration of circulating tumor cells," *Cytometry A*, vol. 71, pp. 154–162, Mar 2007.

CHAPTER 3

Circulating Tumor Cell - Trapping Devices

Frank A.W. Coumans, Sjoerd T. Ligthart, Joost Swennenhuis, Leon W.M.M. Terstappen

Chapter in "Biofunctional Surface Engineering in Medicine" in the "Nanobiotechnology" series, Pan Stanford Publishing, Singapore. Edited by Prof. Dr. Martin Scholz. In press, expected 2012.

Abstract

Presence of tumor cells in blood of carcinoma patients is associated with poor outcome and may be used as a 'liquid biopsy" to enable personalized treatment of cancer patients. Here we review the frequency of tumor cells in blood and its association with survival followed by the description of the enrichment and staining of circulating tumor cells (CTC) and their identification and enumeration as performed by the CellSearch system. Challenges in entrapment of the rare CTC by immunomagnetic enrichments and the identification of treatment targets on these CTC are highlighted.

3.1 Introduction

The increase in life expectancy since the early 20th century has been accompanied by a relative and absolute increase in people diagnosed with and treated for cancer. Death from cancer is or will soon be the primary cause of death in the developed world. Cause of death can mostly be attributed to the effects of metastasis rather than the primary tumor [1]. Tumor cells induce blood-vessel growth (angiogenesis) and may invade these

Table 3.1: Immunohistochemical staining of monoclonal antibodies *used in the CellSearch system on paraffin embedded tissue sections and tissue microarrays of breast cancer patients*

Antigen	cytokeratin 8,18	cytokeratin 19	EpCAM
Antibody	C11	A53	VU-1D9
Samples (N)	280	272	282
Positive samples (N)	273	272	278
Positive samples (%)	97.5	100	98.6

blood vessels or the lymphatic system. After entering in the blood directly or through the lymphatic system these cells are termed circulating tumor cells (CTC). The majority of CTC are destroyed by the reticuloendothelial system, but some escape, exit the blood stream and form distant metastases. The ability to identify and characterize CTC holds the promise of a liquid biopsy that can pave the way towards personalized care for cancer patients. The frequency of these CTC is extremely rare and quite some technological challenges arise in the development of CTC trapping devices. Here we will review the Cell Search platform, which is the first clinically validated platform for the detection of CTC.

3.2 Frequency and clinical relevance of Circulating Tumor Cells

CTC are very rare cells in blood of cancer patients and have previously only been observed in blood smears of patients with extensive metastatic disease [2, 3, 4, 5, 6]. The CellSearch system identifies CTC in 7.5 mL of blood and has been extensively validated for patients with metastatic carcinoma [7]. Modeling of the CTC distribution in 7.5 mL of blood from patients with metastatic breast, colorectal and prostate cancer was used to arrive at the CTC frequency distribution in all 5 liters of blood [8]. Figure 3.1 depicts the cumulative probability in which CTC can be detected as a function of blood volume in patients with metastatic carcinomas. The figure also shows the frequency of erythrocytes, platelets and leukocytes in blood and highlights the difficulty of detecting CTC in all patients. Ten CTC per mL of blood can only be detected in 20% of patients, 1 CTC per mL of blood in 40% of patients and 100 CTC per liter of blood in 80% of patients.

The CellSearch system detects CTC that express both the Epithelial Cell Adhesion Molecule (EpCAM) [9, 10, 11, 12] and Cytokeratin 8, 18 or 19 (CK) [12, 13, 14, 15]. Reactivity of the antibodies used in the CellSearch system on tumor tissue of breast cancer patients is shown in table 3.1.

While expression was detected in the majority of breast cancer tissue samples, this does not imply that all the tumor cells in the tissue express

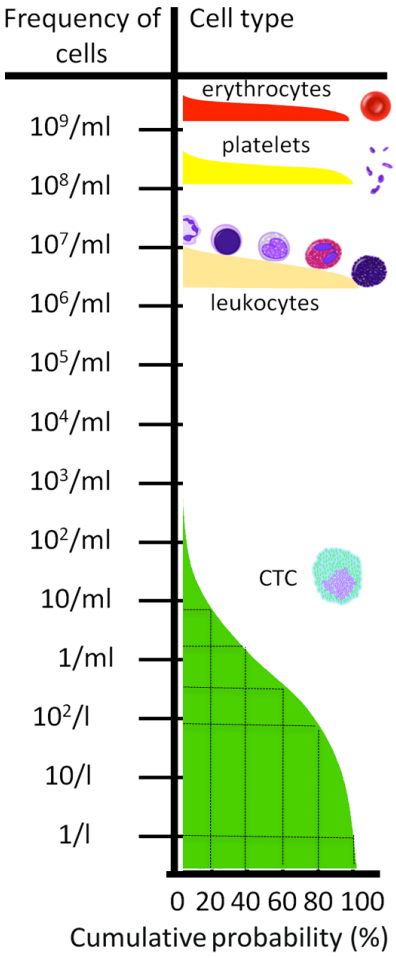

Figure 3.1: Frequency of erythrocytes, platelets, leukocytes and circulating tumor cells in blood of metastatic carcinoma patients. *Cumulative probability of finding at least 1 cell in a given sample volume is shown on the x-axis.*

these antigens nor does it imply that these antigens are preserved during cell migration from tissue to blood. The CTC frequency may therefore be underestimated. While the impact of EpCAM+CK+DNA+CD45- CTC on outcome is well established, the relation between CTC with alternative phenotypes and clinical outcome remains to be determined. Various technologies are currently being explored to identify CTC by other means and should further improve our understanding of CTC [16, 17, 18, 19, 20, 21, 22, 23, 24, 25]. The CellSearch system may simply miss some EpCAM+, CK+ cells, however enumeration of EpCAM+ CTC in 100 µL of whole blood showed that the CTC yield can only be increased 3.3 fold [8, 12]. The CTC definition used in the flowcytometric analysis is less strict and a high false positive rate in the flow assay is the most likely explanation for the largest portion of this discrepancy. The definition of a CTC in the CellSearch system was

set in as series of preclinical studies and was used in system validation studies [7, 26] as well as in prospective multicenter studies for breast, colon, and prostate cancer [27, 28, 29]. These studies showed that metastatic patients that had equal or more CTC than a certain cut-off (five CTC for breast and prostate cancer, three for colon cancer) had significant lower probability of overall survival and thus a worse prognosis than the group that was below this cut-off. Re-analysis of prostate cancer data furthermore showed that a continuous relationship exists between the number of CTC and survival [8, 30] and that fragments of tumor cells or tumor micro particles (TMPs), CK+, CD45- objects that are < 4 µm, are present at a much higher frequency and that their presence also indicates a worse prognosis [31]. Next to these three major types of carcinomas, CTC were enumerated in patients suffering from lung cancer [32, 33], neuroendocrine tumors [34], gastric cancer [35], bladder cancer [36] and ovarian cancer [37]. The relation between CTC and overall survival is illustrated in figure 3.2 by Kaplan-Meier plots for 296 metastatic breast and prostate cancer patients.

For this analysis CTC were identified by an automated algorithm [38]. Panel A shows the Kaplan-Meier of patients before initiation of therapy. Patients with 0 CTC (N=96, 32%, green line) had a median survival of 33.1 months, patients with 1–3 CTC (N=61, 21%, light blue line) had a median survival of 21.9 months, patients with 4–19 CTC (N=71, 24%, dark blue line) had a median survival of 15.8 months and patients with > 20 CTC (N=68, 23%, red line) had a median survival of only 9.5 months. Panel B shows the Kaplan-meier of patients at first follow-up after initiation of therapy. The number of patients with 0 CTC increased (N=134, 45%) and had a median survival of 23.5 months, patients with 1–3 CTC also increased (n=73, 25%) with a median survival of 21.3 months, patients with 4–19 CTC, decreased (N=43, 15%) with a median survival of 10.6 months and patients with >20 CTC also decreased (N=46, 16%) with an even shorter median survival 5.5 months. Panel C shows the Kaplan-Meier of patients subdivided by the changes in CTC counts upon treatment. CTC remained above 20 in 58 of the 68 patients with a median survival of 5.7 months (red line) indicating that therapy did not have a sufficiently beneficial effect. Survival also did not improve for those patients with lower (4–19 CTC) but unchanged CTC with a median survival of 10.6 months (orange line) or who gained CTC during therapy median survival 15.2 months (purple line). The 108 patients with 0 CTC (green line) before and after initiation of therapy had a median survival of 29.6 months. Survival of the 65 patients with a CTC reduction (blue line) to below 4 clearly improved and patients that remained with low counts (light blue line) did not significantly change. The low numbers of CTC detected urges the need for elimination of error in the assignments of CTC as is achieved by the automation of the image analysis and also is strongly dependent on the Poisson error [39]. Patients in which 0 CTC were detected in 7.5 mL of blood have metastatic disease and the question arises whether this is a distinct group of patients, CTC

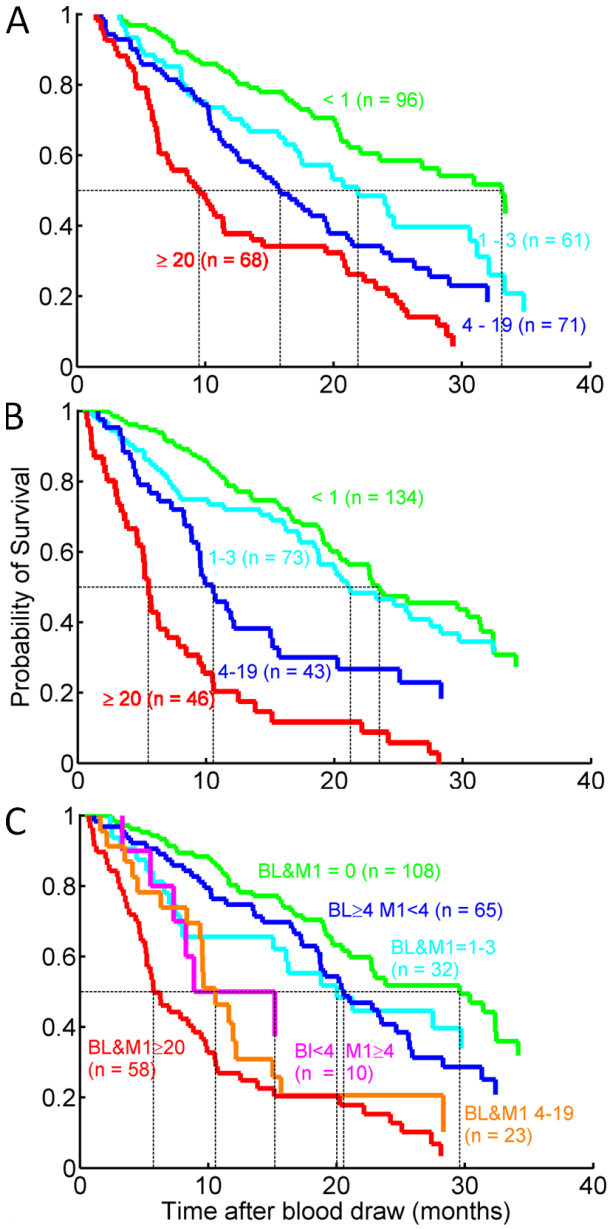

Figure 3.2: CTC and the probability of overall survival for 296 metastatic breast and prostate cancer patients. *Panel A shows patients before therapy, Panel B shows patients 2–5 weeks after initiation of therapy, Panel C shows changes in CTC after initiation of therapy.*

are missed by the CellSearch system or the volume of blood examined is simply too low. Extrapolation of the sample volume to 5 liters of blood predicted that 99% of patients had at least 1 CTC before initiation of therapy, which decreased to 97% after the first cycles of therapy. Survival chances of patients with EpCAM+CK+DNA+CD45- CTC are reduced by 6.6 months for each tenfold CTC increase [8]. These results suggest that a technological leap is needed to identify CTC in all patients with metastatic disease and likely those patients with primary disease that are at risk for disease recurrence.

3.3 CTC enrichment and staining with the CellTracks AutoPrep

The CellTracks AutoPrep is an automated sample preparation device that is part of the CellSearch System. Blood is collected from a patient by venipuncture or from a venous port into a CellSave Preservative Tube®. These tubes contain EDTA as anticoagulant and a cellular preservative to avoid degradation of the blood sample for up to 96 hours while it is being transported to a facility where an AutoPrep system is present. Before placement on the AutoPrep the blood is diluted, mixed by inversion, and centrifuged. The AutoPrep first detects the interface between plasma and blood and then aspirates and discards the plasma. Next ferrofluid conjugated to the epithelial cell adhesion molecule (EpCAM) is added as well as dilution and system buffers. The sample is placed between magnets, which causes the ferrofluid labeled cells to travel to the area within the tube that has the highest magnetic gradient. After the magnetically labeled cells and the free ferrofluid are captured at the wall of the tube, the remaining blood is aspirated and discarded. Buffers are added and the magnetic separation is repeated. Next, fluorescent markers for DNA (4',6-diamidino-2-phenylindole: DAPI), antibodies directed to cytokeratins 8, 18, and 19 labeled to phycoerythrin (PE), and CD45 to allophycocyanin (APC) are added and the sample is left to incubate. After another magnetic separation step and more aspiration steps, the remaining 300 µL is transferred to the analysis cartridge, which is placed in a CellTracks MagNest® cell presentation device, see figure 3.3. This MagNest consists of two magnets that create an upward magnetic force, pulling the ferrofluid labeled cells to a cover slip within the cartridge. Simulated particle trajectories due to the magnetic field in the Magnest are shown in figure 3.4 [40], with the square box slightly underneath the magnets representing a cross section of the sample cartridge. As can be seen in figure 3.4, the magnets are designed in such a way that cells will move straight up; their distribution across the analysis surface is therefore homogeneous.

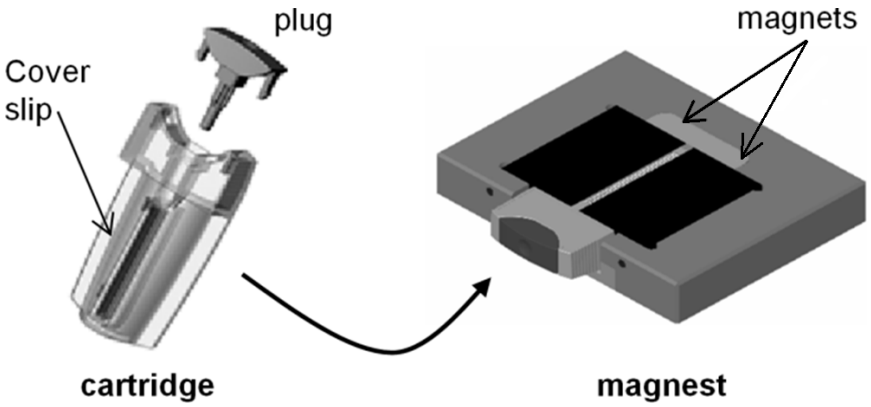

Figure 3.3: Analysis cartridge to which the enriched sample is transferred and magnest in which cells are magnetically pulled to the cover slip

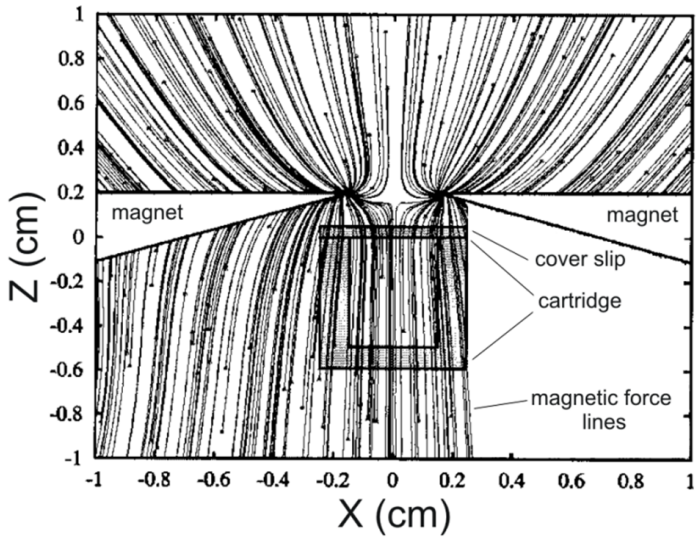

Figure 3.4: Simulation of magnetic particle trajectories inside the MagNest. *Adapted from [40]. Cells are pulled towards the cover slip inside the cartridge in a trajectory perpendicular to the cover slip. The force lines in the lower right part of the figure were erased for viewing purposes*

3.4 Imaging and enumeration of CTC with the Celltracks Analyzer

The CellTracks Analyzer is a semi-automated fluorescence microscope that is part of the CellSearch System. After the cells are settled, the MagNest is placed in the CellTracks Analyzer II, a semi-automatic epi-fluorescence microscope. Employing a mercury arc lamp, a 10X/0.45NA objective, the whole cartridge is scanned at four fluorescence channels: channels for the detection of DNA-DAPI, CK-PE, and CD45-APC, and a fourth channel termed "FITC". This fourth channel may be used for control cells or an extra biomarker, but is generally used to verify if objects are auto-fluorescent (and thus debris). Images are captured with a charge-coupled device (CCD) camera with an effective pixel size of 0.65 x 0.65 μm^2. When a scan is complete, the CellSearch software identifies objects that are positively stained for DNA and CK, and creates a thumbnail gallery showing these objects. Figure 3.5 shows an example of such a gallery. Next to the four fluorescence channels an overlay of the DAPI and PE channels is shown. A trained reviewer must now distinguish CTC from leukocytes and debris that were carried over during the enrichment procedure. The reviewers have a set of rules in determining whether an object is a CTC or not, which is shown in figure 3.6. These rules were set and tested by means of preclinical studies [41, 42, 43, 44]. By scoring the cells according to this set of rules, object A from figure 3.5 is a CTC next to a leukocyte. Object B are two bright CTC close together that have some spill-over signal in the CD45-APC channel. Object C fails rule 2 (and also has questionable morphology), and object D fails rule 5. Although these examples are relatively straightforward, not all images are unambiguous, as is exemplified by the two objects in E and F. These seem to be small cells and are a bit speckled suggesting that they are undergoing apoptosis [45]. When shown to reviewers, it was found that these objects give rise to the highest inter-reviewer variability. The variability for classification of CTC between reviewers was reported to be between 4% and 31% (median 14%), and a variability of 7.5% between laboratories [46]. The rules for qualifying objects are mostly quantitative, because a reviewer cannot view the number of grey levels in the image easily. Reviewers may therefore be biased by the auto-scaling of these images, which is done purely for viewing purposes. If a bright object is located near a dim object, this dim object may be classified wrongly due to this effect.

3.5 Immunomagnetic enrichment

For enrichment of the rare CTC a high recovery of the CTC and a low carryover of the blood cells is of utmost importance. In the CellSearch system the choice was made to use immunomagnetic enrichment of CTC. EpCAM was chosen as the antigen as it was expressed on the majority

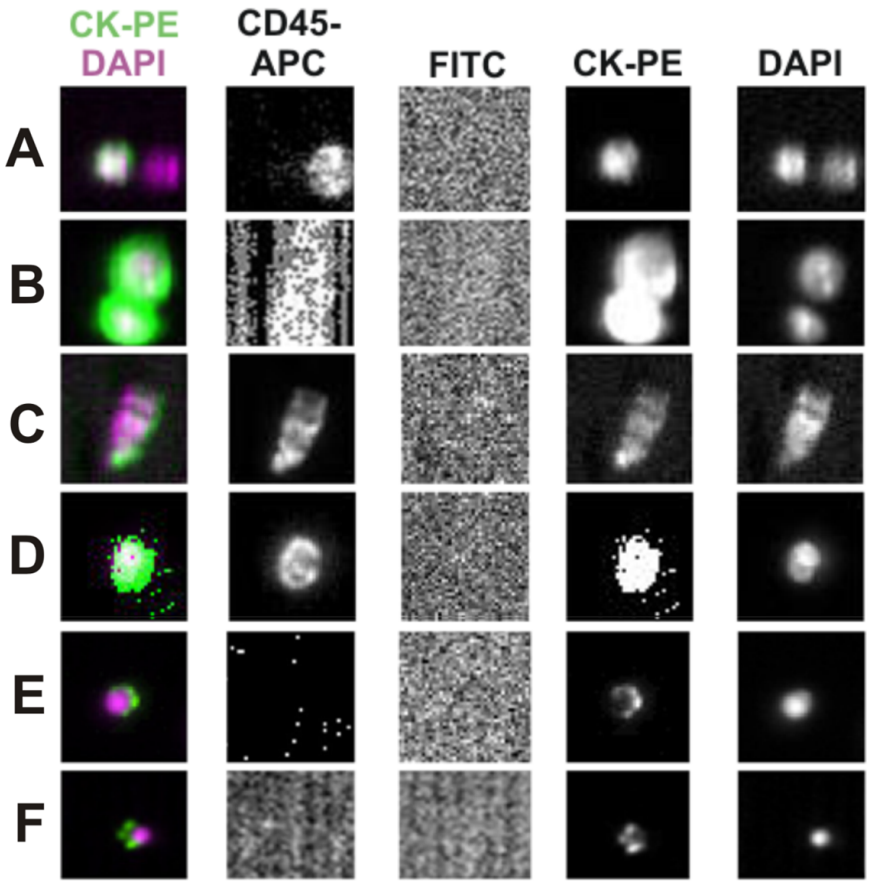

Figure 3.5: CellSearch thumbnail gallery. *The CellSearch software presents all objects that are both positive for CK and DAPI. Panels A–D show examples of CTC (A/B) and debris (C/D). Whether some of the cells encountered are CTC or not is questionable (E/F), and these lead to discrepancies between reviewers*

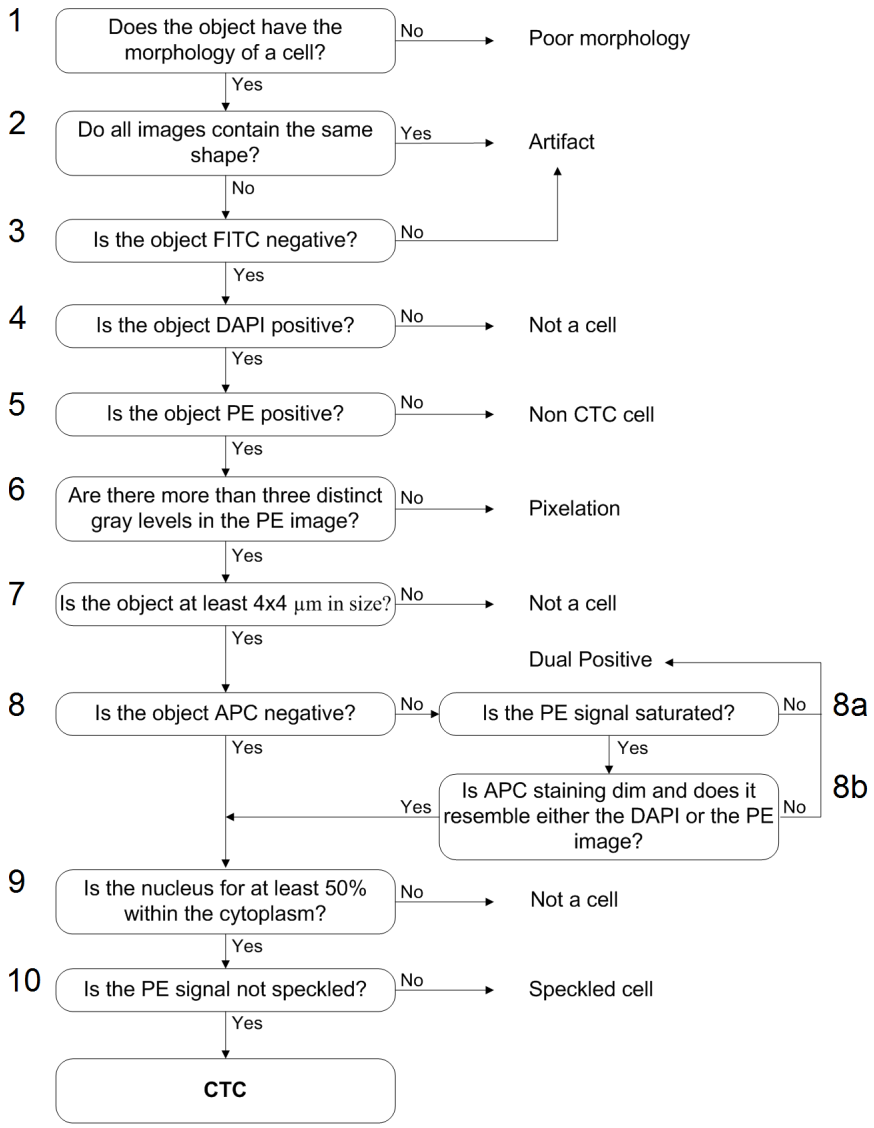

Figure 3.6: Decision tree showing how the trained reviewers classify whether or not an object is a CTC

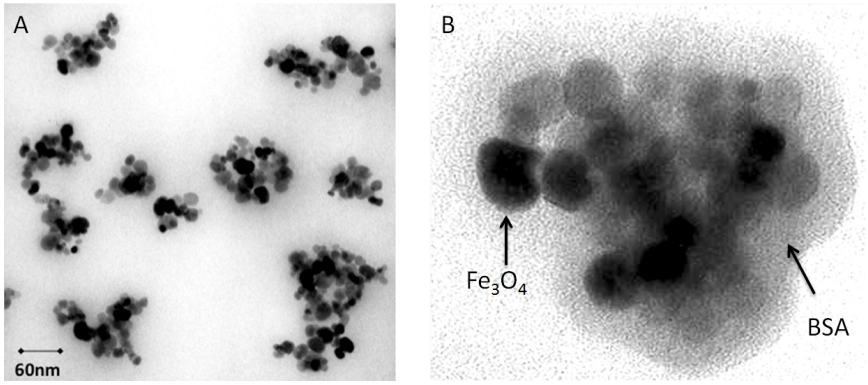

Figure 3.7: Ferrofluids visualized by electronic microscopy. *Panel B shows particles imaged at higher resolution than panel A. BSA: bovine serum albumin.*

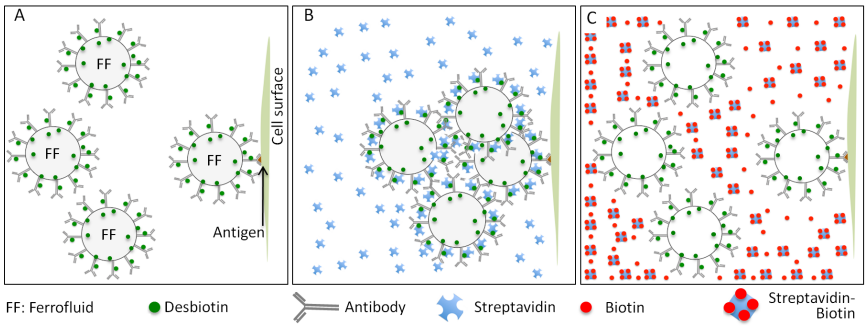

Figure 3.8: Transient increase in magnetic loading to improve the selection of CTC with low EpCAM expression. *Panel A: EpCAM desthiobiotinilated ferrofluid binds EpCAM antigen at the cell surface. The majority of ferrofluid particles remain in suspension because the bound ferrofluids sterically hinder the binding sites. Panel B: Streptavidin is added, recruiting unbound ferrofluids. This leads to an increase in magnetic loading per cell . Panel C: unconjugated biotin is added, which replaces the desthiobiotin in the streptaividin linkers. This results in a release of the recruited ferrofluids.*

of breast cancer carcinomas (table 3.1), and other carcinomas [10], it was not expressed on cells of hematopoietic origin and was expressed at the cell surface. Cell surface markers do not need cell permeabilization, which is needed for intracellular antigens such as cytokeratin. The drawback of the antibody approach is that CTC not expressing the target antigen will be missed. As magnetic particle the choice was made for ferrofluids with sub micron sized particles as they would not reduce the ability to visualize the cells as much as µm sized magnetic particles. However the ferrofluids need to have sufficient magnetic properties to be separated in an open magnetic field and avoid entrapment in mesh like structures. This base ferrofluid is made by sonification of magnetite while adding BSA under controlled conditions to arrive at an average particle size of 120 nm [47]. This ferrofluid consists of small clusters of Fe_3O_4 covered with BSA as illustrated in the electron micrographs in figure 3.7. The VU1D9 monoclonal antibody directed against the EpCAM antigen is conjugated by standard coupling chemistry to the ferrofluid [48]. Although this ferrofluid can be used to capture cells expressing the EpCAM antigen from blood it was noted that the recovery of cells with a relatively low EpCAM expression was considerably less as compared to those expressing larger densities of the EpCAM antigen [12]. To overcome this issue a process called "controlled aggregation" was developed which resulted in high cell recoveries along a larger range of antigen densities [12]. To achieve this the EpCAM ferrofluid is conjugated to desthiobiotin using N-hydroxysuccinimide-DL-desthiobiotin [49]. After addition of EpCAM desthiobiotin ferrofluid to the blood it will bind the EpCAM antigen at the cell surface (figure 3.8, panel A) upon addition of a buffer containing streptavidin more ferrofluids will bind to the cell surface (figure 3.8, panel B) thereby increasing the ability to separate the cells in a magnetic field and reduce variability of cell recovery due to variations in antigen densities [12]. After the enrichment has taken place a buffer can be added containing biotin, which will replace the desthiobiotin in the streptavidin and releases the additional ferrofluid from the cells (figure 3.8, panel C). Removal of the ferrofluid from the cells is needed to reduce attenuation of fluorescence signals from the cells by ferrofluid. This increases the ability to visualize the cells and thus aids in their identification. Aggregation of ferrofluid can also take place under the influence of plasma components in blood samples from some individuals. To reduce the influence of these factors the blood samples are diluted and the plasma is aspirated and discarded by the CellTracks Autoprep system. A ferrofluid that does not interact with plasma components is desirable because with the discard of the plasma the majority of tumor micro particles (TMP) that are contained within the plasma fraction cannot be captured [50, 51].

3.6 Detection of predicitve biomarkers on CTC

After identification of CTC, the presence of treatment targets on these CTC can be assessed. Expression of these targets may be used to prescribe therapies directed against these targets. Expression of cell surface or intracellular treatment target antigens can be assessed by addition of additional monoclonal antibodies labeled with fluorochromes not overlapping with the ones used for the identification of CTC. Examples are the expression of Her-2 [52, 53], uPAR [54] and IGF-1R [55, 56]. The ability to revisit the CTC in the CellSearch system provides the opportunity to examine the gene by fluorescence-in-situ-hybridization (FISH) [57] and investigate gene amplification of Her-2, AR, deletion of PTEN and rearrangement of ERG [58, 59]. Alternative approaches are the examination of gene expression by multiplex PCR. For this approach one can use an immunomagnetically enriched sample obtained after processing 7.5 mL whole blood by the CellTracks Autoprep profile kit (Veridex, Raritan, NJ, USA). This typically results in a 900 µL sample volume containing 1000 leukocytes and varying number of CTC. This material has been used successfully to detect the expression of numerous genes in CTC by multiplex PCR [60, 61, 62]. Drawback of this approach is that only genes can be examined that have no or low expression in leukocytes [61, 63]. A method that can deplete the residual leukocytes from a CTC enriched sample could increase the number of genes that can be examined by PCR methods. One such approach is the depletion of leukocytes by a CD45 depletion column. A concept for a depletion column is shown in figure 3.9, panel A. The sample with leukocytes and CTC is loaded onto the column, containing beads coated with the leukocyte specific antibody CD45. Leukocytes will be retained by the column while CTC pass through for further processing. The composition of the coating is illustrated in panel B of figure 3.9. On a glass substrate a layer of 3-aminopropyltriethoxysilane (APTES, Sigma Aldrich, St. Louis, USA) is formed. This layer covalently binds BSA-biotin molecules (Sigma Aldrich). Streptavidin (Thermo Fisher Scientific, Rockford, IL, USA) has four binding sites for biotin and is used as a linker between the BSA-biotin and biotinylated antibodies. When a cell expresses antigens to this antibody on the membrane, the cell can be captured. The construction of the depletion column is illustrated in panel C of figure 3.9. The container for the column consists of a 3 mL syringe barrel (BD, Franklin Lakes, NJ, USA). The substrate for the column consists of 210–300 µm soda lime glass beads (Sigma Aldrich); with maximum packing density this leaves gaps large enough for cells to pass between the beads (> 30 µm), while the coated surface area of a 2 mL column is approximately $113 \cdot 10^3\,\mathrm{mm}^2$. The beads are held in place on both ends by a nylon mesh (30 µm poresize, Spectrum Laboratories, Rancho Dominguez, CA, USA). The output flow rate of the column is controlled by squeezing a piece of flexible tubing (Tygon, Saint Gobain Plastics, Paris, France), which is connected to the output of the syringe. To test

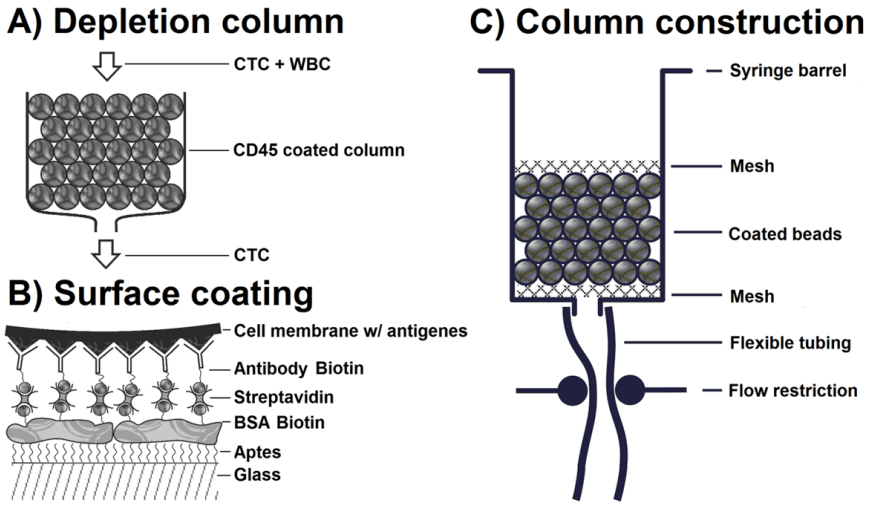

Figure 3.9: Design of a depletion column. *Panel A shows the concept of cell depletion on a column. The sample containing CTC and leukocytes is loaded onto the column, which is coated with CD45. The leukocytes are trapped while passing through the column, and CTC pass through and can be captured for further processing. Panel B shows the different layers the antibody coating is constructed of. The substrate is glass. The glass is coated with silane (APTES) to which BSA-biotin is covalently bound. The streptavidin binds to the biotin, which in turn binds a biotinilated antibody. Cells expressing the membrane antigens to the antibody are captured this way. Panel C shows the column construction. Antibody coated beads are contained in between two layers of mesh and the barrel of a syringe to keep the column in place. The flow rate is controlled by squeezing a short length of flexible tubing connected to the outlet of the syringe barrel.*

whether cells could indeed be efficiently passed through a column the beads in the column depicted in figure 3.9 were coated with BSA. Leukocytes were obtained after ammonium chloride lysing of whole blood and passed through the column at a flow rate of 0.85 mm/s in a volume of 1 mL at concentrations of $0.25 \cdot 10^6$, $1.00 \cdot 10^6$, $1.75 \cdot 10^6$ and $2.50 \cdot 10^6$ leukocytes/ mL.

Recovery was determined by centrifugation of the filtrate and resuspending the cells in 0.1 mL. This sample was then stained with 8 µmol Hoechst 33342 and enumerated on a counting chamber (Neubauer, Lauda-Königshofen, Germany). The results in figure 3.10 show a recovery of 92% minus an offset of 97.000 leukocytes. Inspection of the component parts of the functionalized column did not show any large accumulation of cells on the surface of the syringe barrel, nor on the mesh used to contain the beads.

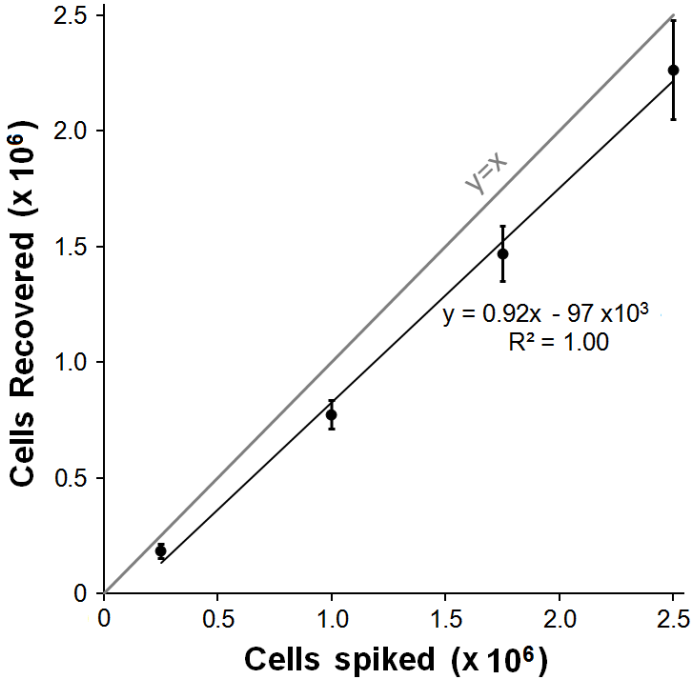

Figure 3.10: Leukocytes were passed through a column coated with BSA and their recovery was determined. *Whiskers indicate one standard deviation Poisson error. A linear fit shows 92% recovery combined with a large offset of 97.000 cells lost per sample.*

Inspection of the beads did not show many cells either, but due to the very large surface area of the beads it is not possible to exclude that the lost cells could be found on the beads. Although a recovery of 92% is not that bad for rare event detection, the offset of 97.000 leukocytes is worrisome. To investigate cell capture on coated surfaces a flow chamber was constructed. The bottom of the chamber was coated with two lanes of BSA-biotin, one lane of streptavidin, two lanes of mouse IgG monoclonal antibody specific for SKBR-3 culture cells and one blank as illustrated in panel A of figure 3.11. SKBR-3 cells were flowed through the chamber and the number of SKBR-3 cells captured on each lane is shown at the bottom of panel A. The fields with antibody captured an average of 36 cells while those without antibody captured an average of 17 cells. The antibody coated lanes do capture more cells than the lanes without antibody, but the non-specific capture is too large. The use of BSA to reduce non-specific adhesion is clearly not sufficient and either the coating needs to be improved by eliminating the "non-specific binding spots" or a different coating needs to be used that prevents cells from binding non-specifically. In panel B of figure

3.11 the Poiseuille flow and the flow velocity profile within this chamber is illustrated. To study the effect of flow on the capture, biotinylated beads were flowed through a flow chamber of which all lanes were coated with streptavidin. A few fragments of a video of the biotinylated beads flowing through the chamber at a maximum flow speed of 1.3 mm/s are shown in panel C of figure 3.11. The beads in the figure are labeled A–E. Bead A is decelerating, while bead B is accelerating. Bead C is attaching and did not move from the last position in the following 20 seconds, while bead D is already attached to the surface at the beginning of this movie fragment. Bead E has a higher speed (further from surface), and is therefore elongated and appears dimmer. While the beads at low speed manage to slow down and adhere to the surface, the fast beads appear to stay in the middle of the flow. This shows the importance of the flow profile of cells / beads passing a functionalized surface. Cells and beads in an aqueous media will have a low Reynolds number giving rise to laminar flow, which prevents contact with the functionalized area. Design of a flow chamber thus needs to be such that a maximum number of collisions between cells and the functionalized surface are obtained.

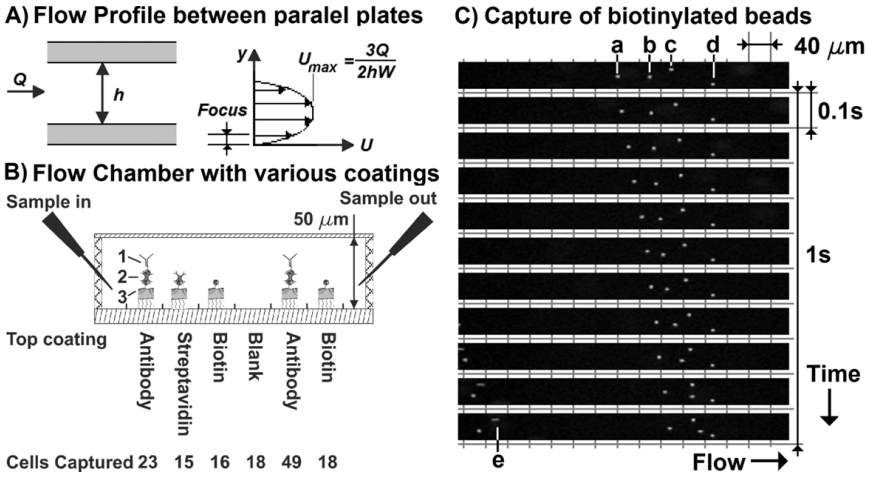

Figure 3.11: Capture of cells and beads in a flow chamber. *Panel A Shows a flow chamber with multiple coating regions, cartoons show which components are present on each area; BSA-biotin (1), streptavidin (2), biotinilated antibody (3). Cells which should be captured by the antibody were flowed through. The number of captured cells for each region are shown below the diagram. Panel B shows the Poiseuille flow between two parallel plates and the flow velocity (U) profile between the plates. The depth of focus of the microscope is shown on the right of the profile. Panel C shows a series of images taken of 1 μm biotinylated beads moving through a streptavidin coated flow chamber. Beads of interest are labeled with letters A–E.*

3.7 References

[1] M. B. Sporn, "The war on cancer," *Lancet*, vol. 347, pp. 1377–1381, May 1996.

[2] R. W. Carey, P. D. Taft, J. M. Bennett, and S. Kaufman, "Carcinocythemia (carcinoma cell leukemia). An acute leukemia-like picture due to metastatic carcinoma cells," *Am. J. Med.*, vol. 60, pp. 273–278, Feb 1976.

[3] H. C. Engell, "Cancer cells in the circulating blood; a clinical study on the occurrence of cancer cells in the peripheral blood and in venous blood draining the tumour area at operation," *Ugeskr. Laeg.*, vol. 117, pp. 822–823, Jun 1955.

[4] M. V. Gallivan and J. J. Lokich, "Carcinocythemia (carcinoma cell leukemia). Report of two cases with English literature review," *Cancer*, vol. 53, pp. 1100–1102, Mar 1984.

[5] R. L. Myerowitz, P. A. Edwards, and G. P. Sartiano, "Carcinocythemia (carcinoma cell leukemia) due to metastatic carcinoma of the breast: report of a case," *Cancer*, vol. 40, pp. 3107–3111, Dec 1977.

[6] L. T. Yam and A. J. Janckila, "Immunocytodiagnosis of carcinocythemia in disseminated breast cancer," *Acta Cytol.*, vol. 31, pp. 68–72, 1987.

[7] W. J. Allard, J. Matera, M. C. Miller, M. Repollet, M. C. Connelly, C. Rao, A. G. Tibbe, J. W. Uhr, and L. W. Terstappen, "Tumor cells circulate in the peripheral blood of all major carcinomas but not in healthy subjects or patients with nonmalignant diseases," *Clin. Cancer Res.*, vol. 10, pp. 6897–6904, Oct 2004.

[8] F. Coumans, S. T. Ligthart, and L. W. M. Terstappen, "Challenges in the enumeration and phenotyping of CTC," *Clinical Cancer Research*, 2012.

[9] D. Herlyn, M. Herlyn, A. H. Ross, C. Ernst, B. Atkinson, and H. Koprowski, "Efficient selection of human tumor growth-inhibiting monoclonal antibodies," *J. Immunol. Methods*, vol. 73, pp. 157–167, Oct 1984.

[10] F. Momburg, G. Moldenhauer, G. J. Hammerling, and P. Moller, "Immunohistochemical study of the expression of a Mr 34,000 human epithelium-specific surface glycoprotein in normal and malignant tissues," *Cancer Res.*, vol. 47, pp. 2883–2891, Jun 1987.

[11] S. Szala, M. Froehlich, M. Scollon, Y. Kasai, Z. Steplewski, H. Koprowski, and A. J. Linnenbach, "Molecular cloning of cDNA for the carcinoma-associated antigen GA733-2," *Proc. Natl. Acad. Sci. U.S.A.*, vol. 87, pp. 3542–3546, May 1990.

[12] C. G. Rao, D. Chianese, G. V. Doyle, M. C. Miller, T. Russell, R. A. Sanders, and L. W. Terstappen, "Expression of epithelial cell adhesion molecule in carcinoma cells present in blood and primary and metastatic tumors," *Int. J. Oncol.*, vol. 27, pp. 49–57, Jul 2005.

[13] W. W. Franke, E. Schmid, M. Osborn, and K. Weber, "Intermediate-sized filaments of human endothelial cells," *J. Cell Biol.*, vol. 81, pp. 570–580, Jun 1979.

[14] R. Moll, W. W. Franke, D. L. Schiller, B. Geiger, and R. Krepler, "The catalog of human cytokeratins: patterns of expression in normal epithelia, tumors and cultured cells," *Cell*, vol. 31, pp. 11–24, Nov 1982.

[15] V. Barak, H. Goike, K. W. Panaretakis, and R. Einarsson, "Clinical utility of cytokeratins as tumor markers," *Clin. Biochem.*, vol. 37, pp. 529–540, Jul 2004.

[16] C. Griwatz, B. Brandt, G. Assmann, and K. S. Zanker, "An immunological enrichment method for epithelial cells from peripheral blood," *J. Immunol. Methods*, vol. 183, pp. 251–265, Jun 1995.

[17] G. Vona, A. Sabile, M. Louha, V. Sitruk, S. Romana, K. Schutze, F. Capron, D. Franco, M. Pazzagli, M. Vekemans, B. Lacour, C. Brechot, and P. Paterlini-Brechot, "Isolation by size of epithelial tumor cells : a new method for the immunomorphological and molecular characterization of circulating tumor cells," *Am. J. Pathol.*, vol. 156, pp. 57–63, Jan 2000.

[18] S. Nagrath, L. V. Sequist, S. Maheswaran, D. W. Bell, D. Irimia, L. Ulkus, M. R. Smith, E. L. Kwak, S. Digumarthy, A. Muzikansky, P. Ryan, U. J. Balis, R. G. Tompkins, D. A. Haber, and M. Toner, "Isolation of rare circulating tumour cells in cancer patients by microchip technology," *Nature*, vol. 450, pp. 1235–1239, Dec 2007.

[19] C. Alix-Panabieres, J. P. Brouillet, M. Fabbro, H. Yssel, T. Rousset, T. Maudelonde, G. Choquet-Kastylevsky, and J. P. Vendrell, "Characterization and enumeration of cells secreting tumor markers in the peripheral blood of breast cancer patients," *J. Immunol. Methods*, vol. 299, pp. 177–188, Apr 2005.

[20] P. R. Gascoyne, J. Noshari, T. J. Anderson, and F. F. Becker, "Isolation of rare cells from cell mixtures by dielectrophoresis," *Electrophoresis*, vol. 30, pp. 1388–1398, Apr 2009.

[21] J. P. Gleghorn, E. D. Pratt, D. Denning, H. Liu, N. H. Bander, S. T. Tagawa, D. M. Nanus, P. A. Giannakakou, and B. J. Kirby, "Capture of circulating tumor cells from whole blood of prostate cancer patients using geometrically enhanced differential immunocapture (GEDI) and a prostate-specific antibody," *Lab Chip*, vol. 10, pp. 27–29, Jan 2010.

[22] H. J. Kahn, A. Presta, L. Y. Yang, J. Blondal, M. Trudeau, L. Lickley, C. Holloway, D. R. McCready, D. Maclean, and A. Marks, "Enumeration of circulating tumor cells in the blood of breast cancer patients after filtration enrichment: correlation with disease stage," *Breast Cancer Res. Treat.*, vol. 86, pp. 237–247, Aug 2004.

[23] R. T. Krivacic, A. Ladanyi, D. N. Curry, H. B. Hsieh, P. Kuhn, D. E. Bergsrud, J. F. Kepros, T. Barbera, M. Y. Ho, L. B. Chen, R. A. Lerner, and R. H. Bruce, "A rare-cell detector for cancer," *Proc. Natl. Acad. Sci. U.S.A.*, vol. 101, pp. 10501–10504, Jul 2004.

[24] R. Konigsberg, E. Obermayr, G. Bises, G. Pfeiler, M. Gneist, F. Wrba, M. de Santis, R. Zeillinger, M. Hudec, and C. Dittrich, "Detection of EpCAM positive and negative circulating tumor cells in metastatic breast cancer patients," *Acta Oncol*, vol. 50, pp. 700–710, Jun 2011.

[25] S. J. Tan, R. L. Lakshmi, P. Chen, W. T. Lim, L. Yobas, and C. T. Lim, "Versatile label free biochip for the detection of circulating tumor cells from peripheral blood in cancer patients," *Biosens Bioelectron*, vol. 26, pp. 1701–1705, Dec 2010.

[26] S. Riethdorf, H. Fritsche, V. Muller, T. Rau, C. Schindibeck, B. Rack, W. Janni, C. Coith, K. Beck, F. Janicke, S. Jackson, T. Gornet, M. Cristofanilli, and K. Pantel, "Detection of circulating tumor cells in peripheral blood of patients with metastatic breast cancer: A validation study of the CellSearch system," *Clinical Cancer Research*, vol. 13, pp. 920–928, 2007.

[27] M. Cristofanilli, G. T. Budd, M. J. Ellis, A. Stopeck, J. Matera, M. C. Miller, J. M. Reuben, G. V. Doyle, W. J. Allard, L. W. Terstappen, and D. F. Hayes, "Circulating tumor cells, disease progression, and survival in metastatic breast cancer," *N. Engl. J. Med.*, vol. 351, pp. 781–791, Aug 2004.

[28] S. J. Cohen, C. J. Punt, N. Iannotti, B. H. Saidman, K. D. Sabbath, N. Y. Gabrail, J. Picus, M. Morse, E. Mitchell, M. C. Miller, G. V. Doyle, H. Tissing, L. W. Terstappen, and N. J. Meropol, "Relationship of circulating tumor cells to tumor response, progression-free survival, and overall survival in patients with metastatic colorectal cancer," *J. Clin. Oncol.*, vol. 26, pp. 3213–3221, Jul 2008.

[29] J. S. de Bono, H. I. Scher, R. B. Montgomery, C. Parker, M. C. Miller, H. Tissing, G. V. Doyle, L. W. Terstappen, K. J. Pienta, and D. Raghavan, "Circulating tumor cells predict survival benefit from treatment in metastatic castration-resistant prostate cancer," *Clin. Cancer Res.*, vol. 14, pp. 6302–6309, Oct 2008.

[30] H. I. Scher, X. Y. Jia, J. S. de Bono, M. Fleisher, K. J. Pienta, D. Raghavan, and G. Heller, "'Circulating tumour cells as prognostic markers in progressive, castration-resistant prostate cancer: a reanalysis of IMMC38 trial data," *Lancet Oncology*, vol. 10, pp. 233–239, 2009.

[31] F. A. Coumans, C. J. Doggen, G. Attard, J. S. de Bono, and L. W. Terstappen, "All circulating EpCAM+CK+CD45- objects predict overall survival in castration-resistant prostate cancer," *Ann. Oncol.*, vol. 21, pp. 1851–1857, Sep 2010.

[32] M. G. Krebs, R. Sloane, L. Priest, L. Lancashire, J. M. Hou, A. Greystoke, T. H. Ward, R. Ferraldeschi, A. Hughes, G. Clack, M. Ranson, C. Dive, and F. H. Blackhall, "Evaluation and prognostic significance of circulating tumor cells in patients with non-small-cell lung cancer," *Journal of Clinical Oncology*, vol. 29, pp. 1556–1563, 2011.

[33] F. Tanaka, K. Yoneda, N. Kondo, M. Hashimoto, T. Takuwa, S. Matsumoto, Y. Okumura, S. Rahman, N. Tsubota, T. Tsujimura, K. Kuribayashi, K. Fukuoka, T. Nakano, and S. Hasegawa, "Circulating tumor cell as a diagnostic marker in primary lung cancer," *Clin. Cancer Res.*, vol. 15, pp. 6980–6986, Nov 2009.

[34] M. S. Khan, T. Tsigani, M. Rashid, J. S. Rabouhans, D. Yu, T. V. Luong, M. Caplin, and T. Meyer, "Circulating tumor cells and EpCAM expression in neuroendocrine tumors," *Clin. Cancer Res.*, vol. 17, pp. 337–345, Jan 2011.

[35] S. Matsusaka, K. Chin, M. Ogura, M. Suenaga, E. Shinozaki, Y. Mishima, Y. Terui, N. Mizunuma, and K. Hatake, "Circulating tumor cells as a surrogate marker for determining response to chemotherapy in patients with advanced gastric cancer," *Cancer Science*, vol. 101, pp. 1067–1071, 2010.

[36] M. Rink, F. K. Chun, S. Minner, M. Friedrich, O. Mauermann, H. Heinzer, H. Huland, M. Fisch, K. Pantel, and S. Riethdorf, "Detection of circulating tumour cells in peripheral blood of patients with advanced non-metastatic bladder cancer," *BJU Int.*, vol. 107, pp. 1668–1675, May 2011.

[37] A. Poveda, S. B. Kaye, R. McCormack, S. Wang, T. Parekh, D. Ricci, C. A. Lebedinsky, J. C. Tercero, P. Zintl, and B. J. Monk, "Circulating tumor cells predict progression free survival and overall survival in patients with relapsed/recurrent advanced ovarian cancer," *Gynecol. Oncol.*, vol. 122, pp. 567–572, Sep 2011.

[38] S. Ligthart, F. Coumans, G. Attard, A. Cassidy, J. de Bono, and L. Terstappen, "Unbiased and automated identification of a circulating tumour cell definition that associates with overall survival," *PloS one*, vol. 6, no. 11, p. e27419, 2011.

[39] A. G. Tibbe, M. C. Miller, and L. W. Terstappen, "Statistical considerations for enumeration of circulating tumor cells," *Cytometry A*, vol. 71, pp. 154–162, Mar 2007.

[40] A. G. Tibbe, B. G. de Grooth, J. Greve, G. J. Dolan, C. Rao, and L. W. Terstappen, "Magnetic field design for selecting and aligning immunomagnetic labeled cells," *Cytometry*, vol. 47, pp. 163–172, Mar 2002.

[41] M. Kagan, D. Howard, T. Bendele, J. Mayes, J. Silvia, M. Repollet, J. Doyle, J. Allard, N. Tu, T. Bui, T. Russell, C. Rao, M. Hermann, H. Rutner, and L. Terstappen, "A sample preparation and analysis system for identification of circulating tumor cells," *J Clinical Ligand Assay*, vol. 25, pp. 104–50, 2002.

[42] J. G. Moreno, S. M. O'Hara, S. Gross, G. Doyle, H. Fritsche, L. G. Gomella, and L. W. Terstappen, "Changes in circulating carcinoma cells in patients with metastatic prostate cancer correlate with disease status," *Urology*, vol. 58, pp. 386–392, Sep 2001.

[43] E. Racila, D. Euhus, A. J. Weiss, C. Rao, J. McConnell, L. W. Terstappen, and J. W. Uhr, "Detection and characterization of carcinoma cells in the blood," *Proc. Natl. Acad. Sci. U.S.A.*, vol. 95, pp. 4589–4594, Apr 1998.

[44] L. W. Terstappen, C. Rao, S. Gross, and A. J. Weiss, "Peripheral blood tumor cell load reflects the clinical activity of the disease in patients with carcinoma of the breast," *Int. J. Oncol.*, vol. 17, pp. 573–578, Sep 2000.

[45] C. J. Larson, J. G. Moreno, K. J. Pienta, S. Gross, M. Repollet, S. M. O'hara, T. Russell, and L. W. Terstappen, "Apoptosis of circulating tumor cells in prostate cancer patients," *Cytometry A*, vol. 62, pp. 46–53, Nov 2004.

[46] J. Kraan, S. Sleijfer, M. H. Strijbos, M. Ignatiadis, D. Peeters, J. Y. Pierga, F. Farace, S. Riethdorf, T. Fehm, L. Zorzino, A. G. Tibbe, M. Maestro, R. Gisbert-Criado, G. Denton, J. S. de Bono, C. Dive, J. A. Foekens, and J. W. Gratama, "External quality assurance of circulating tumor cell enumeration using the CellSearch system: a feasibility study," *Cytometry B Clin Cytom*, vol. 80, pp. 112–118, Mar 2011.

[47] P. Liberti, G. Rao, and J. Chiarappa, "Methods for the manufacture of magnetically responsive particles," US patent 5698271, December 1997.

[48] L. Terstappen, G. Rao, J. Uhr, E. Racila, and P. Liberti, "Methods and reagents for the rapid and efficient isolation of circulating cancer cells," US patent 7332288, February 2008.

[49] P. Liberti, G. Rao, and L. Terstappen, "Increased separation efficiency via controlled aggregation of magnetic nanoparticles," US patent 5698271, September 2003.

[50] T. Pawlowski, R. Akhavan, A. Tasinato, M. Millis, Y. Kojima, J. S. Zhong, and C. Kuslich, "Expression of Mir-497 in circulating microvesicles is a potential biomarker for the early detection of NSCLC," *J. Thoracic Oncol.*, vol. 6, pp. S1079–S1080, Jun 2011.

[51] E. van der Pol, A. G. Hoekstra, A. Sturk, C. Otto, T. G. van Leeuwen, and R. Nieuwland, "Optical and non-optical methods for detection and characterization of microparticles and exosomes," *J. Thromb. Haemost.*, vol. 8, pp. 2596–2607, Dec 2010.

[52] D. F. Hayes, T. M. Walker, B. Singh, E. S. Vitetta, J. W. Uhr, S. Gross, C. Rao, G. V. Doyle, and L. W. Terstappen, "Monitoring expression of HER-2 on circulating epithelial cells in patients with advanced breast cancer," *Int. J. Oncol.*, vol. 21, pp. 1111–1117, Nov 2002.

[53] S. Riethdorf, V. Muller, L. Zhang, T. Rau, S. Loibl, M. Komor, M. Roller, J. Huober, T. Fehm, I. Schrader, J. Hilfrich, F. Holms, H. Tesch, H. Eidtmann, M. Untch, G. von Minckwitz, and K. Pantel, "Detection and HER2 expression of circulating tumor cells: prospective monitoring in breast cancer patients treated in the neoadjuvant GeparQuattro trial," *Clin. Cancer Res.*, vol. 16, pp. 2634–2645, May 2010.

[54] S. Meng, D. Tripathy, S. Shete, R. Ashfaq, H. Saboorian, B. Haley, E. Frenkel, D. Euhus, M. Leitch, C. Osborne, E. Clifford, S. Perkins, P. Beitsch, A. Khan, L. Morrison, D. Herlyn, L. W. Terstappen, N. Lane, J. Wang, and J. Uhr, "uPAR and HER-2 gene status in individual breast cancer cells from blood and tissues," *Proc. Natl. Acad. Sci. U.S.A.*, vol. 103, pp. 17361–17365, Nov 2006.

[55] D. D. Karp, M. N. Pollak, R. B. Cohen, P. D. Eisenberg, P. Haluska, D. Yin, A. Lipton, L. Demers, K. Leitzel, M. L. Hixon, L. W. Terstappen, L. Garland, L. G. Paz-Ares, F. Cardenal, C. J. Langer, and A. Gualberto, "Safety, pharmacokinetics, and pharmacodynamics of the insulin-like growth factor type 1 receptor inhibitor figitumumab (CP-751,871) in combination with paclitaxel and carboplatin," *J Thorac Oncol*, vol. 4, pp. 1397–1403, Nov 2009.

[56] J. S. de Bono, G. Attard, A. Adjei, M. N. Pollak, P. C. Fong, P. Haluska, L. Roberts, C. Melvin, M. Repollet, D. Chianese, M. Connely, L. W. Terstappen, and A. Gualberto, "Potential applications for circulating tumor cells expressing the insulin-like growth factor-I receptor," *Clin. Cancer Res.*, vol. 13, pp. 3611–3616, Jun 2007.

[57] J. F. Swennenhuis, A. G. Tibbe, R. Levink, R. C. Sipkema, and L. W. Terstappen, "Characterization of circulating tumor cells by fluorescence in situ hybridization," *Cytometry A*, vol. 75, pp. 520–527, Jun 2009.

[58] G. Attard, J. F. Swennenhuis, D. Olmos, A. H. Reid, E. Vickers, R. A'Hern, R. Levink, F. Coumans, J. Moreira, R. Riisnaes, N. B. Oommen, G. Hawche, C. Jameson, E. Thompson, R. Sipkema, C. P. Carden, C. Parker, D. Dearnaley, S. B. Kaye, C. S. Cooper, A. Molina, M. E. Cox, L. W. Terstappen, and J. S. de Bono, "Characterization of ERG, AR and PTEN gene status in circulating tumor cells from patients with castration-resistant prostate cancer," *Cancer Res.*, vol. 69, pp. 2912–2918, Apr 2009.

[59] S. Meng, D. Tripathy, S. Shete, R. Ashfaq, B. Haley, S. Perkins, P. Beitsch, A. Khan, D. Euhus, C. Osborne, E. Frenkel, S. Hoover, M. Leitch, E. Clifford, E. Vitetta, L. Morrison, D. Herlyn, L. W. Terstappen, T. Fleming, T. Fehm, T. Tucker, N. Lane, J. Wang, and J. Uhr, "HER-2 gene amplification can be acquired as breast cancer progresses," *Proc. Natl. Acad. Sci. U.S.A.*, vol. 101, pp. 9393–9398, Jun 2004.

[60] S. M. O'Hara, J. G. Moreno, D. R. Zweitzig, S. Gross, L. G. Gomella, and L. W. Terstappen, "Multigene reverse transcription-PCR profiling of circulating tumor cells in hormone-refractory prostate cancer," *Clin. Chem.*, vol. 50, pp. 826–835, May 2004.

[61] D. A. Smirnov, B. W. Foulk, G. V. Doyle, M. C. Connelly, L. W. Terstappen, and S. M. O'Hara, "Global gene expression profiling of circulating endothelial cells in patients with metastatic carcinomas," *Cancer Res.*, vol. 66, pp. 2918–2922, Mar 2006.

[62] A. M. Sieuwerts, J. Kraan, J. Bolt, P. van der Spoel, F. Elstrodt, M. Schutte, J. W. Martens, J. W. Gratama, S. Sleijfer, and J. A. Foekens, "Anti-epithelial cell adhesion molecule antibodies and the detection of circulating normal-like breast tumor cells," *J. Natl. Cancer Inst.*, vol. 101, pp. 61–66, Jan 2009.

[63] M. Kowalewska, M. Chechlińska, S. Markowicz, P. Kober, and R. Nowak, "The relevance of RT-PCR detection of disseminated tumour cells is hampered by the expression of markers regarded as tumour-specific in activated lymphocytes," *Eur. J. Cancer*, vol. 42, pp. 2671–2674, Nov 2006.

CHAPTER 4

All circulating EpCAM+CK+CD45- objects predict overall survival in castration resistant prostate cancer

F.A.W. Coumans, C.J.M. Doggen, G.W. Attard, J.S. de Bono, L.W.M.M. Terstappen

Annals of Oncology 21: 1851 – 1857, 2010

Abstract

Presence of ≥ 5 circulating tumor cells (CTC) in patients with metastatic carcinomas is associated with poor survival. Although many objects positive for epithelial cell adhesion molecules and cytokeratin (EpCAM+CK+) are not counted as CTC, they may be an important predictor for survival. We evaluated the association between these objects and survival in patients with prostate cancer. Included in this follow-up study were 179 patients with castration-resistant prostate cancer. CellSearch was used to isolate EpCAM+ objects and to stain DNA, cytokeratin and CD45. All EpCAM+CK+ objects were subdivided into 7 classes based on pre-defined morphology in 63 independent samples. Association of each class with survival was studied using Kaplan-Meier and Cox regression analyses. Each EPCAM+CK+CD45- class showed a strong association with overall survival ($p < 0.001$). This included small tumor micro particles(S-TMP), which did not require a nucleus and thus are unable

to metastasize. A higher number of objects in any class was associated with decreased survival. A good prediction model included large tumor cell fragments (L-TCF), age, hemoglobin and lactate dehydrogenase. Models with S-TMP or CTC instead of L-TCF performed similarly. EpCAM+CK+CD45- that do not meet strict definitions for CTC are strong prognostic markers for survival.

4.1 Background

Tumor cells that shed into the blood during metastasis have the potential to become generic biomarkers for many cancers. Considerable technological efforts have been made over the past two decades to develop platforms that reliably identify and count circulating tumor cells (CTC). The CellSearch system has demonstrated in multicenter, prospective studies that the presence of ≥ 5 CTC identified using the CellSearch system was associated with reduced overall survival in pre- and on treatment patients with metastatic breast, metastatic colorectal, and castration resistant prostate (CRPC) cancer [1, 2, 3, 4, 5, 6, 7, 8]. In these studies a CTC was defined as a nucleated object that was positive for epithelial cell adhesion molecule (EpCAM+) and cytokeratin 8, 18 or 19 (CK+) and negative for CD45 (CD45-), was at least 4 x 4 μm^2 in size and had specific morphological and immunological features identified by trained operators [9, 10]. Enriched were all objects with $\geq$ 2000 EpCAM antigens [11]. The frequency of objects classified as CTC ranged from 0–10,000/7.5 mL of blood and approximately a third of patients with advanced breast, colorectal or prostate cancer did not have any circulating objects that met these criteria. High CTC heterogeneity was observed and could result in inter-operator error in CTC counting [10, 12, 13]. Although only intact and viable CTC have the potential to form metastases, the presence of apoptotic CTC or other epithelial objects in blood could have independent prognostic relevance. Alternative technologies utilizing less stringent criteria for counting CTC have reported substantially larger numbers of CTC [14, 15, 16, 17, 18, 19, 20, 21, 22, 23, 24]. As an increasing number of clinical studies now incorporate the evaluation of CTC in their design, it has become critical that the definition of what constitutes a CTC is clarified and that the different EpCAM+ objects that are detected using CellSearch are more thoroughly studied. To address this issue, images of all EpCAM+CK+ objects previously acquired during a CTC study in CRPC patients, were reanalyzed to evaluate the relationship between different EpCAM+CK+ classes and overall survival.

4.2 Patients and Methods

4.2.1 Patients and Data Collection

Samples were collected from castration-resistant prostate cancer (CRPC) patients enrolled in a prospective, multi-center clinical trial, IMMC-38 [8]. The primary aim of this study was to investigate the association between the presence of ≥ 5 CTC identified using CellSearch prior to the start of first or later lines of cytotoxic chemotherapy and overall survival in advanced CRPC patients. Patients with histologically confirmed prostate cancer that was metastatic and progressing despite castrate levels of testosterone (< 50 ng/ mL) and who were commencing a new cytotoxic therapy were eligible. Other eligibility criteria included a PSA level of ≥ 5 ng/ mL; ECOG performance status of 0 to 2; a 4-week (6 weeks for nilutamide, bicalutamide) washout after discontinuation of an active treatment, and no radiation or radionuclide therapy within 30 days of entry into the study. Patients with brain metastases or a history of other malignancies within the last 5 years were excluded. Sixty-five clinical centers in the United States and Europe participated. A total of 276 CRPC patients were enrolled into the original study [8]. 42 patients were excluded as they did not meet one or more of the listed eligibility criteria. Three patients met the eligibility criteria, but the CDs with image data were unreadable. For 179 patients, samples from baseline and a first follow-up were available and a bone scan was performed. The baseline data of these 179 patients was used as a validation data set. The 55 remaining patients were missing either a baseline (22), a follow up sample (25) or a bone scan (8). Some patients missing a bone scan supplied two samples; the 63 samples from these patients were used for development of the classification. The study design for the original study has been described in detail elsewhere [8]. Briefly, blood (7.5 mL) was collected into a CellSaveTM tube (Veridex LLC, Raritan, NJ) before and every 4 weeks after starting a new cytotoxic treatment and shipped to a central laboratory where isolation and enumeration of CTC was performed using CellSearch. Samples were also analyzed for serum PSA, lactate dehydrogenase (LDH), alkaline phosphatase (ALP), testosterone, albumin and hemoglobin. Samples from 67 healthy individuals used in previous studies [5] were also analyzed to assess the background level for each of the classes of objects studied. All patients consented to trial protocols that had been approved by ethics review committees at the participating centers.

4.2.2 Isolation of EpCAM+ objects

Isolation and image capture of EPCAM+ objects was performed using the CellSearch system (Veridex Raritan, NJ). The system consists of a CellTracks Autoprep for sample preparation and a CellTracks Analyzer II for sample analysis [9, 10, 12]. The CellTracks Autoprep immunomagnetically

enriches epithelial cells from 7.5 mL of blood using ferrofluids coated with epithelial cell specific EpCAM antibodies and stains the enriched samples with phycoerythrin conjugated antibodies directed against cytokeratins 8, 18 and 19, an allophycocyanin conjugated antibody to CD45 and the nuclear dye DAPI. The CellTracks Analyzer II is a four-color semi-automated fluorescence microscope that captures digital images of the entire surface of the cartridge for four different fluorescent dyes. From the captured images, a gallery of objects is presented to a trained operator who makes a final interpretation for each object.

4.2.3 Reanalysis of captured images

Images were imported into the Linux software of the CellTracks Analyzer II. The automated algorithm in this software was used to identify objects that were positive for CK and/or DAPI. The algorithm identified objects at least 2 x 2 μm^2 in size and of medium to high contrast in the DAPI and/or CK channels. If more than one channel was selected for analysis, objects in the selected channels had to be connected in order to be selected. Two sets of analysis were performed. In one set, objects with CK and DAPI staining were presented to the reviewer; in the other set objects with only CK staining were presented. Monochrome images revealed staining in DAPI, CK and CD45 channels as well as a false color overlay of DAPI and CK to show degree of overlap between channels. A single operator assigned objects to the 7 classes presented in this study for all samples, the CellSearch CTC numbers were taken from the IMMC-38 study. Inter operator variability could not be established, but is expected to be comparable to the inter operator variability for CTC [12]. The human reviewer was blinded to all sample information. After a total of 150 objects were assigned to a class, the results were extrapolated to calculate the total number of objects in the sample for each class.

4.2.4 Statistical Analysis

The primary endpoint was overall survival, measured as the time from the date of the first CTC blood draw (baseline) to date of death from any cause. Patients who were lost to follow-up or still alive at the end of study were censored at the last date they were known to be alive or at the end of study date. 63 samples were selected for use as an independent data set. 7 EpCAM+CK+ classes were defined using this data set. Every EpCAM+CK+ class was then categorized into four groups of similar number to optimize the power of this analysis [25]. The group boundaries for each class were set on the 25, 50 and 75 percentile of the independent data set (Group 1 (G1) was 0–25%; G2, 26–50%; G3, 51–75%; G4, 76–100%). The group (G1) with the lowest number of objects (lowest density) was used as the reference for calculation of hazard ratios. Serum data were

also categorized into four groups using the data for the samples in the independent set. For all classes, overall survival was calculated using the Kaplan-Meier method and survival plots were generated. Log-rank tests were used to compare survival between groups. Cox regression models were used to determine hazard ratios (HR) of death for the different groups within each class with the appropriate 95% confidence intervals (95% CI). Age was included as a continuous variable in all Cox regression models. Correlation between EpCAM+CK+ classes was determined using a two tailed Spearman's Rho test. As several classes were highly correlated (see results), the final multivariate model was built by starting with a full model including all prognostic variables from the univariate analyses. In each successive step one variable was deleted, and the new model compared to the former model, using the likelihood ratio test with the appropriate degrees of freedom to obtain a parsimonious model. The final model was confirmed by using forward conditional Cox regression analyses (p-in 0.05 and p-out 0.10). In this final model the variable with the highest impact was replaced by all other variables to test whether any could replace the highest impact variable without degrading the model. Race and processing site were also available, but did not contribute to survival and therefore were not included in any model. Statistical analysis was performed in SPSS Windows version 16.0 (SPSS Inc., Chicago, IL, USA).

4.3 Results

4.3.1 Patient characteristics

For the 179 patients in the validation set, baseline blood draw was performed between October 2004 and February 2006. If possible, patients were followed up to a visit with the oncologist in the 35^{th}–39^{th} month. Median duration of follow up was 16 months (range 0.2–38.7 months). Overall 134 (75%) patients died during follow-up. Their average age was 70 years (range 49–92 years), 138 (77%) were treated in the USA (41, 23% in Europe). Most patients (120, 67%) were starting first line cytotoxic therapy after baseline, while 29 (16%) were going on second line and the remaining 30 (17%) started 3^{rd}–6^{th} line therapy. The cytotoxic therapy included Docetaxel for 129 (72%) patients and Mitoxantrone for 17 (9%) patients. Metastasis to the bones were found in 158 (88%) of patients. Descriptive statistics for serum markers can be found in table 4.1.

4.3.2 CellSearch identifies different classes of circulating EpCAM+ objects

Samples from the 63 patients assigned to the independent set were used to define the criteria for classification of EpCAM+ classes. We assumed that only a few CTC had the ability to form metastasis, and the majority of

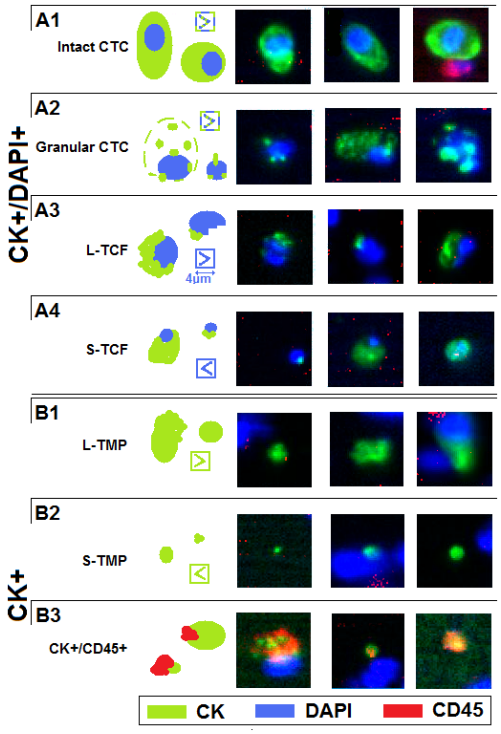

Figure 4.1: Representation and three typical false-color images of the seven CTC classes. *Green represents the cytokeratin-phycoerythrin staining; the blue, the DAPI staining and the red, the CD45 staining. The cartoons show the classification rules explained in the text. All classes except CK+/ CD45+ were CD45 negative. In the first analysis (panel A) that included both CK and DAPI staining, the four distinct classes of EpCAM+CK+CD452 objects were as follows-A1: intact CTC with a round or ellipsoid nucleus (DAPI) entirely surrounded by a uniform CK stain at least 4 × 4 µm^2 in size and negative staining for CD45; A2: granular CTC with nucleus of any shape connected to at least three higher intensity dots of CK, at least 4 × 4 µm^2 in size; A3: L-TCF with a nucleus of at least 4 × 4 µm^2 with any size CK; A4: S-TCF with a nucleus smaller than 4 × 4 µm^2 with any size CK. In the second analysis (panel B) that considered just CK+ objects, the three distinct classes of EpCAM+CK+ objects were as follows: B1: L-TMP with a CK staining area larger than 4 × 4 µm^2 and with or without a nucleus; B2: S-TMP with a cytokeratin staining area smaller than 4 × 4 µm^2, with or without a nucleus; B3: CK+/CD45+ object with or without a nucleus (control). CTC, circulating tumor cells; L-TCF, large tumor cell fragment; S-TCF, small tumor cell fragment; L-TMP, large tumor microparticles; S-TMP, small tumor microparticles; EpCAM+CK+, positive for epithelial cell adhesion molecules and cytokeratin.*

CTC were at different stages of disintegration. We did not investigate, prior to this classification, whether or not the defined EpCAM+CK+ objects were observed in blood of healthy individuals. Seven different classes of EpCAM+CK+ objects, with different morphological and size criteria were outlined. Intact CTC, Granular CTC, Large and Small Tumor Cell Fragments (L-TCF and S-TCF) required the presence of a nucleus or DNA staining (see figure 4.1, panel A1–A4), while the Large and Small Tumor Particles (L-TMP and S-TMP) did not require the presence of DNA (figure 4.1, panel B1, B2). Intact CTC had an intact nucleus, entirely surrounded by intact CK. Granular CTC had at least 3 higher intensity CK dots connected to a nucleus. Intact CTC and Granular CTC required a nucleus of at least 4×4 µm^2. The large and small TCF and TMP were assigned based on whether the size of the CK stain was smaller or larger than 4×4 µm^2. This size cutoff was chosen because a larger than 4 µm requirement is applied in the CellSearch CTC definition [1, 5, 8, 10]. All classes were negative for CD45, except CK+ / CD45+ (figure 4.1, panel B3) which represents white blood cells staining non-specifically with CK and/or CTC staining non-specifically with CD45. The CK+CD45+ class was not expected to correlate with survival and was used as control. An object could be assigned to only one class in each review or not assigned at all. Since objects identified with the CK/DAPI filter and the CK filter were analyzed separately it is probable that objects assigned to one of the 4 classes in the CK/DAPI set were also assigned as S/L-TMP in the CK alone set.

4.3.3 Less stringent CTC definitions increase object counts in CRPC patients but increases false positive object counts in healthy individuals

Figure 4.2 shows the distribution of CTC identified with the original CellSearch definition and the number of objects within each of the EpCAM+CK+ classes for the CRPC patients at baseline and the control group of healthy individuals. For every class except CK+CD45+ a clear separation is found between the control healthy subject group and the samples from cancer patients. Only the CellSearch CTC and Intact CTC classes had zero objects in all samples from healthy individuals. The lowest counts were for Intact CTC and Granular CTC, followed by CellSearch CTC, L-TCF and S-TCF. The highest counts were found for S-TMP and L-TMP, but these also had the highest counts in healthy individuals. The median number of S-TMP was 17 times the median CellSearch CTC count.

4.3.4 All EpCAM+CK+CD45- objects predict survival in CRPC

All EpCAM+CK+CD45- classes were associated with survival (all log rank $p < 0.001$). Figure 4.3 shows the KM curves for all classes and the number

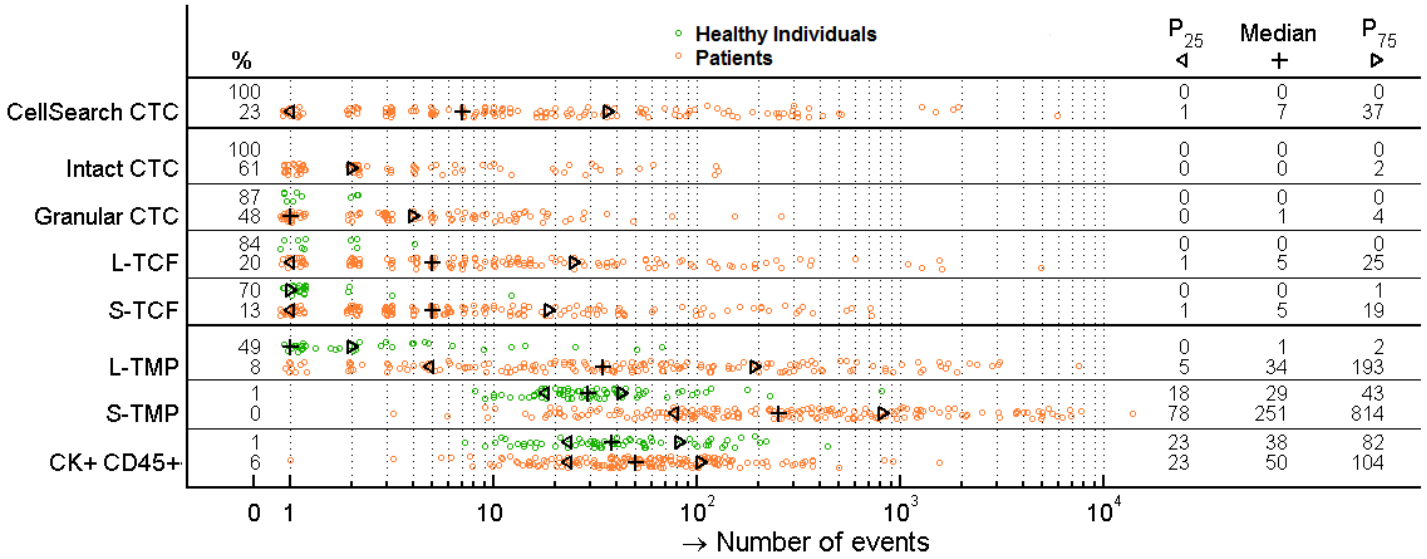

Figure 4.2: Distribution of the number of objects in each CTC class for healthy normals (green) and CRPC patients (orange). *The percentage of samples with 0 objects is shown on the left and each data point is given a random amount of jitter (< 0.5) to show the density of samples in case of overlap. Markers indicate the 25 percentile, median and 75 percentile. At the right side of the figure the actual values are shown.*

Table 4.1: Descriptive statistics for patients at baseline showing mean, SD, median and range for several serum markers.

	Patients at baseline			
	N	Mean ± SD	Median	Range
PSA (ng/ mL)	179	452 ± 1213	126	1.9–13246
LDH (IU/ mL)	170	301 ± 248	224.5	114–2092
Testosterone (ng/ mL)	173	0.20 ± 0.17	0.14	0.10–1.44
ALP (IU/ mL)	173	223 ± 233	137	39–1801
Hemoglobin (g/ dL)	176	12.3 ± 1.6	12.3	8.2–15.7
Albumin (g/ dL)	173	4.2 ± 3.9	3.8	2.1–41

SD: standard deviation, PSA: prostate specific antigen, LDH: lactate dehydrogenase, ALP: Alkaline Phosphatase.

of patients assigned to each group. For Intact CTC there were too few different values and only three groups were created. EpCAM+CK+CD45+ objects were not associated with survival. Survival prospects decreased with increasing number of objects for all other CTC classes as evidenced by the shortest survival for the group with the highest number of objects (G4) followed by G3, G2 and then G1, with the lowest number of objects. Patients who appear in the highest group of one CTC class tend to appear in the highest groups of the other classes too.

Figure 4.4 shows the hazard ratios of groups 2–4 (G2–G4) relative to the reference group (G1). The highest HR was found for L-TCF. Age was prognostic for survival with a typical HR of 1.018/year (95% CI of 0.999 to 1.037). For CellSearch CTC, S/L-TCF and S/L-TMP it is clear that a patient in a higher group, with more objects, has a poorer prognosis compared to a patient in a lower group. For Granular CTC and Intact CTC there is little difference between G2 and G1.

4.3.5 L-TCF, S-TMP and CellSearch CTC are the best predictors of survival

Parameters associated with survival in univariate analyses were used as input parameters for multivariate analysis (MVA, table 4.2, figure 4.3). The input variables were all CTC classes, LDH, ALP, hemoglobin, albumin, PSA as categorical variables and age as a continuous variable. Table 4.2 shows the results of this analysis. The final model contained age, hemoglobin, LDH and L-TCF. The correlation between CTC classes was high (mean Spearman's ρ 0.70, range 0.40–0.92). The performance of models containing S-TMP or CellSearch CTC instead of L-TCF was similar, while models with other CTC classes were performing worse.

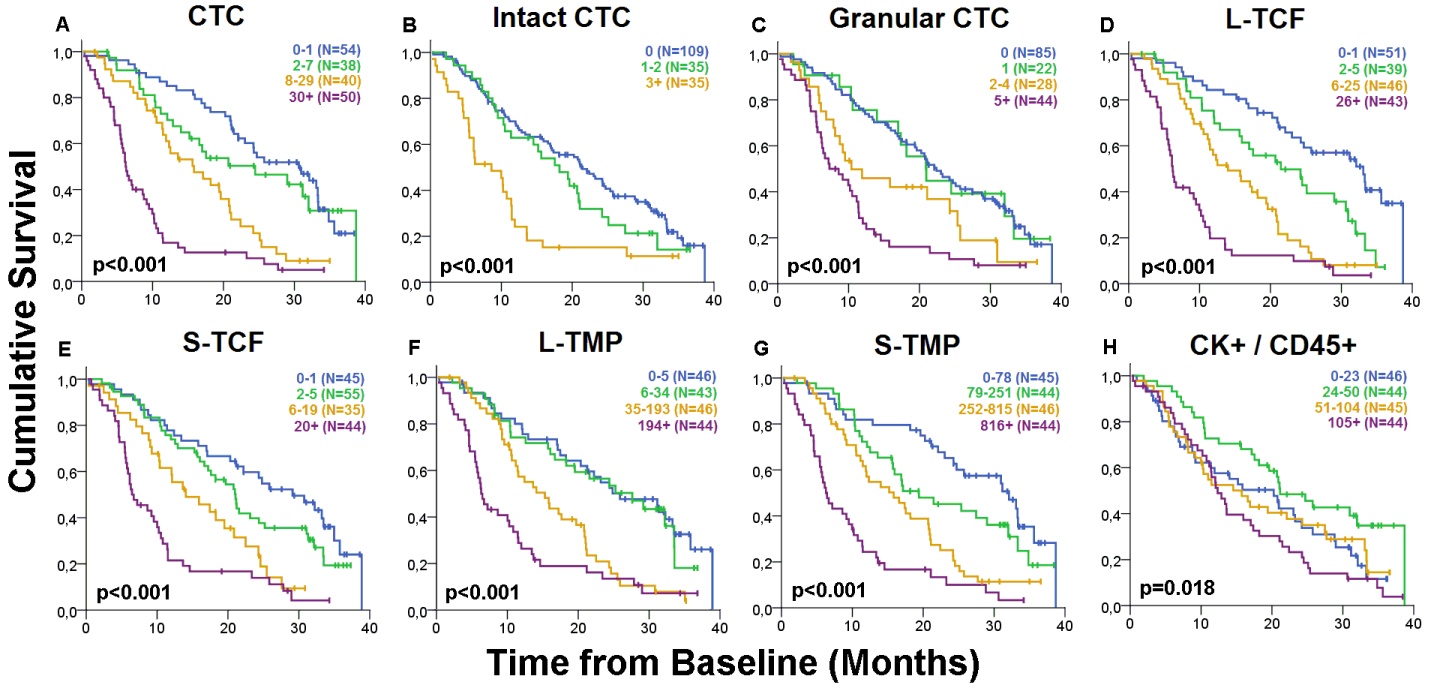

Figure 4.3: Kaplan Meier plots of overall survival of CRPC patients for all EpCAM+CK+ objects *(panels A–H). The vertical markers represent censored patients. The number of patients in each group and the group boundaries are shown in the top right corner of each plot. Due to the large number of samples with zero objects for many EpCAM+ classes, the reference group G1 includes a larger than 25% share of the samples. P values of the log-rank test are shown in the bottom left of each plot. Units for all EpCAM+,CK+ classes are number of objects/7.5 mL.*

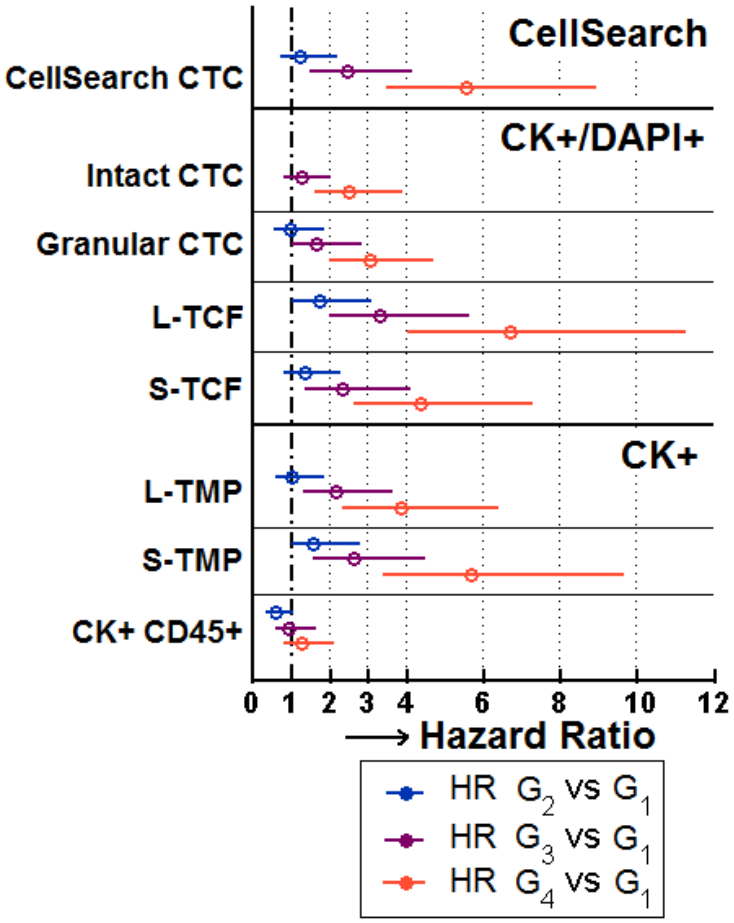

Figure 4.4: Hazard ratios (HR) of groups 2–4 relative to group 1 with 95% confidence intervals. *In the control class (CK+CD45), the confidence interval includes 1 (no change in hazard) for all groups. For all other classes, the HR shows a continuous increase across. While the confidence interval for group 2 (G2) includes 1 for most classes, the confidence interval of group 4 (G4) clearly shows high HR and excludes one. Highest HR are found for S-TMP and CellSearch CTC, closely followed by L-TMP, L-TCF and S-TCF.*

Table 4.2: Results of the Cox proportional hazard analysis of the markers associated with survival at baseline (BL). *The hazard ratios for univariate analysis and the three equivalent multivariate models are shown.*

Variable	Range	HR (95%CI)			
		Univariate	MVA with L-TCF	MVA with CS CTC	MVA with S-TMP
Age (year)	Cont.	1,018 (0,999–1,037)	1,021 (1,000–1,043)	1,023 (1,002–1,044)	1,023 (1,002–1,045)
LDH (IU/ mL)	≤ 173	1 (ref)	1 (ref)	1 (ref)	1 (ref)
	174-228	1,11 (0,63–1,96)	0,87 (0,48–1,57)	0,84 (0,46–1,53)	0,75 (0,41–1,38)
	229-313	1,46 (0,81–2,63)	0,83 (0,44–1,56)	0,76 (0,39–1,45)	0,84 (0,44–1,62)
	314+	3,94 (2,19–7,12)	1,99 (1,03–3,82)	1,9 (0,98–3,65)	1,77 (0,90–3,49)
Hemoglobin	13.5+	1 (ref)	1 (ref)	1 (ref)	1 (ref)
(g/ dL)	12.6-13.4	1,26 (0,70–2,27)	1,03 (0,55–1,92)	1,13 (0,60–2,12)	1,07 (0,57–2,02)
	11.3-12.5	3,00 (1,81–5,00)	1,70 (0,97–2,97)	1,92 (1,10–3,36)	1,93 (1,07–3,48)
	≤ 11.2	4,28 (2,57–7,13)	2,26 (1,26–4,05)	2,25 (1,26–4,04)	2,98 (1,66–5,37)
L-TCF	0-1	1 (ref)	1 (ref)		
(# /7.5 mL blood)	2-5	1,92 (1,12–3,3)	1,52 (0,87–2,69)		
	6-25	3,30 (1,98–5,49)	2,13 (1,19–3,81)		
	26+	6,57 (3,94–10,95)	4,00 (2,20–7,27)		
CTC	0-1	1 (ref)		1 (ref)	
(#/7.5 mL blood)	2-7	1,20 (0,70–2,06)		1,05 (0,60–1,84)	
	8-29	2,39 (1,46–3,91)		1,64 (0,94–2,88)	
	30+	5,20 (3,25–8,32)		3,36 (1,87–6,07)	
S-TMP	0-78	1 (ref)			1 (ref)
(#/7.5 mL blood)	79-251	1,55 (0,91–2,65)			1,26 (0,71–2,26)
	252-815	2,66 (1,59–4,43)			1,58 (0,87–2,85)
	816+	5,50 (3,28–9,24)			3,43 (1,90–6,19)

CS: CellSearch, HR: hazard ratio, CI: confidence interval, MVA: multivariate analysis, L-TCF: large tumor cell fragments, CTC: circulating tumor cells, S-TMP: small tumor microparticles, LDH: lactate dehydrogenase.

4.4 Discussion

Multicenter prospective clinical studies have demonstrated a significant relation between the presence of CTC defined by the CellSearch CTC definition and poor progression free and overall survival [1, 2, 3, 4, 5, 6, 7, 8]. The definition of CellSearch CTC was set before the initiation of these studies and no subsequent analysis has been performed to determine whether less or more stringent definitions of CTC were similarly associated with worse outcome. Moreover, multiple conflicting CTC reports, utilizing different technologies, and describing very different CTC counts have led to questions being raised as to whether different methods are counting different CTC subclasses. This has resulted in an urgent need for guidelines on what is the best definition of a clinically relevant CTC. Our study is the first to have comprehensively evaluated all EpCAM+CK+ objects isolated by immunomagnetic selection using the CellSearch system, which remains the only technology for isolating CTC to have been studied in multi-center, prospective Phase III studies. We report that all circulating EpCAM+CK+CD45- objects identified in CRPC patients predict survival. On multivariate analysis the CD45- large tumor cell fragments with a nucleus at least 4 x 4 μm^2 and any size CK staining (L-TCF) as well as the more strict CellSearch definition for CTC, and the less stringent definition of small tumor micro particles (S-TMP) that are smaller than 4 x 4 μm^2 and do not require DNA staining, were equally prognostic.

These observations have very significant implications for future prognostic studies of CTC. Applying the strictest morphological definition of CTC that have the strongest likelihood of being viable tumor cells (Intact CTC) is not necessary and even less significant than other classes. There are many patients with no Intact CTC found, which could result in a reduction of median survival of the reference group (G1), and thus reduce the HR of the other groups. Tumor micro-particles may be better indicators of disease burden in these patients, because they occur at higher frequency. The presence of TMP could infer that intact CTC are present albeit at a frequency below 1 per 7.5 mL of blood. Overall, it appears that very different morphological CTC definitions can be applied. Many of the patients who appear in the highest group of one CTC class, tend to appear in the highest groups of the other classes too. To investigate whether the level of CTC in each class matters we applied a 4 level categorization of the data wherever possible to show the continuous behavior of the classes without estimating a linearization transformation for Cox regression. The ranking within each subclass was based on an independent set of 63 samples. A higher number of EpCAM+CK+ objects resulted in a reduced survival for CellSearch CTC, L/S-TCF and L/S-TMP. We expect this relationship between the number of events and survival to hold true for metastatic breast and colon cancer. Determining which class is most suitable for prognostication is difficult. From the univariate Cox regression, we find that CellSearch CTC,

L/S-TCF and L/S-TMP all have high hazard ratios. Multivariate regression showed that CellSearch CTC, L-TCF and S-TMP had similar predictive value. Other desirable properties are low counts in healthy volunteers and a quick, objective and reproducible determination. CellCearch CTC determination performs best from the point of view of being generally absent in healthy volunteers. TMP were most prevalent and easier to enumerate, while CellSearch CTC and L/S-TCF require the most operator training. Nonetheless TMPs are unlikely to have the same potential as Intact CTC for the assessment of treatment targets by FISH [26, 27, 28, 29], proteins [24, 30] and RNA [31]. Fully automated CTC enumeration is desirable to increase reproducibility in object assignment. Importantly, the fully automated CTC counting with less stringent definitions for CTC will be easier to achieve than enumerating CTC as defined by CellSearch. Finally, these data need to be replicated in other CRPC studies and their broader significance in other tumor types needs to be investigated. In conclusion, these data have important implications to the future evaluation of CTC. We have investigated the prognostic value of different CTC (DAPI+) or TMP (DAPI+/-) definitions from 179 baseline samples from a CRPC study [8] and have shown that all EpCAM+CK+CD45- classes were prognostic for survival. For CellSearch CTC, L-TCF, S-TCF, L-TMP and S-TMP we found that the presence of a larger number of objects predicted shorter survival. Overall, CellSearch CTC had the lowest background, while the highest number of objects in a tube of blood was for S-TMP. We recommend that reproducibility of CTC assignment needs to be improved, preferably by the use of automated image analysis.

4.5 Acknowledgements

The authors acknowledge Frances Tanney, Arjan Tibbe, and Bjorn Lunter for retrieving the archive CDs, Craig Miller for supplying survival and demographic data and Doug Paynter for configuring the analysis software.

4.6 References

[1] M. Cristofanilli, G. T. Budd, M. J. Ellis, A. Stopeck, J. Matera, M. C. Miller, J. M. Reuben, G. V. Doyle, W. J. Allard, L. W. Terstappen, and D. F. Hayes, "Circulating tumor cells, disease progression, and survival in metastatic breast cancer," *N. Engl. J. Med.*, vol. 351, pp. 781–791, Aug 2004.

[2] M. Cristofanilli, D. F. Hayes, G. T. Budd, M. J. Ellis, A. Stopeck, J. M. Reuben, G. V. Doyle, J. Matera, W. J. Allard, M. C. Miller, H. A. Fritsche, G. N. Hortobagyi, and L. W. Terstappen, "Circulating tumor cells: a novel prognostic factor for newly diagnosed metastatic breast cancer," *J. Clin. Oncol.*, vol. 23, pp. 1420–1430, Mar 2005.

[3] G. T. Budd, M. Cristofanilli, M. J. Ellis, A. Stopeck, E. Borden, M. C. Miller, J. Matera, M. Repollet, G. V. Doyle, L. W. Terstappen, and D. F. Hayes, "Circulating

tumor cells versus imaging–predicting overall survival in metastatic breast cancer," *Clin. Cancer Res.*, vol. 12, pp. 6403–6409, Nov 2006.

[4] D. F. Hayes, M. Cristofanilli, G. T. Budd, M. J. Ellis, A. Stopeck, M. C. Miller, J. Matera, W. J. Allard, G. V. Doyle, and L. W. Terstappen, "Circulating tumor cells at each follow-up time point during therapy of metastatic breast cancer patients predict progression-free and overall survival," *Clin. Cancer Res.*, vol. 12, pp. 4218–4224, Jul 2006.

[5] S. J. Cohen, C. J. Punt, N. Iannotti, B. H. Saidman, K. D. Sabbath, N. Y. Gabrail, J. Picus, M. A. Morse, E. Mitchell, M. C. Miller, G. V. Doyle, H. Tissing, L. W. Terstappen, and N. J. Meropol, "Prognostic significance of circulating tumor cells in patients with metastatic colorectal cancer," *Ann. Oncol.*, vol. 20, pp. 1223–1229, Jul 2009.

[6] D. Olmos, H. T. Arkenau, J. E. Ang, I. Ledaki, G. Attard, C. P. Carden, A. H. Reid, R. A'Hern, P. C. Fong, N. B. Oomen, R. Molife, D. Dearnaley, C. Parker, L. W. Terstappen, and J. S. de Bono, "Circulating tumour cell (CTC) counts as intermediate end points in castration-resistant prostate cancer (CRPC): a single-centre experience," *Ann. Oncol.*, vol. 20, pp. 27–33, Jan 2009.

[7] J. Tol, M. Koopman, M. C. Miller, A. Tibbe, A. Cats, G. J. Creemers, A. H. Vos, I. D. Nagtegaal, L. W. Terstappen, and C. J. Punt, "Circulating tumour cells early predict progression-free and overall survival in advanced colorectal cancer patients treated with chemotherapy and targeted agents," *Ann. Oncol.*, vol. 21, pp. 1006–1012, May 2010.

[8] J. S. de Bono, H. I. Scher, R. B. Montgomery, C. Parker, M. C. Miller, H. Tissing, G. V. Doyle, L. W. Terstappen, K. J. Pienta, and D. Raghavan, "Circulating tumor cells predict survival benefit from treatment in metastatic castration-resistant prostate cancer," *Clin. Cancer Res.*, vol. 14, pp. 6302–6309, Oct 2008.

[9] M. Kagan, D. Howard, T. Bendele, J. Mayes, J. Silvia, M. Repollet, J. Doyle, J. Allard, N. Tu, T. Bui, T. Russell, C. Rao, M. Hermann, H. Rutner, and L. Terstappen, "A sample preparation and analysis system for identification of circulating tumor cells," *J Clinical Ligand Assay*, vol. 25, pp. 104–50, 2002.

[10] W. J. Allard, J. Matera, M. C. Miller, M. Repollet, M. C. Connelly, C. Rao, A. G. Tibbe, J. W. Uhr, and L. W. Terstappen, "Tumor cells circulate in the peripheral blood of all major carcinomas but not in healthy subjects or patients with nonmalignant diseases," *Clin. Cancer Res.*, vol. 10, pp. 6897–6904, Oct 2004.

[11] C. G. Rao, D. Chianese, G. V. Doyle, M. C. Miller, T. Russell, R. A. Sanders, and L. W. Terstappen, "Expression of epithelial cell adhesion molecule in carcinoma cells present in blood and primary and metastatic tumors," *Int. J. Oncol.*, vol. 27, pp. 49–57, Jul 2005.

[12] A. G. Tibbe, M. C. Miller, and L. W. Terstappen, "Statistical considerations for enumeration of circulating tumor cells," *Cytometry A*, vol. 71, pp. 154–162, Mar 2007.

[13] C. J. Larson, J. G. Moreno, K. J. Pienta, S. Gross, M. Repollet, S. M. O'hara, T. Russell, and L. W. Terstappen, "Apoptosis of circulating tumor cells in prostate cancer patients," *Cytometry A*, vol. 62, pp. 46–53, Nov 2004.

[14] S. Nagrath, L. V. Sequist, S. Maheswaran, D. W. Bell, D. Irimia, L. Ulkus, M. R. Smith, E. L. Kwak, S. Digumarthy, A. Muzikansky, P. Ryan, U. J. Balis, R. G. Tompkins, D. A. Haber, and M. Toner, "Isolation of rare circulating tumour cells in cancer patients by microchip technology," *Nature*, vol. 450, pp. 1235–1239, Dec 2007.

[15] K. Pachmann, O. Camara, A. Kavallaris, S. Krauspe, N. Malarski, M. Gajda, T. Kroll, C. Jorke, U. Hammer, A. Altendorf-Hofmann, C. Rabenstein, U. Pachmann, I. Runnebaum, and K. Hoffken, "Monitoring the response of circulating epithelial tumor cells to adjuvant chemotherapy in breast cancer allows detection of patients at risk of early relapse," *J. Clin. Oncol.*, vol. 26, pp. 1208–1215, Mar 2008.

[16] H. J. Kahn, A. Presta, L. Y. Yang, J. Blondal, M. Trudeau, L. Lickley, C. Holloway, D. R. McCready, D. Maclean, and A. Marks, "Enumeration of circulating tumor cells in the blood of breast cancer patients after filtration enrichment: correlation with disease stage," *Breast Cancer Res. Treat.*, vol. 86, pp. 237–247, Aug 2004.

[17] R. T. Krivacic, A. Ladanyi, D. N. Curry, H. B. Hsieh, P. Kuhn, D. E. Bergsrud, J. F. Kepros, T. Barbera, M. Y. Ho, L. B. Chen, R. A. Lerner, and R. H. Bruce, "A rare-cell detector for cancer," *Proc. Natl. Acad. Sci. U.S.A.*, vol. 101, pp. 10501–10504, Jul 2004.

[18] C. Alix-Panabieres, J. P. Brouillet, M. Fabbro, H. Yssel, T. Rousset, T. Maudelonde, G. Choquet-Kastylevsky, and J. P. Vendrell, "Characterization and enumeration of cells secreting tumor markers in the peripheral blood of breast cancer patients," *J. Immunol. Methods*, vol. 299, pp. 177–188, Apr 2005.

[19] H. Schwarzenbach, C. Alix-Panabieres, I. Muller, N. Letang, J. P. Vendrell, X. Rebillard, and K. Pantel, "Cell-free tumor DNA in blood plasma as a marker for circulating tumor cells in prostate cancer," *Clin. Cancer Res.*, vol. 15, pp. 1032–1038, Feb 2009.

[20] H. B. Hsieh, D. Marrinucci, K. Bethel, D. N. Curry, M. Humphrey, R. T. Krivacic, J. Kroener, L. Kroener, A. Ladanyi, N. Lazarus, P. Kuhn, R. H. Bruce, and J. Nieva, "High speed detection of circulating tumor cells," *Biosens Bioelectron*, vol. 21, pp. 1893–1899, Apr 2006.

[21] E. Racila, D. Euhus, A. J. Weiss, C. Rao, J. McConnell, L. W. Terstappen, and J. W. Uhr, "Detection and characterization of carcinoma cells in the blood," *Proc. Natl. Acad. Sci. U.S.A.*, vol. 95, pp. 4589–4594, Apr 1998.

[22] L. W. Terstappen, C. Rao, S. Gross, and A. J. Weiss, "Peripheral blood tumor cell load reflects the clinical activity of the disease in patients with carcinoma of the breast," *Int. J. Oncol.*, vol. 17, pp. 573–578, Sep 2000.

[23] J. G. Moreno, M. C. Miller, S. Gross, W. J. Allard, L. G. Gomella, and L. W. Terstappen, "Circulating tumor cells predict survival in patients with metastatic prostate cancer," *Urology*, vol. 65, pp. 713–718, Apr 2005.

[24] D. F. Hayes, T. M. Walker, B. Singh, E. S. Vitetta, J. W. Uhr, S. Gross, C. Rao, G. V. Doyle, and L. W. Terstappen, "Monitoring expression of HER-2 on circulating epithelial cells in patients with advanced breast cancer," *Int. J. Oncol.*, vol. 21, pp. 1111–1117, Nov 2002.

[25] H. F. E. Jr., *Regression Modeling Strategies: With Applications to Linear Models, Logistic Regression and Survival Analysis*. Springer, New York, NY, USA, 2001.

[26] J. F. Swennenhuis, A. G. Tibbe, R. Levink, R. C. Sipkema, and L. W. Terstappen, "Characterization of circulating tumor cells by fluorescence in situ hybridization," *Cytometry A*, vol. 75, pp. 520–527, Jun 2009.

[27] S. Meng, D. Tripathy, S. Shete, R. Ashfaq, B. Haley, S. Perkins, P. Beitsch, A. Khan, D. Euhus, C. Osborne, E. Frenkel, S. Hoover, M. Leitch, E. Clifford, E. Vitetta, L. Morrison, D. Herlyn, L. W. Terstappen, T. Fleming, T. Fehm, T. Tucker, N. Lane, J. Wang, and J. Uhr, "HER-2 gene amplification can be acquired as breast cancer progresses," *Proc. Natl. Acad. Sci. U.S.A.*, vol. 101, pp. 9393–9398, Jun 2004.

[28] G. Attard, J. F. Swennenhuis, D. Olmos, A. H. Reid, E. Vickers, R. A'Hern, R. Levink, F. Coumans, J. Moreira, R. Riisnaes, N. B. Oommen, G. Hawche, C. Jameson, E. Thompson, R. Sipkema, C. P. Carden, C. Parker, D. Dearnaley, S. B. Kaye, C. S. Cooper, A. Molina, M. E. Cox, L. W. Terstappen, and J. S. de Bono, "Characterization of ERG, AR and PTEN gene status in circulating tumor cells from patients with castration-resistant prostate cancer," *Cancer Res.*, vol. 69, pp. 2912–2918, Apr 2009.

[29] S. Meng, D. Tripathy, S. Shete, R. Ashfaq, H. Saboorian, B. Haley, E. Frenkel, D. Euhus, M. Leitch, C. Osborne, E. Clifford, S. Perkins, P. Beitsch, A. Khan, L. Morrison, D. Herlyn, L. W. Terstappen, N. Lane, J. Wang, and J. Uhr, "uPAR and HER-2 gene status in individual breast cancer cells from blood and tissues," *Proc. Natl. Acad. Sci. U.S.A.*, vol. 103, pp. 17361–17365, Nov 2006.

[30] J. S. de Bono, G. Attard, A. Adjei, M. N. Pollak, P. C. Fong, P. Haluska, L. Roberts, C. Melvin, M. Repollet, D. Chianese, M. Connely, L. W. Terstappen, and A. Gualberto, "Potential applications for circulating tumor cells expressing the insulin-like growth factor-I receptor," *Clin. Cancer Res.*, vol. 13, pp. 3611–3616, Jun 2007.

[31] D. A. Smirnov, D. R. Zweitzig, B. W. Foulk, M. C. Miller, G. V. Doyle, K. J. Pienta, N. J. Meropol, L. M. Weiner, S. J. Cohen, J. G. Moreno, M. C. Connelly, L. W. Terstappen, and S. M. O'Hara, "Global gene expression profiling of circulating tumor cells," *Cancer Res.*, vol. 65, pp. 4993–4997, Jun 2005.

CHAPTER 5

Automated identification of Circulating Tumor Cells

Sjoerd T. Ligthart, Frank A.W. Coumans, Gerhardt Attard, Amy M. Cassidy, Johann S. de Bono, and Leon W.M.M. Terstappen
PlosOne, doi:10.1371/journal.pone.0027419, 2011

Abstract

Circulating tumor cells (CTC) in patients with metastatic carcinomas are associated with poor survival and can be used to guide therapy. Classification of CTC remains however subjective, as they are morphologically heterogeneous. We acquired digital images, using the Cellsearch system, of objects positive for the epithelial cell adhesion molecule captured from the blood of 185 castration resistant prostate cancer (CRPC) patients and 68 healthy subjects to define CTC by computerized algorithms. Patient survival data was used as the training parameter for the computer defined CTC. The computer-generated CTC definition was then validated on a separate CRPC dataset comprising 96 patients. The optimal CTC definition was selected based on: 1.) High Cox hazard ratio (HR) for both baseline and follow-up samples; 2.) Higher HR for follow-up than baseline samples since these patients were being administered drugs with antitumor activity; 3.) Low relative and absolute count in control samples. Our computer-generated CTC definition resulted in HRs of 2.8 for baseline and 3.9 for follow-up samples, which is comparable to the manual Cellsearch CTC definition (baseline HR 2.9, follow-up HR 4.5). Validation resulted in HRs at baseline/follow-up of 3.9/5.4 for computer and 4.8/5.8 for Cellsearch definitions. Processing of a sample using the automated classifier required no operator intervention, compared to up to 39 minutes of review per sample by highly trained

operators in the Cellsearch method. We have created and validated a definition for CTC using automated counting that compares favorably to manual counting by the Cellsearch definition, but is rapid and reproducible.

5.1 Introduction

In recent years several studies have reported that counting circulating tumor cells (CTC) can indicate whether a therapy for advanced cancer is effective after treatment [1, 2, 3, 4, 5, 6, 7, 8]. At present, the Cellsearch method is the only validated method for CTC enumeration [9]. In this system, objects that are positive for epithelial cell adhesion molecule (EpCAM) antibodies are enriched from 7.5 mL of blood and identified as cytokeratin-phycoerythrin (CK-PE) positive, CD45-allophycocyan (CD45-APC) negative objects > 4 µm in size, staining with the nuclear dye DAPI and cell-like morphology. The recorded fluorescence images of CK, DNA, CD45 and a debris-FITC channel are segmented on the basis of being positive for CK and DNA and are then presented to a trained reviewer for CTC identification. This procedure is very laborious, time-consuming and can be highly subjective. Moreover, CTC are known to be morphologically heterogeneous [1] and in fact different laboratories have slightly different definitions of what constitutes a CTC, especially in the case of objects that are dead or apoptotic [10]. Because CTC occur at very low frequencies, misjudging a few events may be very significant [11]. Also, the a-priori definition of what to call a CTC that has been used to date may not be optimal. Our group recently reported that Tumor Micro Particles (TMPs), EpCAM+CK+CD45- objects smaller than 4 µm, have the same prognostic value as manually counted "CTC" [12], suggesting alternative methods for CTC evaluation should be considered. Here we present the results of a new approach to identify CTC in images recorded by ten Cellsearch systems from samples from castration-resistant prostate cancer (CRPC) patients [13, 14, 15]. We recorded images before treatment (baseline samples) and from the first follow-up sample. Our hypothesis was that using solely survival data as a training feature, an automated algorithm could be optimized to automatically count CTC with the same fidelity as the manual Cellsearch method. We stipulated that such an algorithm needed to identify candidate CTC, extract several relevant properties and compare the candidate to a range of known parameters. This automated CTC (aCTC) definition would then need to be validated on an independent data set confirming that it was associated with Cox hazard ratios (HR) comparable to when the manual Cellsearch CTC (mCTC) definition is applied. This would allow replacement of manual CTC counting with an automated approach, significantly increasing processing speed and eliminating inter- and intra-laboratory variation.

5.2 Results

5.2.1 Processing of images

Stored images from the 185 CRPC patients with samples taken at baseline and at first follow-up (2–5 weeks after baseline) and 68 healthy donors were imported. Figure 5.1 shows a schematic representation of the procedure that was used for acquiring an optimal classifier for selecting aCTC. Detailed results of each step are described below.

5.2.2 Optimal channel for segmentation

Segmentation in the four image channels, the PE/DAPI sum and the maximum intensity profile was performed on 185 baseline samples. The HR after dichotomization on the median number of objects found was 1.2 in the FITC channel, 1.3 in the APC channel, 1.6 in the DAPI and the DAPI/PE sum channels, 1.7 in the maximum intensity profile and 2.3 in the PE channel. In the 185 baseline samples a total of 262282 objects were found within the PE channel, these objects were used for the feature selection step in the algorithm development process.

5.2.3 Features with highest impact on HR

The values of the 24 measured properties -called features hereafter- were determined for each object. For each feature, all objects were tested against thresholds at various levels and for each level the HR was determined. The maximum HR was determined for each feature. Figure 5.2 shows the results for four of these analyses, including only events that exceed a minimum "peak signal intensity" in the four channels.

Panel A and C show that selecting on this feature results in a higher HR. Panel B shows that objects have very low FITC peak values, already at a low minimum value the HR is near 1, and the median count drops to 0. Panels D shows that a minimum CD45-APC peak intensity results in lower HRs than the base HR after segmentation. The object features with the best discriminatory power based on the above analysis were: Size (HR 3.0), total PE intensity (HR 3.0), total DAPI intensity (HR 3.0), Standard deviation of the PE intensity (HR 2.8), mean PE intensity (HR 2.8), peak PE intensity (HR 2.8), peak DAPI intensity (HR 2.8), mean DAPI intensity (HR 2.8), total APC intensity (HR 2.8), standard deviation DAPI intensity (HR 2.6), peak APC intensity (HR 2.5). After deriving the covariance matrix of these features, the correlation coefficients were determined. The feature with the highest HR was chosen first. Next, features were chosen in descending order of HR provided they had a correlation coefficient of less than 0.4 with features already chosen. As a result the total intensity features were not selected as they had too much correlation with the size

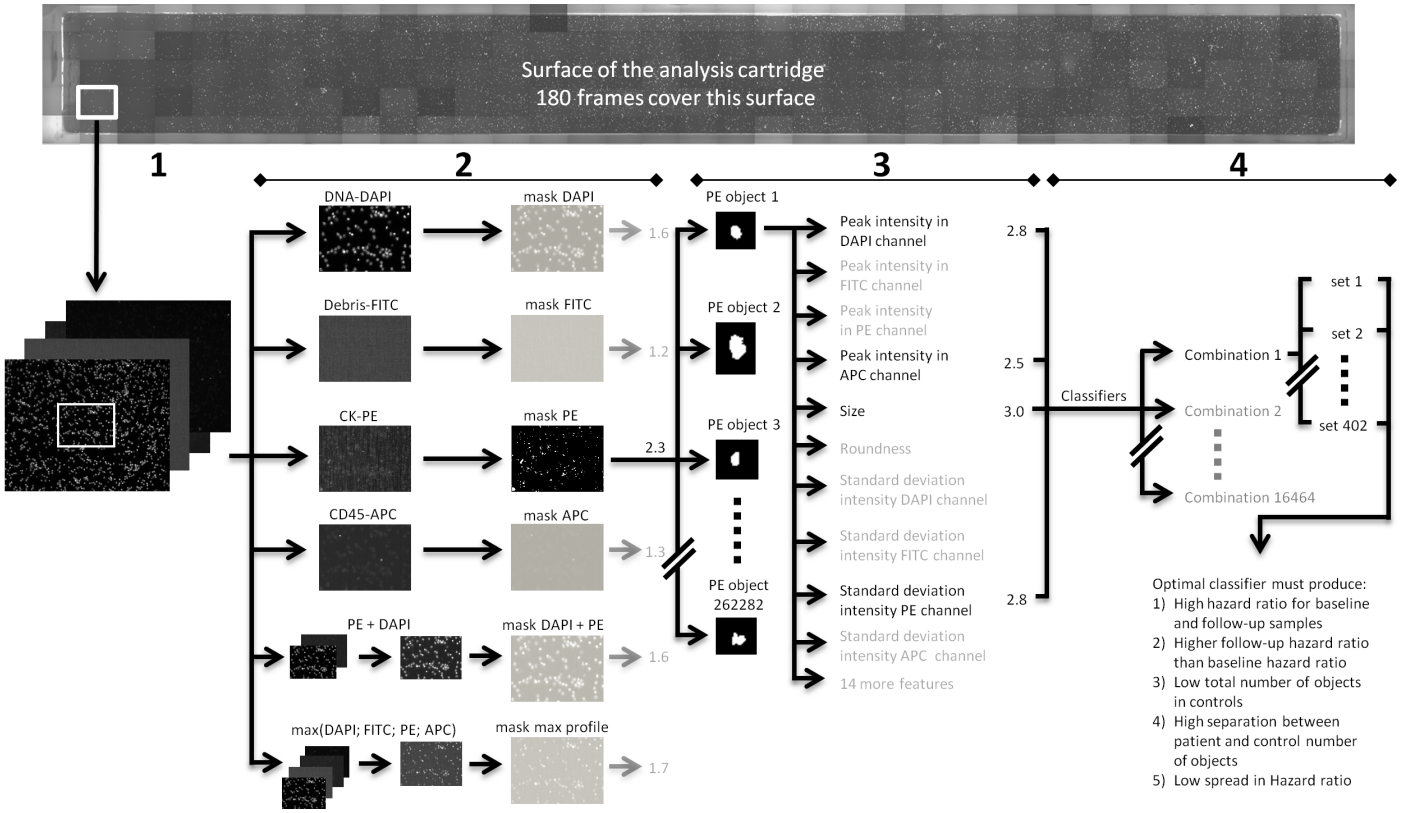

Figure 5.1: Schematic overview of the aCTC classifier development process. *1: image acquisition, 2: object segmentation, 3: feature measurements, 4: creation and selection of classifiers.*

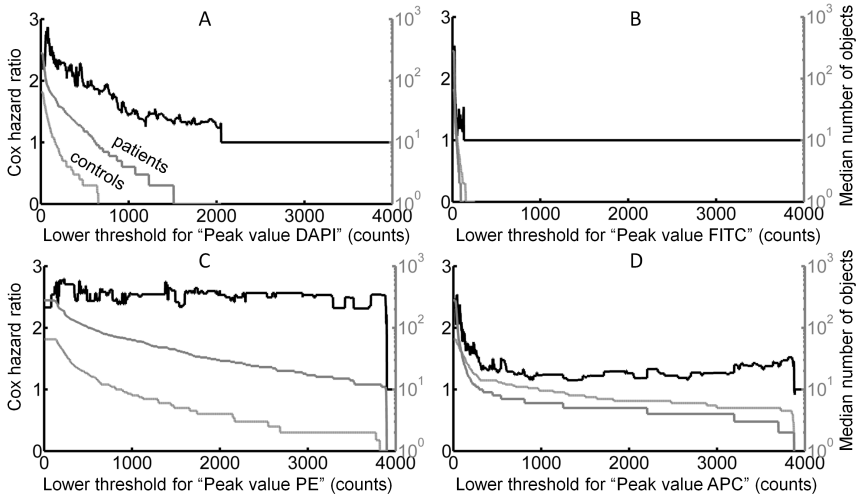

Figure 5.2: Example of the influence of thresholding of a feature on the Cox hazard ratio. *After segmentation of objects in the PE channel, the patient group is dichotomized on the median count and a base HR is derived. Varying a lower threshold from 0–4000 grey level counts on the feature "peak value" for all four channels DAPI, FITC, PE, and APC (panel A–D respectively) resulted in a varying HR (black line) and decreased the median number of particles of the patients and controls (grey lines) that were included.*

of the feature. Four features with both high influence on the HR and low inter feature correlation were selected for further analysis:

1. Size of object.
2. Standard deviation of signal in the PE-CK channel.
3. Peak value of signal in the DAPI-DNA channel.
4. Peak value of signal in the APC-CD45 channel.

5.2.4 Rules to assign aCTC

A classifier was constructed by creating an acceptance range for each feature, an object had to fall within the acceptance range for each feature to be classified as an aCTC. The acceptance ranges were varied simultaneously to construct 16464 different classifiers. Each of these classifiers was tested by means of bootstrapping; the acquired variation in HR was used as a measure for the robustness of the classifier. Follow-up samples from 185 patients and 68 control samples were now included to determine the optimal

classifier. Figure 5.3, panel A shows the average HR after bootstrapping of the baseline samples from the 16464 classifiers plotted against the HR on the follow-up samples, after patient groups were dichotomized on the median number of objects.

The figure illustrates that many classifiers in this data set can be chosen that provide a higher HR for both baseline and follow-up samples as compared to the manual Cellsearch CTC definition (indicated with the red cross in the figure). Figure 5.3, panel B shows the performance of the classifiers on 4 of our 5 selection rules (the spread of the HR after bootstrapping is not shown in this figure). The optimal classifier is indicated by the arrow in figure 5.3, panels A and B. On this data set the selected classifier has only one background object classified as aCTC in the 68 controls, a high mean bootstrapped HR of 4.2 and a HR for follow-up samples that is 1.5 times higher than the baseline HR. The optimal classifier included objects with a PE-CK standard deviation higher than 50 counts, a size range of 75–500 pixels (34–224 μm^2), a DAPI-DNA peak value of at least 170 counts and a APC-CD45 peak value less than 60 counts. SD of the spread of the HR after bootstrapping for this classifier was 0.7 and 1.3 for baseline and follow-up samples respectively.

5.2.5 Processing time and reproducibility of the algorithm

Automated counting and classification of aCTC took about 5 minutes per sample. Identification of candidate mCTC in the current system takes approximately 5 minutes. However, classification of these mCTC by a human operator takes 0.5–39 minutes per sample (median 5.0 min, mean 7.9 min, SD 8.4 min, n=43) according to the main Veridex LLC Cellsearch processing lab. The reproducibility of counting aCTC by the algorithm is 100%.

5.2.6 Automatic CTC count versus manual CTC count in patients and controls

In the baseline samples the aCTC counts ranged from 0 to 3384 (total 14439, median 5, mean 78, SD 333) compared to mCTC counts of 0 to 5925 (total 18706, median 7, mean 101, SD 497). The R^2-correlation between aCTC and mCTC was 0.80 (slope = 1.33, intercept = -3.03). In the follow-up samples the aCTC counts ranged from 0 to 870 (total 4992, median 2, mean 27, SD 86) compared to mCTC counts of 0 to 545 (total 5546, median 2, mean 30, SD 87). The R^2-correlation was 0.67 (slope = 0.85, intercept = 7.18). In the 68 control samples 1 object was classified as aCTC and 0 objects as mCTC.

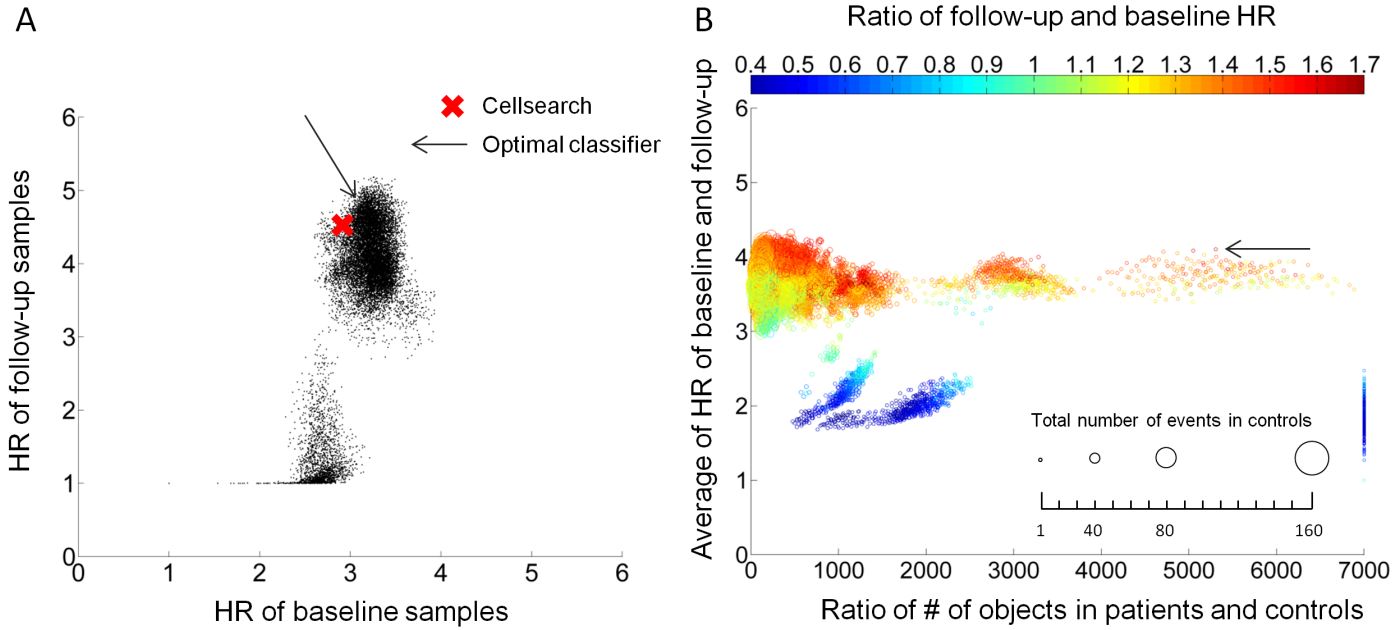

Figure 5.3: Scatter plots showing the relation between the HR of 185 baseline and 185 follow-up samples and the 16464 classifiers. *Panel A shows the HRs of baseline versus follow-up samples for all classifiers. The arrow depicts our optimal classifier, the red cross depicts the HR derived using the Cellsearch CTC definition. Panel B shows the mean HR of baseline and follow up samples versus the mean number of particles found in patient samples divided by the mean number of objects found in control samples of all classifiers. The color indicates the HR of the follow-up samples divided by the HR of the baseline samples and the size of the circles indicates the number of objects classified in all 68 control samples. The ratio of # of objects in patients / # of objects in controls was set to 7000 if no were objects found in the control samples.*

5.2.7 CTC cut off value for aCTC and mCTC

The influence of the CTC cut-off value from > 1–10 CTC on the number of patients affected, the median overall survival, HR and its significance for both baseline and follow-up samples were determined and shown in tables 5.1 and 5.2 (p-values for all HRs < 0.0001, except baseline cut-off=1: $p = 0.0003$ for classifier and $p = 0.004$ for Cellsearch). To arrive at a cut-off value for aCTC comparable to the mCTC cutoff of 5 used in routine clinical practice we used the slope of 1.33 of the correlation between aCTC and mCTC. This resulted in a cut-off of 4 aCTC. Kaplan Meier plots were generated for 185 baseline and 185 follow-up samples using the standard cut-off value of 5 CTC for mCTC and the cut-off value for aCTC of 4. Figure 5.4, panel A shows the Kaplan Meier plot for the baseline samples. Cox regression yielded a HR of 2.8 (95% confidence interval, CI, 1.9–4.1) for aCTC and a HR of 2.9 (95% CI 2.0–4.4) for mCTC. Figure 5.4, panel B shows the Kaplan Meier plot for the follow-up samples. For first follow-up samples we found a HR of 3.9 (95% CI (2.6–5.9) for aCTC and a HR of 4.5 (95% 3.0–6.8) for mCTC.

5.2.8 Validation of the automated CTC count

To validate the aCTC count an independent data set from metastatic prostate cancer patients treated with Abiraterone on Phase I and II studies reported previously [16, 17] was used. 4296 objects were classified as aCTC in the 93 baseline samples and 7489 objects classified as aCTC in the 96 follow-up samples. In the baseline samples the aCTC counts range was 0–1258 (median 3, mean 46, SD 152) and a range of 0–1108 (median 6, mean 53 SD 151) was found for mCTC. R^2-correlation between aCTC and mCTC was 0.28 (slope = 0.52, intercept = 28.78). A single outlier contributed to this result, exclusion of this outlier resulted in a R^2 of 0.90 (slope 0.52, intercept 5.40). In the follow-up samples the aCTC counts range was 0–2490 (median 2, mean 78, SD 326) and a range of 0–3573 (median 2, mean 74, SD 390) with mCTC. The R^2-correlation between aCTC and mCTC both was 0.83 (slope = 1.09, intercept = -11.43). Kaplan Meier plots were generated for 93 baseline and 96 follow-up samples using the standard CTC cut off of 5 CTC for mCTC and 4 CTC for aCTC. Figure 5.4, panel C shows the Kaplan Meier plot from the baseline samples. Cox regression resulted in a HR of 3.9 (95% CI 2.4–6.6) for aCTC and a HR of 4.8 (95% CI 2.8–8.3) for mCTC. The Kaplan Meier plot from the follow-up samples are presented in figure 5.4, panel D. A HR of 5.4 (95% CI 3.2–8.9) was found for aCTC and a HR of 5.8 (95% CI 3.4–9.8) for mCTC (p-values for all HRs < 0.0001). Tables 5.1 and 5.2 show the influence of other cut off values.

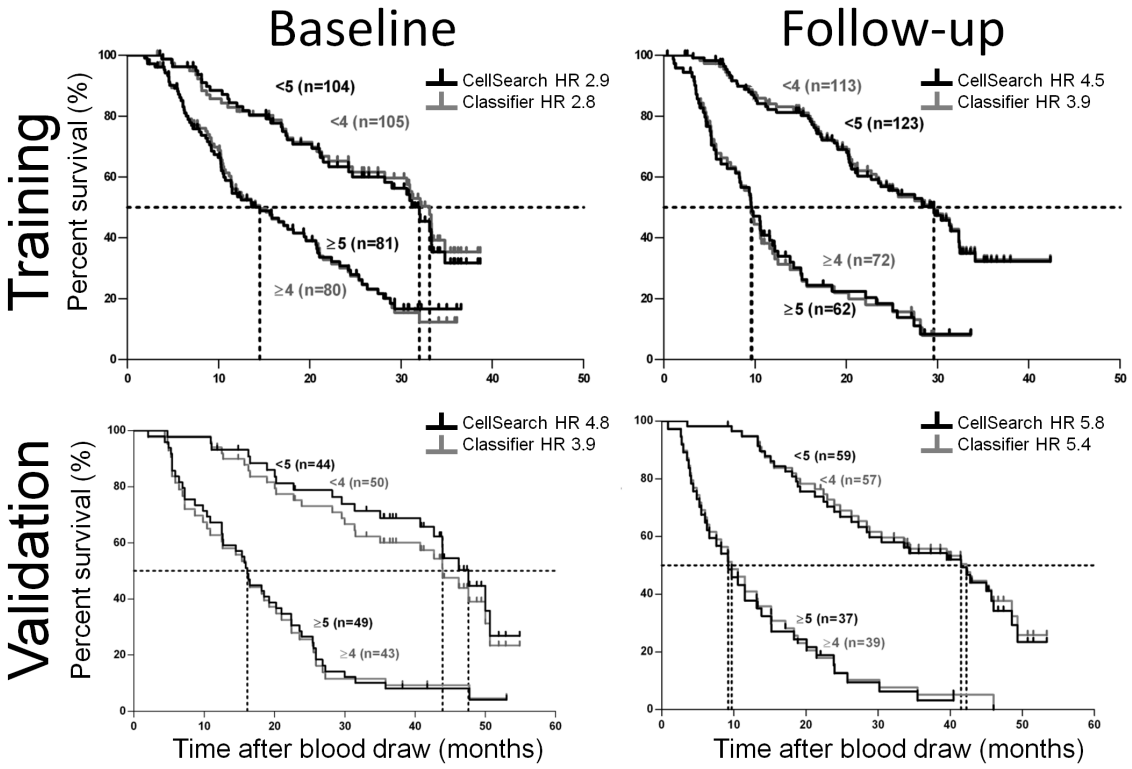

Figure 5.4: Kaplan-Meier plots of the classifier (grey lines) and the original Cellsearch (black lines) definition in the test and validation sets. *The patient group was dichotomized on a threshold. For CellSearch this threshold was the currently clinically used 5 mCTC. The threshold for the classifier was determined by dividing the Cellsearch threshold by the linear regression slope between Cellsearch and classifier of 1.33, resulting in 4 aCTC. Kaplan Meier plots for the training set are shown in panel A (baseline, $N = 185$) and panel B (follow-up, $N = 185$). Kaplan Meier plots for the validation set are shown in panel C (baseline, $N = 93$) and panel D (follow-up, $N = 96$).*

Table 5.1: aCTC and mCTC cut-off values with HRs (95% CI), median Overall Survival, for baseline and first follow-up samples for the training set IMMC-38.

	Classifier				**Cellsearch**			
Cut Off (CO)	$n \geq$ CO (%)	50% OS $<$ CO	50% OS $>$ CO	HR	n $\geq$ CO (%)	50% OS $<$ CO	50% OS $>$ CO	HR
Baseline ($n = 185$)								
1	147 (79)	33.0	17.5	2.6 (1.6–4.5)	145 (78)	32.0	17.4	2.0 (1.2–3.2)
2	126 (68)	33.3	15.8	3.0 (1.9–4.8)	128 (69)	33.3	15.6	2.8 (1.8–4.4)
3	115 (62)	33.3	15.2	3.0 (1.9–4.6)	118 (64)	33.1	15.2	2.9 (1.9 4.4)
4	105 (57)	33.1	14.5	2.8 (1.9–4.1)	108 (58)	32.1	14.5	2.5 (1.7–3.7)
5	93 (50)	31.2	13.6	3.1 (2.1–4.7)	104 (56)	32.0	14.5	2.9 (2.0–4.4)
6	87 (47)	32.0	12.5	3.0 (2.0–4.5)	96 (52)	32.0	13.6	2.8 (1.9–4.2)
7	82 (44)	31.0	11.5	3.2 (2.2–4.8)	95 (51)	32.0	13.6	3.1 (2.1–4.5)
8	75 (41)	30.6	11.4	3.1 (2.1–4.6)	87 (47)	31.2	11.5	3.2 (2.1–4.7)
9	72 (39)	30.6	11.4	3.0 (2.0–4.4)	84 (45)	31.2	11.4	3.4 (2.3–5.0)
10	70 (38)	29.0	11.4	2.9 (1.9–4.3)	78 (42)	30.6	10.6	3.2 (2.1–4.7)
Follow-up ($n = 185$)								
1	129 (70)	31.4	15.2	2.3 (1.6–3.5)	110 (59)	33.4	12.5	3.0 (2.1–4.5)
2	98 (53)	29.6	11.6	3.6 (2.4–5.3)	94 (51)	31.1	11.5	3.9 (2.6–5.7)
3	79 (43)	29.6	9.8	4.0 (2.7–5.9)	81 (44)	31.2	10.3	4.4 (2.9–6.5)
4	72 (39)	29.6	9.6	3.9 (2.6–5.9)	77 (42)	31.2	10.3	3.8 (2.5–5.6)
5	67 (36)	28.3	9.5	4.8 (3.2–7.3)	71 (38)	30.6	10.5	4.5 (3.0–6.8)
6	62 (34)	28.3	9.4	4.4 (2.9–6.6)	64 (35)	29.3	10.2	4.7 (3.1–7.1)
7	57 (31)	25.7	9.4	4.4 (2.9–6.6)	62 (34)	29.3	10.2	4.5 (3.0–6.8)
8	57 (31)	25.7	9.4	4.5 (2.9–6.8)	58 (31)	28.2	9.2	4.7 (3.1–7.1)
9	53 (29)	25.7	9.4	4.0 (2.6–6.1)	55 (30)	28.2	9.2	4.7 (3.1–7.2)
10	49 (26)	25.6	9.4	3.9 (2.6–6.0)	51 (28)	27.5	9.2	4.3 (2.8–6.6)

CO: Cut Off, OS: Overall Survival, HR: Hazard Ratio

Table 5.2: aCTC and mCTC cut-off values with HRs (95% CI), median Overall Survival, for baseline and first follow-up samples for the validation set Abiraterone.

	Classifier				**Cellsearch**			
Cut Off (CO)	$n \geq$ CO (%)	50% OS $<$ CO	50% OS $>$ CO	HR	n $\geq$ CO (%)	50% OS $<$ CO	50% OS $>$ CO	HR
Baseline ($n = 93$)								
1	69 (74)	50.0	20.3	4.3 (2.2–8.7)	60 (65)	50.0	18.5	3.8 (2.1–6.9)
2	54 (58)	46.2	18.1	3.3 (2.0–5.7)	56 (60)	47.6	18.1	4.0 (2.3–7.0)
3	49 (53)	46.2	16.3	4.0 (2.4–6.8)	50 (54)	47.6	16.1	4.8 (2.8–8.4)
4	43 (46)	44.0	16.1	3.9 (2.4–6.6)	49 (53)	47.6	16.1	4.8 (2.8–8.3)
5	43 (46)	44.0	16.1	3.9 (2.8–6.6)	49 (53)	47.6	16.1	4.8 (2.8–8.3)
6	41 (44)	43.9	15.9	3.8 (2.3–6.2)	47 (51)	46.2	16.1	4.4 (2.6–7.4)
7	37 (40)	43.9	15.4	3.6 (2.2–5.9)	45 (48)	44.0	16.3	3.9 (2.3–6.5)
8	36 (39)	42.7	14.5	3.5 (2.2–5.8)	43 (46)	44.0	16.1	3.8 (2.3–6.4)
9	35 (38)	42.7	15.4	3.3 (2.0–5.4)	41 (44)	43.9	15.9	3.6 (2.2–5.9)
10	33 (35)	40.7	15.4	3.0 (1.8–4.9)	40 (43)	43.9	15.7	3.5 (2.1–5.7)
Follow-up ($n = 96$)								
1	58 (60)	48.5	13.8	5.4 (3.0–9.9)	55 (57)	48.5	13.8	5.4 (3.1–9.6)
2	51 (53)	45.0	13.3	5.0 (2.9–8.6)	50 (52)	45.0	11.5	5.0 (2.9–8.5)
3	40 (42)	42.2	9.7	5.6 (3.4–9.4)	44 (46)	42.2	11.1	4.8 (2.9–8.0)
4	39 (41)	42.2	9.7	5.4 (3.2–8.9)	40 (42)	42.2	9.7	6.6 (3.8–11.4)
5	37 (39)	41.5	9.7	4.9 (3.0–8.1)	37 (39)	41.5	9.2	5.8 (3.4–9.8)
6	34 (35)	41.5	9.2	6.8 (3.9–11.6)	36 (38)	41.5	9.2	6.2 (3.7–10.5)
7	33 (34)	41.5	9.2	6.6 (3.8–11.1)	36 (38)	41.5	9.2	6.2 (3.7–10.5)
8	32 (33)	41.5	9.2	6.1 (3.6–10.4)	35 (36)	41.5	9.2	5.9 (3.5–10.0)
9	30 (31)	39.5	9.2	6.2 (3.6–10.5)	32 (33)	39.5	7.6	5.3 (3.2–8.9)
10	28 (29)	34.4	9.2	5.5 (3.3–9.5)	32 (33)	39.5	7.6	5.3 (3.2–8.9)

CO: Cut Off, OS: Overall Survival, HR: Hazard Ratio

5.3 Discussion

Multicenter prospective clinical studies have shown a significant relation between the presence of mCTC defined by the Cellsearch CTC definition and poor progression-free and overall survival; studies are underway to evaluate whether a fall in CTC is a surrogate of overall survival from advanced prostate cancer [2, 3, 4, 5, 6, 7, 8, 13]. It is envisioned that the clinical use of CTC studies will rapidly increase in the near future. These translational studies are, however, hindered by the laborious, manual, CTC identification process, which increases study costs and is associated with variability of the CTC classification by different operators. We have recently shown that all circulating EpCAM+CK+CD45- objects predict overall survival in castration-resistant prostate cancer and that different morphological definitions for CTC can be used supporting the possibility that automated and clinically relevant CTC identification is feasible [12]. Utilizing overall survival from two cohorts of patients with metastatic castration resistant prostate cancer receiving either chemotherapy (training cohort) or the highly active hormonal agent abiraterone (validation cohort) we have evaluated all the EpCAM positive circulating objects detected by ten Cellsearch systems to determine the most clinically relevant automated algorithm for CTC identification. We have now shown that automated count of EpCAM+ CK+ objects is fast, 100% reproducible and comparable to the manual count performed utilizing the established method. It must be stressed that our automatic count was only compared to the one manual count performed during the study [13]. In an earlier study it was found that in only 50% of cases two independent readers will read the same number of mCTC [11].
There are many ways of testing and optimizing classifiers to improve robustness. However, most of these methods require a training set for which an absolute ground truth is known. Unfortunately in this research, this ground truth cannot be established. After enrichment of the blood sample, many objects still remain that have no influence on patient survival. The impact on survival of each object cannot be verified by inspecting it. The Cox hazard ratio and the number of objects in controls are our measure if a classifier is working properly. This indirect measure, which can only be evaluated by looking at a group of patients, cannot assure which objects are 100% responsible for patient survival. By using the bootstrap method we have chosen the classifier, that is least influenced by certain dominating patients and gives consistent results for every subset of the total patient group. In this way we reduced the risk of over-training of the classifier. We found that the classifiers that were the most promising had an equal spread in HR.
Many pre-processing steps may be applied to the images that are recorded. Before segmentation, edge enhancement may be applied, as well as background correction and many more. The impact of such procedures may increase or reduce the fidelity of a parameter in unpredictable ways. We did

not apply any pre-processing to avoid making any presumptions about what kind of particles we were looking for. This led to an independent analysis of the CTC definition.

The CTC classifier that was chosen resulted in the identification of one object in the control samples. Usually, such an auto-fluorescent object is discarded if it is positive in the FITC channel. However, using the feature "maximum value in the FITC channel" in the classifier did not yield an improvement over the existing classifier. This is advantageous since this channel can now be used to not only detect the presence but also quantify the expression of biomarkers on the CTC [18, 19]. It was furthermore concluded that some of the objects positive in the FITC channel were important for patient survival. This was surprising, as no fluorescent label was used in this channel. Bleed through of fluorescence signal from bright PE objects into this FITC channels was the likely cause for this observation.

For the purpose of the development of the CTC classifier patients were divided into two groups based on the median aCTC count in the training set of 185 baseline samples. This division was chosen to minimize statistical error in the HR. The median count for the chosen aCTC classifier on the baseline samples was 5 aCTC and resulted in a HR of 3.1. The current standard Cellsearch method presents to the reviewer CK+ DAPI+ objects for classification with a threshold of 5 or more mCTC being used to discriminate between those patients with a favorable and unfavorable prognosis. In an earlier study we argued that this threshold of 5 mCTC could be mainly attributed to error introduced by human interpretation [11]. As this error is eliminated by the automated method one could argue that the presence of any CTC with the automated method can be used to identify patients at risk although this algorithm may rarely incorrectly identify CTC. To arrive at a threshold for aCTC we used the correlation statistics between mCTC and aCTC and propose to use a cut-off for aCTC of 4. The Kaplan-Meier plots of baseline and follow-up using aCTC and mCTC illustrated in figure 5.4 show that they are similar.

Our aCTC definition was validated using an independent data set. This validation set showed that our classifier is not likely to be over-trained as comparable HRs to the Cellsearch definition were obtained. Correlation with Cellsearch count was quite low (0.28), due to one outlier. For this patient, our algorithm counted 1344 aCTC, whereas the operator only counted 67 mCTC. The images of this sample revealed a very high cell density, in which it is hard for a human operator to verify whether a CK+ object had the right morphology in combination with a nucleus. Because many CK+ objects were available only the most distinguishable cells were selected which may have resulted in a slight undercounting of mCTC objects. In contrast, the algorithm looks at signal levels rather than morphology and over-counted due to overlapping cells in this sample. A CK+ cell fragment overlapped by a CD45 dim leukocyte could also in this way have potentially been counted as an aCTC; this patient sample had very low CD45-APC

signal levels, reducing the rejection of objects by the classifier on the APC peak value. Nonetheless, the Kaplan-Meier plots of baseline and follow-up using aCTC and mCTC from the validation set illustrated in figure 5.4 strongly supports the use of the aCTC for routine clinical use.
Although the patient groups were dichotomized, it is clear that the presence of larger number of CTC is related to a poorer prognosis; determination of a meaningful increase or decrease in CTC upon treatment is however difficult to assess reliably as the number of CTC that are detected are so low that a decrease or increase is often statistically insignificant. Exploration of alternative definitions that for example include Tumor Micro Particles that occur in larger frequencies may resolve this issue.

5.4 Materials and methods

5.4.1 Patients

Development and validation of image analysis algorithms for automated CTC enumeration were performed on stored images from 10 Cellsearch systems (Veridex LLC, Raritan, NJ) from patients and controls participating in prospective studies, all provided written informed consent. 276 patients were enrolled in IMMC-38 [13], 231 were eligible and for 185 of those patients images could be imported for baseline and first follow-up. A total of 65 clinical centers in the United States and Europe participated in this study. Images of 68 healthy individuals participating in the IMMC-06 study [20, 21] were available. This prospective trial was conducted at 55 clinical centers throughout the US, the Netherlands, and the United Kingdom. Institutional review boards at each center approved both study protocols. For validation of the algorithm images were used from samples from consented patients participating in Phase I and II clinical studies of abiraterone acetate conducted at the Royal Marsden NHS Foundation Trust and reported previously [16, 17]. These studies were approved by the Ethics Review Committees of the Royal Marsden Hospital. Samples collected up to 14 days before initiation of abiraterone acetate (93 samples) and after one cycle (28 days) of therapy (96 samples) were used for this analysis. All patients had histologically confirmed prostate adenocarcinoma, castrate levels of testosterone and progressive disease as defined by three consecutively rising PSA values [22]. Fifty-one baseline and 52 follow-up samples were collected from chemotherapy-naïve patients and 41 baseline and 44 follow-up from docetaxel-pretreated patients. Samples were processed at The Institute of Cancer Research (ICR) and archived images were sent for automated analysis at the University of Twente. The University of Twente was blinded to clinical details and survival data for these samples. Statistical analysis was performed independently by A.M.C. in The ICR.

5.4.2 Isolation of EpCAM+ objects and fluorescence imaging

The Cellsearch system was used to enumerate CTC. The system consists of a CellTracks Autoprep for sample preparation and a CellTracks Analyzer II for sample analysis [1, 9, 11]. The Celltracks Autoprep immuno-magnetically enriches epithelial cells from 7.5 mL of blood using ferrofluids conjugated to epithelial cell adhesion molecule antibodies (EpCAM). The enriched sample is stained with phycoerythrin-conjugated (PE) antibodies directed against cytokeratins (CK) 8, 18 and 19, an allophycocyanin-conjugated (APC) antibody to CD45 and the nuclear dye 4',6-diamidino-2-phenylindole (DAPI). This enriched sample is then transferred to a magnetic cartridge where all ferrofluid labeled objects are pulled towards a cover slip. The entire cartridge cover slip is imaged by the CellTracks Analyzer II, a four-color semi-automated fluorescence microscope that captures digital images for four different fluorescent dyes. It does so using a 10X/0.45 NA objective and a CCD camera with 6.7×6.7 µm^2 sized pixels. Next to the DAPI, PE and APC images, a fourth fluorescence channel (emission 535 ± 25 nm) is imaged as a control channel for exclusion of auto-fluorescent debris. This channel is termed "FITC" channel. Per cartridge, 144–180 4-layer tiff images are saved per patient.

5.4.3 General algorithm development approach

Algorithm development was performed in Matlab 2009a (Mathworks, Natick, MA) using the DIPimage toolbox (TU-Delft, The Netherlands, diplib.org). Figure 5.1 illustrates the method used to develop the classifier, of which the four steps are explained further below.

5.4.4 1. Import of images and selection of analysis area

CDs containing archived images for samples belonging to the respective studies were collected for import to a central hard drive. Detection of the sample border was performed via edge detection in the debris-FITC channel and the area outside the border was excluded from further analysis. All FITC images from a scan were sub-sampled by a factor of 8. Next, images expected to have a certain orientated border were convolved with a line-shape kernel to boost this orientation. Finally, the convolved image was filtered by a gradient magnitude filter (gaussian derivative width 8 pixels) to boost the edges. The resulting images were connected to each other to construct an image of the surface of the cartridge which was then thresholded via the triangle threshold method. After holes in the thresholded areas were filled, the area of interest was selected via a binary propagation algorithm and the result was verified by comparing to the possible area range between 72 and 92 mm^2. If the detected area failed this

check, boundaries were estimated using results from a fixed set of previously analyzed cartridges. This estimation had to be applied for 8 samples (of 370, 2%), whose cartridges had very irregular edges.

5.4.5 2. Determine segmentation channel

First step in automated image analysis is to determine where objects of interest are and what their outline is, so-called segmentation. The samples used for this step were all baseline samples. Objects were segmented using the triangle threshold [23] applied to six different channels: DAPI, FITC, PE, APC, sum of DAPI and PE and a maximum intensity profile of all four channels. The threshold value for each channel was multiplied with a factor in order to be as sensitive as possible, but not to segment large areas of noise (factor range 1.30–1.75). The sum of DAPI and PE channel was chosen because Cellsearch selects objects positive in both PE and DAPI for review. The maximum intensity profile was expected to approach the actual outline of cells in the cartridge most accurately. Objects smaller than 9 pixels and larger than 2000 pixels were rejected. There were too many objects smaller than 9 pixels, most of which looked like noise on close examination. Objects bigger than 2000 pixels (≈ 900 µm^2) cannot be single cellular objects. For each investigated segmentation channel the HR was determined after dichotomization of the patient group on the median number of segmented objects per patient. The channel which yielded the highest HR was selected for further analysis.

5.4.6 3. Select four independent properties with highest impact on HR

For each object that was found in the selected segmentation method 24 features were extracted; peak intensity, standard deviation of intensity, mean intensity and total intensity in the DAPI, FITC, PE, APC channels, as well as roundness, size, height and width, perimeter, first and second moments of inertia, and center of gravity in the segmentation channel. We required at least 15 samples per feature included in the classifier to prevent over fitting, four features were selected because there were only 68 samples in the healthy controls. Selection of high impact features was achieved by univariate analysis. For each feature objects were excluded if they were above or below a variable threshold. At each threshold tested, the HR was determined by dichotomizing patients on the median number of objects found in the patient population. The maximum obtained HR was determined for each feature and features were ranked according to HR. The covariance matrix was also determined for all features. Features with correlation coefficients less than 0.4 with all features ranked higher in HR were selected for further classifier development.

5.4.7 4. Create classifiers and use bootstrap aggregating to test for robustness

A classifier required an object to fall within the inclusion criteria for each of the 4 features. 16464 different classifiers were created by varying the inclusion criteria independently. Performance of each classifier was tested against our training set of baseline and follow-up samples. To prevent over-training of the classifier due to possible high impact of a few dominating samples, the bootstrap aggregating method [24] was employed to test the robustness of each classifier. Each classifier was tested on 402 sets of 185 random pickings -with replacement- from the total of 185 samples. When picking n samples with replacement from a group with N samples using a large set, 63% of the samples are expected to be unique. Taking 402 sets of 185 random numbers results in each sample appearing approximately 402 times with a coefficient of variation of 5%. In this way, strong dependency on a few samples is averaged out. Furthermore, when deriving a HR after 402 picks, the spread of this HR provides a CI and thus a comparative measure for stability. The optimal classifier met the following requirements:

1. The classifier has a high HR in both baseline and follow-up samples.
2. The ratio between the number of objects found in patients and controls is large.
3. The absolute number of particles in the control samples is very low.
4. The HR from the follow-up samples is higher than that of the baseline samples
5. The CI of the HR is not above average.

Acknowledgements

The authors would like to thank the members of the main Veridex LLC CellSearch processing lab for providing data on the review processing time.

5.5 References

[1] W. J. Allard, J. Matera, M. C. Miller, M. Repollet, M. C. Connelly, C. Rao, A. G. Tibbe, J. W. Uhr, and L. W. Terstappen, "Tumor cells circulate in the peripheral blood of all major carcinomas but not in healthy subjects or patients with nonmalignant diseases," *Clin. Cancer Res.*, vol. 10, pp. 6897–6904, Oct 2004.

[2] G. T. Budd, M. Cristofanilli, M. J. Ellis, A. Stopeck, E. Borden, M. C. Miller, J. Matera, M. Repollet, G. V. Doyle, L. W. Terstappen, and D. F. Hayes, "Circulating tumor cells versus imaging–predicting overall survival in metastatic breast cancer," *Clin. Cancer Res.*, vol. 12, pp. 6403–6409, Nov 2006.

[3] S. J. Cohen, C. J. Punt, N. Iannotti, B. H. Saidman, K. D. Sabbath, N. Y. Gabrail, J. Picus, M. A. Morse, E. Mitchell, M. C. Miller, G. V. Doyle, H. Tissing, L. W. Terstappen, and N. J. Meropol, "Prognostic significance of circulating tumor cells in patients with metastatic colorectal cancer," *Ann. Oncol.*, vol. 20, pp. 1223–1229, Jul 2009.

[4] M. Cristofanilli, G. T. Budd, M. J. Ellis, A. Stopeck, J. Matera, M. C. Miller, J. M. Reuben, G. V. Doyle, W. J. Allard, L. W. Terstappen, and D. F. Hayes, "Circulating tumor cells, disease progression, and survival in metastatic breast cancer," *N. Engl. J. Med.*, vol. 351, pp. 781–791, Aug 2004.

[5] M. Cristofanilli, D. F. Hayes, G. T. Budd, M. J. Ellis, A. Stopeck, J. M. Reuben, G. V. Doyle, J. Matera, W. J. Allard, M. C. Miller, H. A. Fritsche, G. N. Hortobagyi, and L. W. Terstappen, "Circulating tumor cells: a novel prognostic factor for newly diagnosed metastatic breast cancer," *J. Clin. Oncol.*, vol. 23, pp. 1420–1430, Mar 2005.

[6] D. F. Hayes, M. Cristofanilli, G. T. Budd, M. J. Ellis, A. Stopeck, M. C. Miller, J. Matera, W. J. Allard, G. V. Doyle, and L. W. Terstappen, "Circulating tumor cells at each follow-up time point during therapy of metastatic breast cancer patients predict progression-free and overall survival," *Clin. Cancer Res.*, vol. 12, pp. 4218–4224, Jul 2006.

[7] D. Olmos, H. T. Arkenau, J. E. Ang, I. Ledaki, G. Attard, C. P. Carden, A. H. Reid, R. A'Hern, P. C. Fong, N. B. Oomen, R. Molife, D. Dearnaley, C. Parker, L. W. Terstappen, and J. S. de Bono, "Circulating tumour cell (CTC) counts as intermediate end points in castration-resistant prostate cancer (CRPC): a single-centre experience," *Ann. Oncol.*, vol. 20, pp. 27–33, Jan 2009.

[8] J. Tol, M. Koopman, M. C. Miller, A. Tibbe, A. Cats, G. J. Creemers, A. H. Vos, I. D. Nagtegaal, L. W. Terstappen, and C. J. Punt, "Circulating tumour cells early predict progression-free and overall survival in advanced colorectal cancer patients treated with chemotherapy and targeted agents," *Ann. Oncol.*, vol. 21, pp. 1006–1012, May 2010.

[9] M. Kagan, D. Howard, T. Bendele, J. Mayes, J. Silvia, M. Repollet, J. Doyle, J. Allard, N. Tu, T. Bui, T. Russell, C. Rao, M. Hermann, H. Rutner, and L. Terstappen, "A sample preparation and analysis system for identification of circulating tumor cells," *J Clinical Ligand Assay*, vol. 25, pp. 104–50, 2002.

[10] J. Kraan, S. Sleijfer, M. H. Strijbos, M. Ignatiadis, D. Peeters, J. Y. Pierga, F. Farace, S. Riethdorf, T. Fehm, L. Zorzino, A. G. Tibbe, M. Maestro, R. Gisbert-Criado, G. Denton, J. S. de Bono, C. Dive, J. A. Foekens, and J. W. Gratama, "External quality assurance of circulating tumor cell enumeration using the CellSearch system: a feasibility study," *Cytometry B Clin Cytom*, vol. 80, pp. 112–118, Mar 2011.

[11] A. G. Tibbe, M. C. Miller, and L. W. Terstappen, "Statistical considerations for enumeration of circulating tumor cells," *Cytometry A*, vol. 71, pp. 154–162, Mar 2007.

[12] F. A. Coumans, C. J. Doggen, G. Attard, J. S. de Bono, and L. W. Terstappen, "All circulating EpCAM+CK+CD45- objects predict overall survival in castration-resistant prostate cancer," *Ann. Oncol.*, vol. 21, pp. 1851–1857, Sep 2010.

[13] J. S. de Bono, H. I. Scher, R. B. Montgomery, C. Parker, M. C. Miller, H. Tissing, G. V. Doyle, L. W. Terstappen, K. J. Pienta, and D. Raghavan, "Circulating tumor cells predict survival benefit from treatment in metastatic castration-resistant prostate cancer," *Clin. Cancer Res.*, vol. 14, pp. 6302–6309, Oct 2008.

[14] A. H. Reid, G. Attard, D. C. Danila, N. B. Oommen, D. Olmos, P. C. Fong, L. R. Molife, J. Hunt, C. Messiou, C. Parker, D. Dearnaley, J. F. Swennenhuis, L. W. Terstappen, G. Lee, T. Kheoh, A. Molina, C. J. Ryan, E. Small, H. I. Scher, and J. S. de Bono, "Significant and sustained antitumor activity in post-docetaxel, castration-resistant prostate cancer with the CYP17 inhibitor abiraterone acetate," *J. Clin. Oncol.*, vol. 28, pp. 1489–1495, Mar 2010.

[15] G. Attard, J. F. Swennenhuis, D. Olmos, A. H. Reid, E. Vickers, R. A'Hern, R. Levink, F. Coumans, J. Moreira, R. Riisnaes, N. B. Oommen, G. Hawche, C. Jameson, E. Thompson, R. Sipkema, C. P. Carden, C. Parker, D. Dearnaley, S. B. Kaye, C. S. Cooper, A. Molina, M. E. Cox, L. W. Terstappen, and J. S. de Bono, "Characterization of ERG, AR and PTEN gene status in circulating tumor cells from patients with castration-resistant prostate cancer," *Cancer Res.*, vol. 69, pp. 2912–2918, Apr 2009.

[16] G. Attard, A. H. Reid, T. A. Yap, F. Raynaud, M. Dowsett, S. Settatree, M. Barrett, C. Parker, V. Martins, E. Folkerd, J. Clark, C. S. Cooper, S. B. Kaye, D. Dearnaley, G. Lee, and J. S. de Bono, "Phase I clinical trial of a selective inhibitor of CYP17, abiraterone acetate, confirms that castration-resistant prostate cancer commonly remains hormone driven," *J. Clin. Oncol.*, vol. 26, pp. 4563–4571, Oct 2008.

[17] G. Attard, A. H. Reid, R. A'Hern, C. Parker, N. B. Oommen, E. Folkerd, C. Messiou, L. R. Molife, G. Maier, E. Thompson, D. Olmos, R. Sinha, G. Lee, M. Dowsett, S. B. Kaye, D. Dearnaley, T. Kheoh, A. Molina, and J. S. de Bono, "Selective inhibition of CYP17 with abiraterone acetate is highly active in the treatment of castration-resistant prostate cancer," *J. Clin. Oncol.*, vol. 27, pp. 3742–3748, Aug 2009.

[18] S. Meng, D. Tripathy, S. Shete, R. Ashfaq, H. Saboorian, B. Haley, E. Frenkel, D. Euhus, M. Leitch, C. Osborne, E. Clifford, S. Perkins, P. Beitsch, A. Khan, L. Morrison, D. Herlyn, L. W. Terstappen, N. Lane, J. Wang, and J. Uhr, "uPAR and HER-2 gene status in individual breast cancer cells from blood and tissues," *Proc. Natl. Acad. Sci. U.S.A.*, vol. 103, pp. 17361–17365, Nov 2006.

[19] J. S. de Bono, G. Attard, A. Adjei, M. N. Pollak, P. C. Fong, P. Haluska, L. Roberts, C. Melvin, M. Repollet, D. Chianese, M. Connely, L. W. Terstappen, and A. Gualberto, "Potential applications for circulating tumor cells expressing the insulin-like growth factor-I receptor," *Clin. Cancer Res.*, vol. 13, pp. 3611–3616, Jun 2007.

[20] S. J. Cohen, R. K. Alpaugh, S. Gross, S. M. O'Hara, D. A. Smirnov, L. W. Terstappen, W. J. Allard, M. Bilbee, J. D. Cheng, J. P. Hoffman, N. L. Lewis, A. Pellegrino, A. Rogatko, E. Sigurdson, H. Wang, J. C. Watson, L. M. Weiner, and N. J. Meropol, "Isolation and characterization of circulating tumor cells in patients with metastatic colorectal cancer," *Clin Colorectal Cancer*, vol. 6, pp. 125–132, Jul 2006.

[21] S. J. Cohen, C. J. Punt, N. Iannotti, B. H. Saidman, K. D. Sabbath, N. Y. Gabrail, J. Picus, M. Morse, E. Mitchell, M. C. Miller, G. V. Doyle, H. Tissing, L. W. Terstappen, and N. J. Meropol, "Relationship of circulating tumor cells to tumor response, progression-free survival, and overall survival in patients with metastatic colorectal cancer," *J. Clin. Oncol.*, vol. 26, pp. 3213–3221, Jul 2008.

[22] G. J. Bubley, M. Carducci, W. Dahut, N. Dawson, D. Daliani, M. Eisenberger, W. D. Figg, B. Freidlin, S. Halabi, G. Hudes, M. Hussain, R. Kaplan, C. Myers, W. Oh, D. P. Petrylak, E. Reed, B. Roth, O. Sartor, H. Scher, J. Simons, V. Sinibaldi, E. J. Small, M. R. Smith, D. L. Trump, and G. Wilding, "Eligibility and response guidelines for phase II clinical trials in androgen-independent prostate cancer: recommendations from the Prostate-Specific Antigen Working Group," *J. Clin. Oncol.*, vol. 17, pp. 3461–3467, Nov 1999.

[23] G. W. Zack, W. E. Rogers, and S. A. Latt, "Automatic measurement of sister chromatid exchange frequency," *J. Histochem. Cytochem.*, vol. 25, pp. 741–753, Jul 1977.

[24] L. Breiman, "Bagging predictors," *Machine Learning*, vol. 24, pp. 123–140, 1996.

CHAPTER 6

Interpretation of changes in circulating tumor cell counts

S.T. Ligthart *, F.A.W. Coumans *, and L.W.M.M. Terstappen
Translational Oncology, in press, 2012
* both authors contributed equally to this work

Abstract

The presence of circulating tumor cells (CTC) in the blood of cancer patients may guide the use of therapy. We investigated how to evaluate a reduction in the number of CTC after administration of therapy. CTC were enumerated with the CellSearch system in 111 metastatic breast and 185 metastatic prostate cancer patients before start of a new line of chemotherapy and after initiation of therapy. CTC were enumerated by manual review and by an automated algorithm using four selection criteria. Different means to express changes in CTC counts were evaluated with respect to progression free (PFS) and overall survival (OS). A static CTC cut-off is the best method to determine whether a therapy is effective. This is exemplified by the highest Cox hazard ratios for OS of 2.1–3.0 and for PFS of 2.0–2.9 for all CTC definitions; three methods to express relative differences performed worse. We furthermore show that a very strict CTC definition is the most useful because of low background in healthy controls. A look-up table is provided from which the significance of a change in CTC can be derived. The aim of therapy should be elimination of all CTC. An automated CTC count with a low background is the best means to measure CTC elimination. A

period of 10–12 weeks of therapy is needed to reach the treatment effect on CTC.

6.1 Introduction

Circulating tumor cells (CTC) leave the tumor site(s), invade the blood stream, and may give rise to distant metastases. The presence of CTC has been associated with poor survival in melanoma, breast, colorectal, prostate, gastric, and non-small cell lung cancer [1, 2, 3, 4, 5, 6]. The association between the presence of CTC and poor prognosis holds true before and at various time intervals after initiation of therapy [3, 4, 7]. Transition from unfavorable ($\geq$ 5 CTC/7.5 mL of blood) to favorable CTC ($<$ 5 CTC/7.5 mL of blood) improves survival and as such can be used as a predictive factor for treatment response [2, 3, 4, 7]. This transition can already be measured after the first cycle of therapy, which is considerably earlier compared to treatment response measured by imaging. Moreover conversion to favorable or unfavorable CTC may be a better indicator of therapy response as compared to imaging [3, 8, 9]. Although conversion to no detectable CTC most likely gives the best outcome, the time needed to assure whether or not this target is reached under the current treatment regimen is unknown. Change in therapy before ineffectiveness of the current therapy has been proven is undesirable. Accurate measurement of a decline in CTC is hampered by the low frequency of CTC in most patients with metastatic disease [10]. Not only the continuous relationship between CTC concentration and survival but also the Poisson sampling error suggests that dichotomization may not be the best approach to detect effective chemotherapy [11, 12, 13]. The goal of this study was to investigate how to optimally define a true decrease in the number of CTC and to determine whether less strict definitions of CTC could aid in the assessment of a CTC reduction. To address these questions we estimated the prognostic power of various methods to express a change in the CTC number.

6.2 Materials and methods

6.2.1 Patient data

For this study we used stored images of CTC measurements from patients before initiation of a new cycle of cytotoxic chemotherapy (baseline) and at several follow-up time-points in a thirteen-week period after initiation of therapy. Samples from patients enrolled into the IMMC-01 metastatic breast cancer [2] and IMMC-38 metastatic prostate cancer [4] studies were used. This study included 111 baseline samples and 265 follow up samples from 111 metastatic breast cancer patients and 185 baseline and 425 follow-up samples from 185 metastatic prostate cancer patients. 205 samples

Table 6.1: Patient characteristics. *Numerical data are shown as median (min-max) or % of total N. The sample size n is given in parenthesis if different from the total N.*

	Breast	Prostate
N	111	185
Age	58 (27–86)	69 (49–92)
OS [a] of Px [b]	16.1 (1.5–48.6)	16.9 (1.9–38.7)
PFS [c] of Px [b]	5.5 (0.7–45.2)	5.0 (0.6–34.5)
Follow-up of censored Px [b]	20.7 (5.5–48.6, $N = 47$)	25.9 (2.4–38.9, $N = 67$)
Types of Tx [d] (1/2/3) [e]	57.8%/5.5%/36.7%	8.2%/91.8%/0%
Tx [d] line (1/2/3+)	43.2%/15.3%/41.5%	67.0%/16.2%/16.8%
Bone mets (yes/no)	90.6%/9.4%	87.4%/12.6%
PSA [f] (ng/mL)	N/A [g]	128 (1.9–17800)
LDH [h] (IU/mL)	N/A	236 (4.7–2364, $N = 139$)
ALP [i] (IU/mL)	N/A	126 (3.29–1558, $N = 179$)
Hemoglobin (g/dl)	N/A	12.4 (8.2–15.7, $N = 182$)
Albumin (g/dl)	N/A	3.8 (2.1–41, $N = 179$)
CA15.3 [j]	169.5 (0.9–19315, $N = 22$)	N/A
CA27.29 [k]	96 (9.9–23204, $N = 65$)	N/A
CEA [l]	8.2 (0.5–3920, $N = 38$)	N/A
mCTC [m]	6 (0–10194)	7 (0–5925)

[a] Overall survival, [b] Patients, [c] Progression free survival, [d] Treatment, [e] Tx types: 1 = chemo+other; 2 = chemo, hormone+other; 3 = hormone+other, [f] Prostate specific antigen, [g] Not applicable, [h] Lactate dehydrogenase, [i] Alkaline phosphatase, [j] Mucin 1 glycoprotein, [k] Milk mucin antigen, [l] Carcinoembryonic antigen, [m] Manual CellSearch circulating tumor cells.

from healthy controls were available [10, 14]. All patients provided written informed consent. The institutional review boards at each participating center approved the respective study protocols. Table 6.1 shows a summary of the patient characteristics.

6.2.2 CTC enumeration

The CellSearch system (Veridex LLC, Raritan, USA) was used for enumeration of CTC. The system consists of a CellTracks Autoprep for sample preparation and a CellTracks Analyzer II for sample analysis [10]. The CellTracks Autoprep immuno-magnetically enriches epithelial cells from 7.5 mL of blood using ferrofluids conjugated to EpCAM. The enriched sample is stained with phycoerythrin-conjugated (PE) antibodies directed against cytokeratins (CK) 8, 18 and 19, an allophycocyanin-conjugated (APC) antibody to CD45 and the nuclear dye 4',6-diamidino-2-phenylindole (DAPI). The enriched sample ($\sim$300 µL in volume) is transferred to a cartridge placed in a CellTracks Magnest where all magnetically labeled objects are pulled towards the imaging surface. The surface is imaged by the CellTracks Analyzer II and records digital images for four different fluorescent dyes, using a 10X/0.45 NA objective. Per cartridge, 144–180 four layer tiff images

Table 6.2: Characteristics of the mCTC and aCTC definitions A through D used to test different reduction criteria. *Thresholds for each parameter were defined elsewhere [15]. Size is shown as a diameter assuming a round cell. Log-rank $p < 0.0001$ for all HRs*

CTC definition	CK[b]	DNA	CD45	Size (µm)	Median count BL[c]	Median count FU1[d]	HR[a] BL	HR[a] FU1
mCTC	+	+	−	> 4	7	1	2.6	3.8
aCTC A	> 50	> 170	< 60	6–16	2	1	2.3	3.0
aCTC B	> 80	> 120	< 160	3–30	10	5	3.2	3.7
aCTC C	> 40	> 80	< 180	2–30	22	13	3.0	3.4
aCTC D	> 20	any	any	6–30	68	40	2.6	2.8

[a] Hazard ratio, [b] Cytokeratin 8, 18, 19, [c] Baseline measurement, [d] First follow-up measurement.

are recorded. To arrive at a final CTC count, objects that are CK+DAPI+ are selected by an algorithm and presented in a gallery to a trained reviewer. The reviewer scores events as manual CTC (mCTC) when the objects are CD45 negative, larger than 4 µm and have a cell-like morphology.
For automated CTC enumeration (aCTC) the same 144–180 tiff images are used as input to count aCTC by a fully automated algorithm [15]. This algorithm selects the outline of potential aCTC by object segmentation in the CK channel and measures properties of the object within these outlines. Next, the algorithm applies criteria to arrive at a final aCTC count. For this study four different definitions of aCTC were developed using overall survival as training parameter. A classifier is defined as a combination of selection criteria; by changing these criteria we can change the sensitivity and specificity of the classifier. The characteristics of the four aCTC definitions -together with the mCTC definition- used in this study are provided in table 6.2 [15]. These definitions were then used to gauge whether one of these definitions was particularly suited for assessment of a change in CTC number.

6.2.3 Poisson model for reduction in CTC count

The tree major sources of variation in CTC counting are [12]: 1) the Poisson distribution of the number of CTC present in a randomly drawn sample; 2) the variability in the enrichment efficiency and 3) the intra- and inter-reader variability. The latter source of error disappears when counting with an automated algorithm. With $80 \pm 15\%$ assay efficiency [12], the sampling error is dominant up to 44 CTC and only this error will be taken into account. When taking a sample from a large blood volume with an average concentration λ objects/sample volume, the probability that we find k objects in that sample is given by the Poisson distribution:

$$P(X = k) = \frac{e^{-\lambda}\lambda^k}{k!} \text{ for } k = 0, 1, 2, ... \tag{6.1}$$

The probability that a pair of successive measurements represents a reduction in the true mean number of CTC was determined in Matlab 2009a (Mathworks, Natick, MA). Briefly, for two measurements k_1 and k_2 the probability was derived that λ_2 is smaller than λ_1, as is represented in equation 6.2:

$$P(\lambda_2 < \lambda_1) = \int_0^\infty \left(P(X = k_2) \int_{\lambda_1 \geq \lambda_2}^\infty P(X = k_1)\, \mathrm{d}\lambda_1 \right) \mathrm{d}\lambda_2 \tag{6.2}$$

In which k_1, λ_1 represent the first and k_2, λ_2 the second CTC measurement. This equation compares two distributions of underlying true means λ that were derived from two measured k. First, for the two k, the probability is simulated that it originates from a certain mean λ, this distribution is normalized to 1. Second, for every λ from k_2 the probability is determined that it is lower than the λ from k_1. This total is summed to determine the total probability that k_2 came from a lower true mean than k_1. There is an infinite number of λ were a CTC measurement could originate from, in our simulation we chose a λ distribution with 0.01 CTC spacing. Using equation 6.2, we can determine the confidence for a CTC reduction given any pair of measurements. For each combination of baseline and follow-up measurement ranging from 0–50, the confidence for a true reduction was calculated. For aCTC definitions with high background noise, the range where the Poisson error is dominant is reduced

6.2.4 CTC reduction criteria

Several criteria to express CTC reduction were tested for their ability to predict favorable outcome. Only patients with ≥ 5 mCTC at baseline were used for this analysis ($N = 164$). The traditional CTC numbers and the four different aCTC definitions were used in this comparison. Tested criteria were:

1. Conversion to favorable group (from $\geq x$ to $< x$ CTC): a static cut-off.
2. Reduction confidence larger than x%: a cut-off according to equation 2.
3. Measurement 2 is x smaller than measurement 1: an absolute reduction cut-off.
4. Measurement 2 is x times smaller than measurement 1: a proportional reduction cut-off.

The parameter x was determined for each reduction criterion and CTC definition as described in statistical analysis.

6.2.5 Statistical analysis

The Cox proportional hazard ratio (HR) for each aCTC classifier was determined by dichotomizing on the median of the number of aCTC found at baseline. For reference, the HR for mCTC was also determined in the same way. We did not apply the cut-off of 5 (which is clinically used for mCTC) to the aCTC definitions, because this would distort the relative size of favorable and unfavorable groups. For each criterion, the HR was determined for OS unless otherwise stated. A method which delivers a high HR, but distinguishes very few metastatic patients is of no practical use. To determine how well different criteria stratify patients into two groups, the relative size of the two groups resulting from each criterion must be balanced. To achieve this, the x in the criterion 1 through 4 was set such that the percentages of patients in the favorable and unfavorable groups were similar to the clinically validated mCTC cutoff in criterion 1. The percentage of patients who remained unfavorable was found to be 59% using criterion 1 for $x = 5$ mCTC. Thus for each of the mCTC and aCTC definitions from table 6.2, the variable x was set for each criterion to approximate the unfavorable group at 59%. OS was measured from the time of blood draw to time of death from any cause. Patients were censored at last follow-up if progression or death had not occurred. Survival curves were compared with the use of log-rank testing. Progression free survival (PFS) was defined as the elapsed time between the date of the blood draw and the date of progression by CT scans and/or clinical signs and symptoms or death.

6.3 Results

6.3.1 Overall survival as a function of CTC number

mCTC were enumerated with the CellSearch system in 296 blood samples at the first follow-up after initiation of a new line of therapy in 111 metastatic breast and 185 metastatic prostate cancer patients. Patients were divided into those with 0 mCTC/7.5 mL of whole blood ($N = 123$, 42%), those between 1 and 4 mCTC ($N = 67$, 23%), those between 5 and 24 mCTC ($N = 55$, 19%) and those with ≥ 25 mCTC ($N = 51$, 17%). Figure 6.1 shows the Kaplan- Meier plot of these 296 patients. Log-rank p for a comparison between the survival curves of patients with 0 versus 1–4 mCTC was $p = 0.044$, 1–4 mCTC versus 5–24 mCTC $p = 0.002$, and 5–24 mCTC versus ≥ 25 mCTC $p = 0.003$, all other $p < 0.0001$.

6.3.2 Changes in the number of CTC and overall survival

Metastatic breast and prostate cancer patients were separated into 164 (55%) patients with unfavorable mCTC (≥ 5 mCTC) and 132 (45%) patients with

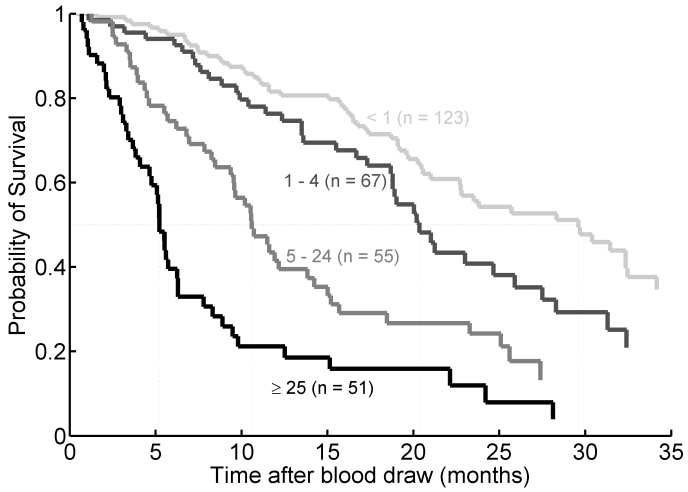

Figure 6.1: Overall survival time of metastatic breast and prostate cancer patients was calculated from the date of the first follow-up blood draw after initiation of a new line of therapy. *Kaplan-meier plots of the probability of overall survival for 123 patients with < 1 CTC, 67 patients with 1–4 CTC, 55 patients with 5–24 CTC and 51 patients with ≥ 25 CTCs are shown.*

favorable mCTC (< 5 mCTC) at baseline. To illustrate the relationship between changes in mCTC count and overall survival, patients were further subdivided into groups that survived 1–6, 6–12, 12–24 and 24–36 months. From the 296 patients 690 blood samples were taken in 4–6 week intervals after initiation of therapy. Smoothed spline fits were used to show the relationship between the median number of mCTC and time for the different survival groups. Figure 6.2 shows the median number of mCTC as a function of time for patients with unfavorable baseline CTC in Panel A and favorable baseline mCTC in Panel B. The patients that survived for only 1–6 months showed a clear trend of increasing mCTC for both the patients groups with unfavorable and with favorable baseline mCTC. In absolute terms, the changes are less severe for patients with < 5 mCTC at baseline. In relative terms they are comparable: a 3–4 fold increase in mCTC over a three month period. For patients surviving 6–12 months with unfavorable baseline mCTC a trend of slight mCTC decrease followed by an increase was observed and a trend of steadily increasing numbers for those with favorable baseline mCTC. For patients surviving 12–24 and 24–36 months a clear trend of decreasing mCTC was observed that reached 0 mCTC after 10–12 weeks of therapy.

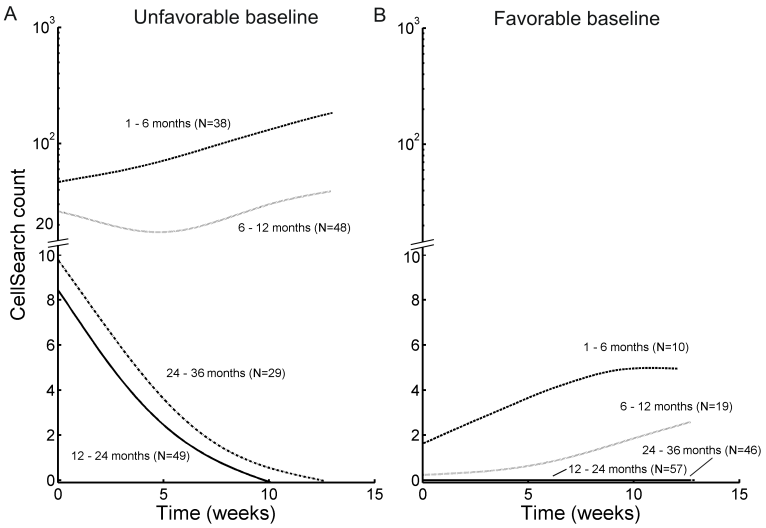

Figure 6.2: mCTC trends for patients that survived 1–6, 6–12, 12–24 and 24–36 months after initiation of therapy. *mCTC trends were obtained by smoothed spline fits to the number of follow-up mCTC at several time points. Panel A shows 164 baseline and 369 follow-up samples from patients with Unfavorable mCTC before initiation of therapy and panel B shows 132 baseline and 312 follow-up samples from patients with Favorable mCTC before initiation of therapy.*

6.3.3 True CTC changes determined using a Poisson model

Measurements on samples taken from a patient at successive time points may show a decline in CTC. For low CTC number this decline may reflect a true decline in the number of CTC in the patient's blood, but it may also be due to the Poisson sampling error. A look-up table shown in figure 6.3 was created that can be used as a reference to determine confidence for a true CTC reduction in the range of 0–50 CTC. For example, in case the baseline measurement is 7 CTC: detecting 0–1 CTC at follow-up provides a CTC reduction confidence $> 95\%$ (see the lower arrow in figure 6.3), whereas for a CTC follow-up count of 5 to 9 this confidence reduces to 25–75%. A follow-up measurement of 10–14 CTC gives confidence of 5–25% and for a follow up count above 14 CTC confidence of reduction is less than 5%, or 95% confidence of an increase (see the upper arrow in figure 6.3). For larger CTC numbers, the relative width of each confidence window is narrower, making it easier to detect changes in the CTC number.

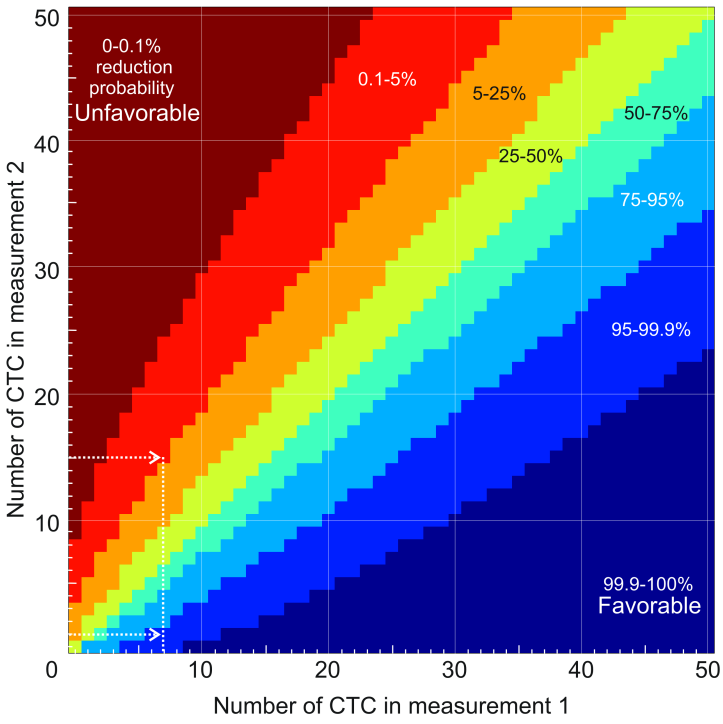

Figure 6.3: Look-up table for the probability of a true reduction in CTC count between two measurements. *A true reduction occurs when the true average present in a patient at the time of the second measurement is lower than the true average at the time of the first measurement.*

6.3.4 Relation between CTC definitions and clinical outcome

The look-up table in figure 6.3 illustrates that low CTC numbers result in a large uncertainty when a change in the true average CTC number present in a patient is determined. To evaluate whether it is possible to reduce this uncertainty by applying less stringent definitions of CTC, resulting in more reported CTC, aCTC were identified by a computer algorithm and classified according to different criteria as shown in table 6.2. The table also shows the median CTC count for each CTC definition at baseline and at the first follow-up sample as well as the resulting HR. All CTC definitions resulted in a significant difference in survival of both groups ($p < 0.0001$ for all) and HRs ranged between 2.3 (95% CI 1.7–3.2) and 3.2 (95% CI 2.3–4.3) at baseline and between 2.8 (95% CI 2.0–3.8) and 3.8 (95% CI 2.8–5.1) at first follow-up.

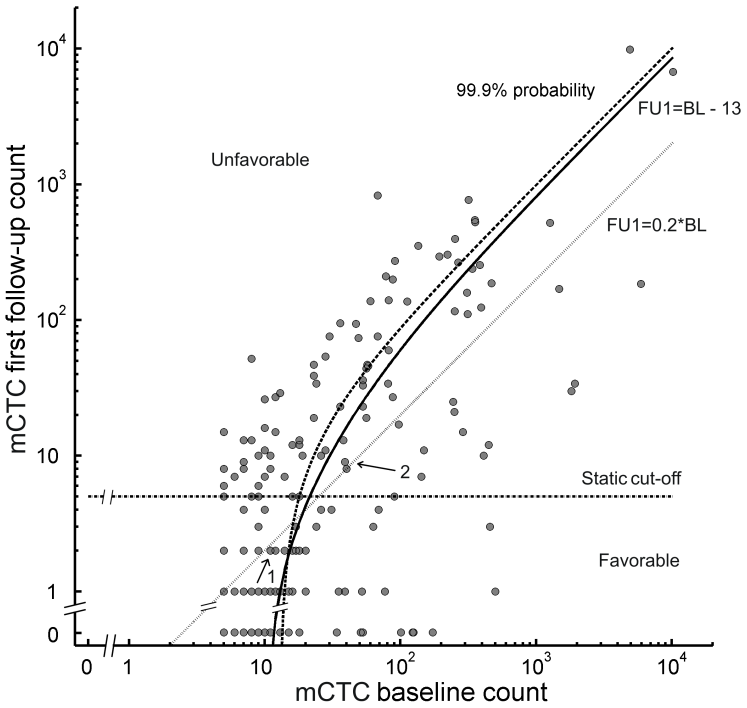

Figure 6.4: Conversion from unfavorable to favorable CTC using the classic CTC definition of 296 metastatic breast and prostate cancer patients. *Four different criteria of assessing a CTC reduction are indicated with different lines. Arrows indicate patients described in more detail in the text. BL = CTC at baseline, FU1 = CTC at first follow-up.*

6.3.5 Changes in CTC that correlate with survival

Four different criteria for CTC reduction were evaluated together with the different CTC definitions. We tested a static cut-off, a confidence of reduction, a proportional reduction, and an absolute reduction. The boundaries for each criterion when applied to the mCTC definition are shown in figure 6.4. The figure shows the mCTC number at baseline and first-follow-up of 164 of 296 (65%) patients with unfavorable mCTC at baseline. For the standard mCTC definition the static cut-off for unfavorable mCTC is 5 CTC, the 99.9% probability for mCTC reduction was based on the Poisson model, the minimum relative reduction was set at five fold and the minimum absolute reduction was set at 13 mCTC. Using these specific values in each approach resulted in a dichotomization that had 59% of the patients in the unfavorable group, thus the group sizes remained constant.

Table 6.3: HRs using OS/PFS (% unfavorable patients) using different criteria for CTC reduction for mCTC and aCTC definitions *($N = 164$, all patients ≥ 5 mCTC at baseline). Cells with gray fill show HRs that had a logrank $p < 0.05$ for both OS and PFS.*

CTC definition	Static cut-off FU1[a] <constant	Reduction confidence >% certain	Relative reduction FU1 <BL[b] / constant	Absolute reduction FU1 <BL – constant
mCTC	2.1/2.5 (59%)	0.8/0.7 (62%)	1.5/1.9 (59%)	0.7/0.8 (58%)
aCTC A	2.7/2.8(49%)	1.0/1.1 (61%)	1.5/1.5 (60%)	0.9/0.8 (60%)
aCTC B	3.0/2.9 (58%)	1.0/1.0 (60%)	1.5/1.5 (58%)	0.8/0.9 (59%)
aCTC C	2.6/2.4 (59%)	1.0/1.0 (53%)	1.4/1.4 (57%)	0.8/0.8 (59%)
aCTC D	2.3/2.0 (60%)	1.5/1.5 (38%)	1.3/1.4 (61%)	0.9/1.1 (59%)

[a] First follow-up measurement, [b] Baseline measurement.

For illustration purposes, two arrows are shown in figure 6.4 to exemplify the implications of applying these criteria. Arrow 1 is a patient that started with 11 mCTC, which reduced to 2 mCTC at first follow-up. According to static mCTC cut-off and relative mCTC reduction this patient has a favorable prognosis, but using the 99.9% mCTC reduction confidence or the absolute mCTC decrease this patient has an unfavorable prognosis. The opposite case is indicated by arrow 2, where a patient had 39 mCTC at baseline and 9 mCTC at first follow-up; static mCTC cut-off and relative mCTC reduction give this patient an unfavorable prognosis but 99.9% mCTC reduction confidence and absolute mCTC decrease indicate a favorable prognosis. The HRs for OS and PFS for the different CTC definitions and methods to express CTC changes for patients with unfavorable CTC at baseline (≥ 5 mCTC) are shown in table 6.3. The static cut-off predicted a significant difference in OS and PFS for all definitions ($p < 0.001$ for all HRs). The aCTC definitions A and B gave the highest predictive power using the static cut-off method, but 95% confidence intervals overlapped for all definitions (data not shown). Using the confidence reduction method, only the aCTC D definition was significant ($p < 0.05$) for OS/PFS ($p = 0.029/0.001$), although the group size could not match that of the mCTC definition. Applying the relative model showed that only aCTC definitions A ($p = 0.046/0.035$) and B ($p = 0.045/0.040$) predicted significant differences in OS/PFS, while the absolute method did not predict a significant difference in survival for all definitions ($p > 0.06$ for all HRs). Confidence of reduction (with mCTC) was at least 50% for 74% of patients, and at least 95% confidence for 56% of patients.

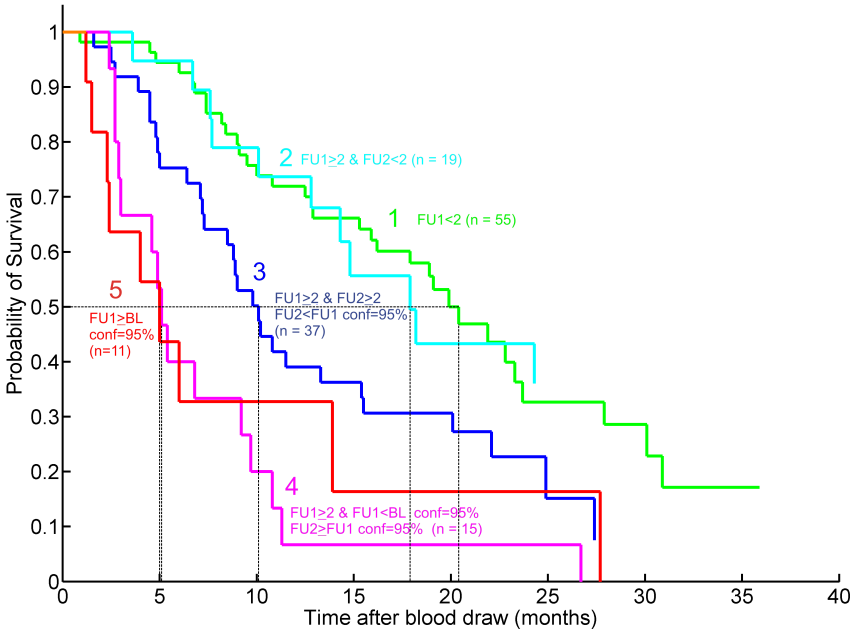

Figure 6.5: Kaplan-Meier plot of patients with $\geq$ 2 aCTC at baseline who were monitored at two subsequent follow-up time points ($N = 137$). *Patients were grouped (see text) according to a drop below a cut-off of 2 mCTC, 95% confidence of a rise, or in between both. BL = baseline measurement; FU1 = first follow-up measurement; FU2 = second follow-up measurement.*

6.3.6 Applying criteria for mCTC change to multiple time points

In order to create clear-cut rules for deciding whether or not a certain therapy is working, survival of the group of unfavorable patients at baseline was assessed for two subsequent follow-up measurements: the first between 2–5 weeks and the second between 6–8 weeks after initiation of therapy. Figures 6.1 and 6.2 show that it is important to treat patients until the number of CTC becomes zero. It was found that the number of mCTC and aCTC in healthy controls ranged from 0–1 mCTC: one of 205 healthy controls had one mCTC (0.5%), six controls had one aCTC (2.9%). Therefore, the cut-off for deciding if a patient was unfavorable was set to $\geq$ 2 mCTC. This reduction of the cut-off from five to two aCTC allowed for 137 patients to be included in the analysis.

The Kaplan-Meier survival plot of this analysis is shown in figure 6.5,

for which the patients were divided into five groups: 1.) patients who changed to favorable (< 2 mCTC) at first follow-up (green line in figure 6.5); 2.) patients who stayed unfavorable at first follow-up, but changed to at second follow-up (cyan line); 3.) patients who stayed unfavorable at first and second follow-up, but did not show a significant rise in the number of mCTC (blue line); 4.) patients who stayed unfavorable at first follow-up without significant rise that change to a significant rise at second follow-up (magenta line); 5.) patients who showed a significant rise at first follow-up (red line). In these cases, a significant rise was defined from figure 6.2, panel A: the unfavorable group with survival from 1–6 months showed a relative rise of 50% (or factor 1.5 increase). This increase represents 95% confidence of a true change as calculated by our model. For patients that had lower than 20 mCTC, the factor of 1.5 does not give 95% confidence due to the higher Poisson noise at these lower numbers: a rise from two to three mCTC would then already be significant. For these patients, the look-up table shown in figure 6.3 was used to determine if a rise was significant. If two subsequent measurements are located in the bright or dark red part of this look-up table, the rise was at least 95% confident. Median survival for groups 1–5 was 20.4, 17.9, 10.1, 5.1, and 5.0, respectively. Log-rank p for comparison between the survival curves of patients of group 1 and group 2, and between groups 4 and 5 were $p > 0.8$; 2 and 3 had $p = 0.07$. Comparison of group 3 to group 5 (group 5 is closer to 3 than to group 4) resulted in $p = 0.17$.

6.4 Discussion

Evidence is increasing that CTC are an independent prognostic and predictive biomarker for patients treated for metastatic carcinomas [2, 3, 4, 5, 6, 7, 8, 9, 16, 17, 18, 19, 20]. Whether an early switch of treatment based on persistence of CTC after the first cycle of therapy can prolong survival is still being investigated in ongoing clinical studies (SWOG 0500 - NCT00382018). A difficulty that arises in applying the results of a CTC assay to evaluate therapy response is the low number of CTC that are usually found in patients. Using the CellSearch system -that has been validated for CTC enumeration- patients are divided into two groups: those with favorable CTC (< 5 CTC / 7.5 mL of blood) and those with unfavorable CTC (≥ 5 CTC / 7.5 mL of blood). Examination of patient survival as a function of the number of CTC however clearly shows a significant correlation between the CTC load and survival prospects as illustrated for breast and prostate cancer patients in figure 6.1. CTC of metastatic breast and prostate cancer patients were combined for this analysis to illustrate that an interpretation of CTC results can be made regardless of origin of the disease or treatment. Elimination of all CTC clearly is the most desired outcome, the time needed for a CTC reduction may however vary (figure 6.2) and it is of importance

to have the proper tools to evaluate changes in CTC numbers. Using Poisson statistics, a measure was given of the confidence that two CTC measurements represent a true change in the underlying average number of CTC found in patients. A look-up table (figure 6.3) was created to assist physicians in determining whether or not a change in CTC is significant. This look-up table shows that for 0–10 CTC, most possible combinations of CTC at baseline and follow-up have confidence less than 95% for determining decrease or increase. At baseline, 57% of patients in prostate and 66% in breast have 0–10 mCTC. For 56% of patients in our data set, the observed reduction is significant with at least 95% confidence. However, this reduction does not result in an improvement of OS and PFS unless the absolute number of mCTC is reduced below 5 and preferably approaches 0. We attribute this inconsequential reduction to cytotoxic chemotherapy, which kills cells in most patients, but probably does not target all malignant cells in those patients with brief survival. This also suggests that when CTC are found after therapy was initiated, these CTC are resistant to the current therapy and of special interest for characterization.
In patients where the number of mCTC is reduced but survival does not improve, therapy possibly affects only part of the metastases that give rise to CTC, or alternative therapy is given at insufficient dose or frequency to achieve a durable effect. This is reflected in the changes in CTC counts for patients that survived 1–6, 6–12, 12–24 and 24–36 months in figure 6.2 panel A. The group with 6–12 month survival showed some decline of CTC in response to therapy in the first five weeks after initiation of therapy, but deteriorated at subsequent time points. This figure further shows that a period of 10–12 weeks may be needed before definitive conclusions can be drawn whether a count is going to zero. Figure 6.5 further confirms this conclusion, in which patient samples of two follow-up time points were used. The cut-off for unfavorable patients was lowered to 2 mCTC for this analysis, as (i) we showed that we only found up to one mCTC in healthy controls [10, 14], and (ii) to include the maximum number of patients of whom multiple time points were available. It can be seen that patients who stay unfavorable at first follow-up may improve at second follow-up, which is reflected in their survival chances. Patients who have a rise in number of mCTC with at least 95% confidence deteriorate rapidly. Figure 6.2, panel B shows that also for those patients with < 5 mCTC at baseline a strong upward trend is an indicator for poor prognosis, even though the majority of patients with 6–12 month survival have fewer than the clinically used cutoff of 5 mCTC after 12 weeks. It is unknown whether these patients have a subtype of cancer which sheds fewer mCTC into the blood, or whether they rapidly deteriorated after the last follow-up measurement. The therapeutic regimen of the majority of these patients included chemotherapy and the rate of CTC decline may be dependent on the type of therapy.

To determine the best definition of a change in CTC count, several re-

duction criteria were tested. Four criteria were used to measure a reduction using modeled confidence of reduction, static, absolute and proportional cut-offs. Next, using our automated classifiers [15] different definitions of what constitutes an aCTC were applied, each having significant impact on survival of patients as measured by HRs at baseline, shown in table 6.2. The different definitions ranged from strict to loose, where the strictest definition excluded most false positives and part of the true positives, while the most inclusive definition included most true positives and some false positives. This allowed us to explore the hypothesis that using more objects from a patient improves the ability to measure a reduction in aCTC count. This hypothesis was generated after the observation that tumor micro particles (EpCAM+CK+CD45–, < 4 µm diameter), present at a 20 fold higher frequency as compared to mCTC, are equally prognostic as the CellSearch manually counted mCTC [21].

These different CTC definitions were combined with different criteria to measure CTC reduction. For patients who started with five or more mCTC, a count below a static cut-off after 6 weeks of therapy remains the best indicator of treatment success for all CTC definitions. Combined with figure 6.1, we can again conclude that treatment should focus on getting the number of CTC to zero. Table 6.3 shows that HRs were comparable for all definitions, indicating that the reduction in Poisson sampling noise with looser CTC definitions is roughly offset by an increase in background due to inclusion of more false positives. The aCTC D definition encompasses tumor fragments; the presence of similar particles in healthy controls however hampers their use as a surrogate for detection of the presence of CTC. Reduction of the background of aCTC D may improve the ability to use these tumor fragments as a means to measure the presence of CTC. This however will require alteration of the assay, such as addition of an extra fluorescent marker, which may result in such reduction of the numbers that it defeats the purpose. Improving the yield of CTC with CellSearch will not significantly increase the numbers as ∼80% of tumor cells spiked in blood are already recovered by the system [10]. Chasing CTC phenotypes that are currently not detected by the CellSearch system is likely to identify subgroups of patients in whom no CTC are detected, but will not significantly increase the number of CTC in those patients, in whom few CTC are detected. Moreover, clinical studies will have to be conducted to demonstrate the prognostic and predictive value of CTC that do not express EpCAM and cytokeratins 8, 18 or 19.

The approach that truly will reduce the Poisson error is to sample a larger blood volume. Extrapolation of the CTC frequency in patients with metastatic breast and colon cancer showed that by increasing the blood volume to 5 liters CTC will be detected in all patients [13]. This however can only be achieved through in-vivo measurements [22, 23] or apheresis-based systems [24]. Using the current blood volume of 7.5 mL, the automated aCTC A definition is the preferred method of measuring

if a patients CTC number approaches zero, because it eliminates reviewer variability. When reviewers assess two subsequent measurements, their variability in determining a change will propagate by the square root of the sum of the variability of the individual measurements squared. We conclude that (i) CTC are best measured by means of an automated CTC count with a low background (aCTC A), (ii) aim of treatment should be the eliminating of all CTC, (iii) while reduction to 0 CTC can be seen after 4–6 weeks, to reach this aim 10–12 weeks of therapy may be needed for some patients, and (iv) if the number does not decrease within this time span, treatment is not effective.

6.5 References

[1] C. Rao, T. Bui, M. Connelly, G. Doyle, I. Karydis, M. R. Middleton, G. Clack, M. Malone, F. A. W. Coumans, and L. W. M. M. Terstappen, "Circulating melanoma cells and survival in metastatic melanoma," *International Journal of Oncology*, vol. 38, pp. 755–760, 2011.

[2] M. Cristofanilli, G. T. Budd, M. J. Ellis, A. Stopeck, J. Matera, M. C. Miller, J. M. Reuben, G. V. Doyle, W. J. Allard, L. W. Terstappen, and D. F. Hayes, "Circulating tumor cells, disease progression, and survival in metastatic breast cancer," *N. Engl. J. Med.*, vol. 351, pp. 781–791, Aug 2004.

[3] S. J. Cohen, C. J. Punt, N. Iannotti, B. H. Saidman, K. D. Sabbath, N. Y. Gabrail, J. Picus, M. Morse, E. Mitchell, M. C. Miller, G. V. Doyle, H. Tissing, L. W. Terstappen, and N. J. Meropol, "Relationship of circulating tumor cells to tumor response, progression-free survival, and overall survival in patients with metastatic colorectal cancer," *J. Clin. Oncol.*, vol. 26, pp. 3213–3221, Jul 2008.

[4] J. S. de Bono, H. I. Scher, R. B. Montgomery, C. Parker, M. C. Miller, H. Tissing, G. V. Doyle, L. W. Terstappen, K. J. Pienta, and D. Raghavan, "Circulating tumor cells predict survival benefit from treatment in metastatic castration-resistant prostate cancer," *Clin. Cancer Res.*, vol. 14, pp. 6302–6309, Oct 2008.

[5] S. Matsusaka, K. Chin, M. Ogura, M. Suenaga, E. Shinozaki, Y. Mishima, Y. Terui, N. Mizunuma, and K. Hatake, "Circulating tumor cells as a surrogate marker for determining response to chemotherapy in patients with advanced gastric cancer," *Cancer Science*, vol. 101, pp. 1067–1071, 2010.

[6] M. G. Krebs, R. Sloane, L. Priest, L. Lancashire, J. M. Hou, A. Greystoke, T. H. Ward, R. Ferraldeschi, A. Hughes, G. Clack, M. Ranson, C. Dive, and F. H. Blackhall, "Evaluation and prognostic significance of circulating tumor cells in patients with non-small-cell lung cancer," *Journal of Clinical Oncology*, vol. 29, pp. 1556–1563, 2011.

[7] D. F. Hayes, M. Cristofanilli, G. T. Budd, M. J. Ellis, A. Stopeck, M. C. Miller, J. Matera, W. J. Allard, G. V. Doyle, and L. W. Terstappen, "Circulating tumor cells at each follow-up time point during therapy of metastatic breast cancer patients predict progression-free and overall survival," *Clin. Cancer Res.*, vol. 12, pp. 4218–4224, Jul 2006.

[8] G. T. Budd, M. Cristofanilli, M. J. Ellis, A. Stopeck, E. Borden, M. C. Miller, J. Matera, M. Repollet, G. V. Doyle, L. W. Terstappen, and D. F. Hayes, "Circulating tumor cells versus imaging–predicting overall survival in metastatic breast cancer," *Clin. Cancer Res.*, vol. 12, pp. 6403–6409, Nov 2006.

[9] U. De Giorgi, V. Valero, E. Rohren, M. Mego, G. V. Doyle, M. C. Miller, N. T. Ueno, B. C. Handy, J. M. Reuben, H. A. Macapinlac, G. N. Hortobagyi, and M. Cristofanilli, "Circulating tumor cells and bone metastases as detected by fdg-pet/ct in patients with metastatic breast cancer," *Annals of Oncology*, vol. 21, pp. 33–39, 2010.

[10] W. J. Allard, J. Matera, M. C. Miller, M. Repollet, M. C. Connelly, C. Rao, A. G. Tibbe, J. W. Uhr, and L. W. Terstappen, "Tumor cells circulate in the peripheral blood of all major carcinomas but not in healthy subjects or patients with nonmalignant diseases," *Clin. Cancer Res.*, vol. 10, pp. 6897–6904, Oct 2004.

[11] H. I. Scher, X. Y. Jia, J. S. de Bono, M. Fleisher, K. J. Pienta, D. Raghavan, and G. Heller, "'Circulating tumour cells as prognostic markers in progressive, castration-resistant prostate cancer: a reanalysis of IMMC38 trial data," *Lancet Oncology*, vol. 10, pp. 233–239, 2009.

[12] A. G. Tibbe, M. C. Miller, and L. W. Terstappen, "Statistical considerations for enumeration of circulating tumor cells," *Cytometry A*, vol. 71, pp. 154–162, Mar 2007.

[13] F. Coumans, S. T. Ligthart, and L. W. M. Terstappen, "Challenges in the enumeration and phenotyping of CTC," *Clinical Cancer Research*, 2012.

[14] M. R. de Groot, H. M. Croonen, W. J. T. Mastboom, I. Vermes, A. G. J. Tibbe, H. Tissing, and L. W. M. M. Terstappen, "Circulating tumor cells (ctc) in newly diagnosed breast or colorectal cancer," *Proc Ann Meet Am Soc Clin Onc*, vol. 25, 2007.

[15] S. Ligthart, F. Coumans, G. Attard, A. Cassidy, J. de Bono, and L. Terstappen, "Unbiased and automated identification of a circulating tumour cell definition that associates with overall survival," *PloS one*, vol. 6, no. 11, p. e27419, 2011.

[16] S. Riethdorf, H. Fritsche, V. Muller, T. Rau, C. Schindibeck, B. Rack, W. Janni, C. Coith, K. Beck, F. Janicke, S. Jackson, T. Gornet, M. Cristofanilli, and K. Pantel, "Detection of circulating tumor cells in peripheral blood of patients with metastatic breast cancer: A validation study of the CellSearch system," *Clinical Cancer Research*, vol. 13, pp. 920–928, 2007.

[17] H. Yagata, S. Nakamura, M. Toi, H. Bando, S. Ohno, and A. Kataoka, "Evaluation of circulating tumor cells in patients with breast cancer: multi-institutional clinical trial in japan," *International Journal of Clinical Oncology*, vol. 13, pp. 252–256, 2008.

[18] F. C. Bidard, C. Mathiot, A. Degeorges, M. C. Etienne-Grimaldi, R. Delva, X. Pivot, C. Veyret, L. Bergougnoux, P. de Cremoux, G. Milano, and J. Y. Pierga, "Clinical value of circulating endothelial cells and circulating tumor cells in metastatic breast cancer patients treated first line with bevacizumab and chemotherapy," *Annals of Oncology*, vol. 21, pp. 1765–1771, 2010.

[19] D. R. Shaffer, M. A. Leversha, D. C. Danila, O. Lin, R. Gonzalez-Espinoza, B. Gu, A. Anand, K. Smith, P. Maslak, G. V. Doyle, L. Terstappen, H. Lilja, G. Heller, M. Fleisher, and H. I. Scher, "Circulating tumor cell analysis in patients with progressive castration-resistant prostate cancer," *Clinical Cancer Research*, vol. 13, pp. 2023–2029, 2007.

[20] M. C. Liu, P. G. Shields, R. D. Warren, P. Cohen, M. Wilkinson, Y. L. Ottaviano, S. B. Rao, J. Eng-Wong, F. Seillier-Moiseiwitsch, A. M. Noone, and C. Isaacs, "Circulating tumor cells: A useful predictor of treatment efficacy in metastatic breast cancer," *Journal of Clinical Oncology*, vol. 27, pp. 5153–5159, 2009.

[21] F. A. Coumans, C. J. Doggen, G. Attard, J. S. de Bono, and L. W. Terstappen, "All circulating EpCAM+CK+CD45- objects predict overall survival in castration-resistant prostate cancer," *Ann. Oncol.*, vol. 21, pp. 1851–1857, Sep 2010.

[22] Y. C. Chang, J. Y. Ye, T. P. Thomas, Z. Y. Cao, A. Kotlyar, E. R. Tkaczyk, J. R. Baker, and T. B. Norris, "Fiber-optic multiphoton flow cytometry in whole blood and in vivo," *Journal of Biomedical Optics*, vol. 15, p. 047004, 2010.

[23] E. I. Galanzha, E. V. Shashkov, T. Kelly, J. W. Kim, L. L. Yang, and V. P. Zharov, "In vivo magnetic enrichment and multiplex photoacoustic detection of circulating tumour cells," *Nature Nanotechnology*, vol. 4, pp. 855–860, 2009.

[24] R. L. Eifler, J. Lind, D. Falkenhagen, V. Weber, M. B. Fischer, and R. Zeillinger, "Enrichment of circulating tumor cells from a large blood volume using leukapheresis and elutriation: Proof of concept," *Cytometry Part B-Clinical Cytometry*, vol. 80B, pp. 100–111, 2011.

CHAPTER 7

Challenges in the Enumeration and Phenotyping of CTC

F.A.W. Coumans, S.T. Ligthart, J. Uhr , L.W.M.M. Terstappen *Clinical Cancer Research, doi:10.1158/1078-0432.CCR-12-1585, 2012*

Abstract

Presence of circulating tumor cells (CTC) in metastatic carcinoma is associated with poor survival. Phenotyping and genotyping of CTC may permit "real-time" treatment decisions, provided CTC are available for examination. Here we investigate what is needed to detect CTC in all patients. CTC enumerated in 7.5 mL of blood together with survival from 836 metastatic breast, colorectal and prostate cancer patients were used to predict the CTC concentration in the 42% of these patients in whom no CTC were found and to establish the relation of concentration of CTC with survival. Influence of different CTC definitions were investigated by automated cell recognition and a flow cytometry assay without an enrichment or permeabilization step. A log-logistic regression of the log of CTC yielded a good fit to the CTC frequency distribution. Extrapolation of the blood volume to 5 liters predicted that 99% of patients had at least 1 CTC before therapy initiation. Survival of patients with EpCAM+ CK+ CD45– nucleated CTC is reduced by 6.6 months for each tenfold CTC increase. Using flow cytometry, the potential threefold recovery improvement is not sufficient to detect CTC in all patients in 7.5 mL of blood. EpCAM+ cytokeratin+ CD45– nucleated CTC are present in all metastatic breast, prostate and colorectal cancer patients and

their frequency is proportional to survival. To serve as a liquid biopsy for the majority of patients, a substantial improvement of CTC yield is needed, which can only be achieved by a dramatic increase in sample volume.

7.1 Introduction

In recent years a variety of technologies have emerged for the detection of circulating tumor cells (CTC) [1, 2, 3, 4, 5, 6, 7, 8, 9]. The CTC phenotype employed by these technologies vary greatly and as a result the reported CTC frequencies can vary up to a few orders of magnitude in similar patient groups. At present, CellSearch is the only validated method for enumeration of CTC in which the presence of CTC detected has been related with poor clinical outcome in multicenter prospective studies [10, 11, 12]. Definition of a CTC in this system was set before these studies were initiated. They were defined as: EpCAM enriched objects from 7.5 mL of blood that express cytokeratin 8, 18 or 19 (CK), lack CD45, are > 4 µm in size and have cell-like morphology including a nucleus, determined by staining with 4',6-diamidino-2-phenylindole (DAPI). In these studies 20–50% of the processed samples were found to have 0 CTC. The prognosis of these patients is much better than the prognosis of patients with CTC.
The majority of the emerging CTC technologies report higher frequencies of CTC, contributed to either a more efficient capture and detection or based on other immunological or physical properties [1, 2, 3, 4, 5, 6, 7, 8, 9]. Retrospective analysis of recorded fluorescence images captured with the CellSearch system using a variety of different phenotypic and morphological criteria showed that different definitions of CTC resulted in a wide range of "CTC" frequencies with varying degrees of clinical significance [13]. These observations explained some of the discrepancies between technologies. An important question with regard to the 20–50% of patients who did not have CTC in 7.5 mL of blood is whether they had no EpCAM+CK+CD45–DNA+ CTC, or they had such CTC but they were not detected. Absence of EpCAM+CK+CD45–DNA+ CTC in carcinoma patients could be explained by either lack of expression by the primary tumor or loss of the antigens during the epithelial mesenchymal transition [14, 15, 16, 17, 18, 19]. In this study, we could only test 2 alternative hypotheses, namely, either insufficient sample volume or insufficient assay sensitivity caused patients with CTC to have no CTC in the CellSearch test. The sample volume is addressed by means of a distribution function fit to the CTC frequency distribution of patients in whom CTC were detected. This fit can be used to predict the frequency distribution in patients in whom no CTC were detected in 7.5 mL of blood. The sensitivity is addressed by two means; first the definition of CTC is varied to determine whether a different CTC definition may yield higher number of cells while maintaining prognostic value, second CTC were determined on patients blood with both CellSearch and a flow assay

detecting all EpCAM+DNA+CD45– CTC in the blood sample, albeit with lower specificity than CellSearch.
In the past, most CellSearch CTC studies dichotomized patients into high and low CTC groups. To test whether the absolute number of CTC counted by CellSearch is useful, the continuous survival function as a function of CTC-count was determined.

7.2 Materials and methods

7.2.1 Patients and clinical trials

7.5 mL blood samples were collected in CellSave vacutainers (Veridex, NJ) in prospective, multi center clinical trials in breast (IMMC-01), colorectal (IMMC-06) and prostate cancer (IMMC-38) patients [10, 11, 12]. Included were 177 breast, 428 colorectal and 231 prostate cancer patients. All participants provided written informed consent. Samples were taken prior to commencement of a new line of therapy and at first follow up after initiation of therapy. The primary aim of these studies was to investigate the association between the presence of CTC and progression free and overall survival. The primary study endpoint was death of any cause. As control samples for CTC enumeration by the automated classifier stored images from CellSearch data from healthy volunteers from the IMMC-06 and IMMC-01 studies ($N = 68$, $N = 136$ respectively) and patients with benign neoplasm from the IMMC-01 study ($N = 190$) were used. For comparison between CTC enumeration by flow cytometry and CellSearch 186 blood samples were collected in EDTA vacutainers (BD, Franklin Lakes, NJ) from 140 metastatic carcinoma patients from a study reported earlier were analyzed [20]. Of the 140 patients, 65 (46%) had breast cancer, 24 (17%) lung cancer, 16 (11%) colorectal cancer, 12 (9%) ovarian cancer, 7 (5%) prostate cancer and 16 (11%) had other carcinomas. Patient inclusion for all studies, detailed inclusion criteria, study characteristics and patient demographics are detailed in paragraph 7.5.

7.2.2 CTC enumeration by CellSearch

The CellSearch system employs immunomagnetic enrichment targeting the epithelial cell adhesion molecule (EpCAM) and immunofluorescence labeling and detection for enumeration of CTC [2]. Fluorescence images of the enriched cells are recorded and a trained operator identifies CTC defined as EpCAM enriched cells larger than 4 µm, meeting morphology criteria of cells, expressing cytokeratins 8, 18 or 19 (CK), lacking the leukocyte specific antigen CD45 and staining with the nucleic acid DAPI from thumbnail images generated by a computer algorithm containing objects staining with both DAPI and CK [2]. The trained operator is blinded to patient information at the time of review.

7.2.3 Automated CTC classifier

An automated classifier of CTC was used to identify CTC with different characteristics in the archived images from the multicenter prospective studies. This classifier compares each found object to a predefined CTC phenotype to determine whether this object is a CTC or not. The phenotype is constructed of 4 parameters; size, signal in CK, CD45 and DNA channels and the CTC definition was optimized using patient overall survival [21]. To test the impact of other phenotypes on both prognostic value as well as frequency of found objects we retrained the classifier using different EpCAM+ phenotypes; DNA+, CK+, DNA+CK+, DNA+CK+CD45–, CK+CD45– CK+CD45+, DNA+CD45–. Size was included in each classifier to allow filtering of excessively large or small objects. The dataset for training included the baseline samples of the entire population of eligible patients from breast, prostate and colorectal studies, whose archive images could be read, in the breast ($N = 163$), colorectal ($N = 72$) and prostate ($N = 185$) studies. Controls were healthy volunteers from the colorectal and breast studies ($N = 68$ and $N = 136$) and patients with benign neoplasm from the breast study ($N = 190$).

7.2.4 CTC enumeration by flow cytometry

The frequency of CTC was determined using flow cytometry and compared to CellSearch CTC enumeration using blood from 186 metastatic cancer patients. We wanted to have approximately 50 samples with at least 1 CTC/90 µL of blood. To achieve this, we needed to run 200 comparisons assuming (1) 25% of patients have 11 or more CTC/ mL blood, (2) the flow assay has at least comparable recovery to CellSearch, and (3) 10% of samples fails. An aliquot of 100 µL of blood was stained with 10 µL each of EpCAM-PE (Veridex LLC, Raritan, NJ, USA), CD45–PerCP (BD Biosciences, San Jose, CA, USA) and the nucleic acid dye used in procount (BD Biosciences). After 15 minutes of incubation, 0.5 mL of FACSlyse (BD Biosciences) was added. The samples were analyzed on a FACSCalibur flow cytometer (BD Biosciences) and CTC were defined as EpCAM+DNA+CD45– as described elsewhere [20].

7.2.5 Statistical analysis

All statistical analysis was performed in Matlab 2010b with statistics toolbox (Mathworks, Natick, MA, USA). The CTC data from patients in the breast, prostate and colorectal studies at baseline and first follow-up was used to generate empirical cumulative distribution functions (CDF). The % of patients with > 0 CTC was highest with prostate cancer; therefore various functions were fit to the prostate cancer CDF via maximum likelihood estimation to the empirical curve, including the logistic function, Weibull

CDF, normal CDF and exponential CDF. As input variables, all measurements with CTC > 0 and the log thereof were tested. The best fitting distribution was fit to the empirical CDF of each study for the baseline (prior to commencement of chemotherapy) and first follow-up samples (2–8 weeks after baseline). Each fit was extrapolated to a blood volume of 5 liters. The 95% confidence interval (CI) of each fit was determined from the covariance matrix.
All studies were designed to follow patients for up to 36 months; survivals recorded beyond 36 months were censored at 36 months. Cox regression analysis was performed to determine the impact of different automatically counted phenotypes on survival. Patients were dichotomized on the median number of found objects. To show the relationship between survival time and CTC, we produced smoothed Kaplan Meier estimates of the median survival conditional [22, 23], both by study and with all studies grouped together. A 95% confidence interval for the all study relationship was determined by bootstrap aggregation of the data set 400 times.

7.3 Results

7.3.1 99% of patients are predicted to have at least one CTC in circulation

The empirical cumulative distribution function (CDF) using data from a previously reported metastatic castration-resistant prostate cancer study [10] was used to test the fit of various distribution functions; the CDF and the tested fits are shown figure 7.1.

The best function was selected on the basis of log likelihood ratio (LLR). Only distributions fit to the log of CTC had a good fit, with the log-logistic fitting (LLR 1.002) slightly better than the log Weibull and log normal distribution (LLR 1.004 for both). The regular logistic function (LLR 1.078) and the exponential function (LLR 2.080) fit poorly. The log-logistic function was fit to all studies for samples before initiation of therapy (baseline) and after initiation of therapy (first follow-up) and extrapolated to 5 L in figure 7.2.

Included were patients with metastatic cancer originating from the breast (177), prostate (231) and colon or rectum (428). Confidence intervals for the follow-up samples for breast and especially colorectal cancer are large, due to the large fraction of samples with 0 CTC. At baseline, 99% of patients in each study are predicted to have at least 1 CTC in 5 L of blood (breast 98.7%, colorectal 99.1%, prostate 99.5%) while after one month of chemotherapy, 96–99% of patients still have 1 CTC in 5 L of blood (breast 95.8%, colorectal 99.0%, prostate 98.7%).

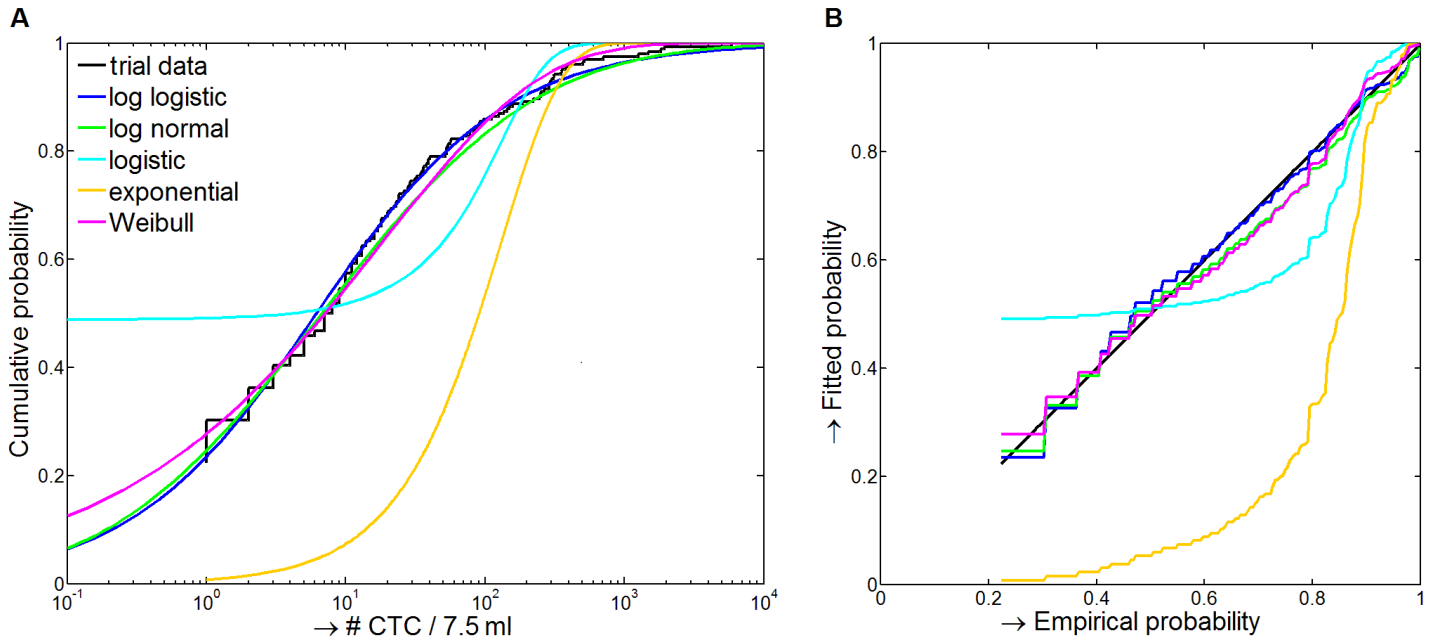

Figure 7.1: Fits to the empirical cumulative distribution function (CDF) of the prostate study baseline samples ***($N = 231$).*** *Fits were performed using all non-zero circulating tumor cell (CTC) counts. Log-logistic regression on the log of CTC yields the closest fit (log likelihood ratio, LLR of 1.002). A log-normal distribution and Weibull distribution on the log of CTC also yields an acceptable fit (LLR 1.004 for both). Log-binominal regression on the number of CTC and a fit of an exponential distribution both are poor fits (LLR 1.076 and 2.079 respectively). Panel A shows the CDF functions and panel B the probability-probability plot where a line with slope of 1 is a perfect fit.*

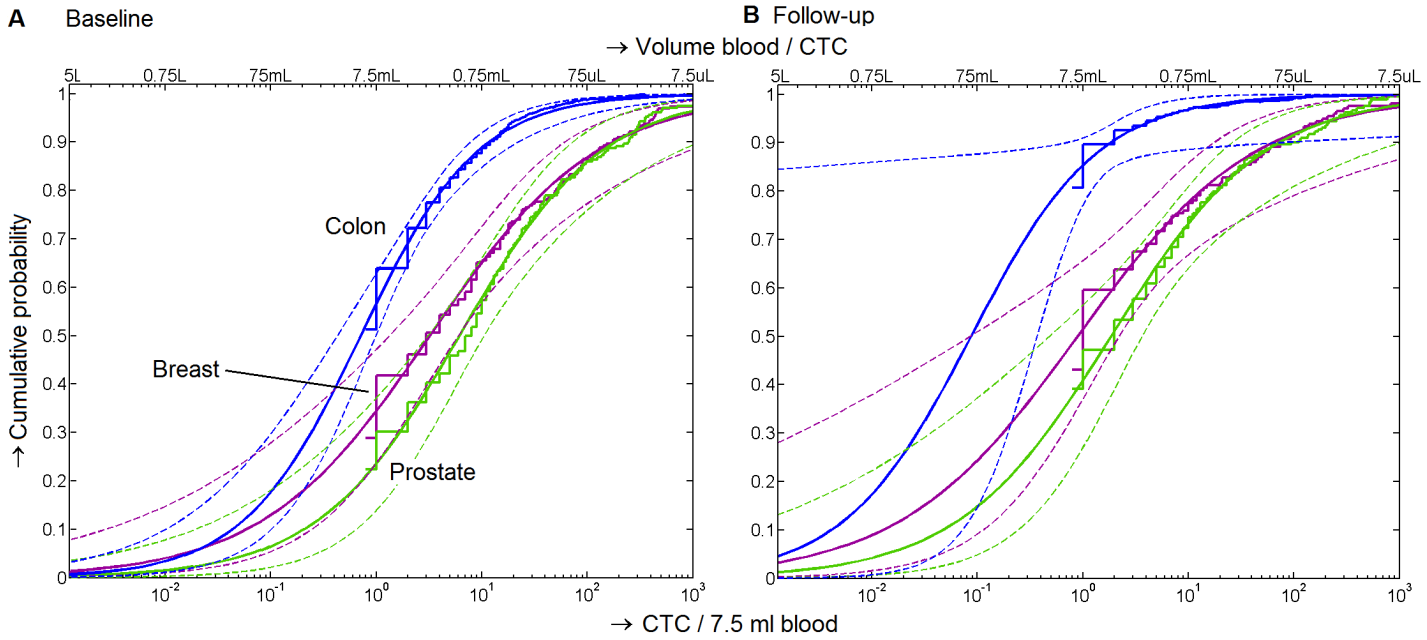

Figure 7.2: Extrapolation of log-logistic fit curves for all studies at baseline and first follow-up. *Stair plots show the empirical CDF, the continuous line the fit and the dashed lines outline the 95% CI for breast ($N = 177$), prostate ($N = 231$) and colorectal patients ($N = 428$). Extrapolation predicts that $> 99\%$ of patients in these studies had CTC at baseline (Panel A) and $> 95\%$ of patients still had CTC at first follow-up (Panel B). The 95% CI are much wider for follow-up because a smaller part of the empirical CDF is available for fitting.*

7.3.2 Survival chance decreases with increasing CTC in metastatic cancer patients

Survival versus CTC number was plotted in a scatter plot in figure 7.3 and a smoothed median survival function was estimated for each study. For this estimate, patients with zero CTC were included as a single group, with a number of CTC equal to the median as predicted from the log-logistic fit. For visualization purposes, the survival data of patients with zero CTC were randomly spread out between 10^{-3} and 0.9 CTC/7.5 mL with a distribution as estimated by the log logistic fit. Survival monotonically declines with increasing CTC number for each study, with the exception of breast cancer patients with zero CTC, who had median survival 1 month less than the 22.4 months of patients with one CTC. The slope of the curve for prostate cancer patients is much steeper than the other slopes. The survival graph for all patients shows that survival chances are reduced by 6.6 months by each tenfold increase in CTC in a 7.5 mL blood volume. The 95% confidence interval by bootstrapping was 4.2–8.2 months for an increase from 100 to 1000 CTC and 4.5–8.1 months for an increase from 10 to 100 CTC. The shape of the survival curves suggests that this can be extrapolated to the higher blood volumes with less CTC.

7.3.3 Increased concentration of CTC can be detected at the cost of clinical significance

Alternative definitions of EpCAM+ objects enriched with the CellSearch method were tested using an automated classifier [21] on all available archived images from the three studies (420 patients, 204 healthy controls, 190 patients with benign disease). The frequency of the alternative CTC definitions and the influence of hazard ratio (HR) are shown in table 7.1.

Manual review of the images using the CellSearch definition resulted in a HR of 2.5 at baseline and 3.4 at follow up. For the automated classifier the EpCAM+, DNA+, CK+, CD45– and EpCAM+, DNA+, CK+ phenotypes had the highest hazard ratio (HR) of 2.7 at baseline and 3.2 at follow up. However, these definitions also had the lowest frequency. Whereas, EpCAM+DNA+ cells were approximately 500 times more frequent than EpCAM+DNA+CK+CD45– cells, the HR was only 1.5 at baseline and 1.3 at follow up. Loosening the criteria that define a CTC increases the frequency of counted objects not only in patients but also in controls and, thereby reduced the hazard ratio.

7.3.4 A 3.3 fold loss of EpCAM+ CTC can be contributed to the enrichment and staining procedure

To evaluate the potential loss of CTC through the immuno-magnetic enrichment and staining procedure a comparison was made between CTC detected

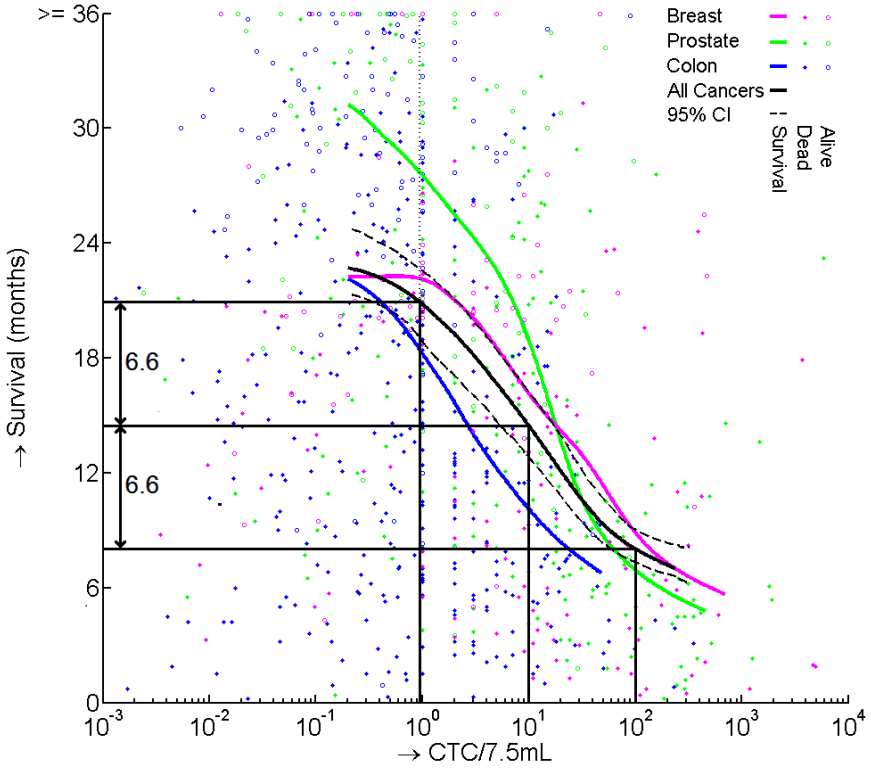

Figure 7.3: Scatter plot of survival versus number of CTC for breast, colorectal and prostate cancer. *Time from baseline to death is indicated by closed symbols, time from baseline to censoring is indicated with open symbols. Survivals exceeding 36 months are truncated at 36 months. Curves show the estimated relationship between median survival time and CTC count for breast ($N = 177$), prostate ($N = 231$), colorectal ($N = 428$) and all patients ($N = 836$). Samples with 0 CTC per 7.5 mL blood were randomly redistributed to a CTC density between 0.001 and 0.9 CTC/7.5 mL of blood with a distribution as predicted by the CDF fits. Median survival monotonically decreases with increasing CTC count for all studies, except the change from 0 to 1 CTC for breast cancer patients, where an increase in survival of 1 month was observed. The 95% confidence interval is shown in dashed lines for the overall curve. In the figure a decrease of 6.6 months in survival for each tenfold increase in CTC is indicated.*

Table 7.1: Impact on survival and CTC frequency using different CTC definitions in metastatic cancers and CTC frequency in healthy donors and patients with benign disease

					Baseline ($N = 420$)				Follow-up ($N = 364$)				Healthy ($N = 204$)			Benign ($N = 190$)		
EpCAM	DNA	CK	CD45	Size	HR	med	min	max	HR	med	min	max	med	min	max	med	min	max
mCTC																		
+	+	+	-	> 4 µm	2.5	4	0	23,618	3.4	4	0	9,864	0	0	1	0	0	12
aCTC																		
+	+	+	-	> 4 µm	2.7	4	0	5,897	3.2	1	0	7,911	0	0	12	0	0	15
+	+	+		> 4 µm	2.7	3	0	5,591	2.8	1	0	6,450	0	0	13	0	0	12
+		+		> 4 µm	2.4	48	0	18,622	2.4	23	0	15,904	11	0	209	15	1	155
+		+	-	> 4 µm	2.3	23	0	16,236	2.7	8	0	8,628	1	0	61	1	0	70
+	+			> 4 µm	1.5	980	0	82,397	1.3	1,263	0	80,810	868	2	70,971	1,094	2	27,302
+	+	+		> 4 µm	2.4	49	0	6,679	2.3	25	0	5,759	15	1	280	16	2	140
+		+	-	> 4 µm	2.2	52	0	13,157	2.9	29	0	9,024	9	0	2,079	5	0	124

mCTC = manual CTC count using the CellSearch CTC definition, aCTC = automated CTC count with different definitions, EpCAM = epithelial cell adhesion molecule, DNA = Hoechst 33342 staining, CK = cytokeratin 8, 18 or 19, HR = Cox hazard ratio, med = median, min = minimum, max = maximum. All HR had $p < 0.0001$ *except for EpCAM+DNA+ CTC with a* $p = 0.02$ *for baseline samples and* $p = 0.03$ *for follow-up samples*

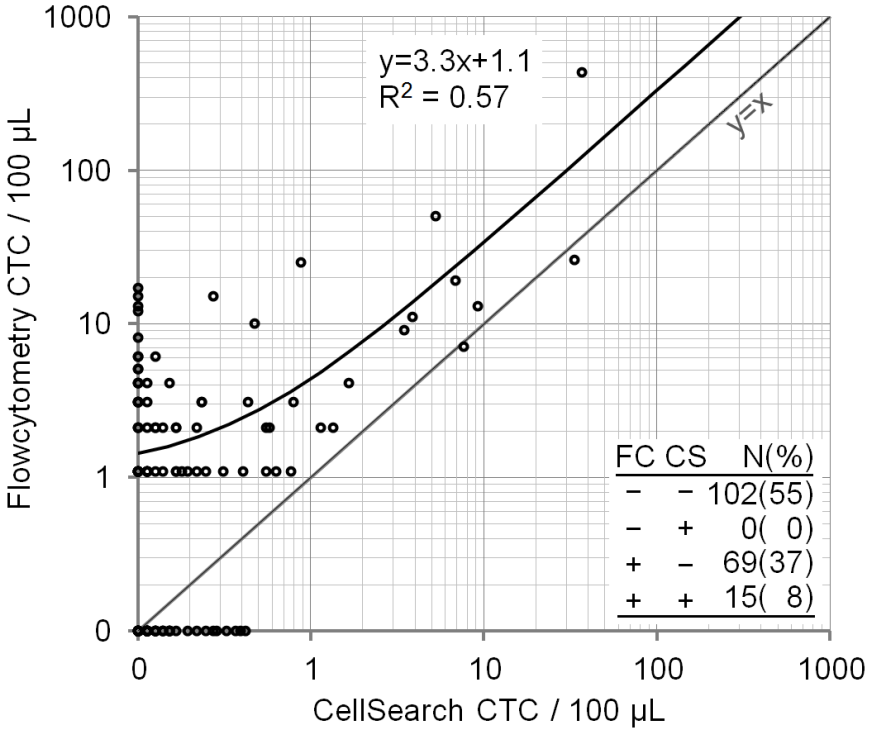

Figure 7.4: Detection of CTC by flow cytometry (FC) versus CellSearch (CS) per 100 µL of blood in metastatic carcinoma patients *($N = 186$)**. CellSearch was performed on 7.5 mL of blood and then divided by 75 to obtain results per 100 µL. The slope between FC and CS is 3.3 indicating that flow cytometry finds more CTC. The number of samples in which ≥ 1 CTC are detected in 100 µL of blood is shown in the bottom right. 55% of samples were negative by both methods, 37% positive by flow only and 8% positive by both flow and CellSearch.*

with the CellSearch system and flow cytometry. For flowcytometric analysis, 100 µL of blood was stained with EpCAM-PE, CD45–PerCP and a nucleic acid dye [20]. Cytokeratin was not stained to avoid potential tumor cell loss due to permeabilization. CTC were detected in blood samples from 186 patients with metastatic carcinoma using both methods. To correct for the different blood volumes the CellSearch results were divided by 75. 105 (55%) samples were negative by both methods.

Figure 7.4 shows the comparison. Both methods correlated with an R^2 of 0.6 and from the slope a higher yield of CTC by the flow cytometry approach can be estimated. The slope is highly dependent on the highest CTC data points, removal of the highest 0–3 values results in slopes of

6.5 (0 points removed), 1.0, 2.5 and 3.1 (3 points removed) respectively. The mean of these four slopes is 3.3, which represents the potential gain in recovery of EpCAM+DNA+CD45- cells.

7.4 Discussion

Tumor cells circulating in blood of cancer patients hold the potential to serve as a liquid biopsy and, thereby, to be used to tailor treatment for the individual patient and to gain insights into the cellular pathways underlying tumor progression [24] or development of clinical cancer dormancy [25] Requirements for fulfilling this potential include the presence of CTC in the sample volume, their isolation and the maintenance of their molecules pertinent to diagnoses and treatment. In studies using CellSearch -the only clinically validated system for CTC detection, 20–50% of blood samples of metastatic cancer patients were found to have 0 CTC in 7.5 mL of blood and, when CTC were detected, only a portion of these cells allowed assessment of treatment targets [10, 11, 12, 26, 27]. The study of RNA, DNA and protein composition of CTC, detected by other methods [28, 29, 4, 30, 31], also suffers from low numbers of CTC per sample. The number of CTC recovered per patient must be increased to yield clinically useful information in all patients. In the present study we investigated possible approaches to achieve this increase; (1) an increase of sample volume, (2) increased recovery of CTC by improved enrichment of cells expressing EpCAM or (3) increased recovery by applying a different morphological definition of a CTC. The frequency of CTC detected in past studies was used to predict the CTC concentration in all 5 liters of blood of these patients. We initially hypothesized that the driving mechanism behind the number of CTC found in patients was self seeding exponential growth with a frequency independent growth rate, and had thus expected a log normal distribution for an optimal fit of the frequency distribution of the CTC [32]. Instead the log-logistic function turned out to better fit the CTC distribution, possibly because the tumor growth rate slows as the tumor increases in size [33, 34, 35, 36]. Application of this function to the data predicts that before initiation of a new line of therapy, 98.7–99.5% of the patients have more than 1 CTC in all 5 L of blood, which decreases to 95.8–99% after these patients receive 1–2 months of cytotoxic chemotherapy, figure 7.2. The low percentage of patients in which CTC disappear after treatment is consistent with the low success rate of treatment in metastatic cancer. The extrapolation down to 5 L hinges on the assumption that the distribution of CTC across patients can be described with a single function. Nevertheless, the close agreement between fit and data shows that an increase in sample volume achieved by drawing more tubes of blood will marginally affect the number of patients in whom CTC are found.

Our results suggest that almost all metastatic patients have EpCAM+CK+

CD45-DNA+ tumor cells circulating in their blood at all times. However, a subset of patients lack the EpCAM and CK antigens in their tumor tissue [37, 38]. For example, in breast cancer the reported percentage of patients whose tumor tissue does not express EpCAM antigens ranges from 3–10% [20, 39, 40]. Possible explanations for this contradiction are that the EpCAM and/or cytokeratin expression is below the detection threshold for immuno-histochemistry, but not for immuno-fluorescence or that the EpCAM- tumor cells in the primary tumor or the metastatic sites represent too small a fraction to be detected during routine immunophenotyping of the tissues.

These EpCAM+ Cytokeratin+ cells may represent a more aggressive phenotype and, thereby, resemble the concept of tumor stem cells [18, 41, 42]. Support for the aggressive phenotype hypothesis is obtained by the monotonic reduction of survival as the number of CTC increases as depicted in figure 7.3. The smoothed survival curves shown in figure 7.3 suggest that survival decreases by 6.6 months for each 10-fold increase in CTC. The steep relationship between number of CTC and survival suggests that this cell population either contains the "killer" cells or contains a different immunophenotype that correlates with the EpCAM+, Cytokeratin+ CTC-concentration.

To test whether the number of patients in which CTC could be detected by increased sensitivity, we first evaluated whether different definitions of CTC can be used to increase the sensitivity of the assay without loss of specificity. To this end, an automated classifier was applied on the stored image sets of the prospective multicenter clinical studies. An increase in the number of CTC can be obtained by using less strict criteria to define a CTC, but this gain reduced the impact on clinical outcome as signified by the HR in all our attempts, table 7.1. This also implies that clinical trials are needed to determine whether the (often higher) CTC number as determined using other CTC enumeration assays is equally or more prognostic for survival than the cells assigned as CTC by the CellSearch method. Next, we evaluated whether significant losses of CTC could have occurred due to either ineffective immunomagnetic enrichment or loss from the staining procedure utilizing permeabilization to enable intra-cytoplasmatic staining of the cytokeratins. To answer this question, a flow cytometry assay was used to detect cells expressing EpCAM and lacking CD45 in 100 µL of blood. Since this assay does not permeabilize the cells and a flow cytometer is an extremely sensitive tool to detect cell surface and intracellular antigens we assume the loss of CTC in this assay to be negligible. Flow cytometry could detect a larger number of CTC as compared to CTC detection by CellSearch in the same blood volume. The highest estimate of this increase was 6.5 fold, but removal of the highest 1–3 measurement values from the fit shows that the true potential improvement is probably closer to 3.3 fold. Furthermore, addition of the cytokeratin requirement in the CTC definition as well as the morphological criteria to the definition will surely reduce

this increase in sensitivity. Still even if a 3.3 fold increase in yield of CTC could be achieved, the CDF fits show that the effect of this increase is limited since the % of samples with ≥ 1 CTC will only increase from 61% to 68%. Additional increases in yield may be achieved by including alternative phenotypes for detection [18, 43, 44, 45, 46], however, proof will be needed that these CTC with a different phenotype are also associated with a bad prognosis and can be used to assess treatment targets.

A solution to the issue would be to significantly increase the sample volume. However, the blood volume taken from the patient cannot be sufficiently increased. This apparent conflict could be solved by in vivo detection methods, in which feasibility has been shown [47, 48, 49, 50]. An alternative approach is to perform leukapheresis for CTC isolation [51]. Although this procedure is more cumbersome compared to a simple blood draw it is more attractive than taking biopsies from the metastatic sites. The utilization of an microfuildic device for CTC detection would require a pre-enrichment step to reduce the sample volume.

The key conclusions from the present study are: 1.) Statistical analysis of the CTC distribution in 7.5 mL of blood detected by CellSearch in metastatic cancer patients suggests that virtually all patients including those that do not have detectable CTCs by CellSearch have at least 1 CTC in 5 L of blood. 2.) A potential 3-fold improvement in the yield of EpCAM+ CTC will not be sufficient to detect CTC in all patients. Therefore, much larger volumes of blood are needed to obtain intact, nucleated, EpCAM+, Cytokeratin+, CD45– CTCs. 3.| Although more "CTC" can be detected by loosening the criteria to define CTC their association with survival decreases. 4.) For every tenfold increase in the number of intact, nucleated, EpCAM+, Cytokeratin +, CD45- CTCs, survival decreases by 6.6 month, supporting the notion that this phenotype of tumor cells may be responsible for metastasis and ultimately death of patients. However, further studies of additional phenotypes are needed.

7.5 Supplemental - Study and patient characteristics

7.5.1 IMMC-01

Inclusion criteria

Patients with progressive, measurable metastatic breast cancer who are commencing a new systemic therapy were eligible. Eastern Cooperative Oncology Group (ECOG) scores for performance status of 0 to 2. Prior adjuvant treatment, treatment of metastatic disease, or both were permitted.

Reasons for exclusion

No patients excluded

Study characteristics and patient demographics

177 female patients, with an median age of 58 years, were included from 20 participating centers in the United States. Patients were enrolled from 2001 to 2003. Of all patients, 47% were enrolled before commencement of the first line of therapy for metastatic disease, 30% started hormone treatment or immunotherapy and 67% chemotherapy (alone or in combination with other therapies). In the 36 months after enrollment, 109 patients died and 68 were censored. The median duration of follow-up of censored patients was 20.8 months. In addition, 145 healthy donors and 200 patients with benign breast carcinoma were enrolled.

7.5.2 IMMC-06

Inclusion criteria

Patients with measurable metastatic colorectal cancer initiating any first- or second-line systemic therapy or third-line therapy with an epidermal growth factor receptor inhibitor. ECOG performance status score of 0 to 2 and hemoglobin of at least 8 g/dL.

Reasons for exclusion

Of 481 patients enrolled, 53 were excluded, 39 did not meet inclusion/exclusion criteria, 6 withdrew consent, 8 were excluded for other reasons.

Study characteristics and patient demographics

428 patients, 45% female, with a median age of 64 years, were included from 55 participating centers in the United States, The Netherlands, and the United Kingdom. Patients were enrolled from 2004 to 2006. Of all patients, 72% were enrolled before commencement of the first line of therapy for metastatic disease, therapy is known for 94% of patients and included Bevacizumab in 56%, Irinotecan in 24%, and/or Oxaliplatin in 59% of patients. In the 36 months after enrollment, 329 patients died and 99 were censored. The median duration of follow-up of censored patients was 29.5 months. In addition, 70 healthy donors were enrolled.

7.5.3 IMMC-38

Inclusion criteria

Patients with histologically confirmed prostate cancer that was metastatic and progressing despite castrate levels of testosterone (<50 ng/mL) and who were commencing a new cytotoxic therapy were eligible. Progression required any or all of the following: a rising PSA as defined by PSA Working Group criteria (53), new osseous lesions, or new or enlarging soft tissue metastases. Other eligibility criteria included a PSA level of >5 ng/mL; ECOG performance status score of 0 to 2; a 4-wk (6-wk for nilutamide, bicalutamide) washout after discontinuation of an antiandrogen, and no radiation or radionuclide therapy within 30 d of entry. A bone scan within 60 d of the first blood draw was also required. Patient with brain metastases or a history of other malignancies within the last 5 years were excluded.

Reasons for exclusion

13 commenced radiotherapy or a new hormonal therapy within 30 days of the baseline blood draw; 10 did not have evaluable baseline blood draws or scans; 8 had insufficient washout from anti-androgens; 7 lacked progressive disease at accrual; 3 had a history of other cancers within the previous 5 years; 2 withdrew consent; 1 had a PSA of <5 ng/mL; 1 was not castration resistant.

Study characteristics and patient demographics

231 male patients, with a median age of 70 years, were included from 65 participating centers in the United States and Europe. Patients were enrolled from 2004 to 2006. Of all patients, 67% were enrolled before commencement of the first line of therapy for metastatic disease, and the first line of therapy after enrollment included Taxotere for 70% of patients. In the 36 months after enrollment, 166 patients died and 65 were censored. The median duration of follow-up of censored patients was 30.0 months.

7.5.4 Flow versus CellSearch

Inclusion criteria

Patients diagnosed with metastatic carcinoma.

Reasons for exclusion

Of 296 patients enrolled for the quantification of EpCAM expression on circulating tumor cells, 140 were randomly selected for a comparison between flowcytometry and CellSearch. The other patients were used for quantitative determination of expression of cytokeratin 8,18, cytokeratin 19, and EpCAM.

Study characteristics and patient demographics

All samples were acquired from a single clinical site in the United States. Patients were enrolled from 2003 to 2005. Therapy was administered at the discretion of the treating oncologist. No therapy or patient demographic information is available.

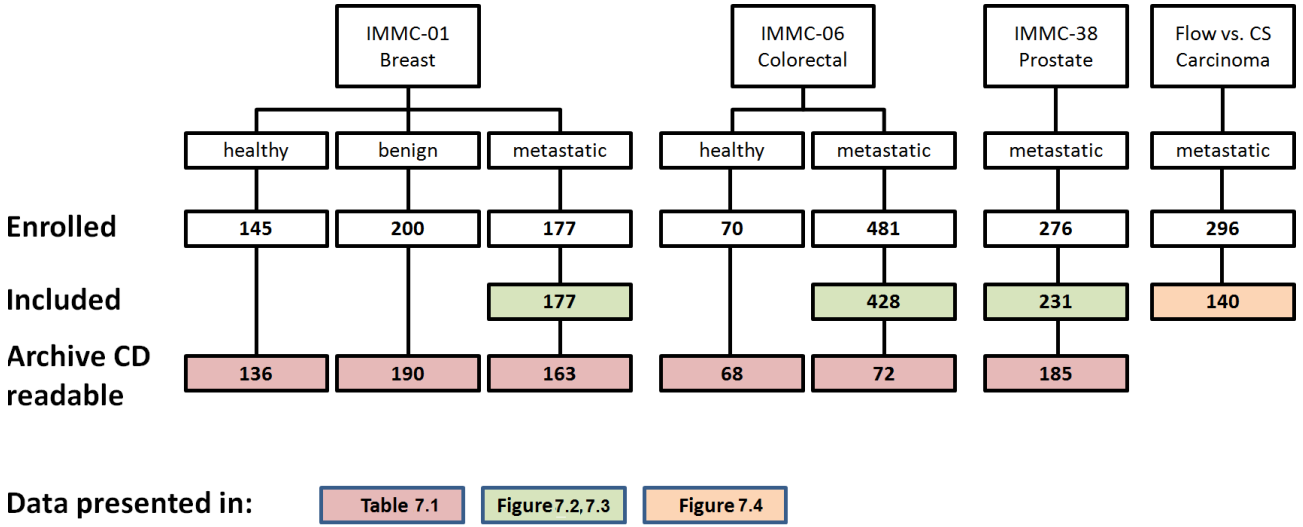

Figure 7.5: Inclusion diagram for all data. *The number of patients enrolled is shown on the first line. For the metastatic patients, the number of patients who met the inclusion criteria is shown on the second line. No inclusion/exclusion was applied to patients with benign carcinoma, or without history of carcinoma (healthy); included is equal to enrolled for these groups. For the automated image analysis in table 7.1, the archive CDs with sample image data needed to be imported. This import failed occasionally due to issues with the CD writers at several sites, damage to the archive CDs or loss of the archive CDs. Cumulatively 14 (8%) metastatic breast, 356 (83%) of metastatic colorectal and 46 (20%) of metastatic prostate cancer patients could not be used for the evaluation of different morphological CTC definitions. The archive CDs from the flowcytometry versus CellSearch (CS) comparison were not available.*

7.6 References

[1] E. Racila, D. Euhus, A. J. Weiss, C. Rao, J. McConnell, L. W. Terstappen, and J. W. Uhr, "Detection and characterization of carcinoma cells in the blood," *Proc. Natl. Acad. Sci. U.S.A.*, vol. 95, pp. 4589–4594, Apr 1998.

[2] W. J. Allard, J. Matera, M. C. Miller, M. Repollet, M. C. Connelly, C. Rao, A. G. Tibbe, J. W. Uhr, and L. W. Terstappen, "Tumor cells circulate in the peripheral blood of all major carcinomas but not in healthy subjects or patients with nonmalignant diseases," *Clin. Cancer Res.*, vol. 10, pp. 6897–6904, Oct 2004.

[3] S. Nagrath, L. V. Sequist, S. Maheswaran, D. W. Bell, D. Irimia, L. Ulkus, M. R. Smith, E. L. Kwak, S. Digumarthy, A. Muzikansky, P. Ryan, U. J. Balis, R. G. Tompkins, D. A. Haber, and M. Toner, "Isolation of rare circulating tumour cells in cancer patients by microchip technology," *Nature*, vol. 450, pp. 1235–1239, Dec 2007.

[4] S. L. Stott, C. H. Hsu, D. I. Tsukrov, M. Yu, D. T. Miyamoto, B. A. Waltman, S. M. Rothenberg, A. M. Shah, M. E. Smas, G. K. Korir, F. P. Floyd, A. J. Gilman, J. B. Lord, D. Winokur, S. Springer, D. Irimia, S. Nagrath, L. V. Sequist, R. J. Lee, K. J. Isselbacher, S. Maheswaran, D. A. Haber, and M. Toner, "Isolation of circulating tumor cells using a microvortex-generating herringbone-chip," *Proc. Natl. Acad. Sci. U.S.A.*, vol. 107, pp. 18392–18397, Oct 2010.

[5] U. Dharmasiri, S. Njoroge, M. Witek, M. Adebiyi, J. Kamande, M. Hupert, F. Barany, and S. Soper, "High-throughput selection, enumeration, electrokinetic manipulation, and molecular profiling of low-abundance circulating tumor cells using a microfluidic system," *Analytical chemistry*, vol. 83, pp. 2301–Ũ2309, 2011.

[6] S. J. Tan, R. L. Lakshmi, P. Chen, W. T. Lim, L. Yobas, and C. T. Lim, "Versatile label free biochip for the detection of circulating tumor cells from peripheral blood in cancer patients," *Biosens Bioelectron*, vol. 26, pp. 1701–1705, Dec 2010.

[7] H. B. Hsieh, D. Marrinucci, K. Bethel, D. N. Curry, M. Humphrey, R. T. Krivacic, J. Kroener, L. Kroener, A. Ladanyi, N. Lazarus, P. Kuhn, R. H. Bruce, and J. Nieva, "High speed detection of circulating tumor cells," *Biosens Bioelectron*, vol. 21, pp. 1893–1899, Apr 2006.

[8] S. Zheng, H. Lin, J. Q. Liu, M. Balic, R. Datar, R. J. Cote, and Y. C. Tai, "Membrane microfilter device for selective capture, electrolysis and genomic analysis of human circulating tumor cells," *J Chromatogr A*, vol. 1162, pp. 154–161, Aug 2007.

[9] J. P. Gleghorn, E. D. Pratt, D. Denning, H. Liu, N. H. Bander, S. T. Tagawa, D. M. Nanus, P. A. Giannakakou, and B. J. Kirby, "Capture of circulating tumor cells from whole blood of prostate cancer patients using geometrically enhanced differential immunocapture (GEDI) and a prostate-specific antibody," *Lab Chip*, vol. 10, pp. 27–29, Jan 2010.

[10] J. S. de Bono, H. I. Scher, R. B. Montgomery, C. Parker, M. C. Miller, H. Tissing, G. V. Doyle, L. W. Terstappen, K. J. Pienta, and D. Raghavan, "Circulating tumor cells predict survival benefit from treatment in metastatic castration-resistant prostate cancer," *Clin. Cancer Res.*, vol. 14, pp. 6302–6309, Oct 2008.

[11] S. J. Cohen, C. J. Punt, N. Iannotti, B. H. Saidman, K. D. Sabbath, N. Y. Gabrail, J. Picus, M. Morse, E. Mitchell, M. C. Miller, G. V. Doyle, H. Tissing, L. W. Terstappen, and N. J. Meropol, "Relationship of circulating tumor cells to tumor response, progression-free survival, and overall survival in patients with metastatic colorectal cancer," *J. Clin. Oncol.*, vol. 26, pp. 3213–3221, Jul 2008.

[12] M. Cristofanilli, G. T. Budd, M. J. Ellis, A. Stopeck, J. Matera, M. C. Miller, J. M. Reuben, G. V. Doyle, W. J. Allard, L. W. Terstappen, and D. F. Hayes, "Circulating tumor cells, disease progression, and survival in metastatic breast cancer," *N. Engl. J. Med.*, vol. 351, pp. 781–791, Aug 2004.

[13] F. A. Coumans, C. J. Doggen, G. Attard, J. S. de Bono, and L. W. Terstappen, "All circulating EpCAM+CK+CD45- objects predict overall survival in castration-resistant prostate cancer," *Ann. Oncol.*, vol. 21, pp. 1851–1857, Sep 2010.

[14] J. Thiery *et al.*, "Epithelial-mesenchymal transitions in tumour progression," *Nature Reviews Cancer*, vol. 2, no. 6, pp. 442–454, 2002.

[15] R. Kalluri and R. Weinberg, "The basics of epithelial-mesenchymal transition," *The Journal of clinical investigation*, vol. 119, no. 6, p. 1420, 2009.

[16] B. Aktas, M. Tewes, T. Fehm, S. Hauch, R. Kimmig, S. Kasimir-Bauer, *et al.*, "Stem cell and epithelial-mesenchymal transition markers are frequently overexpressed in circulating tumor cells of metastatic breast cancer patients," *Breast Cancer Res*, vol. 11, no. 4, p. R46, 2009.

[17] A. Bonnomet, A. Brysse, A. Tachsidis, M. Waltham, E. Thompson, M. Polette, and C. Gilles, "Epithelial-to-mesenchymal transitions and circulating tumor cells," *Journal of mammary gland biology and neoplasia*, vol. 15, no. 2, pp. 261–273, 2010.

[18] C. Raimondi, A. Gradilone, G. Naso, B. Vincenzi, A. Petracca, C. Nicolazzo, A. Palazzo, R. Saltarelli, F. Spremberg, E. Cortesi, *et al.*, "Epithelial-mesenchymal transition and stemness features in circulating tumor cells from breast cancer patients," *Breast cancer research and treatment*, vol. 130, no. 2, pp. 449–455, 2011.

[19] G. Kallergi, M. Papadaki, E. Politaki, D. Mavroudis, V. Georgoulias, S. Agelaki, *et al.*, "Epithelial to mesenchymal transition markers expressed in circulating tumour cells of early and metastatic breast cancer patients," *Breast Cancer Research*, vol. 13, no. 3, p. R59, 2011.

[20] C. G. Rao, D. Chianese, G. V. Doyle, M. C. Miller, T. Russell, R. A. Sanders, and L. W. Terstappen, "Expression of epithelial cell adhesion molecule in carcinoma cells present in blood and primary and metastatic tumors," *Int. J. Oncol.*, vol. 27, pp. 49–57, Jul 2005.

[21] S. Ligthart, F. Coumans, G. Attard, A. Cassidy, J. de Bono, and L. Terstappen, "Unbiased and automated identification of a circulating tumour cell definition that associates with overall survival," *PloS one*, vol. 6, no. 11, p. e27419, 2011.

[22] H. I. Scher, X. Y. Jia, J. S. de Bono, M. Fleisher, K. J. Pienta, D. Raghavan, and G. Heller, "'Circulating tumour cells as prognostic markers in progressive, castration-resistant prostate cancer: a reanalysis of IMMC38 trial data," *Lancet Oncology*, vol. 10, pp. 233–239, 2009.

[23] R. Gentleman and J. Crowley, "Graphical methods for censored data," *Journal of the American Statistical Association*, pp. 678–683, 1991.

[24] B. Vogelstein and K. Kinzler, "Cancer genes and the pathways they control," *Nature medicine*, vol. 10, no. 8, pp. 789–799, 2004.

[25] J. Uhr and K. Pantel, "Controversies in clinical cancer dormancy," *Proceedings of the National Academy of Sciences*, vol. 108, no. 30, p. 12396, 2011.

[26] J. F. Swennenhuis, A. G. Tibbe, R. Levink, R. C. Sipkema, and L. W. Terstappen, "Characterization of circulating tumor cells by fluorescence in situ hybridization," *Cytometry A*, vol. 75, pp. 520–527, Jun 2009.

[27] G. Attard, J. F. Swennenhuis, D. Olmos, A. H. Reid, E. Vickers, R. A'Hern, R. Levink, F. Coumans, J. Moreira, R. Riisnaes, N. B. Oommen, G. Hawche, C. Jameson, E. Thompson, R. Sipkema, C. P. Carden, C. Parker, D. Dearnaley, S. B. Kaye, C. S. Cooper, A. Molina, M. E. Cox, L. W. Terstappen, and J. S. de Bono, "Characterization of ERG, AR and PTEN gene status in circulating tumor cells from patients with castration-resistant prostate cancer," *Cancer Res.*, vol. 69, pp. 2912–2918, Apr 2009.

[28] C. Klein, S. Seidl, K. Petat-Dutter, S. Offner, J. Geigl, O. Schmidt-Kittler, N. Wendler, B. Passlick, R. Huber, G. Schlimok, *et al.*, "Combined transcriptome and genome analysis of single micrometastatic cells," *Nature biotechnology*, vol. 20, no. 4, pp. 387–392, 2002.

[29] S. Riethdorf, V. Muller, L. Zhang, T. Rau, S. Loibl, M. Komor, M. Roller, J. Huober, T. Fehm, I. Schrader, J. Hilfrich, F. Holms, H. Tesch, H. Eidtmann, M. Untch, G. von Minckwitz, and K. Pantel, "Detection and HER2 expression of circulating tumor cells: prospective monitoring in breast cancer patients treated in the neoadjuvant GeparQuattro trial," *Clin. Cancer Res.*, vol. 16, pp. 2634–2645, May 2010.

[30] Y. Hou, L. Song, P. Zhu, B. Zhang, Y. Tao, X. Xu, F. Li, K. Wu, J. Liang, D. Shao, *et al.*, "Single-cell exome sequencing and monoclonal evolution of a JAK2-negative myeloproliferative neoplasm," *Cell*, vol. 148, no. 5, pp. 873–885, 2012.

[31] J. Shaw, K. Page, K. Blighe, N. Hava, D. Guttery, B. Ward, J. Brown, C. Ruangpratheep, J. Stebbing, R. Payne, *et al.*, "Genomic analysis of circulating cell-free dna infers breast cancer dormancy," *Genome Research*, vol. 22, no. 2, pp. 220–231, 2012.

[32] A. Koch, "The logarithm in biology 1. mechanisms generating the log-normal distribution exactly," *Journal of theoretical biology*, vol. 12, no. 2, pp. 276–290, 1966.

[33] J. Spratt, D. Von Fournier, J. Spratt, and E. Weber, "Decelerating growth and human breast cancer," *Cancer*, vol. 71, no. 6, pp. 2013–2019, 1993.

[34] D. Fournier, E. Weber, W. Hoeffken, M. Bauer, F. Kubli, and V. Barth, "Growth rate of 147 mammary carcinomas," *Cancer*, vol. 45, no. 8, pp. 2198–2207, 1980.

[35] I. Millet, E. Bouic-Pages, D. Hoa, D. Azria, and P. Taourel, "Growth of breast cancer recurrences assessed by consecutive MRI," *BMC cancer*, vol. 11, no. 1, p. 155, 2011.

[36] J. Shaeffer, A. El-Mahdi, and W. Constable, "Radiation control of microscopic pulmonary metastases in C3H mice," *Cancer*, vol. 32, no. 2, pp. 346–351, 1973.

[37] S. Joosse, J. Hannemann, J. Spötter, A. Bauche, A. Andreas, V. Müller, and K. Pantel, "Changes in keratin expression during metastatic progression of breast cancer: impact on the detection of circulating tumor cells," *Clinical Cancer Research*, vol. 18, no. 4, pp. 993–1003, 2012.

[38] A. M. Sieuwerts, J. Kraan, J. Bolt, P. van der Spoel, F. Elstrodt, M. Schutte, J. W. Martens, J. W. Gratama, S. Sleijfer, and J. A. Foekens, "Anti-epithelial cell adhesion molecule antibodies and the detection of circulating normal-like breast tumor cells," *J. Natl. Cancer Inst.*, vol. 101, pp. 61–66, Jan 2009.

[39] G. Spizzo, D. Fong, M. Wurm, C. Ensinger, P. Obrist, C. Hofer, G. Mazzoleni, G. Gastl, and P. Went, "EpCAM expression in primary tumour tissues and metastases: an immunohistochemical analysis," *Journal of clinical pathology*, vol. 64, no. 5, pp. 415–420, 2011.

[40] M. Smid, Y. Wang, Y. Zhang, A. Sieuwerts, J. Yu, J. Klijn, J. Foekens, and J. Martens, "Subtypes of breast cancer show preferential site of relapse," *Cancer research*, vol. 68, no. 9, p. 3108, 2008.

[41] M. Wicha, S. Liu, and G. Dontu, "Cancer stem cells: an old ideaŮa paradigm shift," *Cancer research*, vol. 66, no. 4, p. 1883, 2006.

[42] P. Gupta, C. Chaffer, and R. Weinberg, "Cancer stem cells: mirage or reality?," *Nature medicine*, vol. 15, no. 9, pp. 1010–1012, 2009.

[43] B. Mostert, J. Kraan, J. Bolt-de Vries, P. Van Der Spoel, A. Sieuwerts, M. Schutte, A. Timmermans, R. Foekens, J. Martens, J. Gratama, *et al.*, "Detection of circulating tumor cells in breast cancer may improve through enrichment with anti-CD146," *Breast cancer research and treatment*, vol. 127, no. 1, pp. 33–41, 2011.

[44] P. Jacobs and R. Sackstein, "CD44 and HCELL: Preventing hematogenous metastasis at step 1," *FEBS letters*, 2011.

[45] P. Theodoropoulos, H. Polioudaki, S. Agelaki, G. Kallergi, Z. Saridaki, D. Mavroudis, and V. Georgoulias, "Circulating tumor cells with a putative stem cell phenotype in peripheral blood of patients with breast cancer," *Cancer letters*, vol. 288, no. 1, pp. 99–106, 2010.

[46] A. Armstrong, M. Marengo, S. Oltean, G. Kemeny, R. Bitting, J. Turnbull, C. Herold, P. Marcom, D. George, and M. Garcia-Blanco, "Circulating tumor cells from patients with advanced prostate and breast cancer display both epithelial and mesenchymal markers," *Molecular Cancer Research*, vol. 9, no. 8, p. 997, 2011.

[47] P. Smirnov, M. Poirier-Quinot, C. Wilhelm, E. Lavergne, J. Ginefri, B. Combadière, O. Clément, L. Darrasse, and F. Gazeau, "In vivo single cell detection of tumor-infiltrating lymphocytes with a clinical 1.5 Tesla MRI system," *Magnetic Resonance in Medicine*, vol. 60, no. 6, pp. 1292–1297, 2008.

[48] E. I. Galanzha, E. V. Shashkov, T. Kelly, J. W. Kim, L. L. Yang, and V. P. Zharov, "In vivo magnetic enrichment and multiplex photoacoustic detection of circulating tumour cells," *Nature Nanotechnology*, vol. 4, pp. 855–860, 2009.

[49] Y. C. Chang, J. Y. Ye, T. P. Thomas, Z. Y. Cao, A. Kotlyar, E. R. Tkaczyk, J. R. Baker, and T. B. Norris, "Fiber-optic multiphoton flow cytometry in whole blood and in vivo," *Journal of Biomedical Optics*, vol. 15, p. 047004, 2010.

[50] D. Murawa, S. Herold, P. Kim, A. Schmitz, T. Krahn, P. Murawa, M. Zabel, N. Morgenthaler, P. Nowaczyk, and K. Luecke, "A new medical device for in-vivo capturing of circulating tumor cells in breast cancer (BC) patients.," in *Abstract ID 10537, ASCO Annual Meeting 2012*, 2012 Chicago, IL.

[51] R. L. Eifler, J. Lind, D. Falkenhagen, V. Weber, M. B. Fischer, and R. Zeillinger, "Enrichment of circulating tumor cells from a large blood volume using leukapheresis and elutriation: Proof of concept," *Cytometry Part B-Clinical Cytometry*, vol. 80B, pp. 100–111, 2011.

CHAPTER 8

Factors influencing filtration of tumor cells from whole blood

F.A.W. Coumans*, G. van Dalum*, M. Beck, L.W.M.M. Terstappen
* both authors contributed equally

Abstract

Enrichment of circulating tumor cells (CTC) from blood can be achieved by filtration. Key parameters such as flow rate, applied pressure, sample dilution and fixation, vary largely between various assays and their influence is not well understood. Here, we used a filtration system with controlled flow rate, pressure and sample dilution to determine the relation between these parameters. Whole blood, or its major components, with and without spiked tumor cells were filtered through track-etched filters. The apparent viscosity, defined as the viscosity of a cell passing through a pore, of a 15 µm diameter MDA-231 cell is $5 \cdot 10^2$ times larger than the apparent viscosity of a 10 µm white cell and $5 \cdot 10^4$ times larger than that of a 90 fl red cell passing through a 5 µm pore. Fixation increases the pressure needed to pass cells through 8 µm pores by 25-fold and reduces recovery of spiked tumor cells by twofold. Filtration should be performed on unfixed samples at a pressure of about 10 mbar for a 1 cm^2 5 µm pore size track-etched filter. At this pressure MDA-231 cells move through the filter in 1 hour. Sample dilution is not required and has a small negative influence on recovery. If fixation is needed for sample preservation, a gentle fixative is preferable, but will increase apparent viscosity of all cells. The difference in apparent

viscosity between CTC and blood cells is key in optimizing recovery of CTC.

8.1 Introduction

Circulating tumor cells (CTC) are cancer cells shed into the blood from primary or metastatic sites. Clinical trials have shown that the presence of CTC is predictive of survival in several types of cancer, including breast, prostate, colon, gastric, small and non-small cell lung carcinoma and melanoma [1, 2, 3, 4, 5, 6, 7]. The enumeration and characterization of CTC is a great technological challenge [8], which requires a multitude of assay steps. In order to integrate these steps into a single device CTC must be greatly enriched from the rest of the sample in the first processing step(s), as these CTC are extremely rare (typically 1 CTC compared to $5 \cdot 10^6$ white cells and $5 \cdot 10^9$ red cells in 1 mL of blood). On the one hand, it would be desirable to make use of microfluidic technologies to characterize such a small number of cells. On the other hand, the sample volume that can be handled is limited to 1 mL of blood in most lab on a chip devices reported to date [9, 10, 11, 12]. A planar filter integrated in a microfluidic chip [13] can allow larger sample volumes, especially if the captured CTC are moved to another area for further investigation [12].
Selective CTC enrichment is often achieved by either a positive selection, targeting antigens on the cell surface of the CTC not expressed by blood cells, or by a selective depletion of the blood cells targeting antigens not expressed on CTC [14, 15, 16, 9, 17, 11, 18]. The downside of using antibody mediated positive enrichment is that cells with low or no expression of the antigen are lost. Antigen expression independent techniques could select CTC based on physical differences between tumor and blood cells like stiffness [19], density [20], or size by a filter membrane [21, 22, 23, 24, 25, 26, 27, 28, 29] or other filter type [30, 12]. However, large differences in sample fixation, sample dilutions, flow rates and pressures across the filter exist between these approaches as summarized in table 8.1. Here we investigate the parameters important for enrichment of CTC by filtration techniques.

8.2 Materials and methods

8.2.1 Blood samples

Healthy volunteers aged 20–55 consented to the study protocol, which was approved by an ethics board. Blood from EDTA vacutainers (BD, Franklin Lakes, NJ, USA) was processed within 12 hours after draw. Unless otherwise noted, each data point represents the average of three repeat measurements. For each repeat we used blood from a different donor, but a whole experiment was done with the same three donors.

Table 8.1: Filtration methods and conditions

reference	pressure mbar	pore size µm	fixation	sample dilution
Zheng 2011 [28]	35	7[a]	none	1:10
Zheng 2007 [23]	35	10	PFA [c]	1:10
Tan 2010 [12]	50	5[a]	none	none
Vona 2000 [21]	300	8	PFA [c]	1:10 [d]
Desitter 2011 [27]	700 [b]	6.5	none	1:8 [d]
	700 [b]	7.5	PFA [c]	1:7 [d]
Kahn 2004 [22]	N/A [e]	8	50% EtOH	5:4 [d]

[a] Estimated pore size from 3D filter structure, [b] Pressure at start of filtration, [c] Paraformaldehyde, [d] Red blood cells lysed/removed, [e] not available.

8.2.2 Cell culture and cell staining

Spiking experiments were performed with cells from the prostate carcinoma cell line PC3-9 and the breast carcinoma cell lines SKBR-3 and MDA-231. PC3-9 cells were cultured using RPMI (Sigma, St. Louis, MO, USA) while the SKBR-3 and MDA-231 cells were cultured in Dulbecco's Modified Eagle Medium (Sigma). Culture media were supplemented with 10% fetal bovine serum (Gibco, Invitrogen, Carlsbad, CA, USA), 1% penicillin-streptomycin (Gibco) and 1% L-Glutamin (Sigma). PC3-9 were stained with CellTracker Green Bodipy, MDA-231 with CellTracker Orange CMTMR (both Invitrogen) and SKBR-3 with both stains. Cells were incubated in culture media for 24 hours at 37°C with 50 µmol CellTracker Green and/or 5 µmol CellTracker Orange prior to harvesting with 0.05% trypsin (Gibco). While still in the filter holder, the filter was washed with ethanol to fix the cells to the filter, in a series of increasing concentration from 70 to 100%. The filter was dried in vacuum followed by staining of nuclei with 8 µmol Hoechst 33342 (Invitrogen).

8.2.3 Filtration setup

A filtration setup was constructed to allow simultaneous measurement of pressure and control of flow rate, figure 8.1. The flow through the filter consists of two parts, the sample flow and a PBS (phosphate buffered saline) flow. If desired, the PBS flow can be used to dilute the sample. Dilution of 1:x means that 1 part sample is diluted in x-1 parts of PBS. For the sample flow, a sample is loaded into a 1 mL or 50 mL syringe (Plastipak, BD, Franklin Lakes, NJ, USA) with a 21 gauge needle (Microlance 3, BD) and placed onto a NE-1000 syringe pump (New Era Pump Systems, Farmingdale, NY, USA). The PBS flow originates from a stainless steel tank (Alloy products, Waukesha, WI, USA) pressurized with 2 bar N_2. To reduce uptake of N_2 into the PBS, the PBS is contained inside a plastic bladder

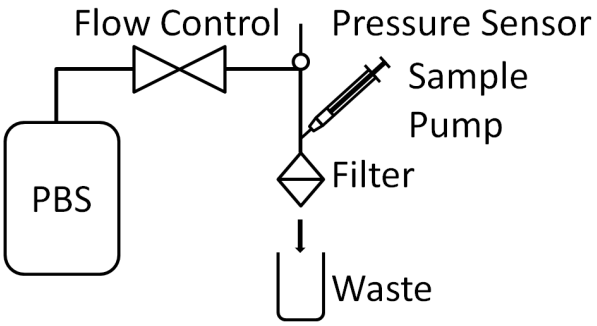

Figure 8.1: Setup for filtration. *The setup allows for control of either pressure, flow rate or sample dilution factor while monitoring the other two parameters.*

inside a water filled tank. PBS is filtered by an inline 0.2 µm filter (mini Kleenpak, Pall, Mijdrecht, The Netherlands) and the flow rate is controlled by a flow sensor (CoriFlow, Bronkhorst, Veenendaal, Netherlands). The pressure difference across the filter is measured by a 0–300 mbar pressure sensor (PR-41X, Keller, Winterthur, Switzerland). During filtration, the pressure increases until a stable situation is reached or pressure exceeds 300 mbar. The stable pressure was recorded.

8.2.4 Filters

Track-etched filters with pore sizes of 5 µm and 8 µm pore size and a diameter of 13 mm were used (Nucleopore, Whatman, GE, Maidstone, UK). The number of pores on a track-etched filter were counted with a bright field image of 1 mm^2 of filter area using a fluorescent microscope with 4x NA=0.13 objective (E-400, Nikon, Melville, NY, USA). The 5 µm pore size filters contained $3.5 \cdot 10^5$ pores and the 8 µm contained $9.2 \cdot 10^4$ pores in a filter surface of 102 mm^2. Inspection of the filters by bright field microscopy indicates that the pores are distributed randomly, that 3–10% of the pores are so closely spaced that one 15 µm diameter cell may block several pores, and that 1–2% of pores consist of merged holes. The pores constitute approximately 5–7% of the filter area. Since filter properties vary between different lots, only one lot of each pore size was used. The filters were mounted in plastic filter holders (Swinney, Pall). Before use, a filter was placed in a holder, primed with PBS and placed in $\approx$ 50 mbar vacuum for 30 minutes, which displaced trapped air form the filter pores, but did not evaporate more than 10% of the PBS.

8.2.5 Relation between number of pores, pressure, and flow rate

The relation between pressure and flow rate for a filter was determined by increasing the flow rate from 0–2000 mL/h in steps of 50 mL/h and recording flow rate and pressure. To determine the impact of the number of pores, we covered parts of the 5 and 8 µm track-etched filters with different aperture plates leaving 2, 4, 8, 16, 32 or 57 mm^2 of the filter area open. Viscosity of PBS was assumed to be equal to water [31], $0.9 \cdot 10^{-3}$ Pa·s.

8.2.6 Impact of sample dilution on pressure

To determine the impact of sample dilution on the pressure difference, we filtered 1 mL of whole blood through a 5 µm track-etched filter with dilutions of 1:1, 1:4 and 1:16 and total flow rates of 50, 200 and 800 mL/h. Dilutions were set at 1:4 for all other experiments.

8.2.7 Filtration of blood fractions, culture cells and beads

Major components of whole blood include white blood cells (WBC), red blood cells (RBC) and serum. Blood was split into fractions by means of centrifugation. A 10 mL tube of blood was centrifuged at 300 x g for 10 minutes. We collected the top 1 mL of serum, the bottom 1 mL of red blood cells as well as the buffy coat layer together with 0.5 mL of serum above and 0.5 mL of red blood cells below this layer. Each fraction was reconstituted to their original concentration with PBS-1%BSA (bovine serum albumin). At a hematocrit of 60%, the 1 mL of serum was diluted with 1.5 mL of PBS-1%BSA and the 1 mL of RBC was diluted with 0.67 mL PBS-1%BSA. The buffy coat was diluted with 9 mL of PBS-1%BSA. We did not lyse the red blood cells in the buffy coat sample to prevent swelling of the WBC. As a result the sample contains RBC but at a concentration ≈ 12 times lower than the RBC sample. For culture cells, we attempted to pass 10^6 MDA-231, PC3-9 and SKBR-3 culture cells through a 5 µm pore track-etched filter with $0.35 \cdot 10^6$ pores, or three times more cells than pores. To test whether very stiff cells that are larger than the pore size are retained on the filter, we filtered a solution with 10^6 of 10 µm, 6 µm and 4 µm polystyrene beads (size calibration beads, Invitrogen) through a 5 µm filter. The filtrate was enumerated on a FACSARIA II flowcytometer (BD) using forward and side scatter signals and the beads on the filter enumerated using brightfield imaging on a microscope with 4x NA=0.13 objective.

8.2.8 Whole blood cell filtration

The force pushing cells through a filter is the pressure ΔP across the filter times the cross section A_{pore} of the pore. The interaction of a cell with a

pore can be modeled by describing the cell as a droplet characterized by an apparent viscosity [32], which is dependent on the cell surface tension, cell and nucleus viscosity [33], the sample temperature [34], and the deformation required to pass through a pore [35]. If the pressure forcing the cell against the pore is larger than the critical pressure to overcome the surface tension, the cell will move into the pore at a rate determined by the apparent viscosity. If the critical pressure for CTC is substantially higher than the critical pressure for white and red blood cells, filtering at a pressure below the CTC critical pressure will be an effective enrichment method. On the other hand, if the CTC critical pressure is similar to that for white and red blood cells, filtration must take place at a pressure in excess of the critical pressure to prevent clogging of the filter. At pressures in excess of the critical pressure, all cells in the sample will pass through the filter at different speeds, which are determined by their apparent viscosity.
For a filter with N pores of diameter d, height h and sufficiently low porosity ($< 10\%$), steady state laminar flow pressure difference across the filter when an incompressible fluid with viscosity μ passes through at flow rate Q is given by [36, 37, 38]:

$$\Delta P = \mu \left[\frac{128h}{\pi d^4} + \frac{24}{d^3} \right] \frac{Q}{N} = \mu R \frac{Q}{N} \tag{8.1}$$

R is the pore resistance, derived for a pore with sharp edges. For all our experimental conditions the Reynolds number is smaller than 100 unless a filter is nearly clogged. It is therefore sufficient to consider laminar flow conditions.

8.2.9 Estimation of cell speed and apparent viscosity

Describing the cells as droplets suspended in a diluent, and assuming that no cells are permanently retained by the filter and fibrin aggregates that may clog the filter are not present, the pressure difference must be equal for each of the components.

$$\Delta P = \mu_{dil} R \frac{Q_{dil}}{N_{dil}} = \mu_{cell}^{app} R \frac{Q_{cell}}{N_{cell}} \tag{8.2}$$

With subscripts used to indicate the contribution of the diluent (dil), cells (cell) or diluent and cells combined (total). Further $Q_{cells} = Q_{total} C_{cell} V_{cell}$, where C_{cell} is the (number) concentration of cells in the sample and V_{cell} is the cell volume. We can now use this equation to determine the number of pores that are needed to pass the sample diluent N_{dil}. The rest of the pores $N_{cell} = N_{total} - N_{dil}$ are occupied by cells passing through. The unknown apparent viscosity μ_{cell}^{app} for each cell type can now be determined by filtering a single cell type with known concentration and cell volume. We assume an average of 90 fl for the red blood cell volume [39]. Other cells are assumed

to be spherical with a radius of 10 µm for WBC and 15 µm for MDA-231. The cell speed v inside the pore is then derived according to equation 8.3, with A_{pore} the cross section of a pore.

$$v = \frac{Q_{cell}}{N_{cell} A_{pore}} \tag{8.3}$$

The data from the filtration of blood fractions and culture cells was used to determine apparent viscosity and cell speed for each cell type. For the WBC/RBC cell mixture in the components experiment, the speed of the WBC was estimated by subtracting the number of pores clogged by RBC as derived from the same experiment.

8.2.10 Spiked samples and cell recovery for different fixations

Thirty mL of blood was collected and spiked with 300 prestained MDA-231, SKBR-3 and PC3-9 per mL of whole blood. The total of 900 cells is low compared to the total number of pores, yet sufficiently high for cell counting. Concentration of cells in the spiking stock was determined by counting at least 200 cells of each type on a counting chamber (Neubauer, Lauda-Königshofen, Germany). The spiked blood was split into three fractions of 10 mL. The first fraction was processed unfixed. To the second fraction the content of a 10 mL CellSave preservative vacutainer tube (Veridex, Raritan, NJ, USA) was added and incubated for 3–5 hours. The third fraction was split into 1 mL aliquots and 10 ± 0.5 minutes prior to commencement of the filtration procedure 1 mL of a 0.8% formaldehyde solution (PFA) was added to each aliquot. For filtering, the total flow rate was set at 100 mL/h, with a 1:4 dilution. The samples were enumerated by imaging the filter on a fluorescence microscope as described above. False color images (CellTracker Orange: red, CellTracker Green: green, Hoechst 33342: blue) were generated in which the PC3-9 appear light green, the MDA-231 pink and the SKBR-3 yellow, figure 8.2. Cells with only a nucleus are assumed to be white blood cells (blue).

8.3 Results

8.3.1 Relation between flow rate, pressure and number of pores is predicted by the model

Figure 8.3 shows the relation between flow rate and pressure for different number of pores of the 5 µm filter. Pressure is linearly dependent on the flow per pore, as predicted by equation 8.1. The resistance R is 1.24 ± 0.02 µm^{-3}, or 48% higher than was expected from entering the thickness and pore size parameters in equation 8.1. For the 8 µm filter, we obtain $R = 0.26 \pm 0.18$

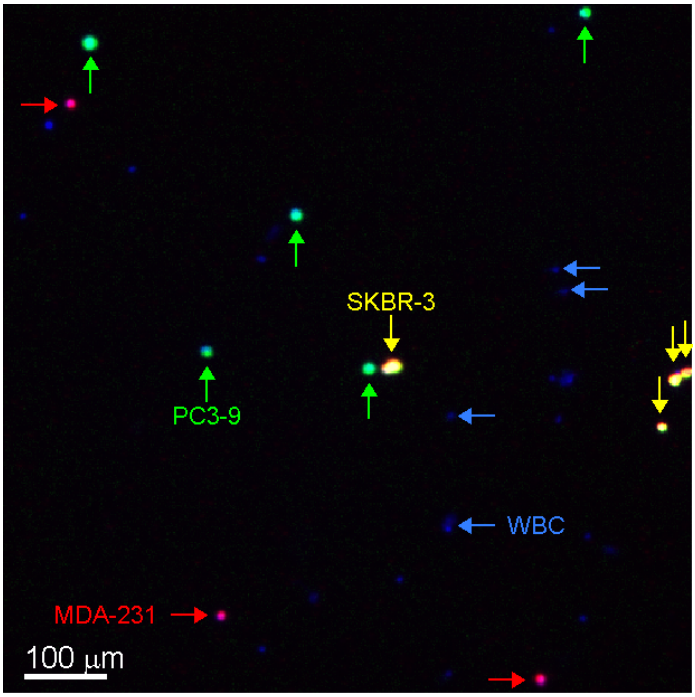

Figure 8.2: Counting cells on a track-etched filter. *False color image of pre-stained culture cells and WBC on a track-etched filter.*

µm^{-3}, with a predicted R of 0.15 µm^{-3}. The variation in R is attributable to experimental repeatability.

8.3.2 In a blood sample the sample flow rate dominates pressure

Figure 8.4, panel A shows the relation between total flow rate, sample dilution and pressure, averaged across 3 donors. At the same total flow rate, pressures are 10 times higher for undiluted blood than for 1:16 diluted samples. Relations between pressure and sample flow rate are linear for each donor (R^2 for each donor at each dilution > 0.94), but the slope between three donors varied by ±40%. Figure 8.4, panel B shows that the pressure is primarily determined by the sample flow rate, not the total flow rate. Three total flow rates (50 mL/h, 200 mL/h, and 800 mL/h) were measured at a sample flow rate of 50 mL/h. In these conditions, the pressure varied from 10.5–17.2 mbar, implying that on average $15 \cdot 10^3$ to $144 \cdot 10^3$ (4–41% of total pores) were needed for the flow of diluent (plasma and PBS), while the rest of the pores ($207 \cdot 10^3$–$336 \cdot 10^3$) were filled with a cell passing at

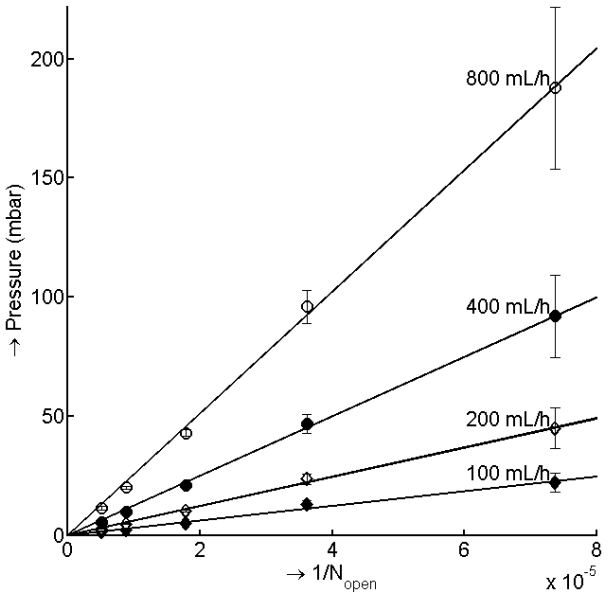

Figure 8.3: Pressure versus inverse of open pores, for different flow rates. *The number of pores on a 5 µm track-etched filter was decreased by reducing the number of available filter pores with aperture plates. The fits through the data were used to estimate an average relationship between pressure (P; mbar), flowrate (Q; mL/h) and number of pores (N_{open}) by fitting the resistance to flow (R); $\Delta P = \mu RQ/N_{open}$. With the viscosity μ at $0.9 \cdot 10^{-3}$ Pa·s, R is 1.28 ± 0.02 μm^{-3}*

much slower speed. For a concentration of $5 \cdot 10^9$ predominantly red blood cells per mL of sample the average speed of a cell passing through a pore is 0.9–1.5 mm/s while the average fluid flow speed is 48–78 mm/s inside the pores.

8.3.3 RBC and WBC contribute most to the pressure

Figure 8.5, panel A shows the relation between pressure and flow rate for blood components. A 1:4 dilution with 3 different total flow rates was used (100, 200 and 400 mL/h). The different components tested include RBC ($5 \cdot 10^9$ / mL), a mixture of RBC ($5 \cdot 10^8$ / mL) and WBC ($5 \cdot 10^6$ WBC / mL), serum and PBS-1%BSA solution. The serum leads to a slight increase in pressure compared with PBS1%BSA. WBC and RBC contribute almost equally to the pressure difference, even though the RBC are 1000 times more numerous. Due to the large relative error in the pressures detected for the 8 µm filters we did not estimate the speed of passage for this pore size.

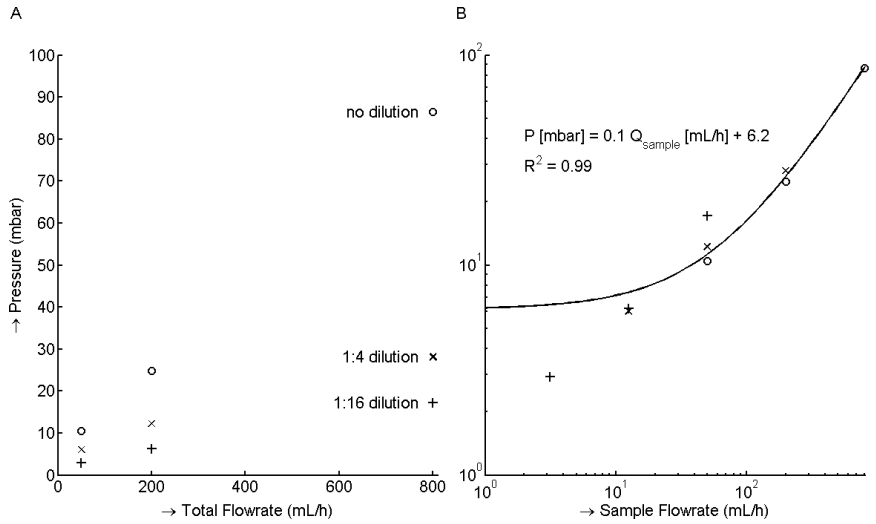

Figure 8.4: Sample flow rate determines pressure drop across filter. *Whole blood was filtered through a 5 µm track-etched filter at total flow rates of 50, 200 and 800 mL/h without sample dilution and with 4x or 16x sample dilution. (Panel A) Total flow rate versus pressure. In contrast with figure 8.3, the total flow rate is not the main factor contributing to the pressure across the filter when cells are present in the sample. (Panel B) Sample flow rate versus pressure. When the pressure difference is plotted as a function of the sample flow rate, there appears to be a linear relation.*

8.3.4 A 15 µm cell can easily pass through a 5 µm pore while a 6 µm bead does not pass

We filtered 10^6 PC3-9, SKBR-3 or MDA-231 culture cells at different flow rates with 5 µm track-etched filters. We expected the filter to clog (pressure to rise above 300 mbar) before $0.35 \cdot 10^6$ culture cells were passed through a track-etched filter with $0.35 \cdot 10^6$ pores, as these cells are more than three times larger than the pore size. PC3-9 and SKBR-3 clogged at all flow speeds when $0.3 \cdot 10^6$ up to $0.5 \cdot 10^6$ cells had been injected. The MDA-231 cells only clogged the filter at the highest total flow speed of 400 mL/h, but 10^6 cells passed the filter at total flow speeds of 50, 100 and 200 mL/h. Figure 8.6 shows the pressures and flow rates for the three cell lines, with each data point representing the average of triplicate measurements and error bars indicating the standard deviation. The implication of MDA-231 not clogging the filter was that a substantial fraction of these cells passed the 5 µm pores. Considering only the ratio of spiked cells to pores, at least 65% of MDA-231 cells passed the filter. The loss is likely to be higher because a single MDA-231 cell could block multiple pores. In addition, the

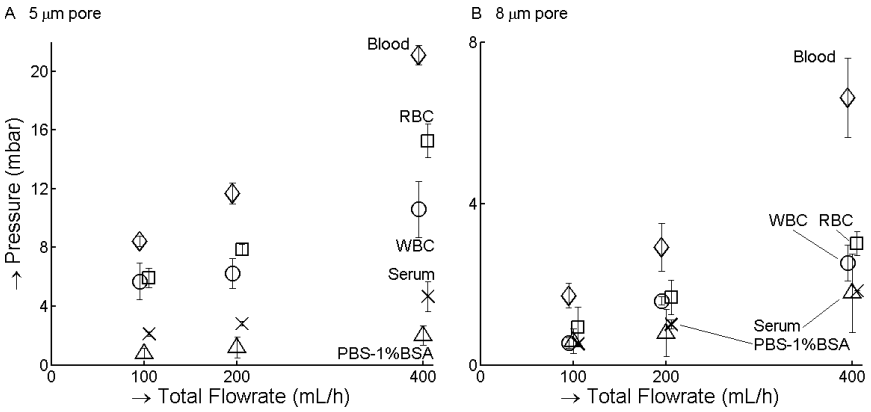

Figure 8.5: All blood components contribute to total pressure. *Major blood components RBC, WBC and serum were filtered across 5 (panel A) and 8 (panel B) µm track-etched filters until pressure reached a plateau (y-axis). Whiskers show the standard deviation from three measurements. Data-points were all measured at flow rates of 100, 200 and 400 mL/h, but were slightly offset to facilitate reading of the graph. Inspection of the filters after filtering using bright field imaging and fluorescence imaging of the Hoechst 33342 stain showed no evidence of capture of RBC, while* 10^3–10^4 *WBC were found on each filter.*

PC3-9 and SKBR-3 runs with the lowest flow speed clogged when more than 40% of the sample had been injected, suggesting that also for these cell lines a substantial fraction of cells had passed the filter. To verify the size selectivity of the 5 µm filter the filtrate of a solution containing 10^6 polystyrene beads with diameters of 4, 6, 10 µm was investigated. We found 26% of the 4 µm beads injected, 0.35% of the 6 and 0.00% of the 10 µm beads had passed the filter. The beads not found in the filtrate were found on the filter.

8.3.5 MDA-231 cells pass at least 4300 times slower through a 5 µm pore than a WBC

Equation 8.3 was used to estimate the speed of a cell passing through a pore for MDA-231, WBC and RBC cells, shown in figure 8.7. From linear fits through the data, we find that at the same pressure, the passage of RBC is approximately 120 fold faster than the passage of WBC, and MDA-231 cells are 430 times slower than the WBC. The average time needed for an MDA-231 cell to pass the filter is 3600 seconds at a pressure of 10 mbar. Assuming this difference in passage time between different cells may be explained by a difference in stiffness, the passage of a cell through a pore

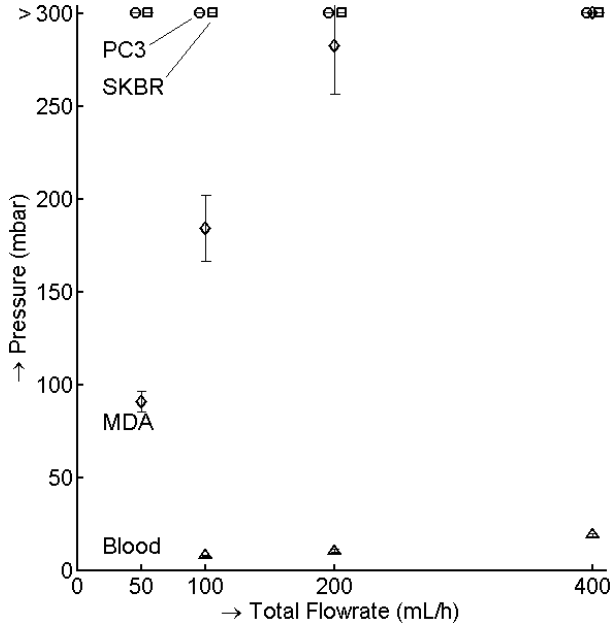

Figure 8.6: Culture cells can pass through small pores at low pressures. *The y-axis shows pressure drops when* $1.0 \cdot 10^6$ *SKBR-3, PC3-9 or MDA-231 cell lines are filtered across 5 µm track-etched filters with* $0.35 \cdot 10^6$ *pores. Data points were all measured at total flow rates of 50, 100, 200 and 400 mL/h, but were slightly offset to facilitate reading of the graph. The median cell diameter of PC3-9 is 19.0 µm, SKBR-3 cells 16.4 µm and MDA-231 15.4 µm and were thus expected to occupy all pores. All samples with SKBR-3 and PC3-9 samples clogged the filter and the sample with MDA-231 clogged at a flow rate of 400 mL/h.*

was modeled as a high viscosity stream passing through a filter. This was used to determine the apparent viscosity of the cells from the slope between pressure and time of passage. The apparent viscosity for 5 µm pores is estimated at 0.035 ± 0.010 Pa·s for RBC ($\Delta P = 5$–16 mbar), 3.2 ± 2.5 Pa·s for WBC ($\Delta P = 5$–13 mbar) and of $1.6 \cdot 10^3 \pm 0.2 \cdot 10^3$ Pa·s for MDA-231 cells ($\Delta P = 85$–300 mbar). The SKBR-3 and PC3-9 cells clogged the filter even at the lowest speed, their apparent viscosity is larger than $2 \cdot 10^3$ Pa·s.

8.3.6 Fixation dramatically increases the pressure needed to push cells through a pore

Recovery of culture cells as a function of fixation was determined by spiking 300 cells of 3 different cell lines into 1 mL of blood. The recovery for each cell line, fixation type and pore size is shown in figure 8.8. Pressure across

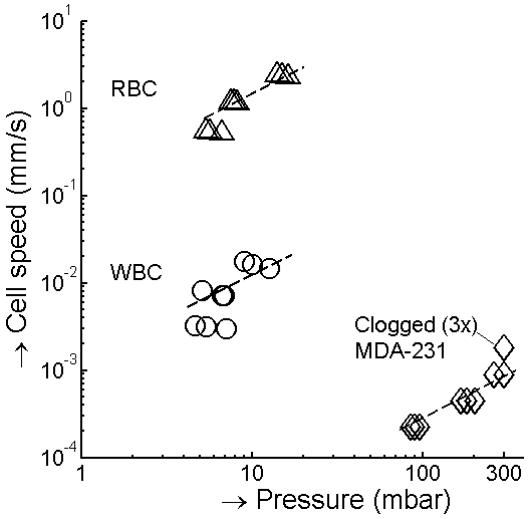

Figure 8.7: Estimated speeds for different cells. *Estimated speed inside a filter pore versus pressure across the filter for white (WBC) and red blood cells (RBC) and MDA-231 culture cells. Dashed lines are fits of* $v \propto \Delta P$*. All three MDA-231 samples at a flow rate of 400 mL/h clogged.*

the filter and sample purity is shown below the x-axis. The purity was defined as the percentage of cancer cells of all cells recovered. Unfixed samples had highest recovery and purity and had lowest pressure. CellSave fixed samples had recovery slightly lower than unfixed samples, with 3–8 fold higher pressures, and lower purity. PFA fixed samples clogged the 5 µm filter. PFA fixed samples on the 8 µm filter had lower recovery and lower purity than the other samples, while the pressure was 25 fold higher compared to unfixed samples. Overall, the 5 µm and 8 µm track-etched filter with unfixed samples performed similarly in terms of recovery but sample purity was an order of magnitude higher on the 8 µm track-etched filter.

8.4 Discussion

A custom filtration setup was used to investigate the influence of pressure, sample dilution and fixation on the enrichment of large cells from whole blood by means of filtration. The influence of filter properties will be discussed elsewhere [40].

A linear relation between the number of pores, total flow rate and pressure across the filter was expected for laminar flow conditions and confirmed on our setup using phosphate buffered saline (PBS). We found a resistance R that is 48–78% higher than what would be predicted based on the geomet-

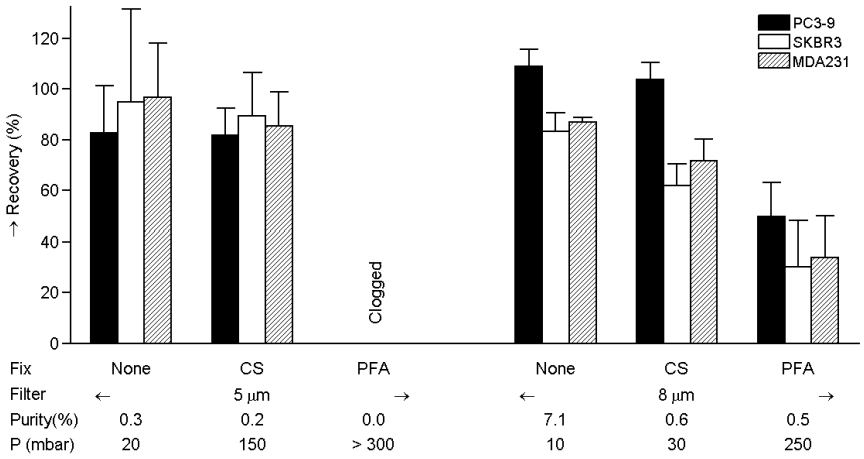

Figure 8.8: Influence of fixation on recovery, pressure across filter and sample purity. *Bars show recovery of three culture cell lines spiked into 1 mL of whole blood as a function of fixation and pore size (5 µm and 8 µm). Samples were not fixed, fixed for 4 hours in CellSave (CS) or 10 minutes in 0.4% formaldehyde (PFA). Whiskers represent 1 standard deviation. Average sample purity is defined as the % cell line of total cells and is shown below the bar plot. Peak pressure (P) is shown below the bar plot as well. Recovery and purity are both highest for no fixation. The pressure needed to pass 1 mL of blood through the filter is much larger with fixed samples, with the pressure required to pass PFA fixed blood through the 5 µm in excess of 300 mbar that could be determined on our setup.*

rical properties. Nevertheless, such deviation from theory is a small error, which could be caused by differences between true and specified thickness of the filter or pore size, or differences in modeled versus real pore shape. We applied equation 8.1 to determine the number of pores that pass PBS and derive the number of pores that pass cells according to equation 8.2. It was possible to pass 15 µm MDA-231 cells through a pore of only 5 µm at relatively low pressures of 80 mbar, while 6 µm polystyrene beads were retained. This difference in behavior between beads and cells may be explained by a difference in stiffness. The passage of a cell through a pore was modeled as a high viscosity stream passing through a filter. We used the setup to determine the speed with which a cell passes through a pore and derive from this the apparent viscosity of a cell relative to the pore. At a pressure of 10 mbar, the speed of a RBC in a 5 µm pore is 1.5 mm/s, compared to $12 \cdot 10^{-3}$ mm/s for a WBC. Literature values are comparable with WBC entry speed into a glass capillary of $36 \cdot 10^{-3}$ mm/s [41] and a 700–1000 fold difference between passage time through a filter of RBC and WBC [42, 43]. At a pressure of 100 mbar an MDA-231 cell

passes in 360 s. Assuming apparent viscosity is independent of pressure, at 10 mbar an MDA-231 cell would pass the filter in one hour. Experiments with granulocytes suggest cells are shear thinning [34, 44], with apparent viscosity reducing from $2.4 \cdot 10^3$–$4.4 \cdot 10^3$ Pa·s [45] at 0.2 mbar to 30–200 Pa·s at pressures near 5 mbar [46, 34, 47, 48]. If this holds true for cultured tumor cells, the time needed to pass a pore is even larger at lower pressures. The estimates for WBC and RBC apparent viscosity as determined here in bulk cell suspensions are similar to those determined using micro pipette aspiration at similar pressures and micropipette pore sizes. We found 3.2 Pa·s for WBC, compared to 30–200 Pa·s for granulocytes reported in the literature [46, 34, 47, 48]. For RBC the apparent viscosity was determined to be $35 \cdot 10^{-3}$ Pa·s and for MDA-231 cells we determined an apparent viscosity of $1.6 \cdot 10^3$ Pa·s at a pressure of 100 mbar and greater than $2 \cdot 10^3$ Pa·s for SKBR-3 and PC3-9 culture cells. An important difference between the apparent viscosities as determined by micropipette aspiration and those determined using a filter is that the entire cell can be aspirated into a capillary, while WBC and MDA-231 cells are larger than the pore; the pore volume is 35% of the WBC volume and 11% of the culture cell volume. As a result, the cells need to deform less to pass through a pore than to enter a long capillary, and thus have lower apparent viscosity. The relative difference between apparent viscosity of blood cells and tumor cells is important because it determines whether captured tumor cells will be on the filter at the end of filtration. It is unknown whether these cultured tumor cells are a good model for CTC as these are extremely rare and very little is known about their physical properties. Many approaches to determine such properties, including the approach we applied, require large numbers of cells, while CTC in patients are extremely rare. Despite differences between our bulk method and micropipette experiments with similar pore size, the latter could be applied to determine the apparent viscosity of real CTC, an advantage since these require only 1 cell per determination. In addition, micropipette experiments could be used to determine the influence of various parameters such as pressure and sample temperature [34] on the apparent viscosities of blood cells and various cultured tumor cells.

Micropipette aspiration experiments have shown that a critical pressure exists for which a cell is not pulled into the pipette, due to surface tension of the cortex. For granulocytes this critical pressure is 0.1 mbar on a 5 µm pore [49], while for various cancer cell lines this pressure is 2–8 mbar [50]. The apparent viscosity is much higher when determined at a pressure slightly above the critical pressure. This suggests that, for a 5 µm pore size, the sample should be filtered at a pressure near 2 mbar in order to retain all captured culture cells. However filtration of 1 mL of blood at this pressure takes approximately 15 minutes on a 1 cm^2 5 µm track etched filter resulting in flow that is extremely slow. This leads to uneven sample distribution across the filter due to gravity, defeating the purpose. While it is not practical to filter at a pressure below the critical pressure, apparent

viscosity is highest near the critical pressure, which suggests that filtration at pressures near the critical pressure of a CTC will yield better results than filtration at much higher pressures.

The sample flow rate we selected for most experiments was 25 mL/h, injecting a 1 mL sample in 2.4 minutes. Higher sample dilution increases pressure, thus slightly reducing recovery. Nevertheless, we decided to set it at 1:4 because it takes much longer to clear the remaining blood from the filter holder after sample injection is stopped if the total flow rate is only 25 mL/h.

Fixation increases the apparent viscosity of a cell, which increases the pressure needed to pass a cell through the same size pore in the same time, or increases the pore size needed at constant pressure and time. In our system, fixation increased the pressure needed to pass a sample through a filter, for PFA fixation this increase was 25 fold and very sensitive to fixation time. The lower sample purity of PFA fixed samples compared to unfixed samples suggests that the difference in passage time between culture cells and white cells is reduced after fixation, and thus the difference in apparent viscosities between blood cells and culture tumor cells is reduced. All experiments presented here were performed with fresh unfixed blood. It is conceivable that processing of older samples requires some form of fixation for sample preservation, for example to allow processing in a remote laboratory. CellSave [51]) is used to preserve CTC in blood prior to immunomagnetic enrichment, and may prove to be a good preservative for enrichment of CTC prior to size based filtration.

From the results in this manuscript and in literature we interpret the filtration process as follows: cells and diluent arrive on the filter. Cells are pulled to a pore by fluid passing through that pore and proceed to slowly pass through, with cells with a higher apparent viscosity passing through slower, which results in a relative enrichment of cells with higher apparent viscosity. A pore is occupied by a cell most of the time and passes diluent in short bursts until the next cell arrives, blocking the pore again. If the pressure during filtration is lower than the critical pressure for only one cell type in the suspension, this cell type has an infinite apparent viscosity and will be retained. If the pressure during filtration is higher than the critical pressure for all cell types, all cells will eventually pass through the filter, resulting in reduced recovery of tumor cells from larger sample volumes (i.e. longer filtration). This could be mitigated by stacking multiple filters on top of each other, thus dramatically increasing the relative difference in passage time between tumor cells and blood cells. If cortical tension returns the cells to the top of the filter when no pressure difference exists, the same could be achieved by intermittent flow, passing blood cells in bursts and then waiting for the tumor cells to return to the top of the filter between bursts.

Filtration should be performed on unfixed samples at a low pressure, in the order of 10 mbar for a 1 cm^2 5 µm pore size filter. This allows enrichment of CTC from whole blood at a speed of 1 mL of blood per 1–2 minutes. Total processing time is limited because CTC move through the filter slowly, at a pressure of 10 mbar filtration should be completed in less than 1 hour for capture of MDA-231 cells. Pores on the filter should be spaced at least 10 µm from each other, to allow identification of boundaries of adjacent cells. Sample dilution is not strictly needed, and has a small negative influence on recovery. If fixation is needed for sample preservation, a gentle fixative should be used, in which case the filtration pressure will probably be higher. The difference in apparent viscosity between blood cells and CTC is key in determining the most efficient way to enrich CTC. Largest challenge will be to measure the apparent viscosity of a large number of CTC in a variety of patients.

8.5 References

[1] M. Cristofanilli, G. T. Budd, M. J. Ellis, A. Stopeck, J. Matera, M. C. Miller, J. M. Reuben, G. V. Doyle, W. J. Allard, L. W. Terstappen, and D. F. Hayes, "Circulating tumor cells, disease progression, and survival in metastatic breast cancer," *N. Engl. J. Med.*, vol. 351, pp. 781–791, Aug 2004.

[2] S. J. Cohen, C. J. Punt, N. Iannotti, B. H. Saidman, K. D. Sabbath, N. Y. Gabrail, J. Picus, M. Morse, E. Mitchell, M. C. Miller, G. V. Doyle, H. Tissing, L. W. Terstappen, and N. J. Meropol, "Relationship of circulating tumor cells to tumor response, progression-free survival, and overall survival in patients with metastatic colorectal cancer," *J. Clin. Oncol.*, vol. 26, pp. 3213–3221, Jul 2008.

[3] J. S. de Bono, H. I. Scher, R. B. Montgomery, C. Parker, M. C. Miller, H. Tissing, G. V. Doyle, L. W. Terstappen, K. J. Pienta, and D. Raghavan, "Circulating tumor cells predict survival benefit from treatment in metastatic castration-resistant prostate cancer," *Clin. Cancer Res.*, vol. 14, pp. 6302–6309, Oct 2008.

[4] S. Matsusaka, K. Chin, M. Ogura, M. Suenaga, E. Shinozaki, Y. Mishima, Y. Terui, N. Mizunuma, and K. Hatake, "Circulating tumor cells as a surrogate marker for determining response to chemotherapy in patients with advanced gastric cancer," *Cancer Science*, vol. 101, pp. 1067–1071, 2010.

[5] M. G. Krebs, R. Sloane, L. Priest, L. Lancashire, J. M. Hou, A. Greystoke, T. H. Ward, R. Ferraldeschi, A. Hughes, G. Clack, M. Ranson, C. Dive, and F. H. Blackhall, "Evaluation and prognostic significance of circulating tumor cells in patients with non-small-cell lung cancer," *Journal of Clinical Oncology*, vol. 29, pp. 1556–1563, 2011.

[6] C. Rao, T. Bui, M. Connelly, G. Doyle, I. Karydis, M. R. Middleton, G. Clack, M. Malone, F. A. W. Coumans, and L. W. M. M. Terstappen, "Circulating melanoma cells and survival in metastatic melanoma," *International Journal of Oncology*, vol. 38, pp. 755–760, 2011.

[7] T. J. N. Hiltermann, J. J. W. Liesker, A. van den Berg, J. H. Schouwink, W. J. A. Wijnands, G. S. M. A. Kerner, H. M. Boezen, M. M. Pore, F. A. E. Kruyt, W. Timens, H. Tissing, A. G. J. Tibbe, L. W. M. M. Terstappen, and H. J. M. Groen, "Circulating tumor cells in small cell lung cancer, a predictive and prognostic factor," *Annals of Oncology*, p. In press, 2012.

[8] J. den Toonder, "Circulating tumor cells: the grand challenge," *Lab on a chip*, vol. 11, pp. 375–377, 2011.

[9] S. Nagrath, L. V. Sequist, S. Maheswaran, D. W. Bell, D. Irimia, L. Ulkus, M. R. Smith, E. L. Kwak, S. Digumarthy, A. Muzikansky, P. Ryan, U. J. Balis, R. G. Tompkins, D. A. Haber, and M. Toner, "Isolation of rare circulating tumour cells in cancer patients by microchip technology," *Nature*, vol. 450, pp. 1235–1239, Dec 2007.

[10] J. P. Gleghorn, E. D. Pratt, D. Denning, H. Liu, N. H. Bander, S. T. Tagawa, D. M. Nanus, P. A. Giannakakou, and B. J. Kirby, "Capture of circulating tumor cells from whole blood of prostate cancer patients using geometrically enhanced differential immunocapture (GEDI) and a prostate-specific antibody," *Lab Chip*, vol. 10, pp. 27–29, Jan 2010.

[11] S. L. Stott, C. H. Hsu, D. I. Tsukrov, M. Yu, D. T. Miyamoto, B. A. Waltman, S. M. Rothenberg, A. M. Shah, M. E. Smas, G. K. Korir, F. P. Floyd, A. J. Gilman, J. B. Lord, D. Winokur, S. Springer, D. Irimia, S. Nagrath, L. V. Sequist, R. J. Lee, K. J. Isselbacher, S. Maheswaran, D. A. Haber, and M. Toner, "Isolation of circulating tumor cells using a microvortex-generating herringbone-chip," *Proc. Natl. Acad. Sci. U.S.A.*, vol. 107, pp. 18392–18397, Oct 2010.

[12] S. J. Tan, R. L. Lakshmi, P. Chen, W. T. Lim, L. Yobas, and C. T. Lim, "Versatile label free biochip for the detection of circulating tumor cells from peripheral blood in cancer patients," *Biosens Bioelectron*, vol. 26, pp. 1701–1705, Dec 2010.

[13] H. Lin, S. Zheng, A. Williams, M. Balic, S. Groshen, H. Scher, M. Fleisher, W. Stadler, R. Datar, Y. Tai, *et al.*, "Portable filter-based microdevice for detection and characterization of circulating tumor cells," *Clinical Cancer Research*, vol. 16, no. 20, pp. 5011–5018, 2010.

[14] W. J. Allard, J. Matera, M. C. Miller, M. Repollet, M. C. Connelly, C. Rao, A. G. Tibbe, J. W. Uhr, and L. W. Terstappen, "Tumor cells circulate in the peripheral blood of all major carcinomas but not in healthy subjects or patients with nonmalignant diseases," *Clin. Cancer Res.*, vol. 10, pp. 6897–6904, Oct 2004.

[15] C. Alix-Panabieres, J. P. Brouillet, M. Fabbro, H. Yssel, T. Rousset, T. Maudelonde, G. Choquet-Kastylevsky, and J. P. Vendrell, "Characterization and enumeration of cells secreting tumor markers in the peripheral blood of breast cancer patients," *J. Immunol. Methods*, vol. 299, pp. 177–188, Apr 2005.

[16] H. B. Hsieh, D. Marrinucci, K. Bethel, D. N. Curry, M. Humphrey, R. T. Krivacic, J. Kroener, L. Kroener, A. Ladanyi, N. Lazarus, P. Kuhn, R. H. Bruce, and J. Nieva, "High speed detection of circulating tumor cells," *Biosens Bioelectron*, vol. 21, pp. 1893–1899, Apr 2006.

[17] A. H. Talasaz, A. A. Powell, D. E. Huber, J. G. Berbee, K. H. Roh, W. Yu, W. Xiao, M. M. Davis, R. F. Pease, M. N. Mindrinos, S. S. Jeffrey, and R. W. Davis, "Isolating highly enriched populations of circulating epithelial cells and other rare cells from blood using a magnetic sweeper device," *Proc. Natl. Acad. Sci. U.S.A.*, vol. 106, pp. 3970–3975, Mar 2009.

[18] U. Dharmasiri, S. Njoroge, M. Witek, M. Adebiyi, J. Kamande, M. Hupert, F. Barany, and S. Soper, "High-throughput selection, enumeration, electrokinetic manipulation, and molecular profiling of low-abundance circulating tumor cells using a microfluidic system," *Analytical chemistry*, vol. 83, pp. 2301–Ű2309, 2011.

[19] H. W. Hou, Q. S. Li, G. Y. Lee, A. P. Kumar, C. N. Ong, and C. T. Lim, "Deformability study of breast cancer cells using microfluidics," *Biomed Microdevices*, vol. 11, pp. 557–564, Jun 2009.

[20] R. Rosenberg, R. Gertler, J. Friederichs, K. Fuehrer, M. Dahm, R. Phelps, S. Thorban, H. Nekarda, and J. R. Siewert, "Comparison of two density gradient centrifugation systems for the enrichment of disseminated tumor cells in blood," *Cytometry*, vol. 49, pp. 150–158, Dec 2002.

[21] G. Vona, A. Sabile, M. Louha, V. Sitruk, S. Romana, K. Schutze, F. Capron, D. Franco, M. Pazzagli, M. Vekemans, B. Lacour, C. Brechot, and P. Paterlini-Brechot, "Isolation by size of epithelial tumor cells : a new method for the immunomorphological and molecular characterization of circulating tumor cells," *Am. J. Pathol.*, vol. 156, pp. 57–63, Jan 2000.

[22] H. J. Kahn, A. Presta, L. Y. Yang, J. Blondal, M. Trudeau, L. Lickley, C. Holloway, D. R. McCready, D. Maclean, and A. Marks, "Enumeration of circulating tumor cells in the blood of breast cancer patients after filtration enrichment: correlation with disease stage," *Breast Cancer Res. Treat.*, vol. 86, pp. 237–247, Aug 2004.

[23] S. Zheng, H. Lin, J. Q. Liu, M. Balic, R. Datar, R. J. Cote, and Y. C. Tai, "Membrane microfilter device for selective capture, electrolysis and genomic analysis of human circulating tumor cells," *J Chromatogr A*, vol. 1162, pp. 154–161, Aug 2007.

[24] T. G. Ntouroupi, S. Q. Ashraf, S. B. McGregor, B. W. Turney, A. Seppo, Y. Kim, X. Wang, M. W. Kilpatrick, P. Tsipouras, T. Tafas, and W. F. Bodmer, "Detection of circulating tumour cells in peripheral blood with an automated scanning fluorescence microscope," *Br. J. Cancer*, vol. 99, pp. 789–795, Sep 2008.

[25] V. Hofman, M. Ilie, C. Bonnetaud, E. Selva, E. Long, T. Molina, J. Vignaud, J. Fléjou, S. Lantuejoul, E. Piaton, *et al.*, "Cytopathologic detection of circulating tumor cells using the isolation by size of epithelial tumor cell method: promises and pitfalls," *American journal of clinical pathology*, vol. 135, no. 1, pp. 146–156, 2011.

[26] Y. K. Chung, J. Reboud, K. C. Lee, H. M. Lim, P. Y. Lim, K. Y. Wang, K. C. Tang, H. Ji, and Y. Chen, "An electrical biosensor for the detection of circulating tumor cells," *Biosens Bioelectron*, vol. 26, pp. 2520–2526, Jan 2011.

[27] I. Desitter, B. Guerrouahen, N. Benali-furet, J. Wechsler, P. Jänne, Y. Kuang, M. Yanagita, L. Wang, J. Berkowitz, R. Distel, *et al.*, "A new device for rapid isolation by size and characterization of rare circulating tumor cells," *Anticancer research*, vol. 31, no. 2, pp. 427–441, 2011.

[28] S. Zheng, H. Lin, B. Lu, A. Williams, R. Datar, R. Cote, and Y. Tai, "3D microfilter device for viable circulating tumor cell (CTC) enrichment from blood," *Biomedical microdevices*, vol. 13, no. 1, pp. 203–213, 2011.

[29] D. Adams, O. Makarova, P. Zhu, S. Li, P. Amstutz, and C. Tang, "Isolation of circulating tumor cells by size exclusion using lithography fabricated precision microfilters," in *Proceedings of the 102nd Annual Meeting of the American Association for Cancer Research*, (Orlando, FL, USA), AACR, April 2011.

[30] S. J. Tan, L. Yobas, G. Y. Lee, C. N. Ong, and C. T. Lim, "Microdevice for the isolation and enumeration of cancer cells from blood," *Biomed Microdevices*, vol. 11, pp. 883–892, Aug 2009.

[31] E. Merrill, "Rheology of blood," *Physiological Reviews*, vol. 49, pp. 863–888, 1969.

[32] A. Yeung and E. Evans, "Cortical shell-liquid core model for passive flow of liquid-like spherical cells into micropipets," *Biophys. J.*, vol. 56, pp. 139–149, Jul 1989.

[33] C. T. Lim, E. H. Zhou, and S. T. Quek, "Mechanical models for living cells–a review," *J Biomech*, vol. 39, no. 2, pp. 195–216, 2006.

[34] E. Evans and A. Yeung, "Apparent viscosity and cortical tension of blood granulocytes determined by micropipet aspiration," *Biophys. J.*, vol. 56, pp. 151–160, Jul 1989.

[35] J. Khato, H. Sato, M. Suzuki, and H. Sato, "Filtrability and flow characteristics of leukemic and non-leukemic tumor cell suspension through polycarbonate filters in relation to hematogenous spread of cancer," *Tohoku J. Exp. Med.*, vol. 128, pp. 273–284, Jul 1979.

[36] Z. Dagan, S. Weinbaum, and R. Pfeffer, "Theory and experiment on the 3-dimensional motion of a freely suspended spherical-particle at the entrance to a pore at low reynolds-number," *Chemical Engineering Science*, vol. 38, pp. 583–596, 1983.

[37] S. Kuiper, R. Brink, W. Nijdam, G. J. M. Krijnen, and M. C. Elwenspoek, "Ceramic microsieves: influence of perforation shape and distribution on flow resistance and membrane strength," *Journal of Membrane Science*, vol. 196, pp. 149–157, 2002.

[38] R. Holdich, S. Kosvintsev, I. Cumming, and S. Zhdanov, "Pore design and engineering for filters and membranes," *Philosophical Transactions of the Royal Society A: Mathematical, Physical and Engineering Sciences*, vol. 364, no. 1838, pp. 161–174, 2006.

[39] G. Lee, T. Bithell, J. Foerster, J. Athens, and J. Lukens, *Wintrobe's clinical hematology*. Lea & Febiger, Philadelphia, PA, 1993.

[40] F. Coumans, G. van Dalum, M. Beck, and L. Terstappen, "Filter requirements for circulating tumor cell enrichment and detection," *submitted*, 2012.

[41] R. M. Hochmuth and D. Needham, "The viscosity of neutrophils and their transit times through small pores," *Biorheology*, vol. 27, no. 6, pp. 817–828, 1990.

[42] U. Bagge and P. Branemark, "White blood cell rheology. An intravital study in man," *Adv Microcirc*, vol. 7, p. 18Ũ28, 1977.

[43] S. Chien, E. A. Schmalzer, M. M. Lee, T. Impelluso, and R. Skalak, "Role of white blood cells in filtration of blood cell suspensions," *Biorheology*, vol. 20, no. 1, pp. 11–27, 1983.

[44] M. A. Tsai, R. S. Frank, and R. E. Waugh, "Passive mechanical behavior of human neutrophils: power-law fluid," *Biophys. J.*, vol. 65, pp. 2078–2088, Nov 1993.

[45] P. A. Valberg and D. F. Albertini, "Cytoplasmic motions, rheology, and structure probed by a novel magnetic particle method," *J. Cell Biol.*, vol. 101, pp. 130–140, Jul 1985.

[46] C. Dong, R. Skalak, K. L. Sung, G. W. Schmid-Schonbein, and S. Chien, "Passive deformation analysis of human leukocytes," *J Biomech Eng*, vol. 110, pp. 27–36, Feb 1988.

[47] R. S. Frank and M. A. Tsai, "The behavior of human neutrophils during flow through capillary pores," *J Biomech Eng*, vol. 112, pp. 277–282, Aug 1990.

[48] D. Needham and R. M. Hochmuth, "Rapid flow of passive neutrophils into a 4 microns pipet and measurement of cytoplasmic viscosity," *J Biomech Eng*, vol. 112, pp. 269–276, Aug 1990.

[49] E. Evans and B. Kukan, "Passive material behavior of granulocytes based on large deformation and recovery after deformation tests," *Blood*, vol. 64, pp. 1028–1035, Nov 1984.

[50] L. Weiss and G. W. Schmid-Schonbein, "Biomechanical interactions of cancer cells with the microvasculature during metastasis," *Cell Biophys.*, vol. 14, pp. 187–215, Apr 1989.

[51] F. Coumans and L. Terstappen, *Methods in Molecular Biology - Circulating Tumour Cells*, ch. Detection and characterization of Circulating Tumor Cells by the Cell Search approach. Humana Press, In press.

CHAPTER 9

Filter requirements for circulating tumor cell enrichment and detection

F.A.W. Coumans*, G. van Dalum*, M. Beck, L.W.M.M. Terstappen
* both authors contributed equally

Abstract

A variety of filters assays have been described to enrich circulating tumor cells (CTC) based on differences in physical characteristics of blood cells and CTC. In this study we evaluate different filter types to derive the properties of the ideal filter for CTC enrichment. 0.1–10 mL of whole blood spiked with cells from tumor cell lines were passed through silicon nitride microsieves, polymer track-etched filters and ultra fine mesh TEM grids with various pore sizes. The recovery and size of 9 different culture cell lines was determined and compared to the size of EpCAM+CK+CD45–DNA+ CTC from patients with metastatic breast, colorectal and prostate cancer. The 8 µm track-etched filter and the 5 µm microsieve had the best performance on MDA-231, PC3-9 and SKBR-3 cells, enriching $> 80\%$ of cells from whole blood. TEM grids had poor recovery of $\approx 25\%$. Median size of cell lines ranged from 10.9–19.0 µm, compared to 13.1, 10.7, and 11.0 µm for breast, prostate and colorectal CTC, respectively. The 11.4 µm COLO-320 cell line had the lowest recovery of 17%. The ideal filter for CTC enrichment is constructed of a stiff, flat material, is inert to blood cells has at least 100,000 regularly spaced 5 µm pores for 1 mL of blood with a $< 10\%$ porosity. While cell size is an important factor in determining recovery, other factors must be

involved as well. To evaluate a filtration procedure, cell lines with a median size of 11–13 µm should be used to challenge the system.

9.1 Introduction

Circulating tumor cells (CTC) predict survival in patients with various metastatic cancers [1, 2, 3, 4, 5, 6, 7, 8]. Enumeration of these CTC is a great technological challenge [9]. The lack of a positive control complicates assay development, as the number of CTC in patient samples is unknown. No detection of CTC in healthy controls and relatively high recovery of tumor cells spiked into blood samples are frequently used to gauge the performance of a given assay, yet without proof that the frequency of these cells relates to survival it remains uncertain whether CTC are really enumerated. CTC are extremely rare cells typically 1–10 CTC among $6 \cdot 10^6$ leukocytes, $2 \cdot 10^8$ platelets and $4 \cdot 10^9$ erythrocytes per/ mL of blood [10]. This implies that any assay for their enumeration must be able to handle a large number of cells. Examination of a large number of immunofluorescently labeled cells increases the influence of non-specific binding which is inherent to immunofluorescence staining of cells. A non-specific background of 0.01% may be acceptable for routine immunophenotyping, but for rare event detection this would result in detection of 100 "CTC" after analysis of 1,000,000 leukocytes. To increase the specificity of CTC detection, the number of analyzed cells needs to be reduced. While some assays only perform an erythrocyte lysis or density separation [11, 12, 13, 14] other assays achieve enhanced enrichment by leukocyte depletion [15, 16], size based filtration [17, 18, 19, 20, 21, 22, 23] or antibody based enrichment [24, 25, 26, 27, 28, 29, 30]. Each approach has its drawback. CTC could be lost due to the effect of erythrocyte lysis agents and CTC could be lost by employing a density separation as the range of densities of CTC is unknown. Size based filtration is antigen expression independent, but will miss smaller CTC and tumor micro particles, both of which are clinically relevant [31]. Antibody based methods are insensitive to variations in size, but don't enrich tumor cells that have low expression of the target antigen. The epithelial cell adhesion (EpCAM) molecule is frequently used for CTC enrichment as it has little or no expression on leukocytes, and is expressed by the CTC in most patients [32, 33, 34, 35, 36].
Filtration was recently proposed for CTC enrichment [17, 18, 19, 20, 21, 22, 23] and previously we have reported on the factors important for enrichment of CTC from whole blood by filtration [37]. In this study we investigate the properties of the ideal filter for CTC recovery such as pore size, spacing between pores, number of pores, filter thickness and filter surface material. In addition, the size distribution of CTC in metastatic breast, prostate and colorectal cancer and a variety of cell lines was determined to aid in choosing a cell line that can be used as an adequate model for optimization

of filtration based CTC assays.

9.2 Materials and methods

9.2.1 Blood samples

Healthy volunteers aged 20–55 provided informed consent prior to donating blood. The study protocol was approved by an ethics committee. Healthy was defined as no prior history of cancer or blood transmittable disease. Blood was drawn into EDTA vacutainers (BD, Franklin Lakes, NJ, USA) and processed within 8 hours after draw. Unless otherwise noted, each data point within one experiment represents the average of measurements on three different donors. Image archives from patients enrolled in studies with metastatic breast (IC 2006-04 [2], $N = 247$), colorectal (CAIRO-2 [3], $N = 487$) and prostate (IMMC-38 [4], $N = 185$) cancer patients were used for determination of CTC size.

9.2.2 Cell Culture

Breast carcinoma cell lines SKBR-3, MDA-231, MDA-468 and MCF-7, prostate carcinoma cell line PC3-9, colorectal carcinoma cell lines COLO-320, SW-480, and hematopoietic cell lines HL-60, K-562 were used in various recovery experiments. PC3-9 were cultured using RPMI (Sigma, St. Louis, MO, USA) while the others were cultured in Dulbecco's modified eagle medium (Sigma). Culture media were supplemented with 10% fetal calf serum (Gibco, Invitrogen, Carlsbad, CA, USA), 1% l-glutamin (Sigma) and 1% penicillin-streptomycin (Gibco). For MDA-468, the penicillin-streptomycin was replaced with 1% gentamicin and 1 mmol pyruvate (Sigma). To eliminate issues with non-specific staining of blood cells or other debris on the filters evaluated, cells were stained before spiking into blood by incubation in culture media for 24 hours at 37°C with 50 µmol CellTracker Green Bodipy and/or 5 µmol CellTracker Orange CMTMR (both Invitrogen). Cells were harvested using 0.05% trypsin (Gibco) for 5 minutes at 37°C. The exact concentration of a cell suspension for spiking was determined using a flow cytometer (FACSAria II, BD) by placing the suspension in Trucount tubes (BD), staining with Hoechst 33342 (Invitrogen) and counting Hoechst and CellTracker positive events, with forward and side scatter signals typical for cells.

9.2.3 Setup

A setup for filtration of blood samples was constructed that allows for precise control of sample flow rate and dilution factor, while monitoring the pressure across the filter as described in detail previously [37]. In summary, the sample flow rate is set at 25 mL/h and is diluted with 75

mL/h phosphate buffered saline (PBS) prior to filtration. The time a cell needs to pass through a smaller pore is dependent on the pressure across the filter [37]. By supplying a constant sample flow, the pressure across the filter increases until equilibrium is achieved between the number of cells that are pushed through the filter and the number of cells that arrive from the incoming sample flow. The setup stops filtering when the pressure exceeds 300 mbar to prevent damage to the setup.

9.2.4 Detection of recovered cells

After sample injection stopped, the PBS flow was increased to 100 mL/h for 2 minutes to clear any residual blood from the filter holder. Next, the filter was fixed with an ethanol series increasing up to 100% [37] and stained with 8 µmol Hoechst 33342 in PBS for 10 minutes. The filter was mounted on a microscope slide with 75% glycerol. Digital images of the staining pattern in three fluorescence channels (DAPI, EGFP, R-PE filter sets, Chroma, Bellows Falls, VT, USA) were acquired with an Eclipse 400 epi-fluorescence microscope (Nikon, Tokyo, Japan) with CCD camera (C4742-95, Hamamatsu, Hamamatsu, Japan) and a 4x/NA0.13 objective or 10x/NA0.45 objective (both Nikon). The number of nucleated cells was enumerated automatically using an algorithm developed in Matlab 2009a (Mathworks, Natick, MA, USA) with DIPimage plugin (Delft Technical University, Delft, Netherlands). The number of cells from the tumor cell lines was determined using false color overlays of the different fluorescent stains, counting all objects of appropriate size and morphology, containing a nucleus, and having the correct color in the false color image.

9.2.5 Different filter types

Filters with diverse properties were selected for evaluation and characterized in figure 9.1 and table 9.1. This included polycarbonate track-etched filters with a pore diameter of 5, 8, and 10 µm (Whatman Nucleopore, GE, Kent, UK), silica nitride microsieves with a pore diameter of 5, 6, 7, 8, 9 and 10 µm (Aquamarijn, Zutphen, Netherlands), and copper and nickel TEM grids with 7.5 µm square pores (Gilder Grids, Grantham, UK). All filters except microsieves were mounted in 13 mm filter holders (Swinney, Pall, Mijdrecht, Netherlands). A custom reducing ring was used for mounting the TEM grids into the filter holders. Microsieves were mounted in custom designed holders (TCO, Twente University, Enschede, Netherlands). Before use, a filter was placed in a holder, primed with PBS and placed in vacuum for 30 minutes. The vacuum was sufficient to make the PBS boil at room temperature thereby displacing any trapped air from the filter pores. At the end of this procedure the filters are still immersed in PBS.

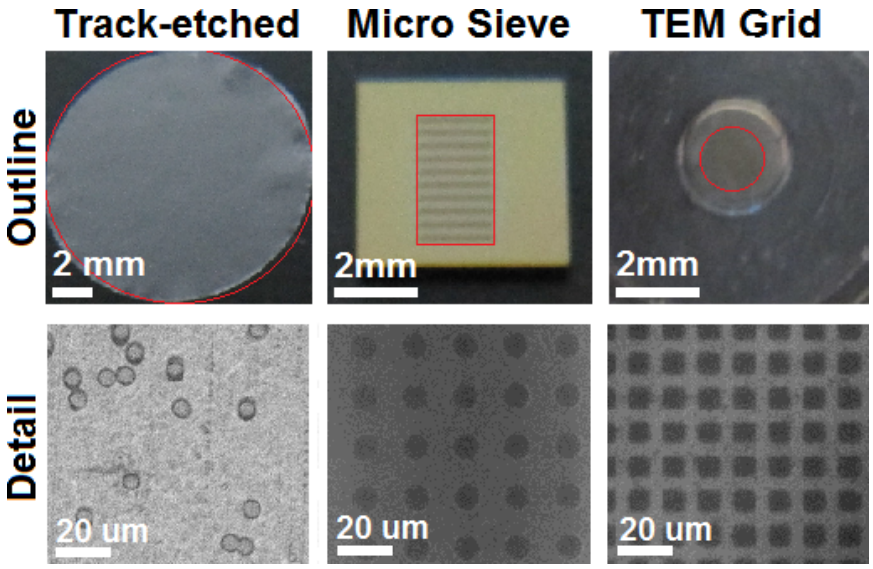

Figure 9.1: Overview of compared filters. *The outline images show a photograph of the track-etch filter, the microsieve and the transmission electron microscopy (TEM) grid. The perforated area of each filter is indicated in red. The microsieve contains perforated horizontal bars alternated by support bars, giving rise to the horizontal pattern. The detail shows dark field images for the three filters. Spacing of the pores is random for the track-etch filters, leading to occasional double pores. Microsieves and TEM grids have periodical pore spacing.*

9.2.6 Comparison of different versions of each filter type

For comparison of the different filters, MDA-231, SKBR-3 and PC3-9 cells were spiked into whole blood at a concentration of 300 cells per mL blood for each cell type. MDA-231 cells were pre-stained with CellTracker orange, PC3-9 were pre-stained with CellTracker green, and SKBR-3 with both CellTracker orange and green. Cell recovery was determined as described above. The best version of each filter type was chosen for further experiments.

9.2.7 Linearity of recovery

To determine linearity of recovery pre-stained MDA-231 cells were spiked into 1 mL of blood at concentrations of 2, 10, 100, 1,000, 10,000, 30,000 (microsieve only), 100,000 (track-etched only) cells. The maximum spike was similar to the number of pores for each filter. MDA-231 cell concentration was determined on the flow cytometer, except for the spikes of (nominally) 2 and 10 cells, where the exact number spiked cells was determined by

Table 9.1: *Properties of all tested filters*

type	material	pore spacing	thick-ness µm	area mm^2	pore size µm	N pores x1000	poro-sity %
track-etched	PC	random	10	102.1	5	350.9	6.7
				"	8	91.8	4.5
				"	10	88.2	6.8
micro-sieve	Si3N4	regular	1	0.6	5	0.16	0.5
				6.2	5	115.4	36.5
				2.7	5	25.9	18.8
				"	6	17.9	18.7
				"	7	15.2	21.7
				"	8	11.8	22.0
				"	9	9.4	22.1
				"	10	7.4	21.5
TEM grid	copper nickel	regular	18	2.6	7.5	17.4	36.0
				"	"	"	"

PC = PolyCarbonate, Si3N4 = Silicon Nitride, TEM = transmission electron microscopy. TEM grid pores are square, others are round.

microscope inspection of each spike drop. To limit the total volume of blood needed for the experiments 1 mL of blood was aspirated into a syringe and then 10 µL of culture cell suspension was pipetted into the front of the syringe. The syringe was inverted and left for a few minutes to allow cells to mix before the sample was used for filtering. Downside of this procedure is that cells are more likely to arrive early on in the filtration process, leading to slightly lower recoveries than when the cells were evenly distributed throughout the blood sample before loading the syringe.

9.2.8 Impact of different sample volumes

The impact of cell enrichment from different volumes of whole blood was tested by spiking 300 MDA-231 cells into blood volumes of 0.1, 1 and 10 mL. The recovery of spiked cells was determined by counting MDA-231 cells on the filters. Additional experiments were conducted to determine recovery while maintaining flow rates per pore that are comparable between track-etched filters and microsieves. The number of pores in a track-etched filter is approximately 10 times higher than the number of pores in a microsieve. Since the flow of cells per pore makes a large difference in pressure across the filter, and thus recovery, the recovery after spiking 30 MDA-231 cells into 0.1 mL of whole blood, when filtered at a total flow rate of 10 mL/h was determined. The flow per pore is then equivalent to flow per track-etched

pore when spiking 300 MDA-231 cells into 1 mL of whole blood at a total flow rate of 100 mL/h.

9.2.9 Cell size determination

The size of the cells was determined by the Coulter principle and by an image analysis algorithm. A Coulter counter pipette (Scepter, Millipore, Billerica, MA, USA) was used to determine the size of all cell lines and leukocytes. Leukocytes were obtained by taking the buffy coat from 10 mL whole blood centrifuged at 300 x g for 10 minutes. Size of cells by imaging was determined by an algorithm developed for automated counting of CTC [38]. This algorithm automatically identifies CK+DNA+CD45– CTC and can output the size of the area occupied by the CTC. Size of CTC from patients with metastatic breast cancer [2], colorectal cancer [3], and prostate cancer [4] was determined using image archives from these studies. For tumor cell lines we used the same CTC algorithm and for detection of leukocytes the algorithm was modified such that CK–DNA+CD45+ objects were counted. Because cells flatten when pulled against the glass slide inside the sample cartridge, the surface area of a cell cannot be used directly to derive the diameter of the cell in suspension. Instead we assumed cells to be cylindrical in shape with a volume of the imaging area A times a constant thickness D:

$$V_{imaging} = D \cdot A_{imaging} = \frac{\pi}{6} d^3_{suspension} \tag{9.1}$$

To find the diameter of a CTC in suspension from imaging, D was least squares fit to size data of SKBR-3, PC3-9, MDA-231 culture cells and leukocytes [39], which were determined using both Coulter and imaging.

9.2.10 Recovery for different cell lines

To determine the relation between the size of cells from the tumor cell lines and recovery, 300 cells were spiked into 1 mL of blood and the spiked samples were filtered through the best filter for each filter type. Spiking was achieved as described in "Linearity of recovery". Tumor cell lines included breast cancer cell lines SKBR-3, MDA-231, MDA-468 and MCF-7, prostate cancer cell line PC3-9, colorectal cancer cell lines COLO-320, SW-480, and hematopoietic cell lines HL-60, K-562. For each cell line the recovery was determined in duplo.

9.2.11 Staining of leukocytes

One mL of unspiked whole blood was filtered through 8 µm track-etched filters to determine whether there is a subpopulation of leukocytes that is preferentially enriched. To preserve antigens, the filters were fixed in 0.4%

PFA (paraformaldehyde) for 10 minutes instead of the ethanol fixation used in other experiments. The filters were then stained for 15 minutes at room temperature with a staining cocktail containing nuclear dye Hoechst 33342 (8 µmol, Invitrogen), and antibody conjugates CD13-PE (BD), CD14-APC (EXBIO, Prague, Czech), CD20-FITC (BioLegend, San Diego, CA, USA), CD4-FITC (MACS, Cologne, Germany), CD8-FITC (BD) at concentrations per the manufacturers' recommendations. The filters were imaged on a fluorescent microscope, followed by cell enumeration. At least 100 nucleated cells were counted and differentiated between granulocytes (CD13+, CD14–), monocytes (CD13+, CD14+), lymphocytes (CD20+ or CD4+ or CD8+, all CD14–) and others (negative for all). As a reference 1 mL of whole blood was stained, and leukocyte types were enumerated in a smear of this sample.

9.3 Results

9.3.1 Cell enumeration is easiest on a stiff filter with low porosity

Images of the filters after filtration of a spiked 1 mL blood sample are shown in figure 9.2. Images were taken with a 4x/NA0.13 objective. The track-etched filter deformed during filtration and as a result could not be imaged with a 10x/NA0.45 objective; 5–15% of the filter was too far out of focus to allow enumeration of positive cells in this area. The high porosity and low number of pores of the microsieves and the TEM grids resulted in a cell density too high to reliably distinguish adjacent cells when imaged with a 4x/NA0.13 objective, see figure 9.2, panels B and C, therefore these filters were imaged with the 10x/NA0.45 objective for all experiments. A large part of the TEM grid is covered with a red blood cell layer, the image in figure 9.2, panel C shows the only part of the filter that was not covered with red blood cells, comprising 17% of the total filter area. The ideal filter should maintain its planar form during filtration, it should not react with the sample and pores should be sufficiently separated to facilitate discrimination of cells.

9.3.2 Increasing pore size leads to lower recovery and higher sample purity

The results of the filter comparison are shown in figure 9.3. In panel A the % recovery is shown per cell type and per filter type. In panel B the pressure across the filter is shown and the sample purity is shown in panel C. The key filter properties are found at the bottom of panel C. Recovery of spiked cells is highest for filters with small pores. When the pore size is increased beyond 6 µm, recovery starts to reduce for MDA-231 cells, but this reduction seems be slower and to occur at a different size for the other

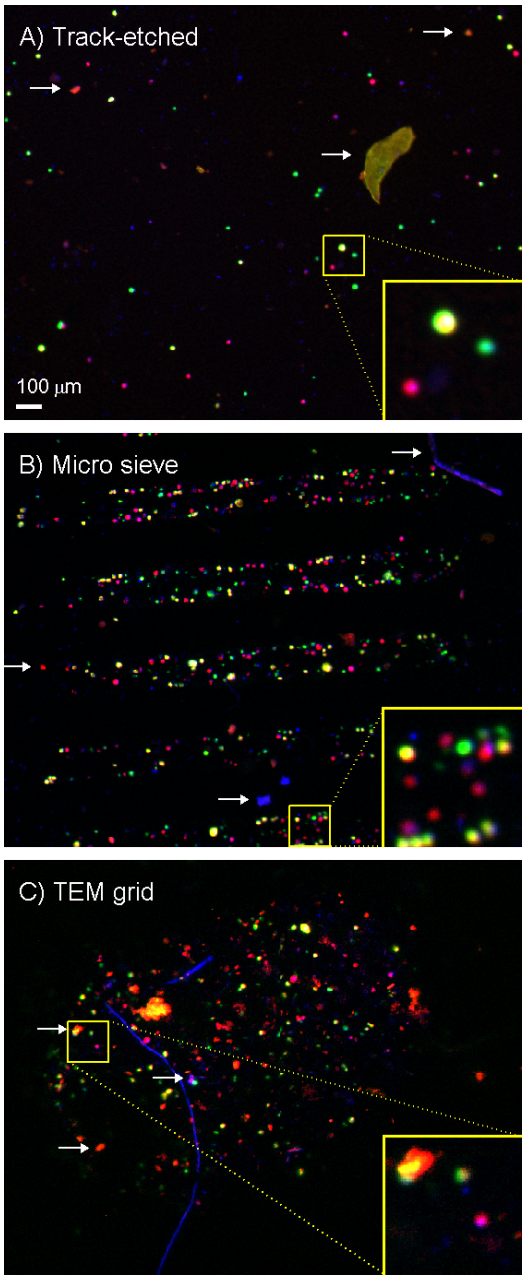

Figure 9.2: Images of cells on all filters. *Panel A shows a track-etched filter, panel B a microsieve filter and panel C a TEM grid filter. The images show false color fluorescent images taken of pre-stained cells enriched from a whole blood sample. Hoechst 33342 stain is shown in blue, Celltracker Orange in red, and Celltracker Green in green. In the false color MDA-231 cells are red, PC3-9 cells green and SKBR-3 cells yellow. Several types of autofluorescent and/or Hoechst positive debris were found on the filters, examples are indicated with white arrows. This debris is also found in unspiked samples. Due to the low number of pores and the high porosity of the microsieves and TEM grids, cells are very close to each other. To better distinguish cells on these filters, imaging with a 10x objective was nescessary for determination of cell recovery. This was not possible with the track-etched filters because they were not sufficiently flat to have all cells in focus.*

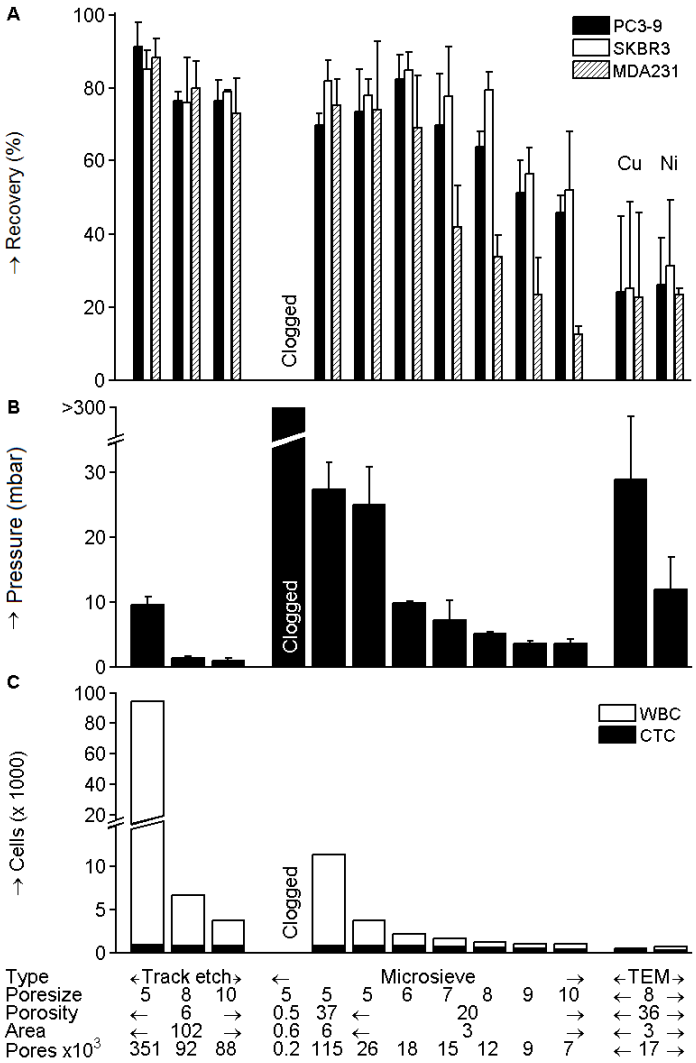

Figure 9.3: Comparison between different filter types. *Panel A shows recovery for SKBR-3, PC3-9 and MDA-231 cell lines. Bar height represents recovery with whiskers showing 1 standard deviation. No recovery was determined for the 0.5% porosity microsieve due to clogging while filtering. Panel B shows the peak pressure achieved during filtration. Whiskers show 1 standard deviation. Panel C shows the number of nucleated cells on the filter, with the CTC fraction also shown. The X-axis summarizes the major differences between the filters and applies to all panels.*

two cell lines, at pores sizes of 7 µm for PC3-9 cells and 8 µm for SKBR-3 cells. The pressure across the filter was lowest for filters with larger pores and filters with more pores. 80–90% of the TEM grid filter was covered with a coat of red blood cells, only a small aperture in the middle remained open. Only 25% of spiked cells were recovered, all found in this aperture, however it is possible that more cells were underneath the red blood cell coat. Recovery was also reduced by the high pressure across the 8 µm TEM grids, which was much higher than the pressure across the 8 µm microsieves, while they have similar numbers of pores. Higher pressure also leads to lower recovery when comparing microsieves to track etched filters. The pressure across the microsieves of similar pore size to the track-etched filters was always higher and recovery was always lower. The 5 µm microsieve with 160 pores needed a pressure in excess of 300 mbar to handle the sample flow, which this setup cannot provide.
As long as there are sufficient pores to pass the sample, recovery seems to be insensitive to the number of pores. There is almost no difference between the microsieves with 115,000 pores and the one with 26,000 pores in terms of spiked cell recovery or pressure across the filter, but the number of leukocytes retained is 3.1 fold higher on the filter with 4.4 fold more pores. The number of leukocytes retained is the highest on the 5 µm track-etched filter. Less than 6% of pores are occupied by leukocytes for 8–10 µm track-etched filters and ≥ 6 µm microsieves.
The filters with highest yield and lowest leukocyte contamination were the 8 µm track-etched filter and the 5 µm microsieve with 26,000 pores, because they recovered $> 70\%$ of the spiked cells, while retaining a low percentage of leukocytes. These two filters were selected for further comparison in the next experiments. The TEM grids had unsatisfactory recovery, and were not used in further experiments.

9.3.3 Recovery is linear until approximately 2% of pores are occupied

The number of MDA-231 cells recovered versus the number spiked cells is shown in figure 9.4. Recovery is linear for spikes of 0–100 cells on the microsieves (58% recovery, $R^2 = 0.98$), and for spikes of 0–10,000 cells on the track-etched filters (67% recovery, $R^2 = 0.98$). When a sufficient fraction of pores on the filter are blocked, the pressure during filtration is increased and recovery reduced [37]. Each cell occupies 3–5 pores on the microsieves, while on the track-etched filters most cells occupy 1 pore. Hundred cells on the microsieve is 1.6% of the available pores, 10,000 cells on the track-etched filters is 2.9% of the available pores. Including all data in the linear fit reduces recovery and correlation both for the microsieves (12% recovery, $R^2 = 0.49$) and for the track-etched filters (51% recovery, $R^2 = 0.91$). One of the microsieves clogged at a spike of 30,000 cells, and average recovery for

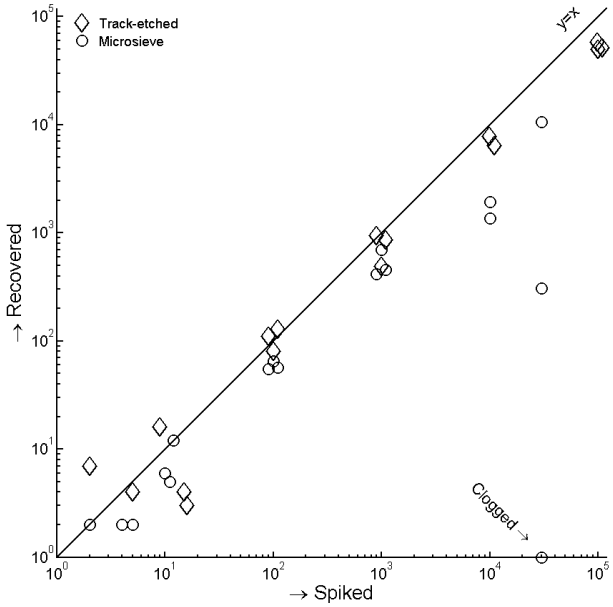

Figure 9.4: Linearity of recovery for 8 µm track-etched filters and 5 µm microsieves. *Whole blood was spiked with 2, 10, 100, 1,000, 10,000, 30,000 (microsieve only) or 100,000 (track-etch only) MDA-231. For spikes with target values of 2 and 10 cells, we determined the actual number of cells by microscope inspection of the cell drop prior to spiking. The counted spikes are shown, not the targets. Spikes of* 10^4 *cells and higher were counted automatically. Spikes of 100 and higher were offset by up to 10% to enhance readability of the graph.*

this spike was 10%. 2–5 false positives cells were counted on the track-etched filters, while none were counted on the microsieves.

9.3.4 The volume that can be filtered is limited by the contaminant concentration

The recovery after spiking 300 MDA-231 cells into 0.1, 1 or 10 mL of whole blood is shown in figure 9.5, panel A. On track-etched filters recovery was 47%, 51%, 36% with volumes of 0.1, 1 and 10 mL respectively. On microsieves recovery was 48%, 30%, 22% with volumes of 0.1, 1 and 10 mL respectively. The amount of the debris, as indicated with white arrows in figure 9.2, as well as the number of leukocytes retained on the filter increased with increasing sample volume, see figure 9.5, panel B. This accumulation of debris leads to a high autofluorescent background as can be seen in figure 9.5, panel D, compared to figure 9.5, panel C. In addition an experiment was

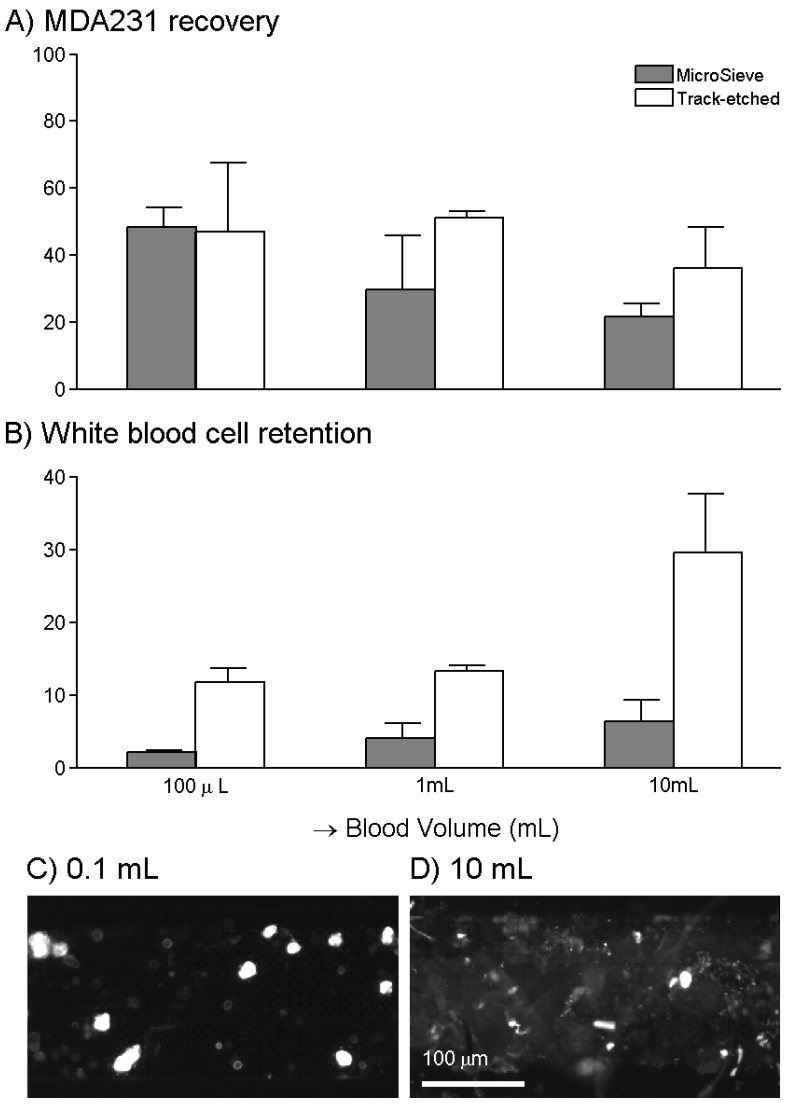

Figure 9.5: Impact of total blood volume. *Recovery of 300 MDA-231 cells spiked into 0.1, 1 and 10 mL of whole blood determined on 5 µm microsieves and 8 µm track-etched filters. Panel A shows the % recovery of MDA-231 cells, panel B the number of white cells found on the filter. The images in panel C and D show the CellTracker Orange signal after microsieve filtration of 0.1 and 10 mL of whole spiked blood respectively. The saturated dots are counted as MDA-231 cells, the weaker fluorescence is autofluorescent material.*

Table 9.2: *Filtration retains slightly more monocytes than other white blood cells. Numbers give % of total ± standard deviation determined on 5 healthy donors. Each data-point was determined by counting at least 300 cells.*

% of total	granulocytes	lymphocytes	monocytes	other
whole blood	65 ± 4	29 ± 5	5 ± 5	1 ± 0
on filter	58 ± 3	27 ± 3	14 ± 2	1 ± 0
% change	-11 ± 3	-5 ± 6	165 ± 37	1 ± 30

conducted where 30 MDA-231 cells were spiked into 0.1 mL of whole blood and filtered through a microsieve at 10 mL/h. This makes the flow per pore and the number of cells per pore equivalent to a spike of 300 MDA-231 cells in 1 mL of whole blood when filtered through a track-etched filter. Recovery under this condition was $57 \pm 31\%$.

9.3.5 Monocytes are retained more than other leukocytes

The selective enrichment of the leukocyte subpopulations on the track-etched filter is shown in table 9.2, the relative proportion of monocytes is increased by 165% at the cost of both granulocytes and lymphocytes. Of the $5 \cdot 10^6$ leukocytes in a 1 mL sample 0.1% was recovered on the filter.

9.3.6 EpCAM+CK+CD45– CTC are smaller than typical cells derived from tumor cell lines

A Coulter pipette was used to determine the size distributions of 9 tumor cell lines and leukocytes, shown in figure 9.6, panel A. The median size of leukocytes was 8.1 µm while cells from the tumor cell lines ranged from 10.9 to 19.0 µm. SKBR-3 shed small vesicles in the culture medium, which leads to a peak in the distribution near 6 µm, comprising up to 15% of total cells. The tumor cell line standard deviation relative to the median size (% CV) ranged between 19% (HL-60, MDA-468) to 31% (MCF-7). The size of MDA-231, SKBR-3 and PC3-9 cell lines was also determined using morphology parameters from an automated CTC counting algorithm, which automatically identifies EpCAM+CK+DNA+CD45– CTC, see figure 9.6, panel B. The cell thickness when imaging was found to be 5.2 µm by fitting the median diameter of these cell lines to the median diameter from the Coulter determination using equation 9.1. With this thickness, deviation between median size by imaging versus Coulter of SKBR-3, MDA-231, PC3-9 and leukocytes was less than 0.4 µm, The % CV of the distributions for imaging/Coulter was 16/26% for PC3-9, 15/30% for SKBR-3, 11/22% for MDA-231 and 16/77% for leukocytes. Applying equation 9.1 the median

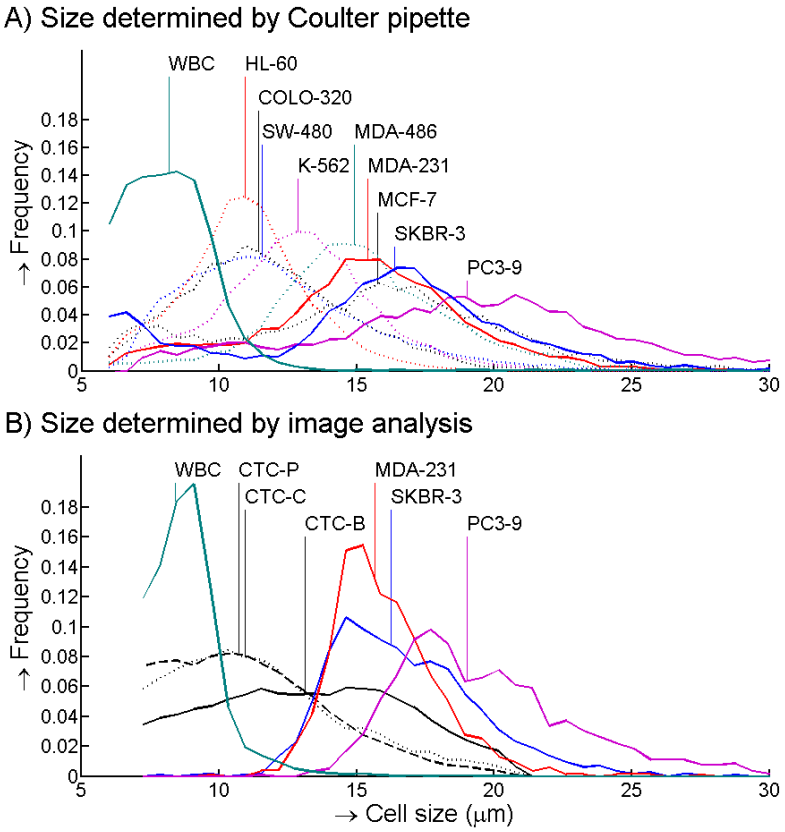

Figure 9.6: Size distribution of blood cells and various cancer cell lines. *Blood cells include white and red blood cells and the hematopoetic cell lines HL-60 and K-562. Cancer cell lines include prostate cancer cell lines PC3-9, colorectal cancer cell lines COLO-320 and SW-480, breast cancer cell lines SKBR-3, MCF7, MDA-231 and MDA-468. Distributions are normalized to unit area. Vertical lines indicate the median size for each cell type. Panel A shows the size distribution as determined using a Coulter pipette. Panel B shows the size distribution as determined using image analysis for MDA-231, SKBR-3, PC3-9, leukocytes (WBC) and CTC from patients with metastatic breast (CTC-B, solid line), colorectal (CTC-C, dotted line) or prostate (CTC-P, dashed line) cancer.*

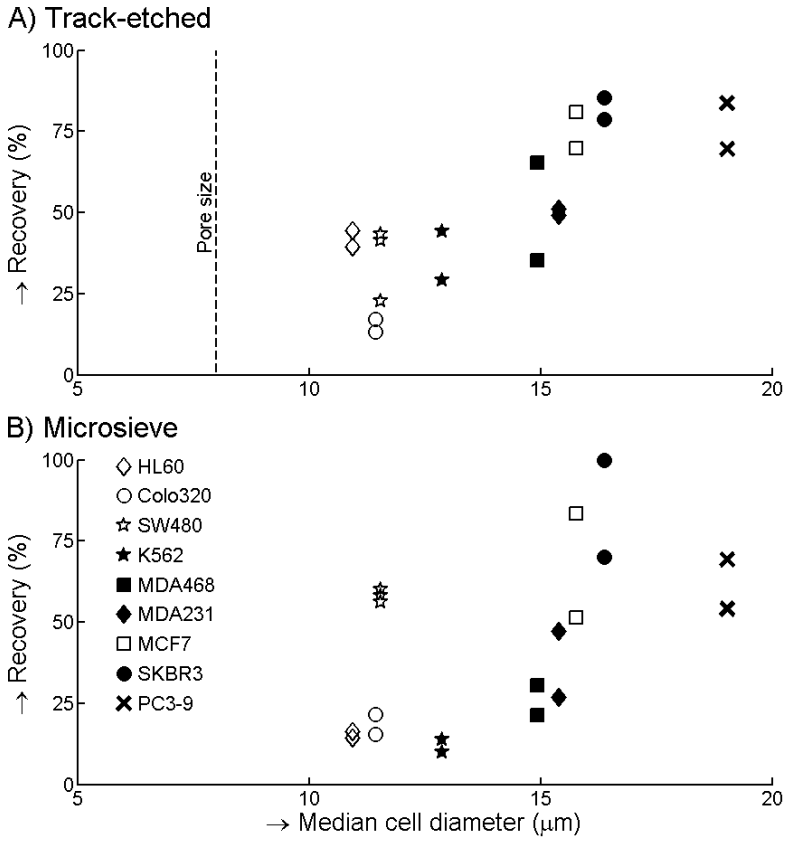

Figure 9.7: Recovery of different cell lines. *300 cells of each cell line were spiked into 1 mL of whole blood. Recovery obtained with 8 µm track-etched filters is shown in panel A, recovery with 5 µm microsieves is shown in panel B.*

diameter of CTC was determined to be 10.7 µm for prostate, 11.0 µm for colorectal and 13.1 µm for breast CTC.

9.3.7 Cell lines with size of CTC typically have low recovery

Three-hundred cells from 9 different tumor cell lines were spiked into 1 mL of blood and filtered through 8 µm track-etched filters and 5 µm microsieves. Recovery for duplicates of each experiment are shown in figure 9.7, panel A for track-etched filters and, panel B for microsieves. The trend for both filter types shows that recovery increases with cell size, however different cell lines of similar size can have two-fold difference in recovery. A larger cell

typically has higher recovery, but this is a weak trend, with large variations in recovery between cells of similar size. Average recovery of cells with sizes (10.8–12.9 µm) on the order of patients CTC (10.7–13.1 µm) was 33% (range 13–44%) on the track-etched filter and 29% (range 13–60%) on the microsieve with Colo-320, SW-480, HL-60 and K-562 cells. The high recovery of SW-480 cells on the microsieves was confirmed by measuring an additional time on both filter types. The third repeat matched the first two, and is thus not due to experimental error. A smaller track-etched pore size may improve recovery. We determined recovery for 5 µm pores by spiking Colo-320 or SW-480 cells into 1 mL of blood. Filtering a spiked sample with Colo-320 increased recovery from 15.2 ± 2.8% (8 µm track-etched) to 19.6 ± 7.5% (5 µm track-etched). With the SW-480 cell line, recovery increased from 35.9 ± 11.3% to 70.8 ± 10.4%.

9.4 Discussion

Methods for CTC enumeration by means of filtration employ different filter designs; track-etched filters with random pore distribution [17, 18], planar filters with predetermined pore distribution and good control of pore size with round [19, 20] or slotted pores [21], or a 3D [22] pore geometry. Lab on a chip (LOC) approaches allow for a more complex filter geometry [23] which may be applied to achieve high CTC recovery while avoiding downsides of dead end filtration. An additional advantage of LOC over the filtration method applied here could be integration of enrichment and sample interrogation in one device, limiting the amount of sample handling needed. A disadvantage of CTC-LOC devices reported to date [23, 24, 25] is their often limited sample volume, using samples up to 1 mL of whole blood. A planar filter integrated in a LOC [20] can allow larger sample sizes. The CTC enriched sample could be stained and then imaged on the filter, or alternatively after capture CTC could be moved to another area for further investigation [23].

We determined the size of CTC in suspension by comparing size determined by the Coulter principle to size determined by imaging. For this comparison, calibration of size by imaging versus size by the Coulter principle is needed. Good agreement on the median size was found, however the % CV on the size was larger by the Coulter principle than by the imaging approach, up to double for the cells from the tumor cell lines and almost five times higher for leukocytes. Possible explanations for these differences: - The imaging approach requires presence of a nucleus, while the Coulter approach determines size on all detected objects, including vesicles produced during culture of some cell lines, increasing CV. - EpCAM-magnetic enrichment and automatic detection of CK staining may favor enrichment and subsequent detection of larger objects, reducing CV with the imaging approach. - Leukocytes are a mixture of three main cell types of different

Table 9.3: Percentage of EpCAM+CK+CD45− CTC that can be recovered for various size cutoffs

size (µm)	breast	colorectal	prostate
8	92	87	84
10	77	61	58
12	60	36	34
14	41	19	16
16	23	9	7

sizes. Relatively high non-specific adhesion of granulocytes means that EpCAM enrichment captures granulocytes relative to other leukocytes and thus the size by imaging represents the size of granulocytes, resulting in a CV that is much lower than a true white blood cell mixture. Median size of EpCAM+CK+DNA+CD45− CTC found by the CellSearch system in metastatic breast is 13.1 µm, prostate 10.7 µm and colorectal cancer is 11.0 µm. This is much smaller than the size of most cells derived from tumor cell lines, figure 9.6. Assuming filtration recovers 100% of all cells in excess of a minimum size, table 9.3 shows an estimate of recovery for minimum size of 8, 10, 12, 14 and 16 µm derived from figure 9.6, panel B. For recoveries of 70% or higher, size based filtration methods need to recover CTC that are larger than 9.2 for prostate, 9.4 for colorectal and 10.8 µm for breast cancer. Unfortunately recovery with such small cells was poor, figure 9.7, and the 8 µm track-etched filter will probably not recover cells of 9.2 µm. Validation of a filtration assay using SKBR-3, MCF-7, PC3-9 or similarly sized cells may not have any relevance to CTC enrichment by means of filtration.

MDA-231 recovery determined during the filter comparison experiment was typically 10–20% higher than the recovery determined using subsequent experiments. This may be due to an error in the spike determination or due to misclassification of some SKBR-3 cells with weak CellTracker Green stain as MDA-231 cells in the comparison experiment or due to the spiking method used in all subsequent experiments. As a result of this method the spiked cells are captured on the filter early in the experiment and have more time to pass through the filter.

In the filter comparison shown in figure 9.3, we chose the 8 µm track-etched filters and the 5 µm microsieve as the best filters. We aimed for recovery $> 70\%$ and the lowest leukocyte contamination possible. The rationale for these targets was that while high CTC recovery is desirable, low leukocyte recovery is also desirable, as they may stain slightly positive for EpCAM or cytokeratin stains. This complicates review and leads to false positives [40]. In addition, leukocytes complicate CTC analysis using techniques such as PCR [41]. However, average recovery was only 33% for cells with a size comparable to CTC. With such recovery high CTC recovery takes precedence over low leukocyte contamination. Changing from 8 to 5 µm

track-etched filters resulted in acceptable recovery of 71% for SW-480 cells, but a still unacceptable 20% for COLO-320 cells. It is unknown which cell line is more similar to CTC.

While there was an association between recovery and cell size, see figure 9.7, it was not sufficient to explain the differences in recovery between the different cell lines. Additional factors contributing to recovery may be the deformability of cells [42, 43] or size of the nucleus [44]. It was surprising that the 5 µm microsieve performed similar to the 8 µm track-etched filter with matched flow per pore conditions. When passing through a 5 µm pore filter, the surface area of a leukocyte needs to increase by approximately 15% for a 1 µm thick filter and 30% for a 10 µm thick filter. As a result, a cell could be squeezed through the 1 µm thick microsieves more easily than through the 10 µm thick track-etched filters, which is countered by the smaller pore size. Ultimately we obtained the best result with a 5 µm pore, 10 µm thick track etched filters. However, we did not study the influence of even thicker filters. If surface tension is important, a 90 µm thick 5 µm pore filter would require a doubling in cell surface area of a MDA-231 cell, while a white blood cell only needs to increase surface area by 40% to pass.

With the leukocytes we expected to see an enrichment of the larger monocytes (8.9–9.6 µm [45]) and depletion of the smaller lymphocytes (6.8–7.7 µm [45]). While table 9.2 shows monocytes were indeed enriched, the ratio between lymphocytes and granulocytes (8.0–9.1 µm [45]) was unchanged. We further expected hematopoietic cell lines to be more flexible than the epithelial cell lines, and thus to have much lower recovery. Surprisingly, recovery of hematopoietic HL-60 and K-562 cells is comparable to similarly sized epithelial SW-480 and COLO-320 cells.

The number of pores needed depends on the number of cells that need to be recovered (figure 9.4), and the number of cells that need to pass the filter (figure 9.5). Recovery on microsieves was lower than recovery on track-etched filters in most experiments, but using an 8 µm track-etched filter and a 5 µm microsieve with comparable numbers of cells per pore, recovery of MDA-231 cells was 51% and 57% respectively. A further factor in determining the number of pores needed is the contamination with debris as seen in figure 9.2. A larger whole blood volume contains more debris, which may block multiple pores. For blood samples of 1 mL, 100,000 pores are adequate, to prevent reduced recovery the number of CTC needs to be less than 2,000 and each cell should block one pore. The number of metastatic patients with more than 2,000 CTC/ mL is less than 2% [46], reduced recovery for these patients would not affect the ability to perform phenotyping of the individual CTC in these patients since there would still be many CTC left.

The number of pores blocked per captured cell has relation to the porosity of the filter. The 5 µm microsieves had high porosity of 20%, blocking 4–6 pores per captured MDA-231 cell, while with the 5% porosity 8 µm track-etched filter less than 10% of MDA-231 cells blocked more than one

pore. These were pores that were close to each other due to random pore location on the track-etched filter. On high porosity filters distinguishing two adjacent cells is complicated by poor separation. This made enumeration of cells on the microsieves more difficult than on the track-etched filter. A porosity of up to 10% on a filter with regularly spaced pores allows for discrimination of cells on adjacent pores, and each cell would block a single pore.

The material of the filter must provide at least two properties. First the material must be compatible with blood. Interaction of erythrocytes with the filter surface resulted in low recovery on the TEM grids. Further, it must allow for imaging of CTC at sufficient resolution to discriminate between false positive leukocytes and true CTC. With the CellSearch platform, a 10x/NA0.45 objective is adequate for this purpose, but we could not image the track-etched filter at this resolution because it had deformed during filtration. The filter material must be sufficiently stiff to prevent deformation during filtration. Imaging at 4x/NA0.13 of the track-etched filters would have been a problem for adequate identification if we had used EpCAM/CK immuno-fluorescence for identification of culture cells, rather than using CellTracker pre-stained cells. While solutions for this problem exist [18], they are time consuming and can be complicated. A third property that is desirable is a CTC specific coating of the filter surface, for example with EpCAM. Such a coating may increase recovery of CTC, while retention of leukocytes is unaffected. Whether a hydrophilic or hydrophobic filter surface has better properties for enrichment of CTC by means of filtration is also of interest. This could be determined by coating microsieves with hydrophilic coatings [47].

In summary, the ideal filter for CTC enrichment has a pore size of about 5 µm, thickness of at least 10 µm, at least 100,000 regularly spaced pores, a porosity of 10% or less and is constructed of a stiff, flat material, which does not interact with blood cells. While cell size is an important factor in determining recovery, other factors must be involved in determining whether a cell can pass as well. To evaluate a filtration procedure, cell lines with a median size of 11–13 µm should be used to challenge the system, such as Colo-320, SW-480 and not cell lines significantly larger than CTC.

9.5 References

[1] M. Cristofanilli, G. T. Budd, M. J. Ellis, A. Stopeck, J. Matera, M. C. Miller, J. M. Reuben, G. V. Doyle, W. J. Allard, L. W. Terstappen, and D. F. Hayes, "Circulating tumor cells, disease progression, and survival in metastatic breast cancer," *N. Engl. J. Med.*, vol. 351, pp. 781–791, Aug 2004.

[2] J. Pierga, D. Hajage, T. Bachelot, S. Delaloge, E. Brain, M. Campone, V. Diéras, E. Rolland, L. Mignot, C. Mathiot, *et al.*, "High independent prognostic and predictive value of circulating tumor cells compared with serum tumor markers in a large prospective trial in first-line chemotherapy for metastatic breast cancer patients," *Annals of Oncology*, vol. 23, no. 3, pp. 618–624, 2011.

[3] J. Tol, M. Koopman, M. C. Miller, A. Tibbe, A. Cats, G. J. Creemers, A. H. Vos, I. D. Nagtegaal, L. W. Terstappen, and C. J. Punt, "Circulating tumour cells early predict progression-free and overall survival in advanced colorectal cancer patients treated with chemotherapy and targeted agents," *Ann. Oncol.*, vol. 21, pp. 1006–1012, May 2010.

[4] J. S. de Bono, H. I. Scher, R. B. Montgomery, C. Parker, M. C. Miller, H. Tissing, G. V. Doyle, L. W. Terstappen, K. J. Pienta, and D. Raghavan, "Circulating tumor cells predict survival benefit from treatment in metastatic castration-resistant prostate cancer," *Clin. Cancer Res.*, vol. 14, pp. 6302–6309, Oct 2008.

[5] C. Rao, T. Bui, M. Connelly, G. Doyle, I. Karydis, M. R. Middleton, G. Clack, M. Malone, F. A. W. Coumans, and L. W. M. M. Terstappen, "Circulating melanoma cells and survival in metastatic melanoma," *International Journal of Oncology*, vol. 38, pp. 755–760, 2011.

[6] S. Matsusaka, K. Chin, M. Ogura, M. Suenaga, E. Shinozaki, Y. Mishima, Y. Terui, N. Mizunuma, and K. Hatake, "Circulating tumor cells as a surrogate marker for determining response to chemotherapy in patients with advanced gastric cancer," *Cancer Science*, vol. 101, pp. 1067–1071, 2010.

[7] M. G. Krebs, R. Sloane, L. Priest, L. Lancashire, J. M. Hou, A. Greystoke, T. H. Ward, R. Ferraldeschi, A. Hughes, G. Clack, M. Ranson, C. Dive, and F. H. Blackhall, "Evaluation and prognostic significance of circulating tumor cells in patients with non-small-cell lung cancer," *Journal of Clinical Oncology*, vol. 29, pp. 1556–1563, 2011.

[8] T. J. N. Hiltermann, J. J. W. Liesker, A. van den Berg, J. H. Schouwink, W. J. A. Wijnands, G. S. M. A. Kerner, H. M. Boezen, M. M. Pore, F. A. E. Kruyt, W. Timens, H. Tissing, A. G. J. Tibbe, L. W. M. M. Terstappen, and H. J. M. Groen, "Circulating tumor cells in small cell lung cancer, a predictive and prognostic factor," *Annals of Oncology*, p. In press, 2012.

[9] J. den Toonder, "Circulating tumor cells: the grand challenge," *Lab on a chip*, vol. 11, pp. 375–377, 2011.

[10] W. J. Allard, J. Matera, M. C. Miller, M. Repollet, M. C. Connelly, C. Rao, A. G. Tibbe, J. W. Uhr, and L. W. Terstappen, "Tumor cells circulate in the peripheral blood of all major carcinomas but not in healthy subjects or patients with nonmalignant diseases," *Clin. Cancer Res.*, vol. 10, pp. 6897–6904, Oct 2004.

[11] H. B. Hsieh, D. Marrinucci, K. Bethel, D. N. Curry, M. Humphrey, R. T. Krivacic, J. Kroener, L. Kroener, A. Ladanyi, N. Lazarus, P. Kuhn, R. H. Bruce, and J. Nieva, "High speed detection of circulating tumor cells," *Biosens Bioelectron*, vol. 21, pp. 1893–1899, Apr 2006.

[12] K. Pachmann, O. Camara, A. Kavallaris, S. Krauspe, N. Malarski, M. Gajda, T. Kroll, C. Jorke, U. Hammer, A. Altendorf-Hofmann, C. Rabenstein, U. Pachmann, I. Runnebaum, and K. Hoffken, "Monitoring the response of circulating epithelial tumor cells to adjuvant chemotherapy in breast cancer allows detection of patients at risk of early relapse," *J. Clin. Oncol.*, vol. 26, pp. 1208–1215, Mar 2008.

[13] C. G. Rao, D. Chianese, G. V. Doyle, M. C. Miller, T. Russell, R. A. Sanders, and L. W. Terstappen, "Expression of epithelial cell adhesion molecule in carcinoma cells present in blood and primary and metastatic tumors," *Int. J. Oncol.*, vol. 27, pp. 49–57, Jul 2005.

[14] R. Rosenberg, R. Gertler, J. Friederichs, K. Fuehrer, M. Dahm, R. Phelps, S. Thorban, H. Nekarda, and J. R. Siewert, "Comparison of two density gradient centrifugation systems for the enrichment of disseminated tumor cells in blood," *Cytometry*, vol. 49, pp. 150–158, Dec 2002.

[15] P. Balasubramanian, L. Yang, J. Lang, K. Jatana, D. Schuller, A. Agrawal, M. Zborowski, and J. Chalmers, "Confocal images of circulating tumor cells obtained using a methodology and technology that removes normal cells," *Molecular pharmaceutics*, vol. 6, no. 5, pp. 1402–1408, 2009.

[16] C. Alix-Panabieres, J. P. Brouillet, M. Fabbro, H. Yssel, T. Rousset, T. Maudelonde, G. Choquet-Kastylevsky, and J. P. Vendrell, "Characterization and enumeration of cells secreting tumor markers in the peripheral blood of breast cancer patients," *J. Immunol. Methods*, vol. 299, pp. 177–188, Apr 2005.

[17] V. Hofman, M. Ilie, C. Bonnetaud, E. Selva, E. Long, T. Molina, J. Vignaud, J. Fléjou, S. Lantuejoul, E. Piaton, *et al.*, "Cytopathologic detection of circulating tumor cells using the isolation by size of epithelial tumor cell method: promises and pitfalls," *American journal of clinical pathology*, vol. 135, no. 1, pp. 146–156, 2011.

[18] G. Vona, A. Sabile, M. Louha, V. Sitruk, S. Romana, K. Schutze, F. Capron, D. Franco, M. Pazzagli, M. Vekemans, B. Lacour, C. Brechot, and P. Paterlini-Brechot, "Isolation by size of epithelial tumor cells : a new method for the immunomorphological and molecular characterization of circulating tumor cells," *Am. J. Pathol.*, vol. 156, pp. 57–63, Jan 2000.

[19] D. Adams, O. Makarova, P. Zhu, S. Li, P. Amstutz, and C. Tang, "Isolation of circulating tumor cells by size exclusion using lithography fabricated precision microfilters," in *Proceedings of the 102nd Annual Meeting of the American Association for Cancer Research*, (Orlando, FL, USA), AACR, April 2011.

[20] H. Lin, S. Zheng, A. Williams, M. Balic, S. Groshen, H. Scher, M. Fleisher, W. Stadler, R. Datar, Y. Tai, *et al.*, "Portable filter-based microdevice for detection and characterization of circulating tumor cells," *Clinical Cancer Research*, vol. 16, no. 20, pp. 5011–5018, 2010.

[21] T. Xu, B. Lu, Y. Tai, and A. Goldkorn, "A cancer detection platform which measures telomerase activity from live circulating tumor cells captured on a microfilter," *Cancer research*, vol. 70, no. 16, pp. 6420–6426, 2010.

[22] S. Zheng, H. Lin, B. Lu, A. Williams, R. Datar, R. Cote, and Y. Tai, "3D microfilter device for viable circulating tumor cell (CTC) enrichment from blood," *Biomedical microdevices*, vol. 13, no. 1, pp. 203–213, 2011.

[23] S. J. Tan, R. L. Lakshmi, P. Chen, W. T. Lim, L. Yobas, and C. T. Lim, "Versatile label free biochip for the detection of circulating tumor cells from peripheral blood in cancer patients," *Biosens Bioelectron*, vol. 26, pp. 1701–1705, Dec 2010.

[24] J. P. Gleghorn, E. D. Pratt, D. Denning, H. Liu, N. H. Bander, S. T. Tagawa, D. M. Nanus, P. A. Giannakakou, and B. J. Kirby, "Capture of circulating tumor cells from whole blood of prostate cancer patients using geometrically enhanced differential immunocapture (GEDI) and a prostate-specific antibody," *Lab Chip*, vol. 10, pp. 27–29, Jan 2010.

[25] S. Nagrath, L. V. Sequist, S. Maheswaran, D. W. Bell, D. Irimia, L. Ulkus, M. R. Smith, E. L. Kwak, S. Digumarthy, A. Muzikansky, P. Ryan, U. J. Balis, R. G. Tompkins, D. A. Haber, and M. Toner, "Isolation of rare circulating tumour cells in cancer patients by microchip technology," *Nature*, vol. 450, pp. 1235–1239, Dec 2007.

[26] S. L. Stott, C. H. Hsu, D. I. Tsukrov, M. Yu, D. T. Miyamoto, B. A. Waltman, S. M. Rothenberg, A. M. Shah, M. E. Smas, G. K. Korir, F. P. Floyd, A. J. Gilman, J. B. Lord, D. Winokur, S. Springer, D. Irimia, S. Nagrath, L. V. Sequist, R. J. Lee, K. J. Isselbacher, S. Maheswaran, D. A. Haber, and M. Toner, "Isolation of circulating tumor cells using a microvortex-generating herringbone-chip," *Proc. Natl. Acad. Sci. U.S.A.*, vol. 107, pp. 18392–18397, Oct 2010.

[27] U. Dharmasiri, S. Njoroge, M. Witek, M. Adebiyi, J. Kamande, M. Hupert, F. Barany, and S. Soper, "High-throughput selection, enumeration, electrokinetic manipulation, and molecular profiling of low-abundance circulating tumor cells using a microfluidic system," *Analytical chemistry*, vol. 83, pp. 2301–Ũ2309, 2011.

[28] T. Stakenborg, C. Liu, O. Henry, E. Borgen, N. Laddach, T. Roeser, M. Ritzi-Lehnert, C. Fermér, S. Hauch, C. OSullivan, *et al.*, "Automated genotyping of circulating tumor cells," *Expert Review of Molecular Diagnostics*, vol. 10, no. 6, pp. 723–729, 2010.

[29] A. H. Talasaz, A. A. Powell, D. E. Huber, J. G. Berbee, K. H. Roh, W. Yu, W. Xiao, M. M. Davis, R. F. Pease, M. N. Mindrinos, S. S. Jeffrey, and R. W. Davis, "Isolating highly enriched populations of circulating epithelial cells and other rare cells from blood using a magnetic sweeper device," *Proc. Natl. Acad. Sci. U.S.A.*, vol. 106, pp. 3970–3975, Mar 2009.

[30] S. Wang, K. Liu, J. Liu, Z. Yu, X. Xu, L. Zhao, T. Lee, E. Lee, J. Reiss, Y. Lee, *et al.*, "Highly efficient capture of circulating tumor cells by using nanostructured silicon substrates with integrated chaotic micromixers," *Angewandte Chemie International Edition*, vol. 50, no. 13, pp. 3084–3088, 2011.

[31] F. A. Coumans, C. J. Doggen, G. Attard, J. S. de Bono, and L. W. Terstappen, "All circulating EpCAM+CK+CD45- objects predict overall survival in castration-resistant prostate cancer," *Ann. Oncol.*, vol. 21, pp. 1851–1857, Sep 2010.

[32] G. Attard, J. F. Swennenhuis, D. Olmos, A. H. Reid, E. Vickers, R. A'Hern, R. Levink, F. Coumans, J. Moreira, R. Riisnaes, N. B. Oommen, G. Hawche, C. Jameson, E. Thompson, R. Sipkema, C. P. Carden, C. Parker, D. Dearnaley, S. B. Kaye, C. S. Cooper, A. Molina, M. E. Cox, L. W. Terstappen, and J. S. de Bono, "Characterization of ERG, AR and PTEN gene status in circulating tumor cells from patients with castration-resistant prostate cancer," *Cancer Res.*, vol. 69, pp. 2912–2918, Apr 2009.

[33] E. Ogura, H. Senzaki, K. Yoshizawa, K. Hioki, and A. Tsubura, "Immunohistochemical localization of epithelial glycoprotein EGP-2 and carcinoembryonic antigen in normal colonic mucosa and colorectal tumors," *Anticancer research*, vol. 18, no. 5B, pp. 3669–3675, 1998.

[34] G. Spizzo, D. Fong, M. Wurm, C. Ensinger, P. Obrist, C. Hofer, G. Mazzoleni, G. Gastl, and P. Went, "EpCAM expression in primary tumour tissues and metastases: an immunohistochemical analysis," *Journal of clinical pathology*, vol. 64, no. 5, pp. 415–420, 2011.

[35] W. Osta, Y. Chen, K. Mikhitarian, M. Mitas, M. Salem, Y. Hannun, D. Cole, and W. Gillanders, "EpCAM is overexpressed in breast cancer and is a potential target for breast cancer gene therapy," *Cancer research*, vol. 64, no. 16, p. 5818, 2004.

[36] S. Mukherjee, A. Richardson, J. Rodriguez-Canales, K. Ylaya, H. Erickson, A. Player, E. Kawasaki, P. Pinto, P. Choyke, M. Merino, *et al.*, "Identification of EpCAM as a molecular target of prostate cancer stroma," *The American journal of pathology*, vol. 175, no. 6, pp. 2277–2287, 2009.

[37] F. Coumans, G. van Dalum, M. Beck, and L. Terstappen, "Factors influencing filtration of tumor cells from whole blood," *submitted*, 2012.

[38] S. Ligthart, F. Coumans, G. Attard, A. Cassidy, J. de Bono, and L. Terstappen, "Unbiased and automated identification of a circulating tumour cell definition that associates with overall survival," *PloS one*, vol. 6, no. 11, p. e27419, 2011.

[39] S. Ligthart, F. Bidard, C. Decraene, T. Bachelot, S. Delaloge, E. Brain, M. Campone, P. Viens, J. Pierga, and L. Terstappen, "Unbiased quantitative assessment of her-2 expression of circulating tumor cells in patients with metastatic and non metastatic breast cancer," *submitted*, 2012.

[40] A. G. Tibbe, M. C. Miller, and L. W. Terstappen, "Statistical considerations for enumeration of circulating tumor cells," *Cytometry A*, vol. 71, pp. 154–162, Mar 2007.

[41] M. Kowalewska, M. Chechlińska, S. Markowicz, P. Kober, and R. Nowak, "The relevance of RT-PCR detection of disseminated tumour cells is hampered by the expression of markers regarded as tumour-specific in activated lymphocytes," *Eur. J. Cancer*, vol. 42, pp. 2671–2674, Nov 2006.

[42] H. W. Hou, Q. S. Li, G. Y. Lee, A. P. Kumar, C. N. Ong, and C. T. Lim, "Deformability study of breast cancer cells using microfluidics," *Biomed Microdevices*, vol. 11, pp. 557–564, Jun 2009.

[43] F. Leong, Q. Li, C. Lim, and K. Chiam, "Modeling cell entry into a micro-channel," *Biomechanics and modeling in mechanobiology*, vol. 10, no. 5, pp. 755–766, 2011.

[44] H. Kan, W. Shyy, H. Udaykumar, P. Vigneron, and R. Tran-Son-Tay, "Effects of nucleus on leukocyte recovery," *Annals of biomedical engineering*, vol. 27, no. 5, pp. 648–655, 1999.

[45] P. Nibbering, T. Zomerdijk, A. Corsèl-Van Tilburg, and R. Van Furth, "Mean cell volume of human blood leucocytes and resident and activated murine macrophages," *Journal of immunological methods*, vol. 129, no. 1, pp. 143–145, 1990.

[46] F. Coumans, S. T. Ligthart, and L. W. M. Terstappen, "Challenges in the enumeration and phenotyping of CTC," *Clinical Cancer Research*, 2012.

[47] A. Nguyen, J. Baggerman, J. Paulusse, C. van Rijn, and H. Zuilhof, "Stable protein-repellent zwitterionic polymer brushes grafted from silicon nitride," *Langmuir*, vol. 27, pp. 2587–Ũ2594, 2011.

CHAPTER 10

Enrichment of CTC from large sample volumes by means of filtration

Frank A.W. Coumans and Leon W.M.M. Terstappen

Abstract

Circulating tumor cell (CTC) load predicts survival for patients with metastatic breast, colon and prostate cancer and survival decreases by 6.6 months for each ten-fold CTC increase. To enable accurate prediction of survival in all patients with metastatic disease 5 L of blood needs to be processed. CTC enrichment by filtration is scalable to larger sample volumes, but pressure during filtration needs to be less than 10 mbar. Whole blood, the buffy coat from 0.5 L of blood, apheresis samples and bovine blood were filtered in a CTC filtration system. The impact of sample aging was evaluated using bovine whole blood. CTC recovery from 100 mL of fresh bovine blood was estimated with spiked SKBR-3 cells. Fibrin aggregates in buffy coats and apheresis samples led to high pressure during filtration, but pressures with apheresis samples were at least ten-fold lower. Fibrin aggregates were formed over time and only the 1 hour old bovine samples approached the 10 mbar target pressure. Recovery of SKBR3 cells from blood in excess of 50% is possible for samples processed within 5 hours. Sample age caused issues with filtration of all the tested sample types. This could be resolved with an extracorporeal circuit with a CTC-trap based on EpCAM enrichment or filtration based on physical characteristics of CTC. Apheresis may be another effective approach for large blood volume CTC enrichment the density of CTC will however need to be determined.

10.1 Introduction

Circulating tumor cell (CTC) load predicts survival for patients with metastatic carcinoma [1, 2, 3, 4, 5, 6, 7]. In a recent study with samples from breast, colorectal and prostate cancer, survival decreased by 6.6 months for each ten-fold CTC increase [8]. The CTC frequency is extremely low and in the standard 7.5 mL blood CTC assay [9], CTC are detected only in 61% of patients with metastatic carcinoma. In addition, one of the promises of CTC technology is to provide a liquid biopsy which reflects the cancer in its current state. Attempts to determine presence of treatment targets on the recovered CTC are limited by the low total number of CTC [10, 11]. Some studies have increased CTC detection sensitivity by processing four tubes of blood instead of one [12, 13, 14, 15], but the impact of such an increase was limited. This can be explained by the log-logistic distribution of CTC number found in patients [8]. Hazard ratio of death from breast cancer is 3.5 when comparing early stage breast cancer patients with CTC to patients without CTC in 30 mL of blood [12]. Nevertheless, 4% of those patients without CTC still died of breast cancer within 4 years. These patients may have had CTC, but at an insufficient frequency to be detected in 30 mL of blood.

To resolve these issues a substantial increase of sample volume is needed, possibly up to 5 L [8]. A 5 L blood sample contains $30 \cdot 10^9$ white blood cells $20 \cdot 10^{12}$ red blood cells and $1 \cdot 10^{12}$ platelets [16]. To allow further analysis of potential CTC by cytometry methods, the total number of cells needs to be reduced to 10^6 or fewer total cells, without loss of CTC. Enrichment of a 5 L blood volume by means of antibody mediated enrichment/depletion [16, 17, 18] would require 2 mg of antibody per test, which is cost prohibitive ($\approx$ €600/test). Other antibody based methods are not scalable to volumes in excess of only 10 mL [19, 20, 21, 22, 23, 24, 25]. Size based filtration is a relatively new approach for CTC enrichment [26, 27, 28, 29, 30, 31], which does not require antibodies. Filters are obtainable in large surface areas and thus potentially suitable for very large sample volumes. For successful enrichment of CTC, the pressure across the filter should not exceed 10 mbar [32] for a filtration that takes 1 hour to complete. A further complication with large samples is that obtaining a sample of only 250 mL several times per year is not feasible for patients. A possible solution is leukapheresis [33] optimized for CTC density. Leukapheresis collects cells within a range of densities and returns cells outside the range to the patient. In this way all or part of the white cells and CTC are obtained, without harming the patient. Here we investigate the possibilities of utilizing a filtration approach for the enrichment of CTC from a blood volume of 5 L, or the apheresis product of such a blood volume.

10.2 Materials and methods

10.2.1 Blood samples

Four sample types were used; blood from healthy donors collected in EDTA tubes (BD), buffy coats from 0.5 L of blood, bovine blood and frozen apheresis products. Buffy coats obtained from the local blood bank were used as a model for leukapheresis products. The blood bank collects 0.5 L of blood in a collection bag (CompoFlow, Fresenius Kabi, Oberursel, Germany) filled with 70 mL citrate phosphate dextrose solution (CPD). After removal of plasma and red blood cells, 50 mL of product is left including most white blood cells present in the original 0.5 L volume, as well as some red blood cells, plasma and platelets. These samples were processed within 20–30 hours after collection. Whole blood from healthy donors was collected in 10 mL EDTA tubes (BD, Franklin Lakes, NJ, USA). All donors signed informed consent, and the study protocols were approved by the Sanquin blood bank and the METC Twente ethics committees. Bovine blood was obtained from a local slaughterhouse via bleeding of the carotid artery. Blood was collected in 5 L containers filled with 300 mL of 66 mmol EDTA in PBS. Apheresis products from 3 patients with hematopoietic malignancies stored for 10+ years in DMSO at -80°C were thawed and processed. These samples were intended for hematopoietic stem cell transplantation, but the patients expired and the samples were discarded according to the procedures of the MST hospital.

10.2.2 Culture cells

The density of breast carcinoma cell lines SKBR-3, MCF-7, MDA-231 and HS-578-T was determined. HS-578-T cells were cultured in RPMI 1640 (Gibco, Invitrogen, Carlsbad, CA, USA) and the other cell lines in Dulbecos Modified Eagle Medium (Sigma Aldrich, St. Louis, MO, USA). All media were supplemented with 10% fetal calf serum (Gibco), 1% penicillin-streptomycin (Gibco) and 1% L-Glutamin (Sigma Aldrich). Cells were harvested using 0.05% trypsin (Gibco) for 5 minutes at 37°C. SKBR-3 were also used in a recovery experiment. To eliminate potential issues with false positive staining of blood cells or other debris for cell enumeration, SKBR-3 cells were pre-stained by incubation in culture media for 24 hours at 37°C with 5 µmol CellTracker Orange CMTMR (Invitrogen). The exact concentration of the cell suspension for spiking was determined with TruCount tubes (BD) and a FACSAria II flow cytometer (BD) by counting cell sized objects staining with Hoechst 33342 (8 µmol in PBS, Invitrogen) and CellTracker Orange.

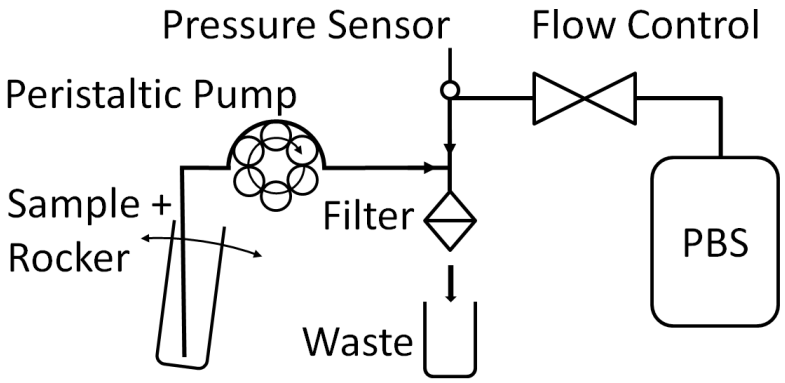

Figure 10.1: System diagram. *The sample is placed inside a rocker to prevent formation of a buffy coat layer. Aspiration of the sample is performed by means of a peristaltic pump, which delivers a constant flow rate to the filter. The pressure across the filter is monitored by a sensor.*

10.2.3 Filtration setup

A filtration setup was constructed as, schematically illustrated in figure 10.1. A detailed description is presented elsewhere [32]. A rocker (PTR-60, Grant Intruments, Shepreth, Cambridgeshire, UK) was added to this system to prevent separation of the blood into its components and the sample injection is performed with a peristaltic pump (Minipulse 2, Gilson, Middleton, WI, USA). The sample stream from the pump passes through either one or four parallel 13 mm track etch filters with 8 µm pores (Whatman Nucleopore, Kent, UK. The pressure across the filter is monitored by a sensor. Due to setup limitations, this pressure cannot exceed 300 mbar.

10.2.4 Density determination with Percoll

Percoll (GE, Piscataway, NJ, USA) was used per the manufacturer's instructions to obtain densities from 1.010 to 1.130 g/ mL [34] in increments of 0.005 g/ mL. The Percoll volume was equal to the sample volume, and samples were centrifuged at 1000 x g for 20 minutes. A Nikon Eclipse 400 epi-fluorescent microscope equipped with a 40x/NA0.6 objective was used together with a Neubauer counting chamber to enumerate the number of cells in each density. Red blood cells were identified by visual appearance, all other cells were enumerated based on 8 µmol Hoechst 33342 (Molecular Probes, Invitrogen) nuclear staining together with additional stainings for the white blood cells. Cells were identified as lymphocytes when staining with either CD20-FITC (Biolegend, San Diego, CA, USA) or CD3-PE (BD), as granulocytes when staining for CD15-PE (BD), as monocytes when staining for CD14-PE (BD) and as platelets when staining for CD41a-FITC

(BD) and/or CD61-FITC (BD). Antibodies were used per manufacturers recommendations. Fibrin aggregates were obtained by filtering a buffy coat through a 30 µm nylon mesh (Spectrum Laboratories, Rancho Dominguez, CA, USA). Relative frequency of fibrin aggregates was determined by visual estimation of the thickness of the layer in each gradient segment. Normal distributions were least squares fit through the measured data using Matlab 2009a (Mathworks, Natick, MA, USA).

10.2.5 Fibrin aggregate removal with Percoll

We diluted 25 mL of three buffy coats with 75 mL PBS-AC (PBS with 0.38% trisodium citrate and 0.5% bovine serum albumin) and split the buffy coats into aggregate rich and aggregate depleted components using Percoll. Both components as well as 25 mL of unprocessed buffy coats were filtered through 4 parallel filters. The filters were stained with CD61-FITC, CD41a-FITC and Hoechst 33342 and imaged on a Nikon Eclipse 400 epi-fluorescent microscope with a 4x/NA0.13 objective.

10.2.6 Blood aging

Fresh bovine blood was used to test the impact of sample age on pressure during filtration. Sample processing was started at 1, 5, 21 and 27 hours after draw. 100 mL of bovine blood was filtered through 4 filters in parallel at a sample flow speed of 100 mL/h. For recovery of culture tumor cells the pressure during a 1 hour filtration needs to be less than 10 mbar to limit loss of captured cells [32]. Three apheresis samples were obtained fresh from patients and stored at -80°C in DMSO. Prior to use, samples were thawed in a water bath, washed with PBS-1%BSA to remove the DMSO, and filtered through a 30 µm mesh to remove aggregates. White blood cells (WBC) from 210 mL of whole blood ($1.25 \cdot 10^9$ WBC in 50 mL) were filtered through 4 filters in parallel at a sample flow speed of 25 mL/h. At these settings, a pressure of 5 mbar is expected [32].

10.2.7 Recovery of SKBR-3 from 100 mL of whole blood

Pre-stained SKBR-3 cells were spiked into 100 mL of whole blood at spikes of 0, 25, 2,500 and 250,000, the latter three representing the 41^{st}, 73^{rd} and 91^{st} percentile of CTC concentrations in patients with metastatic breast cancer [8]. The zero spike was run first, the sequence of the other spikes alternated. The spike of 25 was enumerated under a fluorescent microscope prior to spiking. The filters were imaged on the epi-fluorescence microscope. Recovery was determined manually by inspection of false color overlays for the 25 and 2,500 spikes and determined using an automated algorithm developed in Matlab 2009a for the 250,000 spike since manual enumeration was not practically feasible. The automated algorithm undercounts the

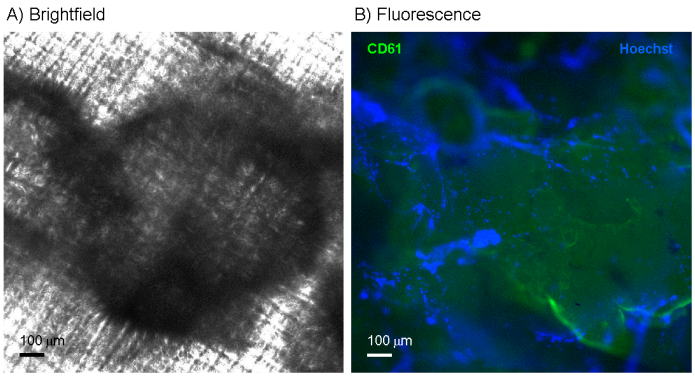

Figure 10.2: Clumps found on 30 µm mesh. *Panel A shows a bright field image fibrin aggregates obtained from a buffy coat on a 30 µm mesh (visible in the background). Clumps of various sizes from 30 µm were found on the filter, the clump in the middle of the image is approximately 950 µm in diameter. The aggregates were washed off the mesh and stained with CD61-FITC and Hoechst. Panel B shows a typical false color image after staining. The bulk of the aggregates are positive for CD61, with some cells attached to the outside.*

manual count by approximately 15% and recovery was revised upwards to take this discrepancy into account.

10.3 Results

10.3.1 Fibrin aggregates prevent processing of human buffy coat

We filtered 9 different 50 mL buffy coats (from 0.5 L of blood) through a single filter at a sample flow rate of 25 mL/h. With 8 samples, the pressure across the filter exceeded 300 mbar after typically 6 mL of the sample was processed (range 2–35 mL). With one sample 50 mL could be processed with a maximum pressure of 107 mbar. After filtering, all filters had a thick coat of cream colored aggregates. For three buffy coats, we used a 30 µm mesh to remove these aggregates from the sample. After pre-filtering, we could process a larger sample volume (7, 11 and 27 mL) before the maximum pressure of 300 mbar was reached. The aggregates retained on the mesh had a similar color and consistency to the aggregates on the filter. Aggregates from 30 µm up to several mm in diameter were observed. A bright field image of a large aggregate is shown in figure 10.2, panel A. The aggregates stain positive for platelet stain CD61-FITC with occasional clusters of Hoechst 33342 positive nuclear material, figure 10.2, panel B.

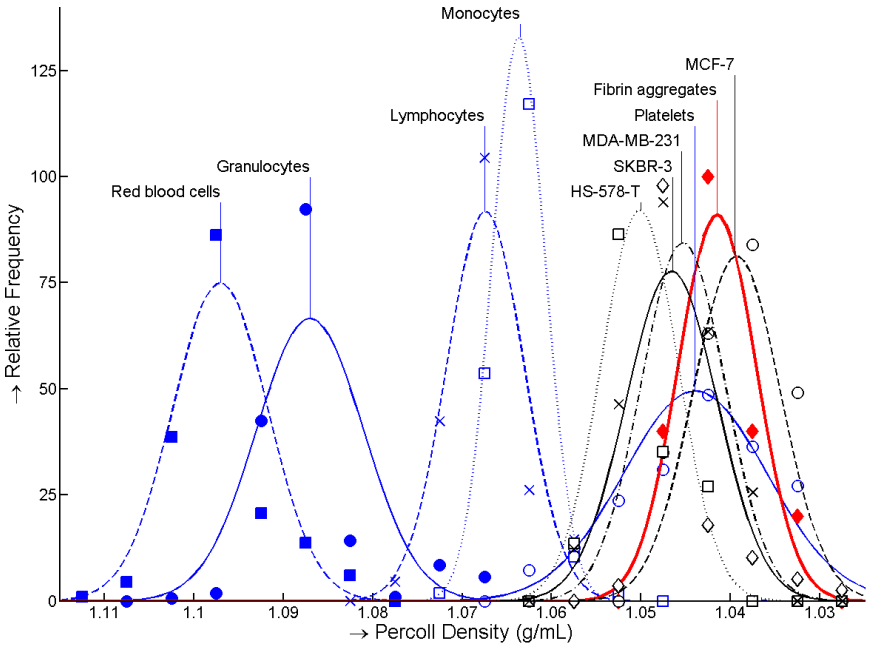

Figure 10.3: Percoll densities of major blood components, four breast cancer cell lines and fibrin clots. *Blue lines show blood components, black lines tumor cell lines and the red line fibrin aggregates. Data points and fit normal curves are shown. The data is normalized to make the area under the curve the same for all cell types.*

10.3.2 Culture cells and fibrin aggregates are lighter than blood cells

The density distributions of blood cells, cells from tumor cell lines and fibrin aggregates are shown in figure 10.3. Cells from the SKBR-3, MCF-7, MDA-231 and HS-578-T tumor cell lines have a density (median 1.040–1.050 g/ mL) similar to the fibrin aggregates (median 1.042) and a lower density than blood cells (median 1.064–1.097 g/ mL). Because CD15 was used for enumeration of granulocytes, some monocytes were also counted, leading to a second peak in the granulocyte data. The normal curve for granulocytes in figure 10.3 is fitted through all points, excluding densities between 1.065 and 1.075 g/ mL resulted in a normal curve with a 43% smaller standard deviation, and a 0.002 g/ mL higher median density. A Percoll density of 1.050 g/ mL separates at least 95% of fibrin aggregates from blood cells.

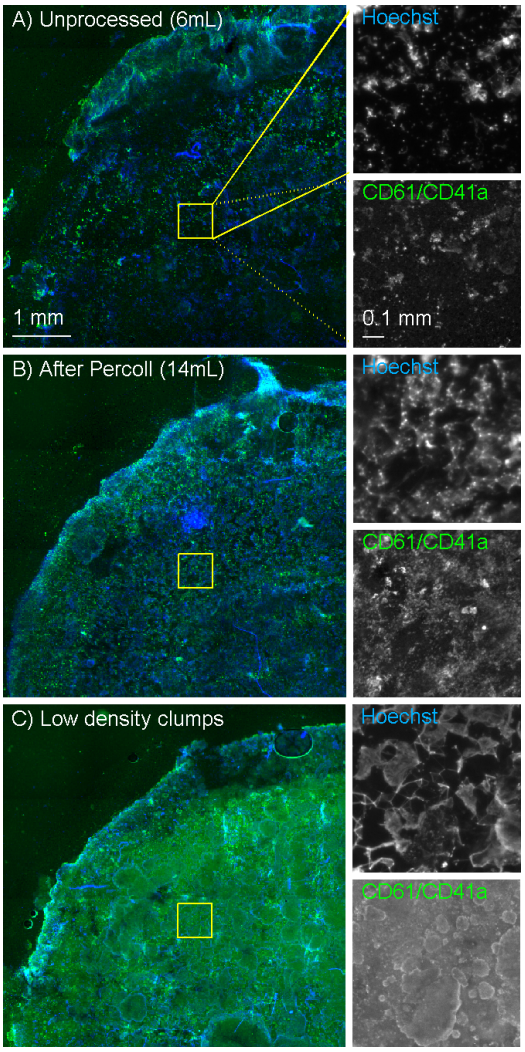

Figure 10.4: Reduction of clumps by Percoll density gradient. *Buffy coat filtrate on 8 µm track etch filter, stained with CD61-FITC, CD41a-FITC and Hoechst. Each panel on the left hand side shows a quarter of the filter with a false color overlay of the Hoechst and CD61/CD41a staining. The yellow square is shown in detail on the right. Three samples from the same 26 hour old buffy coat were filtered. Panel A shows an unprocessed sample. The buffy coat was split with Percoll into an aggregate depleted (panel B) and aggregate enriched fraction (panel C). Values in parenthesis show total buffy coat volume processed until pressure reached 300 mbar.*

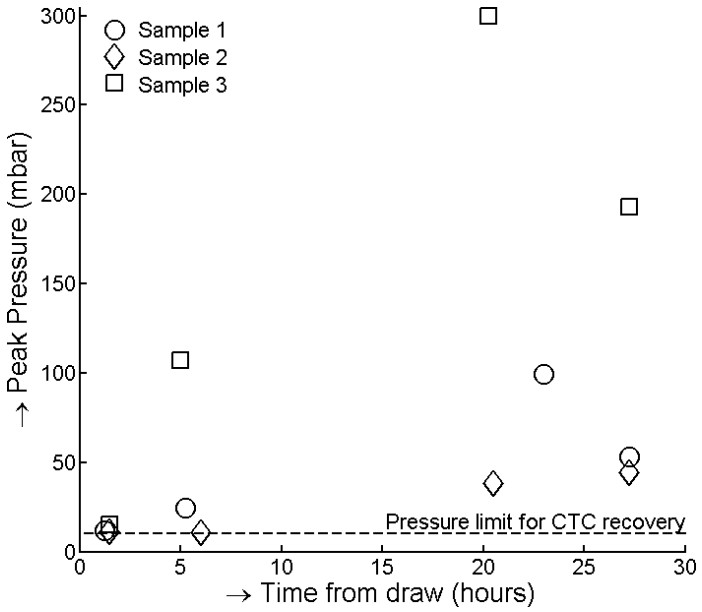

Figure 10.5: Peak pressure achieved during filtration of 100 mL of bovine blood versus sample age. *Whole blood from three cows was filtered through 4 filters in parallel. The peak pressure should not exceed 10 mbar to prevent loss of circulating tumor cells, indicated by the dashed line. This is almost achieved for 1 hour old samples.*

10.3.3 Fibrin aggregates are not eliminated by density separation

Removal of aggregates with Percoll increased the volume of sample that could be processed by approximately two-fold. Of the unprocessed samples we could process 2, 6 and 16 mL, while of the component with density higher than 1.050 g/ mL we could process 5, 14 and 25 mL. Figure 10.4, panels A and B show the distribution of CD41a/CD61 and Hoechst staining on a quarter of the filter from the sample where we could process 6 mL unprocessed sample and 14 mL sample depleted of aggregates. Panel A and B have similar components on the filter, but the processed sample in panel B appears to have many more aggregates. Figure 10.4, panel C shows the same staining of the aggregate enriched component. This filter is covered with a seemingly continuous layer of fibrin aggregates.

10.3.4 Samples need to be processed as fresh as possible

Passage of 100 mL of bovine blood through 4 filters in parallel results in higher pressures for older samples as shown in figure 10.5. The pressure

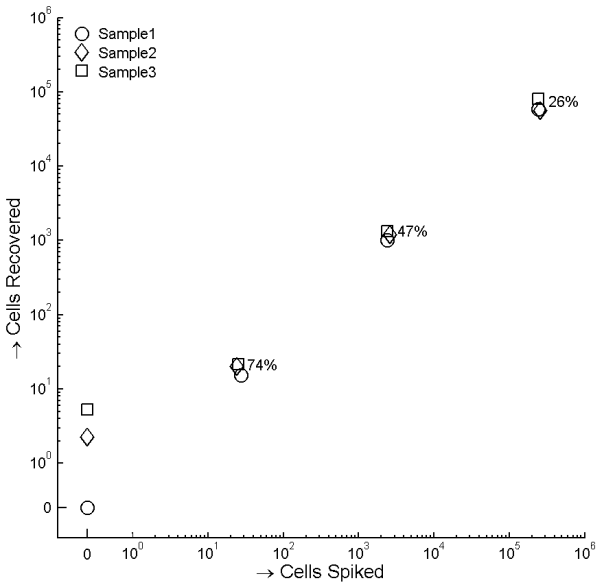

Figure 10.6: Recovery of SKBR3 cells spiked into 100 mL of whole bovine blood. *Cells spiked versus cells recovered is shown in a logarithmic plot, with average recovery in % indicated for each spike level. Blood was less than 5 hours old. The false positive count from samples with no spike was low (0–5 cells).*

exceeds the desired pressure of 10 mbar at all time points. Pressure of blood samples processed the quickest (≈1 hour) was the lowest (11–15 mbar) and close to the target pressure of 10 mbar. The samples with pressure in excess of 100 mbar were covered in a cream coat, while the fresh samples had few clumps on the surface of the four filters. Three apheresis samples were filtered through 4 filters in parallel with white blood cells from 210 mL of whole blood. The complete sample could be filtered, with pressure never exceeding 20, 31, 38 mbar. Due to the low flow speed of 25 mL/h and low cell density, approximately 20% of the sample had sedimented in the tubing before the filters were reached.

10.3.5 Recovery of 50% is possible in 100 mL of fresh bovine blood

Pre-stained SKBR-3 cells were spiked into 100 mL of bovine blood at spikes of 0, 25, 2,500 and 250,000. These samples were filtered within 5 hours from draw. Results are shown in figure 10.6, the spike level for the 2,500 and 250,000 points are offset by up to 10% to improve readability of this graph. A low background of ≤ 5 false positives was found in the controls. Average

recovery with the 25 cell spike was 74%, with the 2,500 spike 47% and 26% with the 250,000 spike. Correcting for 5 false positives, the recovery with the 25 cell spike reduces to an average of 55%. While at the low spikes pressure during filtration was 23 mbar (range 14–34 mbar), with the high spike this pressure had increased to 68 mbar (range 42–89 mbar). Approximately $4 \cdot 10^5$ randomly distributed pores are available on the filter. Because a single cell blocks multiple pores, recovery of 100% on the $2.5 \cdot 10^5$ spike would occupy all pores.

10.4 Discussion

Enrichment of CTC by means of filtration can allow processing of large sample volumes, however this requires that the pressure during filtration is low enough to prevent CTC from passing through the filter within the time needed for processing the sample. One possibility for reducing the pressure during filtration is to increase the filter surface area, but this will also result in more captured white blood cells [35]. We tested buffy coats from whole blood and apheresis samples from humans as well as whole bovine blood. Processing 20–30 hour old buffy coats from 0.5 L of whole blood was not possible due to fibrin aggregates from smaller than 30 µm to larger than 1 mm in diameter. The large aggregates have a density less than 1.05 g/ mL, but removal of components with density less than 1.05 g/ mL did not completely remove the small aggregates. With bovine blood we demonstrated that the age of the sample is the cause of these aggregates, with very few aggregates found in 1 hour old blood and a high density of aggregates in 20+ hour old blood. It is unknown whether these fibrin aggregates form at a quicker rate in buffy coats. The apheresis samples were processed as soon as possible, yet the pressure during filtration was 30 mbar, six-fold higher than expected [32]. This could have been due to aggregates of cells that were found in the sample after thawing. We attempted to remove these aggregates with a 30 µm mesh, but it is possible that some aggregates smaller than 30 µm were present. Sample age is a critical parameter in CTC enrichment by means of filtration.

To demonstrate feasibility of enriching CTC from whole blood, we spiked SKBR-3 into 100 mL of bovine blood. Results of this spike experiment demonstrate that recovery of approximately 50% is achievable with these SKBR-3 cells. From previous experiments we know that MDA-231 cells are a better model of breast CTC found in patients than SKBR-3 [35], and the spike experiment should be repeated with this more challenging cell line. Of patients with breast cancer, 4% has more CTC/ mL than our highest spike. At our highest spike recovery had reduced to 25%, suggesting that a reduced number of CTC would be found in these patients. While this recovery is low, a large number of CTC would still be available for further characterization. During filtration at the high spike, pressure rose from 23

to 68 mbar, increasing the speed at which SKBR-3 move through the filter. Increased filter surface area will increase the number of SKBR-3 and white blood cells captured.

The densities of blood components determined using Percoll match those reported in literature [34], except for platelets. The latter discrepancy can be explained by the size of the platelets, requiring larger g-force to settle to the correct density band. Cells from the SKBR-3, MCF-7, MDA-231 and HS-578-T tumor cell lines were lighter than all blood components except plasma and platelets. This property is exploited in CTC enrichment methods using density separation [36]. While the difference in density between cells from tumor cell lines and blood cells is clear, it is unknown whether the same difference applies to actual CTC. Indeed, cells from tumor cell lines have a relatively narrow size distribution while CTC have a wide size distribution [35] with great variation in the nuclear to cytoplasmatic ratio [37]. Both variations may lead to different densities of CTC, which has implications for the density band that needs to be collected in leukopheresis for CTC. The density of CTC could possibly be determined using the RareCyte system [38]. If the density of CTC matches that of cells derived from tumor cell lines, then a density band of 1.020 to 1.055 g/ mL could be collected, leading to 10^8 monocytes/lymphocytes, all platelets and CTC. However, if all mononuclear cells need to be collected, this band needs to be 1.020 to 1.077 g/ mL, leading to 10^{10} monocytes/lymphocytes. Immunomagnetic CTC enrichment from a sample with 10^8 cells is possible.

Leukapheresis allows for the selective enrichment of cells in a density range that can be set by the operator [39]. Mild complications typically associated with 11–21% normal blood donations [40] are observed in only 2% of apheresis donations because donors who have complications in normal donations are typically not asked for apheresis procedures [41]. Other complications include effects of hypocalcaemia due to prolonged use of anticoagulants in 0.4% of cases, and air embolism or hemolysis in $< 0.01\%$ of cases [42]. Apheresis of mononuclear white blood cells can be performed multiple times per year without significant complications [43]. Post collection platelet concentrations down to $69 \cdot 10^6$ platelets/ mL blood produce no clinically significant problems [44] (2.5–97.5 percentile range in normal donors is $150 \cdot 10^6$–$440 \cdot 10^6$ platelets/ mL blood [45]).

An alternative to leukapheresis is to filter the CTC directly from the blood in an extracorporeal circuit [46]. In such a circuit, whole blood passes through a CTC-trapping device after which it is returned to the patients. The advantage of this circuit is that it eliminates problems associated with sample aging. The device containing CTC may then be separated from the circuit and further processing performed. Complications with a CTC-trap are expected to be similar to the complications with apheresis, provided materials used for the construction of the trap are sufficiently biocompatible. An advantage over apheresis would be that very few blood cells are lost in a CTC-trap. To process a 5 L whole blood sample within one hour

while maintaining a pressure below 10 mbar an 8 µm track-etched filter surface of 1 dm^2 is needed [32]. This will lead to a sample containing CTC and approximately $6 \cdot 10^6$ white blood cells [35]. Such a sample will need further enrichment for use in combination with a standard imaging cytometer, or alternatively a high throughput analysis method [47, 48] is needed. Processing an apheresis sample with 10^{10} cells will require a 0.5 dm^2 filter.

Enrichment of CTC directly from the blood in an extracorporeal CTC-trap would resolve any issues related to sample age. This trap could enrich CTC using EpCAM expression, size filtration or density. CTC enrichment using EpCAM is a clinically proven approach [1, 2, 3, 4, 5, 6, 7], but is possibly a larger challenge to implement in a CTC-trap. While a large area filter is easily constructed, clinical proof for the efficacy of CTC filtration is lacking. Both devices will need to be tested for compatibility with patients. Apheresis is well established for use in patients and CTC enrichment of the apheresis product does not need to be compatible with the patient. The CTC density range should be determined before a CTC apheresis device can be constructed.

Acknowledgements

The authors wish to acknowledge J. van der Linde and N. van der Velde for experimental contributions, H. Vrielink (Sanquin blood banks, Amsterdam, Netherlands) for assistance in obtaining blood bank samples, I. Slomp (Medisch Spectrum Twente, Enschede, Netherlands) for providing apheraesis products.

10.5 References

[1] M. Cristofanilli, G. T. Budd, M. J. Ellis, A. Stopeck, J. Matera, M. C. Miller, J. M. Reuben, G. V. Doyle, W. J. Allard, L. W. Terstappen, and D. F. Hayes, "Circulating tumor cells, disease progression, and survival in metastatic breast cancer," *N. Engl. J. Med.*, vol. 351, pp. 781–791, Aug 2004.

[2] J. S. de Bono, H. I. Scher, R. B. Montgomery, C. Parker, M. C. Miller, H. Tissing, G. V. Doyle, L. W. Terstappen, K. J. Pienta, and D. Raghavan, "Circulating tumor cells predict survival benefit from treatment in metastatic castration-resistant prostate cancer," *Clin. Cancer Res.*, vol. 14, pp. 6302–6309, Oct 2008.

[3] S. Matsusaka, K. Chin, M. Ogura, M. Suenaga, E. Shinozaki, Y. Mishima, Y. Terui, N. Mizunuma, and K. Hatake, "Circulating tumor cells as a surrogate marker for determining response to chemotherapy in patients with advanced gastric cancer," *Cancer Science*, vol. 101, pp. 1067–1071, 2010.

[4] J. Tol, M. Koopman, M. C. Miller, A. Tibbe, A. Cats, G. J. Creemers, A. H. Vos, I. D. Nagtegaal, L. W. Terstappen, and C. J. Punt, "Circulating tumour cells early predict progression-free and overall survival in advanced colorectal cancer patients treated with chemotherapy and targeted agents," *Ann. Oncol.*, vol. 21, pp. 1006–1012, May 2010.

[5] M. G. Krebs, R. Sloane, L. Priest, L. Lancashire, J. M. Hou, A. Greystoke, T. H. Ward, R. Ferraldeschi, A. Hughes, G. Clack, M. Ranson, C. Dive, and F. H. Blackhall, "Evaluation and prognostic significance of circulating tumor cells in patients with non-small-cell lung cancer," *Journal of Clinical Oncology*, vol. 29, pp. 1556–1563, 2011.

[6] C. Rao, T. Bui, M. Connelly, G. Doyle, I. Karydis, M. R. Middleton, G. Clack, M. Malone, F. A. W. Coumans, and L. W. M. M. Terstappen, "Circulating melanoma cells and survival in metastatic melanoma," *International Journal of Oncology*, vol. 38, pp. 755–760, 2011.

[7] T. J. N. Hiltermann, J. J. W. Liesker, A. van den Berg, J. H. Schouwink, W. J. A. Wijnands, G. S. M. A. Kerner, H. M. Boezen, M. M. Pore, F. A. E. Kruyt, W. Timens, H. Tissing, A. G. J. Tibbe, L. W. M. M. Terstappen, and H. J. M. Groen, "Circulating tumor cells in small cell lung cancer, a predictive and prognostic factor," *Annals of Oncology*, p. In press, 2012.

[8] F. Coumans, S. T. Ligthart, and L. W. M. Terstappen, "Challenges in the enumeration and phenotyping of CTC," *Clinical Cancer Research*, 2012.

[9] M. Kagan, D. Howard, T. Bendele, J. Mayes, J. Silvia, M. Repollet, J. Doyle, J. Allard, N. Tu, T. Bui, T. Russell, C. Rao, M. Hermann, H. Rutner, and L. Terstappen, "A sample preparation and analysis system for identification of circulating tumor cells," *J Clinical Ligand Assay*, vol. 25, pp. 104–50, 2002.

[10] J. S. de Bono, G. Attard, A. Adjei, M. N. Pollak, P. C. Fong, P. Haluska, L. Roberts, C. Melvin, M. Repollet, D. Chianese, M. Connely, L. W. Terstappen, and A. Gualberto, "Potential applications for circulating tumor cells expressing the insulin-like growth factor-I receptor," *Clin. Cancer Res.*, vol. 13, pp. 3611–3616, Jun 2007.

[11] S. Riethdorf, V. Muller, L. Zhang, T. Rau, S. Loibl, M. Komor, M. Roller, J. Huober, T. Fehm, I. Schrader, J. Hilfrich, F. Holms, H. Tesch, H. Eidtmann, M. Untch, G. von Minckwitz, and K. Pantel, "Detection and HER2 expression of circulating tumor cells: prospective monitoring in breast cancer patients treated in the neoadjuvant GeparQuattro trial," *Clin. Cancer Res.*, vol. 16, pp. 2634–2645, May 2010.

[12] B. Franken, M. De Groot, L. Terstappen, W. Mastboom, J. Van der Palen, and A. Tibbe, "Circulating tumor cells, disease recurrence and survival in newly diagnosed breast cancer," in *Proceedings of San Antonio Breast Cancer conference*, 2011.

[13] M. Ignatiadis, F. Rothé, C. Chaboteaux, V. Durbecq, G. Rouas, C. Criscitiello, J. Metallo, N. Kheddoumi, S. Singhal, S. Michiels, *et al.*, "Her2-positive circulating tumor cells in breast cancer," *PloS one*, vol. 6, no. 1, p. e15624, 2011.

[14] B. Rack, C. Schindlbeck, A. Schneeweiss, J. Hilfrich, R. Lorenz, M. Beckmann, K. Pantel, W. Lichtenegger, H. Sommer, and W. Janni, "Prognostic relevance of circulating tumor cells (CTCs) in peripheral blood of breast cancer patients before and after adjuvant chemotherapy: The german success-trial," *J Clin Oncol*, vol. 26, no. 15S, p. 503, 2008.

[15] L. Scholten, L. Terstappen, J. van der Palen, W. Mastboom, A. Tibbe, I. Vermes, and M. de Groot, "Circulating tumor cells as a possible prognostic tool in newly diagnosed nonmetastatic colorectal cancer?," in *ASCO Meeting Abstracts*, 2012.

[16] W. J. Allard, J. Matera, M. C. Miller, M. Repollet, M. C. Connelly, C. Rao, A. G. Tibbe, J. W. Uhr, and L. W. Terstappen, "Tumor cells circulate in the peripheral blood of all major carcinomas but not in healthy subjects or patients with nonmalignant diseases," *Clin. Cancer Res.*, vol. 10, pp. 6897–6904, Oct 2004.

[17] C. Alix-Panabieres, J. P. Brouillet, M. Fabbro, H. Yssel, T. Rousset, T. Maudelonde, G. Choquet-Kastylevsky, and J. P. Vendrell, "Characterization and enumeration of cells secreting tumor markers in the peripheral blood of breast cancer patients," *J. Immunol. Methods*, vol. 299, pp. 177–188, Apr 2005.

[18] A. H. Talasaz, A. A. Powell, D. E. Huber, J. G. Berbee, K. H. Roh, W. Yu, W. Xiao, M. M. Davis, R. F. Pease, M. N. Mindrinos, S. S. Jeffrey, and R. W. Davis, "Isolating highly enriched populations of circulating epithelial cells and other rare cells from blood using a magnetic sweeper device," *Proc. Natl. Acad. Sci. U.S.A.*, vol. 106, pp. 3970–3975, Mar 2009.

[19] S. Nagrath, L. V. Sequist, S. Maheswaran, D. W. Bell, D. Irimia, L. Ulkus, M. R. Smith, E. L. Kwak, S. Digumarthy, A. Muzikansky, P. Ryan, U. J. Balis, R. G. Tompkins, D. A. Haber, and M. Toner, "Isolation of rare circulating tumour cells in cancer patients by microchip technology," *Nature*, vol. 450, pp. 1235–1239, Dec 2007.

[20] P. Balasubramanian, L. Yang, J. Lang, K. Jatana, D. Schuller, A. Agrawal, M. Zborowski, and J. Chalmers, "Confocal images of circulating tumor cells obtained using a methodology and technology that removes normal cells," *Molecular pharmaceutics*, vol. 6, no. 5, pp. 1402–1408, 2009.

[21] J. P. Gleghorn, E. D. Pratt, D. Denning, H. Liu, N. H. Bander, S. T. Tagawa, D. M. Nanus, P. A. Giannakakou, and B. J. Kirby, "Capture of circulating tumor cells from whole blood of prostate cancer patients using geometrically enhanced differential immunocapture (GEDI) and a prostate-specific antibody," *Lab Chip*, vol. 10, pp. 27–29, Jan 2010.

[22] T. Stakenborg, C. Liu, O. Henry, E. Borgen, N. Laddach, T. Roeser, M. Ritzi-Lehnert, C. Fermér, S. Hauch, C. OSullivan, *et al.*, "Automated genotyping of circulating tumor cells," *Expert Review of Molecular Diagnostics*, vol. 10, no. 6, pp. 723–729, 2010.

[23] S. L. Stott, C. H. Hsu, D. I. Tsukrov, M. Yu, D. T. Miyamoto, B. A. Waltman, S. M. Rothenberg, A. M. Shah, M. E. Smas, G. K. Korir, F. P. Floyd, A. J. Gilman, J. B. Lord, D. Winokur, S. Springer, D. Irimia, S. Nagrath, L. V. Sequist, R. J. Lee, K. J. Isselbacher, S. Maheswaran, D. A. Haber, and M. Toner, "Isolation of circulating tumor cells using a microvortex-generating herringbone-chip," *Proc. Natl. Acad. Sci. U.S.A.*, vol. 107, pp. 18392–18397, Oct 2010.

[24] U. Dharmasiri, S. Njoroge, M. Witek, M. Adebiyi, J. Kamande, M. Hupert, F. Barany, and S. Soper, "High-throughput selection, enumeration, electrokinetic manipulation, and molecular profiling of low-abundance circulating tumor cells using a microfluidic system," *Analytical chemistry*, vol. 83, pp. 2301–Ũ2309, 2011.

[25] S. Wang, K. Liu, J. Liu, Z. Yu, X. Xu, L. Zhao, T. Lee, E. Lee, J. Reiss, Y. Lee, *et al.*, "Highly efficient capture of circulating tumor cells by using nanostructured silicon substrates with integrated chaotic micromixers," *Angewandte Chemie International Edition*, vol. 50, no. 13, pp. 3084–3088, 2011.

[26] V. Hofman, M. Ilie, C. Bonnetaud, E. Selva, E. Long, T. Molina, J. Vignaud, J. Fléjou, S. Lantuejoul, E. Piaton, *et al.*, "Cytopathologic detection of circulating tumor cells using the isolation by size of epithelial tumor cell method: promises and pitfalls," *American journal of clinical pathology*, vol. 135, no. 1, pp. 146–156, 2011.

[27] H. Lin, S. Zheng, A. Williams, M. Balic, S. Groshen, H. Scher, M. Fleisher, W. Stadler, R. Datar, Y. Tai, *et al.*, "Portable filter-based microdevice for detection and characterization of circulating tumor cells," *Clinical Cancer Research*, vol. 16, no. 20, pp. 5011–5018, 2010.

[28] S. J. Tan, R. L. Lakshmi, P. Chen, W. T. Lim, L. Yobas, and C. T. Lim, "Versatile label free biochip for the detection of circulating tumor cells from peripheral blood in cancer patients," *Biosens Bioelectron*, vol. 26, pp. 1701–1705, Dec 2010.

[29] T. Xu, B. Lu, Y. Tai, and A. Goldkorn, "A cancer detection platform which measures telomerase activity from live circulating tumor cells captured on a microfilter," *Cancer research*, vol. 70, no. 16, pp. 6420–6426, 2010.

[30] M. Takao and K. Takeda, "Enumeration, characterization, and collection of intact circulating tumor cells by cross contamination-free flow cytometry," *Cytometry Part A*, vol. 79, no. 2, pp. 107–117, 2011.

[31] D. Adams, O. Makarova, P. Zhu, S. Li, P. Amstutz, and C. Tang, "Isolation of circulating tumor cells by size exclusion using lithography fabricated precision microfilters," in *Proceedings of the 102nd Annual Meeting of the American Association for Cancer Research*, (Orlando, FL, USA), AACR, April 2011.

[32] F. Coumans, G. van Dalum, M. Beck, and L. Terstappen, "Factors influencing filtration of tumor cells from whole blood," *submitted*, 2012.

[33] R. L. Eifler, J. Lind, D. Falkenhagen, V. Weber, M. B. Fischer, and R. Zeillinger, "Enrichment of circulating tumor cells from a large blood volume using leukapheresis and elutriation: Proof of concept," *Cytometry Part B-Clinical Cytometry*, vol. 80B, pp. 100–111, 2011.

[34] L. Strong, *Encyclopedia of Chemical Technology*, ch. Blood Fractionation, pp. 556–584. Interscience, 1948.

[35] F. Coumans, G. van Dalum, M. Beck, and L. Terstappen, "Filter requirements for circulating tumor cell enrichment and detection," *submitted*, 2012.

[36] R. Rosenberg, R. Gertler, J. Friederichs, K. Fuehrer, M. Dahm, R. Phelps, S. Thorban, H. Nekarda, and J. R. Siewert, "Comparison of two density gradient centrifugation systems for the enrichment of disseminated tumor cells in blood," *Cytometry*, vol. 49, pp. 150–158, Dec 2002.

[37] S. Ligthart, F. Bidard, C. Decraene, T. Bachelot, S. Delaloge, E. Brain, M. Campone, P. Viens, J. Pierga, and L. Terstappen, "Unbiased quantitative assessment of her-2 expression of circulating tumor cells in patients with metastatic and non metastatic breast cancer," *submitted*, 2012.

[38] T. Haubert, V. Contini, S. Grimes, R. Jones, and S. Wardlaw, "Buffy coat separator float system and method," Apr. 15 2008. US Patent 7,358,095.

[39] R. Graw Jr, G. Herzig, R. Eisel, and S. Perry, "Leukocyte and platelet collection from normal donors with the continuous flow blood cell separator," *Transfusion*, vol. 11, no. 2, pp. 94–101, 1971.

[40] B. Newman, "Donor reactions and injuries from whole blood donation," *Transfusion medicine reviews*, vol. 11, no. 1, pp. 64–75, 1997.

[41] B. McLeod, T. Price, H. Owen, D. Ciavarella, I. Sniecinski, M. Randels, and J. Smith, "Frequency of immediate adverse effects associated with apheresis donation," *Transfusion*, vol. 38, no. 10, pp. 938–943, 1998.

[42] J. Winters, "Complications of donor apheresis," *Journal of clinical apheresis*, vol. 21, no. 2, pp. 132–141, 2006.

[43] S. Sandler, J. Nusbacher, *et al.*, "Health risk of leukapheresis donors.," *Haematologia*, vol. 15, no. 1, p. 57, 1982.

[44] R. Rogers, H. Johnson, G. Ludwig, D. Winegarden, M. Randels, and R. Strauss, "Efficacy and safety of plateletpheresis by donors with low-normal platelet counts," *Journal of clinical apheresis*, vol. 10, no. 4, pp. 194–197, 1995.

[45] G. Lee, T. Bithell, J. Foerster, J. Athens, and J. Lukens, *Wintrobe's clinical hematology*. Lea & Febiger, Philadelphia, PA, 1993.

[46] T. Lögters, J. Altrichter, A. Paunel-Görgülü, M. Sager, I. Witte, A. Ott, S. Sadek, J. Baltes, J. Bitu-Moreno, A. Schek, *et al.*, "Extracorporeal immune therapy with immobilized agonistic anti-fas antibodies leads to transient reduction of circulating neutrophil numbers and limits tissue damage after hemorrhagic shock/resuscitation in a porcine model," *Journal of Inflammation*, vol. 7, no. 1, p. 18, 2010.

[47] C. G. Rao, D. Chianese, G. V. Doyle, M. C. Miller, T. Russell, R. A. Sanders, and L. W. Terstappen, "Expression of epithelial cell adhesion molecule in carcinoma cells present in blood and primary and metastatic tumors," *Int. J. Oncol.*, vol. 27, pp. 49–57, Jul 2005.

[48] H. B. Hsieh, D. Marrinucci, K. Bethel, D. N. Curry, M. Humphrey, R. T. Krivacic, J. Kroener, L. Kroener, A. Ladanyi, N. Lazarus, P. Kuhn, R. H. Bruce, and J. Nieva, "High speed detection of circulating tumor cells," *Biosens Bioelectron*, vol. 21, pp. 1893–1899, Apr 2006.

CHAPTER 11

Flat-top illumination profile in an epi-fluorescence microscope by dual micro lens arrays

F.A.W. Coumans, E. van der Pol, L.W.M.M. Terstappen
Cytometry Part A, 81A, p 324–331, doi:10.1002/cyto.a.22029, 2012

Abstract

Low uniformity in illumination across the image plane impairs the ability of a traditional epi-fluorescence microscope to quantify fluorescence intensities. Two Micro Lens Arrays (MLAs) were introduced into the illumination path of two different epi-fluorescence microscope systems to improve the uniformity of the illumination. Measurements of the uniformity of illumination were performed with a CCD camera in the focal plane and with fluorescent beads in the image plane. In semi critical alignment, a uniformity of illumination of 15–23% was found compared to 1–2% in the modified system. Coefficient of variation (CV) of fluorescent beads measured on the unmodified system was 20.4 ± 5.3% in semi critical alignment and 10.8 ± 1.3% in Koehler alignment. On the MLA systems CV was 7.9 ± 2.0% and on a flow cytometer the CV was 6.7 ± 0.7%. Implementation of MLAs in an epi-fluorescence microscope improves the uniformity of illumination, thereby reducing the variation in detection of fluorescent signals of the measured objects and becomes equivalent to that of flow cytometry.

11.1 Introduction

In a traditional epi-fluorescence microscope, there is a tradeoff between the illumination uniformity and power. Koehler illumination is used to achieve high uniformity at the expense of illumination intensity, whereas semi-critical alignment is used to achieve high illumination intensity at the expense of uniformity [1]. In Koehler illumination the light source is focused onto the back pupil of the objective, while in semi-critical illumination, the light source is focused slightly beyond the sample. Poor uniformity results in large spatial intensity variations at the focal plane, while low illumination intensity requires longer illumination times and results in additional bleaching of the sample. With Koehler alignment, an improvement in coefficient of variation CV can be obtained [2]. If a better CV is needed, the signal can be corrected by shading correction [3, 4] or by using the middle 50% of the image [5] to reduce the CV down to 3%. Multiplication is effective in cases where the illumination profile is well known and the signals are bright. In cases where the signal is dim, multiplication is not effective because signal to noise ratio is not changed. Reduction of the field of view increases the time needed for acquisition. A hardware solution that improves the CV without any of these disadvantages is desired. Previously, a double micro lens array (MLA) was used to improve the uniformity of the illumination from a tungsten-halogen lamp [6] and from lasers [7]. Here we demonstrate that epi-fluorescence microscopes equipped with a mercury arc lamp, can be retrofitted with a double MLA system to achieve the uniformity of Koehler alignment, while achieving the illumination intensity of semi-critical alignment. The need for such improvements arises from our desire to improve the sensitivity of detection of rare Circulating Tumor Cells (CTC) [8] and the improvement for the quantification of treatment targets present at low densities on these CTCs such as IGF-1R and Her-2 [9, 10, 11].

11.2 Materials and Methods

11.2.1 Epi-fluorescence microscope

Two epi-fluorescence microscopes were modified to test the implementation of a double MLA system. The first microscope is the CellTracks Analyzer II (Veridex LLC, Raritan, NJ, USA). Figure 11.1, panel A shows the optical diagram of the microscope. The illumination path contains a 100 W HBO lamp (USH-103D, Ushio, Cypress, CA, USA), a collection lens (Quartz Epi-FL Collector Lens, Nikon, Tokyo, Japan) and a plano-concave relay lens (fused silica focal length -150 mm, Edmund optics, Barrington, NJ, USA) to generate a collimated beam. Four custom designed filter cubes (blue: ex 365/20, em LP 400; green: ex 475/20, em 510/20; yellow: ex 547/12, em 578/25; red: ex 620/30, em 580/55; Corion, Franklin, MA, USA) direct a selected wavelength band to a 10x/NA0.45 objective (CFI

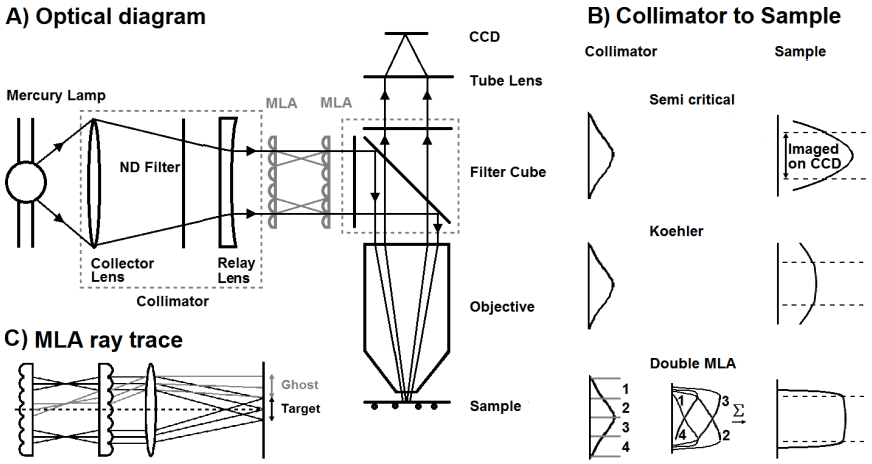

Figure 11.1: Microscope modifications. *(A) Optical diagram of the epi-fluorescence microscope with illumination and detection paths. Rays shown are for semi critical alignment. The collimator was optimized during modification of the microscope. Two micro lens arrays (MLA) were inserted between the relay lens and the filter cube (grey). (B) Cartoons illustrating the truncation of the illumination field in semi critical alignment Koehler alignment and in the MLA system.In the MLA system, the illumination field is split into pieces. Each piece is superimposed to yield a more uniform illumination. (C) Ray trace for MLA system, black lines illustrate how the rays passing through different lenslets are superimposed, grey lines show how incoming light with too high an angle forms a ghost image next to the target.*

plan apochromat, Nikon, Tokyo, Japan). The emitted light is collected by the objective and passed through the filtercube to a tube lens with 200 mm focal length (Infinity tube lens unit for CFI, Nikon, Tokyo, Japan) which forms an image on a TE cooled CCD camera (1412AM, DVC, Austin, TX, USA). In the focal plane, the area imaged is 0.90 x 0.67 mm and referred to as the pickup area. Figure 11.1, panel B illustrates that truncation of the illumination field results in inhomogeneous illumination using the unmodified system. The second system is the Eclipse 400 microscope system (Nikon, Tokio, Japan) equipped with a C4742-95 CCD camera (,Hamamatsu, Hamamatsu, Japan). The optical layout of the Eclipse is equivalent to the CellTracks Analyzer II. The same model 10x objective was used. The filter cubes had the same wavelength specifications, but were manufactured by Chroma (Bellows Falls , VT, USA). After measurements were performed with Koehler alignment the microscope was modified for measurements with the MLA system modification. Figure 11.1, panel C illustrates that the intensity of the illumination is reduced with Koehler alignment.

11.2.2 Double Micro Lens Array (MLA)

If the light bundle from the collimator is uniformly distributed, the illumination on the sample can be perfectly uniform. Typically, the bundle from the illuminator is not uniform, but the non-uniformity is symmetrical around the optical axis. This symmetry is used to achieve uniform illumination with an MLA pair. Two MLAs were introduced in the system as illustrated in figure 11.1, panel A. A MLA contains an array of lenslets, which split the incoming bundle into segments and can be used to produce homogeneous illumination. Each segment is imaged onto the focal plane, superimposed on top of each other as illustrated in figure 11.1, panel B and C. The non flatness of a segment of the incoming bundle is cancelled out by a segment on the opposite side of the optical axis. This results in a 'flat top' illumination profile with sloped sides. Using two MLAs in sequence this slope becomes very steep, reducing the power lost outside the pickup area. The ideal size of the flat top generated by a double MLA is slightly larger than the size of the pickup area to achieve high uniformity while maintaining the majority of illumination power inside the pickup area. The size of the flat top can be calculated with equation 11.1 [12]:

$$Y = \frac{p_L f_F}{f_{L1} f_{L2}}(f_{L1} + f_{L2} - s) \tag{11.1}$$

With Y the flat top cross section, p_L the pitch of the MLA, f_F the focal length of the objective, f_{L1} and f_{L2} the focal length of the first and second MLA respectively and s the distance between the two MLAs. With different pitches for x and y direction, a rectangular flat top is created. CC-Q-1015S and CC-Q-300S are the commercially available MLAs that match the pickup area closest and are made of UV transmitting quartz (SUSS Microoptics, Neuchâtel, Switzerland). The maximum input divergence of these two MLAs is 2 and 4 degrees respectively.

11.2.3 Collimator design

For the introduction of a double MLA in the system, the lenslets of both MLAs need to be aligned. Light that passes through the double MLA at an angle through non aligned lenslets will generate ghost images next to the pickup area, see figure 11.1, panel C. This limits the divergence that the MLA can handle. Various collimators consisting of the collector lens and the relay lens were tested for their power transmission and forward divergence. The collimators that were tested are illustrated in figure 11.2, panels A–E and include a single positive lens, a single negative lens, and a Galilean and Keplerian telescope.

All lenses used were 25 mm diameter fused silica plano-concave or plano-convex lenses (Edmund Optics, Barrington, NJ, USA) with focal lengths as shown in figure 11.2, panel G. The forward divergence and power

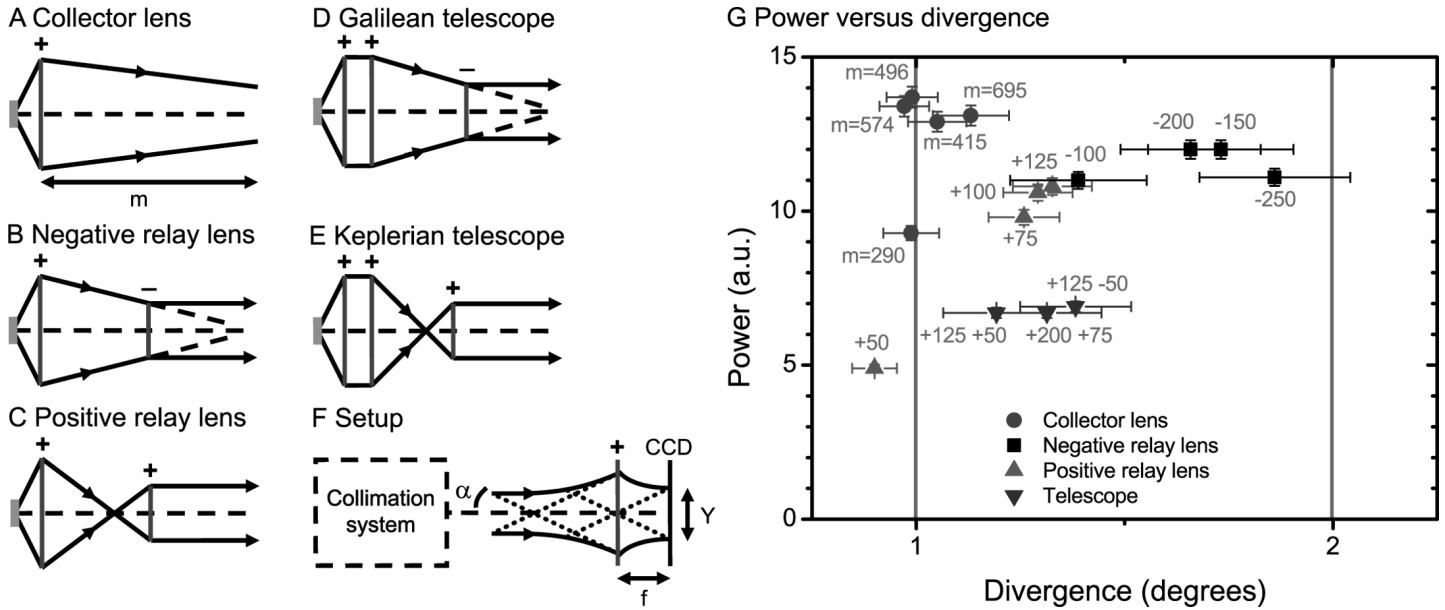

Figure 11.2: Collimator designs. *Consisting of (A) a collector lens only, (B) a negative relay lens, (C) a positive relay lens, (D) a Galilean telescope, and (E) a Keplerian telescope. (F) A CCD camera was placed in the focal plane Y of a positive lens with focal distance f to measure the divergence α and transmission power of each collimator. (G) Power versus normalized mean divergence for various collimators. For the collector lens collimators, the grey labels indicate the distance m. For the other collimators, the lens focal lengths are shown. The solid vertical lines indicate the specified maximum input divergence of two commercially available MLAs. The collector lens collimators have the highest power and the lowest divergence but require a large path length. Negative relay lens collimators perform well on power versus divergence while maintaining a compact system.*

transmission of each collimator were measured by imaging the output of the collimator through a single lens with focal length f=100 mm (50 mm diameter fused silica plano-concave lens, Edmund Optics, Barrington, NJ, USA) onto a CCD camera (1412AM, DVC, Austin, TX, USA), see figure 11.2, panel F. At the focal plane, the divergence α is related to the full width at half maximum of the bundle diameter Y by equation 11.2 [13]:

$$\alpha = \frac{Y}{2f} \tag{11.2}$$

The divergence for two perpendicular directions in the focal plane was determined, averaged, and normalized to the beam size as reduction in beam size increases the divergence linearly. Due to the size of the MLA, each collimator was aligned to achieve a full width at half maximum of less than 10 x 10 mm. The sum of the power on the CCD was taken as the transmitted power.

11.2.4 Calculations

To investigate the impact of each design parameter on the illumination in the focal plane, the Fraunhofer approximation of the scalar Fresnel-Kirchhoff diffraction theory is applied to calculate the one dimensional intensity distribution at the focal plane of the microscope objective as described elsewhere [14]. Our calculations are done in Matlab 2007b (Mathworks, Natick, MA, USA). For reference, a summary of the model components is given in supplemental S1, and the Matlab m-file in supplemental S2. Parameters used are based on the CC-Q-300S MLA and the Nikon 10x NA 0.45 objective.

11.2.5 Measurement of illumination quality

Collimators were implemented in the microscope together with the optimal MLA pair. The impact of this modification was determined on the same system before and after modification was complete for the four filter cubes. To determine the illumination quality, the intensity distribution was measured by placing a CCD camera (Deep sky imager II, monochrome CCD board version camera, Meade Instruments, Irvine, CA, USA) in the focal plane of the objective. The pickup area covers only 8% of the CCD area, therefore the obtained image can be used to measure the fraction η of the total transmitted light that hits the pickup area (equation 11.3) as well as the CV of illumination within the pickup area (equation 11.4). $\sum I_{pixel}$ is the sum of intensities for all pixels.

$$\eta = \frac{\sum_{Pickup} I_{pixel}}{\sum_{CCD} I_{pixel}} \cdot 100\% \tag{11.3}$$

$$CV = \frac{SD_{pickup}}{Mean_{pickup}} \cdot 100\% \tag{11.4}$$

Because the CCD camera did not fit in the Eclipse 400, measurements of the illumination quality were performed only in the CellTracks II.

11.2.6 Measurement of CV using fluorescent beads

Broad spectrum fluorescent magnetic beads (UMC4F COMPEL beads, Bangs Laboratories, Fishers, IN, USA) with diameter 8 µm were chosen in order to use the same sample cartridge used for the routine analysis of clinical samples in the microscope system. The sample cartridge is filled with beads and distributed equally over the analysis surface by means of the specific configuration of the magnets surrounding the chamber [8, 15]. Images were acquired to cover the analysis surface for each of the four fluorescent filter cubes and were analyzed in Matlab 2007b (Mathworks, Natick, MA, USA). In short, thresholds were set on the images at a level of three times the CCD readout noise, objects with sizes more than 20% over or under 8 µm diameter were excluded and the peak intensity of the remaining objects was determined. The bead cartridge was scanned on the unmodified CellTracks in semi critical alignment, the unmodified Eclipse 400 in Koehler alignment, and both microscopes equipped with the MLA systems. In addition the beads were scanned on a flow cytometer (FACSCalibur, BD Biosciences, San Jose, CA, USA) setup according to published guidelines [16]. Due to absence of a UV laser, beads were measured only in the green (FL1 488 - 530/30), yellow (FL2 488 - 585/42) and red (FL4 635 - 661/16) channel. Samples were run at a low flow rate (LO). Acquisition gate was set on forward scatter, minimum 15 (forward scatter of beads $\approx$ 150). No compensation was applied and CV and mean intensity were determined using FCS Express 4 (De Novo Software, Los Angeles, CA, USA). Gates were set around the peak intensity to exclude doublets. Histograms were created for all data and means and CV calculated. Since the detection method differs substantially, the data from the flow cytometer was multiplied by a correction factor to make the mean intensity value fall on the mean of the value measured on the two microscope systems.

11.3 Results

11.3.1 Collimator design

Figure 11.2, panel G shows the results of power and divergence measurements for different collimators. The different collimator designs are shown in annotations next to each data point. Highest power transmission with lowest divergence is achieved by the collector lens focused near infinity. The total path length was varied as needed to achieve best performance. Collimators consisting of just the collector lens were the only ones which

had high power transmission and a forward divergence not exceeding the maximum for the CC-Q-1015S MLA. With these collimators the path length from lens to first MLA will be very long (40–70 cm), which exceeds the size that fits within the microscope enclosure. The telescopes performed poorest on power transmission, possibly due to the 25 mm lens diameter used. The negative relay lens designs had good power transmission, did not exceed the maximum input divergence for the CC-Q-300S MLA and were the most compact collimators. The positive relay lens systems had lower forward divergence, but also lower power transmission and required more space than the negative relay lenses. The -150 mm lens is the most compact and has the highest power, while not exceeding the maximum forward divergence of the CC-Q-300S MLA. This collimator was therefore selected for the MLA system and implemented in the microscopes.

11.3.2 MLA simulations

The calculation parameters are $\alpha_{max} = 1.7°$, $f_F = 20$ mm, $f_L = 4.75$ mm, $N_0 = 32$, $p_L = 0.3$ mm, where α_{max} is the divergence, f_F is the focal length of the objective, f_L is the focal length of the lenslets of the MLA, N_0 is the number of lenslets, and p_L is the pitch of the lenslets. The spectral distribution of the mercury arc lamp was measured (not shown) and included in the model. Figure 11.3, panel A shows the calculated 1D illumination profile for the microscope containing a single MLA.

The illumination profile within the pickup area is homogeneous, but the power efficiency of 8.3% is rather low. Figure 11.3, panel B shows the calculated illumination profile after addition of the second MLA. The distance s between the two MLAs is equal to f_L, resulting in a wide flat top with steep edges and a power efficiency of 37.3%. By increasing s the flat top becomes smaller, with less steep edges. Figure 11.3, panel C shows the calculated illumination profile for two MLAs separated by a distance s equal to 1.5 times f_L. Now, the power efficiency is 64.8% at the expense of homogeneity, since the edges of the flat top also fall within the pickup area.

11.3.3 Measurement of the illumination quality

The results of the measurement of the CV under the objective are shown in figure 11.4 and table 11.1. Figure 11.4 shows the illumination intensity distribution of the CellTracks system before and after modification.

Table 11.1 shows the illumination efficiency η and the CV within the pickup area for all channels. In the unmodified microscope, CVs of 15–23% are measured, while in the MLA modified microscope they are 1.2–1.5%. The illumination efficiency is slightly better for the MLA modified microscope (38–43%) compared to the same microscope before modification (28–40%).

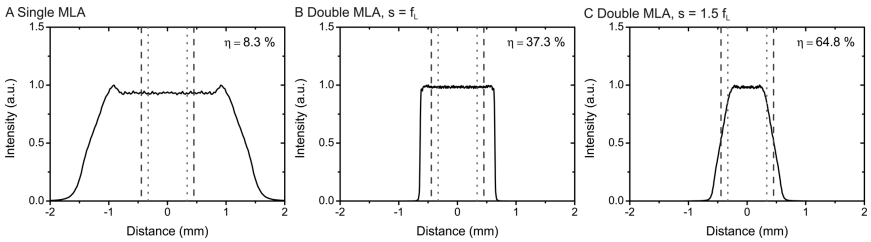

Figure 11.3: Calculated 1D illumination profile for the epi-fluorescence microscope. *Containing (A) a single MLA, (B) two MLAs separated by a distance s equal to the focal length of the lenslets f_L, and (C) two MLAs separated by a distance s equal to 1.5 times f_L. The dashed and dotted lines indicate the pickup area, which is given by the width at the focal plane - in both directions - that is imaged on the CCD chip. The power efficiency η is the ratio between the power at the pickup area and the total power. (A) The illumination profile of the pickup area for a microscope containing a single MLA is homogeneous, but the power efficiency is low. (B) By adding a second MLA at distance $s = f_L$ the illumination profile remains homogeneous and the power efficiency increases 4.5-fold. (C) By increasing the distance s to $1.5f_L$ the power efficiency increases another 1.7-fold at the expense of homogeneity.*

Table 11.1: Illumination efficiency (η,%) and CV (%) measurements on the microscope system before (EPI) and after modification (MLA).

	EPI		MLA	
	η	CV	η	CV
DAPI	28	14.8	38	1.4
FITC	34	18.4	41	1.5
PE	36	18.4	42	1.2
APC	40	23.1	43	1.3

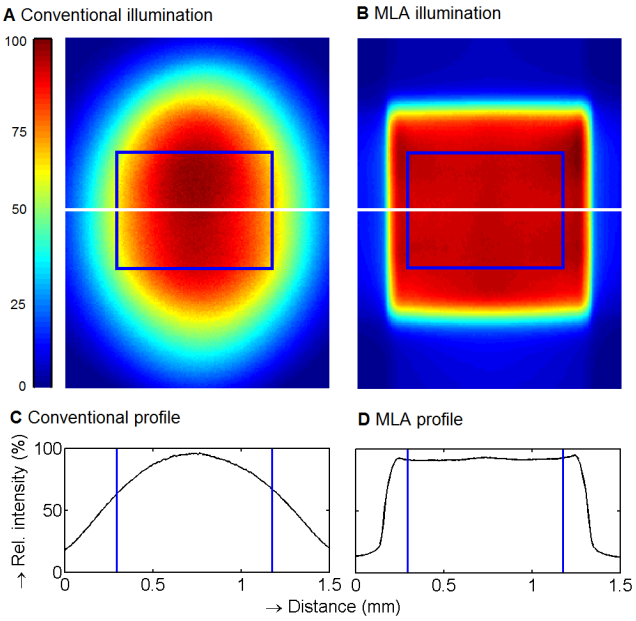

Figure 11.4: Normalized illumination profile. *Of (A) the conventional microscope and (B) the modified microscope containing two MLAs. The solid blue lines mark the pickup area, which is the area that is imaged by the CCD of the microscope. The white horizontal line indicates the position where a cross section of the illumination profile of (C) the conventional microscope and (D) the modified microscope was taken. The illumination profile of the same microscope before and after modification shows a large improvement in homogeneity.*

11.3.4 Measurement of CV using magnetic fluorescent beads

Figure 11.5 shows an image of fluorescent beads with the Nikon in Koehler, semi-critical alignment and with the MLA modification. Figure 11.6 shows histograms for the beads measured with the 4 fluorescence cubes. The histograms show that the *CV* of the MLA CellTracks system is much improved compared to the *CV* measured on the unmodified CellTracks. The intensity on the MLA system is higher than semi-critically aligned microscope by 20–160%. The *CV* on the MLA Eclipse 400 is slightly improved and the signal level is 2–4 fold higher when compared to a Koehler aligned Eclipse 400. The *CV* measured on the flow cytometer equipped with a 488 nm and 633 nm laser was similar to the *CV* found with the MLA systems.

Figure 11.5: Image of beads under epi fluorescence microscope in MLA alignment, semi critical and Koehler alignment. *Arrows point to the enlargements in the corners of the sceen. The bead in the middle (vertical arrow, enlargement on top) is equally bright on both MLA and semi critical system, but dimmer on the Koehler system. The bead in the corner (horizontal arrow enlargement on bottom), is brightest on the MLA, and dimmer on both semi critical (low illumination intensity in corners) and Koehler system (uniform illumination with lower overall intensity)*

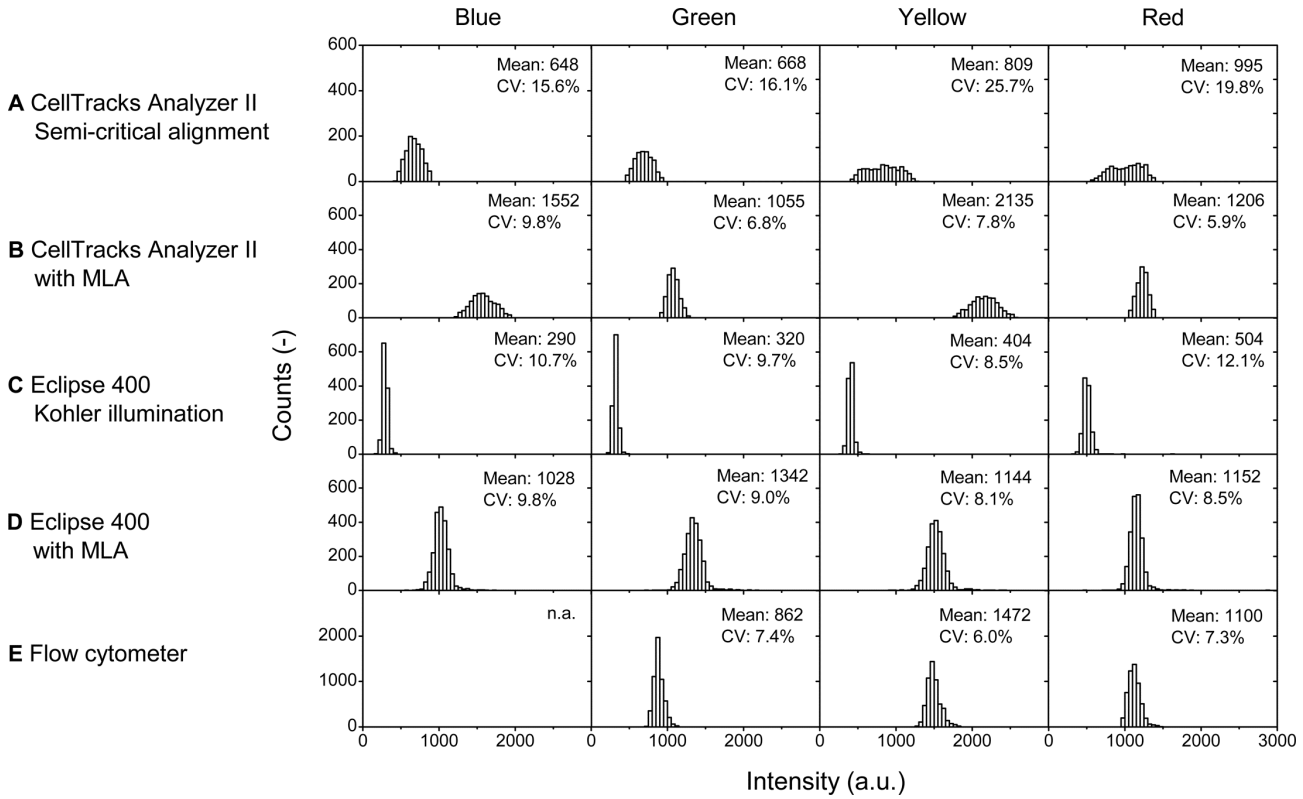

Figure 11.6: Intensity distributions of beads measured by the semi critically aligned CellTracks microscope (A), the Koehler aligned Eclipse 400 (B), the modified Eclipse 400 containing 2 MLAs (C), the modified CellTracks (D) and a flow cytometer (E). *Measurements on the microscopes were performed with filter cubes with blue, green, yellow and red emission. The flowcytometer measurements were performed with 488 nm laser line excitation and filters tuned for yellow and green detection and the 633 nm laser line with filters for red detection. No measurement was available for the UV/blue region because the flowcytometer lacked a UV laser. The intensity distributions obtained by the flowcytometer are scaled on the mean intensities obtained on the conventional and modified microscopes.*

11.4 Discussion

A double MLA is introduced in an epi-fluorescence microscope to improve the homogeneity of the illumination resulting in an improvement in the sensitivity and quantification of fluorescent signals. Automated image analysis algorithms for detection of fluorescently labeled cells can greatly benefit from such improvement as they apply a threshold on the measured fluorescence intensity to discriminate between the labeled and non-labeled cells in the sample. The efficacy of thresholding strongly depends on the homogeneity of the illumination as inhomogeneous illumination will result in a variation of the detection limit across the image and impairs reliable quantification. An application in need for such improvement is the identification of fluorescently labeled CTC in images acquired by fluorescent microscopy in for example the CellSearch system [8]. In this system CTC candidates are identified as objects that express cytokeratin labeled Phycoerythrin (CK-PE). The efficiency of detection of cells with relatively low CK-PE signals will thus vary across the image and can greatly benefit from a homogeneous illumination. For assessment of treatment targets on these tumor cells, low intensity expression will result in some cells being missed, pending on the illumination of the specific area and quantification will be hampered by the lack of uniformity.
A variety of approaches can be applied to improve the homogeneity of the illumination of epi-fluorescence microscopes such as the use of aspheric lenses and mirrors [17], diffractive optics [18], ND filters [19] and engineered diffusers [20]. Aspheric lenses and mirrors perform well with Gaussian beams, but the mercury arc lamp does not produce a Gaussian beam. Diffractive optical elements are designed for a specific wavelength, which makes them unsuitable for use in an application where 4 different illumination bands are used. ND filters can achieve excellent uniformity, but the cost is an order of magnitude reduction in light intensity, making them unsuitable for a low light level application. If custom dimensioned for application in this system, engineered diffusers are expected to be similar in performance to the MLAs presented. Available standard versions would however result in too much loss of power and a custom design was too costly to implement. In addition the images from a Koehlered microscope could be corrected in a post processing step if the illumination profile is known. Such a procedure reduces spatial dependence of signal level, but does not improve signal to noise ratio, which is most important when dealing with dim signals.
Implementation of double MLA in an epi-fluorescence microscope improves the uniformity of illumination without sacrificing illumination intensity when compared to semi critical alignment and improves illumination intensity without sacrifice to illumination uniformity when compared to Koehler alignment. Implementing the MLA system is relatively simple and cost effective. In supplemental S3 we describe how other epi-fluorescence microscopes can be modified and aligned. In contrast to Koehler alignment,

the alignment of the MLA system is stable and does not need frequent optimization. The only alignment that may be needed is that of the lamp after bulb replacement. Because the size of the field of view is matched to the CCD camera the use of binoculars on the same system would result in a smaller field of view and additional modifications would be needed when this is not desired. The distance between the last MLA and back focal plane of the objective needs to be less than 100 mm to achieve optimal performance. To achieve this, we had to remove the objective turret in the Eclipse 400. A sufficiently compact objective turret is possible, but not available from Nikon at this time. This distance limitation could be mitigated by making the system telecentric, but doing so would require much larger micro lens arrays and thus a more extensive modification of our microscopes. Several collimator designs were tested. A single collection lens without further optics performed best with respect to power and forward divergence, but required too much length to make application practical in the microscope. We did implement a negative relay lens collimator, which achieved similar power with a small increase in forward divergence. The differences in the power transmission and divergence with the various collimator designs may be partially explained by a different distance between arc lamp and the collector lens, changing the effective NA of the collector lens.

The 100 W HBO lamp has an arc with a high power density, making it relatively easy to collimate and achieve low divergence angle. Higher power lamps tend to have larger arcs, which are harder to collimate. Selection of an MLA pair with a higher maximum divergence angle may allow for creation of a flat top with a higher power light source, and thus allow higher brightness on the sample.

Modeling shows that the size of the flat top can be tuned by changing the inter MLA distance, allowing compensation of a mismatch between CCD and MLA dimensions at the cost of some illumination power. We measured an illumination CV of 1.2–1.5% and an efficiency of 38–43% using a camera underneath the objective, which matched our theoretical model quite well. We estimate a further 25% increase in illumination intensity could be gained by custom designing an MLA array to match the CCD camera. We did not measure the same low CV using beads in normal imaging mode. In both microscope systems, the MLA modified microscope outperformed the unmodified microscope. The MLA modified CellTracks performed better than the MLA modified Nikon Eclipse. This difference may be attributed to two factors; First the Nikon body design limits dimensions between the different components of the illumination path and second mechanical modifications may not have been sufficiently precise for best results. The CV measured on the flow cytometer was similar to the CV measured on the MLA modified microscope, which makes it likely that the measured CV can mainly be contributed to the CV of the beads. An exact comparison of flow cytometry to the MLA imaging system is not possible because the exclusion of doublets and noise are handled differently due to hardware

differences. Even though the signal intensity was higher on the MLA system compared to the conventional system, comparisons are difficult because the intensities between different microscopes can vary by up to two fold. Implementation of MLAs in epi-fluorescence microscopes is uncomplicated, inexpensive, and can improve the detection of cells with low antigen expression as it no longer depends on the position of a cell in the image. In addition, smaller differences in antigen expression between different cells can be detected which improves the quantification of antigen expression.

Acknowledgements

The authors acknowledge Jan Key for performing flow cytometry on the beads.

11.5 Supplemental S1 - Model for double MLA in mercury based 10x epi fluorescence microscope

For modeling the MLA system, the Fraunhofer approximation of the scalar Fresnel-Kirchoff diffraction theory is applied [21]. Lenses are approximated as infinitely thin. The system is modeled in one lateral dimension, expanding the model to two dimensions is straightforward. Three major steps are taken to construct the double MLA model:

1. Wave passing through single lenslet, equations 11.5 - 11.11, figure 11.7, panel A.
2. Expansion to wave passing through array of lenslets, equations 11.15, 11.12, figure 11.7, panel B/C, and imaged by field lens, panel D.
3. Addition of a second array of lenslets identical to the first, equations 11.17,11.20, figure 11.7, panels E/F.

Notation is as follows (see figure 11.8 for an example for the double MLA); $\mathfrak{F}$ is used for Fourier transformation, z is the distance along the optical axis, y the distance perpendicular to it. Superscript - and + signs denote whether a position before or after the lens is described, subscript L or $L1$ is used for the first MLA or part thereof, subscript $L2$ is used for the second MLA. Subscript F is used for the field lens or objective and subscript O denotes the observation plane, or sample plane. See figure 11.8 for a diagram with this notation. Symbols used are α the angle of incidence, λ the wavelength of the incoming wave, k the wavenumber $(2\pi/\lambda)$, s the distance between two MLA, p the pitch of the MLA, f the focal length, R the radius of curvature and n the refractive index of a lens in the MLA. In

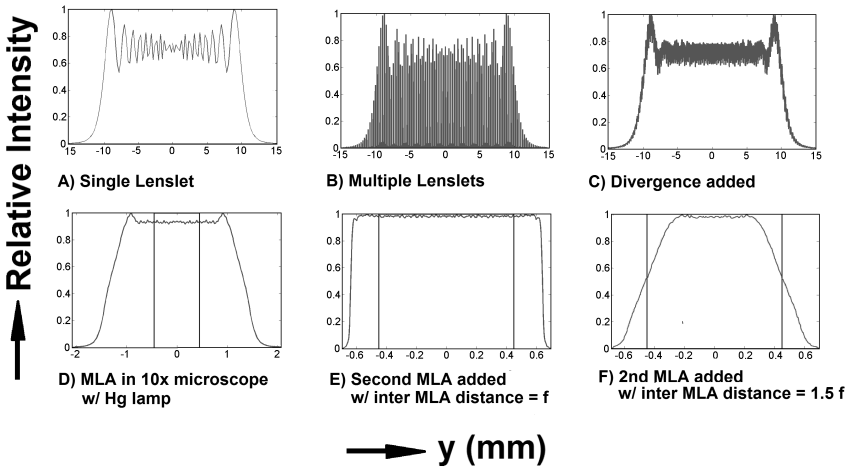

Figure 11.7: Model of an imaging MLA system. *In panels D–F the pickup area is indicated with vertical lines. Panel A shows a monochromatic plane wave that has passed through a single lenslet. Panel B shows a monochromatic plane wave passing through an array of lenslets, an MLA. Panel C shows a monochromatic wave with 0.7° divergence passing through the MLA. Panel D shows the wave passing through an MLA and a 10x objective. The spectrum of a HBO lamp is taken into account. In panels E and F a second MLA is also added. By changing the distance between the MLAs from the MLA focal length (E) to 1.5 times the MLA focal length (F), the width of the flat top is changed, and the power within the vertical lines is changed from 70% of the total (E) to 90% of the total (F).*

the Matlab simulations we started with a monochromatic plane wave of λ = 520 nm, Micro lens array properties p_L 0.3 mm, f_L 4.75 mm and f_F 20 mm, α_{max} was 1.7° and for the polychromatic source the 520 nm HBO arc line was used. We introduced divergence and polychromaticity after the contribution of an array of lenslets was derived. This nicely illustrates the contribution of each parameter to the final distribution. Figure 11.7, panels A–F illustrates the illumination field. All plots are normalized to the maximum value of the distribution.

If we assume the collimator lens is perfect and infinite in size, and our light source is monochromatic, the illumination impinging onto a lenslet can be expressed by a number of plane waves of the form:

$$U_L(y', z_L^-; \alpha, \lambda) = P(\lambda) e^{iky' sin(\alpha)} \tag{11.5}$$

With $P(\lambda)$ the spectral distribution of the light source. The transmitted field immediately behind the lenslet is given by:

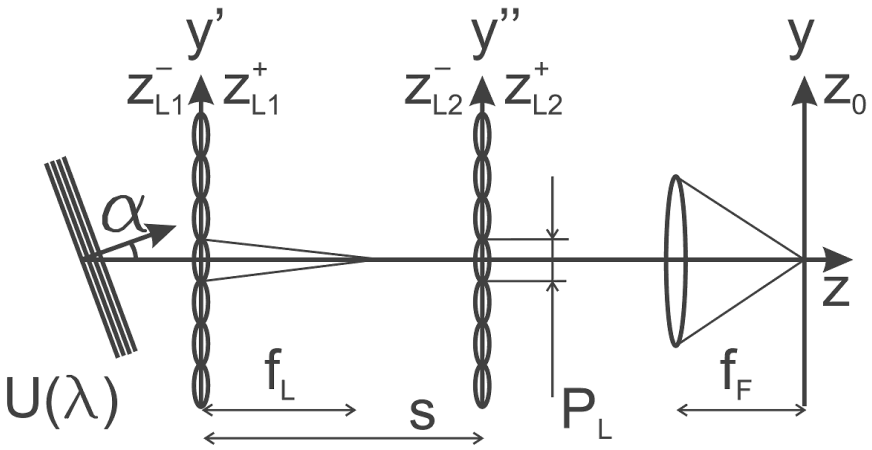

Figure 11.8: Model parameters for double MLA system.

$$U_L(y', z_L^+; \alpha, \lambda) = U_L(y', z_L^-; \alpha, \lambda) T_L(y') \tag{11.6}$$

Under the assumption that the lenslets are parabolic in shape and the fill factor of each lenslet is unity, the transmission function can be described as:

$$T_L(y') = e^{\frac{i\pi y'^2}{\lambda f_L}} rect\left(\frac{y'}{p_L}\right) \tag{11.7}$$

$$rect\left(\frac{y'}{p_L}\right) = \begin{cases} 1 & \text{if } |y'| \leq p_L/2 \\ 0 & \text{if } |y'| > p_L/2 \end{cases} \tag{11.8}$$

The focal distance of a single lenslet is given by $f_L = R_L/(n(\lambda) - 1)$. The amplitude distribution in the observation plane from a single lenslet is obtained by Fourier transformation:

$$\begin{aligned} U_L(y, z_0; \alpha, \lambda) &= \mathfrak{F}_{f_F}\{U_L(y', z_L^+; \alpha, \lambda)\} \\ &= \int_{-\infty}^{\infty} U_L(y', z_L^+; \alpha, \lambda) e^{-\frac{ik}{f_F} y y'} dy' \end{aligned} \tag{11.9}$$

The intensity distribution is proportional to the square of the wave amplitude:

$$I_L(y, z_0; \alpha, \lambda) \propto |U_L(y, z_0; \alpha, \lambda)|^2 \tag{11.10}$$

By integrating over all wavelengths and angles of incidence this is further simplified and we obtain the contribution of a single lenslet:

$$I_L(y, z_0) \propto \int_{\lambda_{min}}^{\lambda_{max}} \int_{\alpha_{min}}^{\alpha_{max}} |U_L(y, z_0; \alpha, \lambda)|^2 d\alpha d\lambda \tag{11.11}$$

The contribution of all lenses in the MLA is expressed by:

$$I(y, z_0) \propto \int_{\lambda_{min}}^{\lambda_{max}} \int_{\alpha_{min}}^{\alpha_{max}} |U_L(y, z_0; \alpha, \lambda) S_{N_0}(\alpha, \lambda, y)|^2 d\alpha d\lambda \tag{11.12}$$

With S_{N_0} derived from equations 11 thru 14 in Buttner and Zeitner [14] as follows: The transmission function of the lens array is a summation over the transmission functions of the individual lenses, which is substituted by a finite shah function and, indeed, a convolution of the transmission function of a single lens located at y' (eq. 11). After applying the shift and convolution theorem, the modulation function is given by:

$$\begin{aligned} S_{N_0}(\alpha, \lambda; y) &= \mathfrak{F}_{f_F}\{ \sum_{l=-N}^{N} \delta(y' - l p_L)\} \\ &= \int_{-\infty}^{\infty} \sum_{l=-N}^{N} \delta(y' - l p_L) e^{\frac{-2\pi i y y'}{\lambda f_F}} dy' \\ &= \sum_{l=-N}^{N} e^{\frac{-2\pi i y l p_L}{\lambda f_F}} \\ &= \sum_{l=-N}^{N} w^l \quad \text{with} \quad w = e^{\frac{-2\pi i y l p_L}{\lambda f_F}} \end{aligned} \tag{11.13}$$

Multiplying every term in the sum by w increases each power of w in the sum by one, giving:

$$\begin{aligned} w S_{N_0}(\alpha, \lambda; y) &= \sum_{l=-N+1}^{N+1} w^l \\ &= S_{N_0}(\alpha, \lambda; y) + w^{N+1} - w^{-N} \end{aligned} \tag{11.14}$$

Resulting in:

$$
\begin{aligned}
S_{N_0}(\alpha,\lambda;y) &= \frac{w^{N+1}-w^{-N}}{w-1} \\
&= \frac{e^{\frac{-2\pi iy(N+1)p_L}{\lambda f_F}} - e^{\frac{-2\pi iyNp_L}{\lambda f_F}}}{e^{\frac{-2\pi iyp_L}{\lambda f_F}} - 1} \\
&= \frac{e^{\frac{-2\pi iy(N+\frac{1}{2})p_L}{\lambda f_F}} - e^{\frac{-2\pi iy(N+\frac{1}{2})p_L}{\lambda f_F}}}{e^{\frac{-\pi iyp_L}{\lambda f_F}} - e^{\frac{\pi iyp_L}{\lambda f_F}}} \\
&= \frac{sin(\frac{N\pi p_L y}{\lambda f_F})}{sin(\frac{\pi p_L y}{\lambda f_F})}
\end{aligned}
\tag{11.15}
$$

by applying Euler's formula and using $N_0 = 2N + 1$. N is the number of lenslets that are being illuminated. From our simulations, N needs to be at least 10 to realize a uniform illumination.

For a monochromatic plane wave equation 11.12 results in interference fringes corresponding to the diffraction orders in the Fourier plane:

$$
y_m = \frac{\lambda_m f_F}{p_L} - \alpha f_F \tag{11.16}
$$

Both wavelength and angle of incidence contribute to the position of the diffraction orders. The derivation for the double MLA is analogous. Neglecting constant phase factors, the field impinging on the second MLA is given by [22]:

$$
U(y'', z_{L2}^-;\alpha,\lambda) = \frac{e^{jkf_L}}{j\lambda f_L}\, d\, e^{\frac{jk}{2f_L}y''^2} \int_{-\infty}^{\infty} U_L(y', z_{L1}^+;\alpha,\lambda) e^{\frac{jk}{2f_L}} e^{-\frac{ik}{f_F}y'y''} dy'' \tag{11.17}
$$

With d a quadratic phase factor compensating for the distance between the MLA, provided $f_L < s \leq 2f_L$

$$
d = e^{\frac{jk}{f_L}\left(1-\frac{s}{f_L}\right)y''^2} \tag{11.18}
$$

Inserting equation 11.6 into equation 11.17, dropping constant phase coefficients and cancelling the parabolic phase curvatures inside the integrand due to opposite signs in the exponent gives a Fourier transformation:

$$
\begin{aligned}
U(y'', z_{L2}^-;\alpha,\lambda) &= d\, e^{\frac{ik}{2f_L}y''^2} \int_{-\infty}^{\infty} |U| e^{iky'sin\alpha} rect\big(\frac{y'}{p_L}\big) e^{-\frac{ik}{f_F}y'y''} dy' \\
&= d\, e^{\frac{ik}{2f_L}y''^2} \mathfrak{F}_{f_L}\Big\{ |U| e^{iky'sin\alpha} rect\big(\frac{y'}{p_L}\big)\Big\} \\
&= d\, e^{\frac{ik}{2f_L}y''^2} \delta(y'' - f_L sin\alpha) \otimes \mathfrak{F}_{f_L}\Big\{ |U| rect\big(\frac{y'}{p_L}\big)\Big\}
\end{aligned}
\tag{11.19}
$$

Which is transformed by the field lens to yield the amplitude distribution in the illumination plane:

$$U(y, z_0; \alpha, \lambda) = e^{\frac{ikf_L}{f_F} y sin\alpha} \mathfrak{F}_{f_F} \left\{ d\, rect(\frac{y''}{p_L}) \, \mathfrak{F}_{f_L} \left\{ |U| rect(\frac{y'}{p_L}) \right\} \right\} \quad (11.20)$$

11.6 Supplemental S2 - Matlab m-file for simulation

Electronic versions of this m-file are available from Cytometry part A or through email (f.a.w.coumans.at.gmail.com).

11.7 Supplemental S3 - Guideline for modifying an epi fluorescence microscope with double MLA

1. Determine the MLA pairs that are suitable for your microscope:

   a) Area of illumination should be larger than the field of view of the CCD, keeping in mind that the larger the excess size is, the lower the intensity you will achieve in the field of view. For equal MLA arrays use equation 11.1 (with $s = f_L$) to determine size of flat top. For combination of different MLA arrays use m-file in supplemental S2 (vary s from smallest of f_{L_1}, f_{L_2} to $f_{L_1} + f_{L_2}$). When using different MLA arrays the pitch must be the same for both.

   b) **Maximum divergence angle should not be larger than what is achievable with a collimator**, see figure 11.2. Higher maximum angle increases alignment stability. If you use a light source that is significantly different in source size from a 100 W Hg arc lamp, you need to repeat the measurements for fig 11.2. The maximum divergence angle is typically given for MLA distance $2f_L$ (worst case) and can easily be determined for other inter MLA-distances using the simulation program.

2. Modify your epi fluorescence module

   a) **Distance between second MLA and back pupil of objective is limited.** We determined this relationship on an optical bench using the Meade CCD camera. For the MLA in this paper, the achievable CV starts to increase at 80 mm distance from 2.5%, to 10% at 200 mm distance. Power is highest at 0 distance, 90% of peak at 80 mm and 80% at 200 mm. If you choose another MLA pair, we strongly recommend you determine this relationship.

b) Modify the epi fluorescence module to achieve the distance between objective and the MLA. This will require some precision machining. Figure 11.9 shows pictures of a Nikon epi fluorescence module before and after modification.

3. Align the system. We used a cage system with premounted MLA from SUSS, one of the two MLA was adjustable perpendicular to the optical axis (xy) and rotationally. The final adjustments are quite precise ($<$ 10 µm), we used long levers to achieve the required precision.

   a) Rotate the adjustable MLA so that the micro lenses are perpendicular with the optical base plate (by eye).

   b) Align the the mutual xy orientation or the MLAs (by eye).

   c) Place the MLAs in the setup.

   d) Turn on the mercury lamp and use a reflective ND 3 filter to attenuate the light. Align the beam on the MLAs by adjusting the xy position of the arc (by eye, that is important!). **Wear UV protective goggles while you do this!**

   e) Place a power meter under the objective. Adjust the z position of the arc to maximize the power throughput.

   f) Turn the x set screw of the adjustable MLA clockwise untill it can't go further. As you turn counterclockwise, the power will fluctuate. Within a displacement equal to the pitch of the MLA there will be a minimum (lenslets misaligned) and a maximum (lenslets aligned). Determine the power at each (local) maximum. The position with the global maximum is where all lenslets of the first MLA have a mate on the second MLA. Set the x alignment to this setting. In subsequent steps, don't move the MLA by more than half a pitch from this setting.

   g) Repeat step F for the y direction.

   h) Remove the power meter and place a CCD camera in the focal plane of the objective (we used the Meade DSI II).

   i) Rotate the adjustable MLA so that you see a rectangular or squared pattern with crisp borders. Take your time to get this as good as possible, this is critical. Smaller pitch MLAs are significantly more difficult to align for this step.

   j) You should see some ghost images. If they are more than 50% in intensity of the central illumination area, the divergence of the collimated bundle is too large. If you see no ghost images, move the collimator lens a little along the optical axis to generate them.

k) Use the set screws on the adjustable MLA to balance the cross talk illumination between left/right and top/bottom. The Meade DSI II software application is horrendous to use here. We saved images, analysed line profiles in x/y direction in ImageJ [1]. Then we adjusted the MLA and checked the alignment again. This will get the lenslets aligned perfectly. A real time feedback system could easily be built in Labview, to make this less cumbersome.

l) The flat top may still be a little asymmetrical. Adjust the xy position of the arc to balance the flat-top. Step K and L have to be repeated untill you are happy with the result. The top should now be nearly flat and most non-flatness is symmetrical around the middle of the illumination area, like figure 11.10.

m) Repeat steps I,K and L. Due to the mechanical design of the rotation adjustment, it can be affected by the xy adjustments.

n) Adjust the lamp along the optical axis to maximize power throughput, this is also the point with maximum flatness.

o) Congratulations, you have successfully aligned your first imaging MLA homogenizer!

p) When replacing a bulb, just perform steps L and N

11.8 References

[1] R. J. Florijn, J. Bonnet, H. Vrolijk, A. K. Raap, and H. J. Tanke, "Effect of chromatic errors in microscopy on the visualization of multi-color fluorescence in situ hybridization," *Cytometry*, vol. 23, pp. 8–14, Jan 1996.

[2] N. Wang, Y. Pan, T. Heiden, and B. Tribukait, "Fluorescence image cytometry for measurement of nuclear DNA content in surgical pathology," *Cytometry*, vol. 22, pp. 323–329, Dec 1995.

[3] M. A. Model and J. K. Burkhardt, "A standard for calibration and shading correction of a fluorescence microscope," *Cytometry*, vol. 44, pp. 309–316, Aug 2001.

[4] A. D. Klein, R. van der Doel, I. T. Young, S. L. Ellenberger, and L. van Vliet, "Quantitative evaluation and comparison of light microscopes," in *Optical investigation of cells In vitro and in vivo* (F. D. L., L. R. C., and T. B. J., eds.), pp. 162–173, Proc SPIE, Progress in Biomedical Optics, 1988.

[5] G. R. Bright, G. W. Fisher, J. Rogowska, and D. L. Taylor, "Fluorescence ratio imaging microscopy: temporal and spatial measurements of cytoplasmic pH," *J. Cell Biol.*, vol. 104, pp. 1019–1033, Apr 1987.

[6] J. K. Ji and Y. Kwon, "Conical microlens arrays that flatten optical-irradiance profiles of nonuniform sources," *Appl Opt*, vol. 34, pp. 2841–2843, 1995.

[7] T. M. Scholtens, F. Schreuder, S. T. Ligthart, J. Swennenhuis, A. G. T. Tibbe, J. Greve, and L. W. M. M. Terstappen, "CellTracks TDI: an image cytometer for cell characterization," *Cytometry Part A*, vol. 79A, pp. 203–213, 2011.

[1] http://rsbweb.nih.gov/ij/

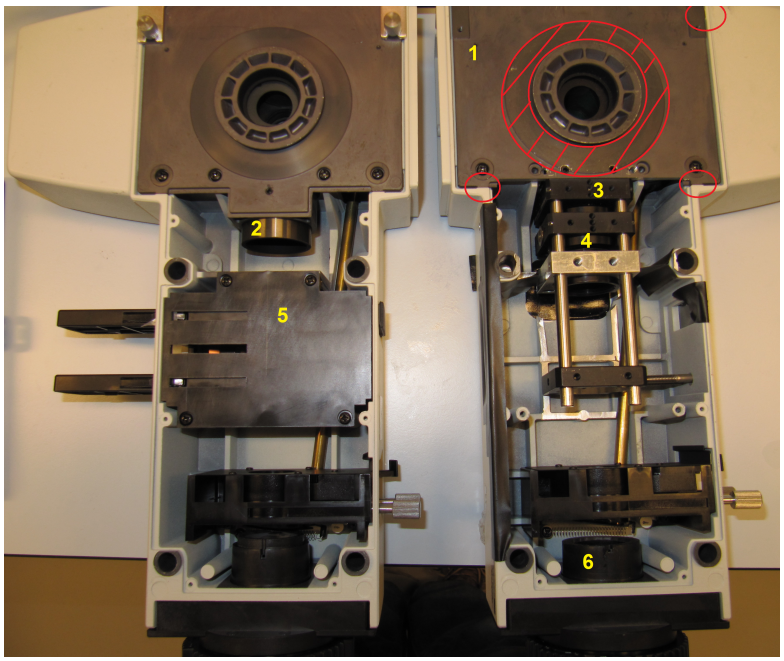

Figure 11.9: Modification of Nikon Eclipse 400 epi fluorescence module. *Steps needed for modification of this module shown in yellow: Plate (1) machined to mount MLA close to filter cube (the surfaced used to mount this piece in the machining vice are shown in red). Lens removed (2/6). MLA (3) and relay lens (4) mounted in cage system. ND filter assembly removed (5).*

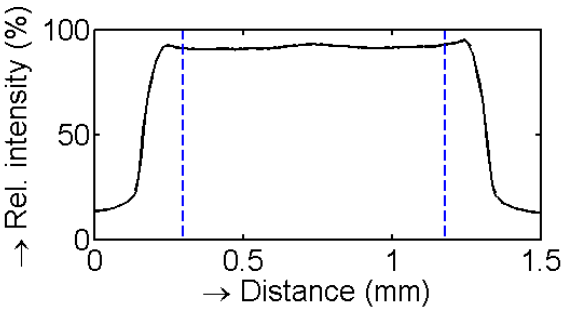

Figure 11.10: Line profile of a well aligned MLA system, with correctly xy aligned arc lamp. *The profile is shown in the long direction of the arc, some residual asymmetry is due to the shape of the arc.*

[8] W. J. Allard, J. Matera, M. C. Miller, M. Repollet, M. C. Connelly, C. Rao, A. G. Tibbe, J. W. Uhr, and L. W. Terstappen, "Tumor cells circulate in the peripheral blood of all major carcinomas but not in healthy subjects or patients with nonmalignant diseases," *Clin. Cancer Res.*, vol. 10, pp. 6897–6904, Oct 2004.

[9] J. S. de Bono, G. Attard, A. Adjei, M. N. Pollak, P. C. Fong, P. Haluska, L. Roberts, C. Melvin, M. Repollet, D. Chianese, M. Connely, L. W. Terstappen, and A. Gualberto, "Potential applications for circulating tumor cells expressing the insulin-like growth factor-I receptor," *Clin. Cancer Res.*, vol. 13, pp. 3611–3616, Jun 2007.

[10] S. Riethdorf, V. Muller, L. Zhang, T. Rau, S. Loibl, M. Komor, M. Roller, J. Huober, T. Fehm, I. Schrader, J. Hilfrich, F. Holms, H. Tesch, H. Eidtmann, M. Untch, G. von Minckwitz, and K. Pantel, "Detection and HER2 expression of circulating tumor cells: prospective monitoring in breast cancer patients treated in the neoadjuvant GeparQuattro trial," *Clin. Cancer Res.*, vol. 16, pp. 2634–2645, May 2010.

[11] E. van der Pol, A. G. Hoekstra, A. Sturk, C. Otto, T. G. van Leeuwen, and R. Nieuwland, "Optical and non-optical methods for detection and characterization of microparticles and exosomes," *J. Thromb. Haemost.*, vol. 8, pp. 2596–2607, Dec 2010.

[12] R. Voelkel and K. J. Weible, "Laser beam homogenizing: Limitations and constraints," in *Optical fabrication, testing and metrology III* (A. Duparre and R. Geyl, eds.), vol. 7102 of *Proceedings of SPIE*, 2008.

[13] D. Wright, P. Greve, J. Fleischer, and L. Austin, "Laser beam width, divergence and beam propagation factor - an international standardization approach," *Optical and Quantum Electronics*, vol. 24, pp. S993–S1000, 1992.

[14] A. Buettner and U. Zeitner, "Wave optical analysis of light emitting diode beam shaping using micro lens arrays," *Opt. Eng.*, vol. 41, pp. 2393–2401, 2002.

[15] A. G. Tibbe, B. G. de Grooth, J. Greve, G. J. Dolan, C. Rao, and L. W. Terstappen, "Magnetic field design for selecting and aligning immunomagnetic labeled cells," *Cytometry*, vol. 47, pp. 163–172, Mar 2002.

[16] H. T. Maecker and J. Trotter, "Flow cytometry controls, instrument setup, and the determination of positivity," *Cytometry A*, vol. 69, pp. 1037–1042, Sep 2006.

[17] J. A. Hoffnagle and C. M. Jefferson, "Design and performance of a refractive optical system that converts a Gaussian to a flattop beam," *Appl Opt*, vol. 39, pp. 5488–5499, Oct 2000.

[18] K. Nemoto, T. Fujii, N. Goto, H. Takino, T. Kobayashi, N. Shibata, K. Yamamura, and Y. Mori, "Laser beam intensity profile transformation with a fabricated mirror," *Appl Opt*, vol. 36, pp. 551–557, Jan 1997.

[19] S. P. Chang, J. M. Kuo, Y. P. Lee, C. M. Lu, and K. J. Ling, "Transformation of gaussian to coherent uniform beams by inverse-gaussian transmittive filters," *Appl Opt*, vol. 37, pp. 747–752, Feb 1998.

[20] T. Sales, "Structured microlens arrays for beam shaping," *Opt. Eng.*, vol. 42, pp. 3084–3085, 2003.

[21] G. R. Fowles, *Introduction to modern optics.* Dover Publications, Mineola, NY, USA, 1975.

[22] M. Bass, *Handbook of optics, Volume I, 2nd edition.* McGraw-Hill, New York, NY, USA, 1995.

Summary

Distant metastases are formed by tumor cells that shed from the primary tumor into the bloodstream. These circulating tumor cells (CTC) may be enumerated in a patients' blood. The number of CTC provides a prognosis, predicts a response to therapy and the expression of certain molecules in the CTC allows for determination of the most appropriate therapy. CellSearch, the standard assay for CTC enumeration from 7.5 mL of blood has shown feasibility of both these concepts, but finds no CTC in up to 50% of metastatic carcinoma patients. In this thesis we investigate several approaches to improve recovery of CTC. Archive data from several large clinical CTC trials were used to test alternative CTC definitions resulting in a higher number of CTC for similar or better prognostic value than the CellSearch definition. Flow cytometry was compared to CellSearch to evaluate whether a higher number of CTC is achievable by improved enrichment. The distribution function of CTC in metastatic patients was determined to estimate the effect of increased sample volume. The increase of sample volume by filtration of apheresis samples was investigated. An improvement to the CellSearch analyzer is presented to allow more accurate measurement of treatment targets on CTC. Increasing the number of CTC by a more inclusive CTC definition reduces the prognostic value of the CTC count when evaluating effectiveness of therapy. A potential threefold increase in EpCAM+CK+DNA+CD45- CTC by improved recovery will not be sufficient to find CTC in all metastatic carcinoma patients. Extrapolation of the EpCAM+CK+DNA+CD45- CTC distribution function in patients, predicts that increasing the sample volume to 5 liters of blood will result in recovery of CTC in 99% of metastatic patients. CTC enrichment by filtration of apheresis samples may allow for the sampling of such a blood volume, but we could not reach the required assay conditions due to sample age. It is critical for CTC enumeration that any cell included in the count is a CTC, even if this means that a large fraction of tumor cell (fragments) are not counted. To recover CTC in all patients, the sample volume must be increased dramatically. Sample age is critical, and CTC recovery in an extracorporeal circuit using antibody or physical based enrichment can circumvent this issue.

Samenvatting

Metastasen worden gevormd door tumorcellen die zich van de primaire tumor afscheiden in de bloedbaan. Het aantal circulerende tumor cellen (CTC) kan bepaald worden in het bloed van patiënten. Het aantal CTC heeft prognostische waarde en kan gebruikt worden om de effectiviteit van bepaalde behandelingen te evalueren. De expressie van bepaalde moleculen op de CTC kan gebruikt worden voor het kiezen van de meest geschikte therapie. CellSearch, de standaard test voor CTC bepaling in 7,5 mL bloed heeft haalbaarheid van beide toepassingen aangetoond, maar er worden geen CTC gevonden in tot 50% van gemetastaseerde carcinoma patiënten. In dit proefschrift onderzoeken we verschillende benaderingen om het aantal gevonden CTC te verhogen. Archief gegevens van verschillende grote klinische CTC proeven werden gebruikt om te testen of het toepassen van alternatieve CTC definities resulteert in een groter aantal CTC met een vergelijkbare, of betere, voorspellende waarde dan de CellSearch definitie. Flow cytometrie werd vergeleken met CellSearch om te beoordelen of een groter aantal CTC kan worden bereikt door verbeterde verrijking. De distributie functie van CTC in metastatische patiënten werd bepaald om het effect van een vergroting van het monstervolume in te schatten. Een toename van monstervolume door CTC-filtratie van aferese monsters werd onderzocht. Een verbetering van de CellSearch Analyzer wordt getoond die een nauwkeuriger meting van "treatment-targets" op CTC mogelijk maakt. Verhoging van het aantal CTC door een meer inclusieve CTC definitie vermindert de prognostische waarde van het aantal CTC bij het evalueren van de effectiviteit van de therapie. Een potentiële drievoudige verhoging van EpCAM+CK+DNA+CD45-CTC door verbeterde verrijking zal niet voldoende zijn om CTC vinden in alle gemetastaseerde patiënten. Extrapolatie van de EpCAM+CK+DNA+CD45-CTC distributie functie in patiënten, voorspelt dat het verhogen van het monster volume naar 5 liter bloed zal resulteren in idenficatie van CTC in 99% van metastatische patiënten. CTC verrijking door middel van filtratie van aferese monsters kan het afnemen van een dergelijk sample volume mogelijk maken, maar het was niet mogelijk om de vereiste test omstandigheden te bereiken als gevolg van de monster leeftijd. Het is van cruciaal belang voor CTC bepaling dat elke meetgetelde cel een CTC is, zelfs als dit betekent dat een groot deel van de tumorcel (fragmenten) niet worden meegeteld. Om CTC te vinden

bij alle patiënten, moet het monster volume drastisch worden verhoogd. Sample leeftijd is kritisch, en CTC verrijking in een extracorporeaal circuit met behulp van antilichamen of op basis van fysieke eigenlschappen kan dit probleem omzeilen.

Outlook

The detection of circulating tumor cells (CTC) will make meaningful contributions to the state of the art of cancer in multiple ways:

First, enumeration of CTC affords insight into the metastatic activity of the tumor. The number of CTC will be used to monitor effectiveness of therapy and will enable the oncologist to find a better balance between benefits and risks of various chemotherapies (chapter 6).

Second, CTC can be a liquid biopsy that represents the current state of the cancer. As the survival of patients is extended with more effective treatments, the difference between the primary tissue and the cancer present in a patient will grow. Characterizing of the CTC at the time therapy is needed will allow identification of effective therapies, which were originally presumed ineffective based on histology data [2].

Third, the methods to study the metastatic process in laboratory animals are not compatible with studies in humans. CTC are a major factor in the metastatic process (chapter 1), and their study could help us understand why the metastatic efficiency of CTC in humans is much lower compared to laboratory animals. Such understanding may yield new therapies that reduce the metastatic efficiency further, and thus halt the metastatic process.

To achieve these promises the number of CTC detected needs to be increased dramatically, but without loss of specificity.

High specificity trumps sensitivity in CTC detection

Enumeration of CTC, with expression of epithelial cell adhesion molecule (EpCAM), cytokeratin 8, 18, 19 (CK), and DNA, but no expression of CD45, in the CellSearch system includes a step where a trained reviewer compares images of possible CTC against a morphological definition to

[2]Patients with Her-2 negative tissue, but Her-2 positive CTC respond to Herceptin: Expression of truncated HER2 receptor in circulating tumor cells (CTCs) of breast cancer patients, G. Kallergi et al., Abstract 2379, Annual conference of the American Association for Cancer Research, Chicago, 2012.

determine whether it is indeed a CTC, or some other type of object. This morphological definition was determined before completion of the first clinical trial. While the results of the clinical trials demonstrated that the original definition was a good estimate (chapters 2 and 3), this result alone should not make this definition gospel. Several alternative definitions were tested both by human inspection (chapter 4) and automated enumeration (chapters 5 and 6) using archive images from prospective clinical trials. This demonstrated that a threefold increase in CTC is possible by applying a more inclusive version of the EpCAM+CK+DNA+CD45- phenotype, with limited reduction in the prognostic value of the CTC count (chapter 6). Even more dramatic, a 35-fold increase in 'CTC' is possible if we enumerate EpCAM+CK+CD45- tumor micro particles (TMP), with similar prognostic value to the CellSearch CTC (chapter 4). Unfortunately, all CTC definitions with a higher frequency in patients suffered from higher false positives in healthy donors. With multiple CTC measurements during therapy, treatment success is best measured by a reduction of the CTC count to 0. The CTC definition most suited to determine whether such a reduction occurred is one with the lowest number of false positives, which is the manual CellSearch, or automated CellSearch-like, CTC definition (chapter 6).

Recovering more CTC from the same sample volume by better false positive elimination

The CellSearch assay includes a CD45-APC stain to eliminate any white blood cells that occasionally stain positive for cytokeratins 8, 18 or 19. A striking observation from the various automated CTC definitions is that the CD45- requirement only has a marginal effect on both the number of CTC recovered and the prognostic value of these CTC. In addition, during the development of the CTC counting algorithm (chapter 5), we observed that while there are ≈10,000 objects in a sample with nuclear material (DAPI+), only ≈500 objects had CD45-APC (allophycocyanin) staining. It is likely that a large fraction of the 9,500 CD45- objects are white blood cells, suggesting that the CD45 staining is ineffective. The culprit for this poor staining is low APC sensitivity of the CellTracks Analyzer II, which is caused by the spectrum of the mercury arc lamp in this system. Solutions for this poor sensitivity can be replacement of the light source by a set of lasers [3], or, a more cost effective solution would be to use a micro lens array based CellTracks Analyzer II (chapter 11) and adding a red laser. With improved CD45 sensitivity, it will be possible to apply a more inclusive CTC definition without increasing the false positive number in healthy controls. Such an improvement may yield up to a threefold higher number

[3] Scholtens, T.M., et al., CellTracks TDI: An image cytometer for cell characterization. Cytometry Part A, 2011. 79(3): p. 203-213.

of CTC from the same blood volume (chapter 7) with better prognostic value than the current CellSearch definition. Improved CD45 sensitivity may also suppress the number of TMP found in healthy controls.

Using physical parameters to enrich CTC requires further optimization

CTC enrichment from whole blood may be achieved by exploiting expression of antigens on CTC which are not expressed on blood cells, or alternatively, by exploiting physical differences such as size, flexibility, or density. With the application of appropriate assay and filter conditions (chapters 8 and 9), it may be possible to enrich CTC exploiting differences in size and flexibility. Because in any practical filtration system all cells will eventually move through the filter (chapter 9), a more elaborate approach is needed to enrich CTC from large sample volumes. Possible approaches to eliminate loss of CTC over time include intermittent flow or multiple filters in series (chapter 9). A substantial fraction of CTC recovered by CellSearch will still be missed by such an approach, as many CTC have a size similar to white blood cells (chapter 10). It is possible that these methods do recover CTC with extremely low expression of EpCAM, however the clinical relevance of EpCAM- CTC needs to be proven. While antigen expression can be estimated from extensive histology databases [4], no comprehensive data source exists for physical characteristics of CTC and white blood cells. Therefore the use of cells from tumor cell lines for evaluation of an assay exploiting physical characteristics entails higher risk than the use of these cells for evaluation of an antibody based assay. To mitigate this risk, any method that applies density, size, flexibility or any other physical parameter for the selective enrichment of CTC should perform a clinical trial much earlier in the assay development process compared to antibody based methods.

Strategies for detecting CTC from a very large sample volume

To identify and characterize CTC in all metastatic patients a large volume of the patients' blood will need to be processed, up to 5 liters (chapter 7). A similar volume will be needed to detect CTC in a patient before the first metastasis has formed (chapter 1). Obviously, such blood volume cannot be taken from a patient and alternative strategies are needed (chapter 10). An approach that selectively enriches the tumor cells from the blood could be apheresis, provided the density of CTC is determined. Attempts to enrich cells from tumor cell lines from buffy coats of 0.5 L of blood were ineffective

[4] e.g. Human protein atlas, www.proteinatlas.org.

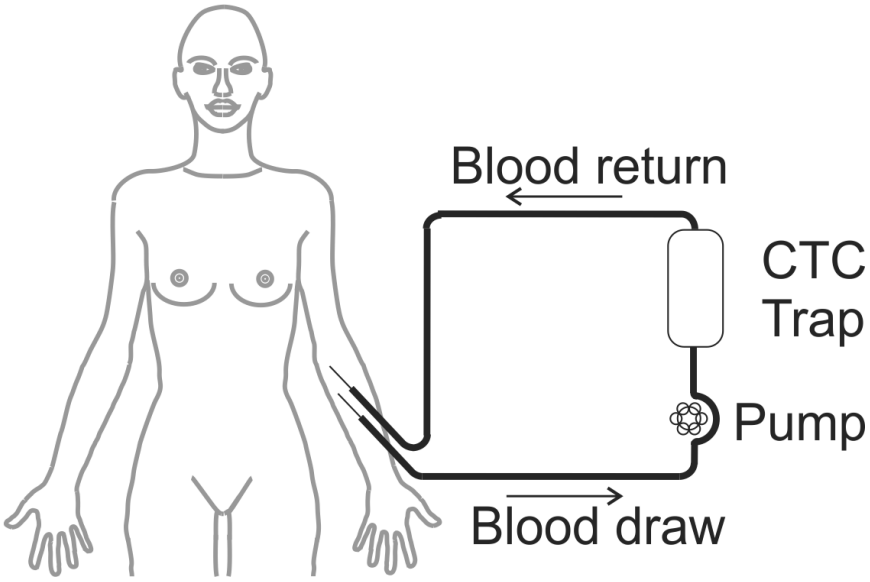

Figure 1: Extracorporeal circuit with CTC trap. A pump draws blood from the patient into the CTC trap. The CTC trap collects CTC and allows CTC depleted blood to exit the trap. This blood is returned to the patient.

due to large fibrin aggregates in the buffy coats, clogging our filters. Tests with bovine blood demonstrated that these aggregates form with sample age. To achieve sample age of less than one hour CTC should be enriched in-vivo [5] or through an extracorporeal circuit (figure 1).

Leukapheresis is an example of such an extracorporeal circuit; a patients' blood is drawn from an arm, pumped through a centrifuge that collects a density fraction, and the rest of the blood is returned to the patient. This extracorporeal circuit needs to contain a CTC-trap; a device that selectively traps circulating tumor cells, but allows blood cells, platelets and plasma to pass. This device could employ a separation technique based on density, cell size or antigen expression, as illustrated in figure 2.

Separation based on density, CTC-apheresis, would need development of a technique that can eliminate the majority of white blood cells. Once this development is complete, it could be quickly implemented as leukapheresis equipment could be used, which already meets all the requirements for patient hook-up. A major risk for CTC-apheresis is the unknown density of CTC. If the density is similar to the density of culture cells (chapter 10),

[5] Galanzha, E.I., et al., In vivo magnetic enrichment and multiplex photoacoustic detection of circulating tumour cells. Nature Nanotechnology, 2009. 4(12): p. 855-860.

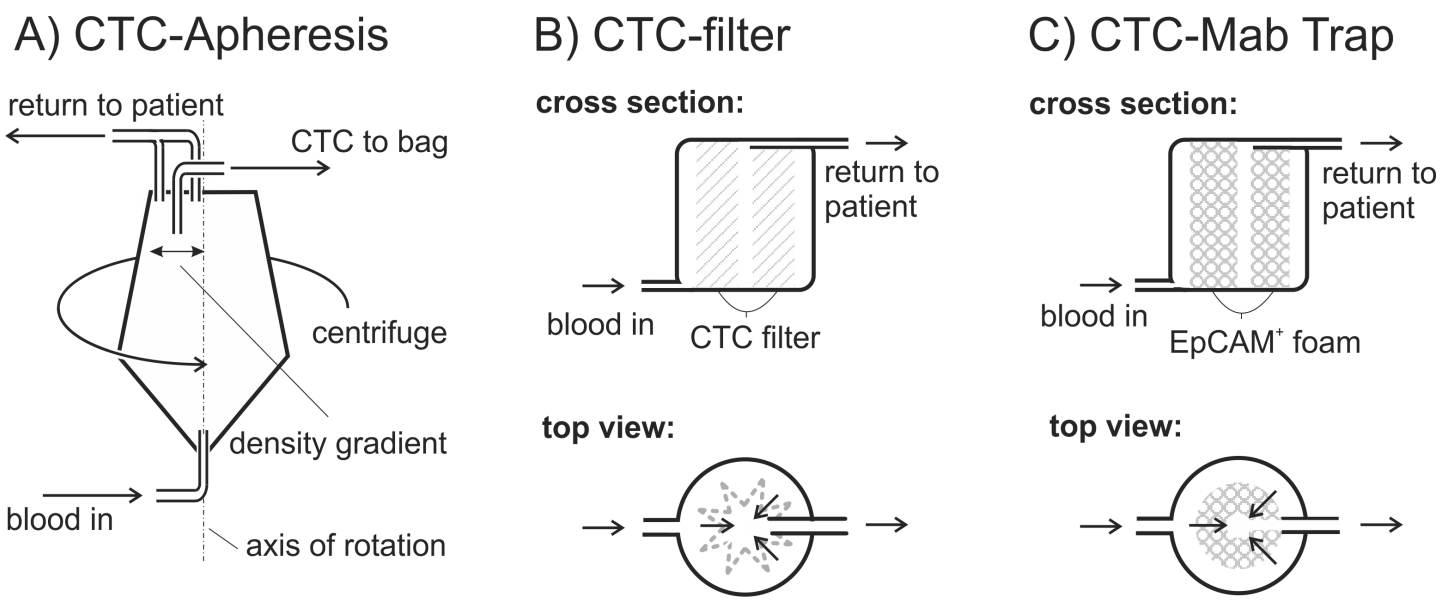

Figure 2: Possible designs for CTC-traps. Panel A shows the apheresis version of the CTC-trap. Blood enters a rotating bowl at the bottom. By the time it reaches the top of the bowl, a density gradient has arisen and the densities of interest are collected in a bag, while the blood components with higher and lower densities are returned to the patient. Panel B shows a filter implementation of the CTC-trap. The trap consists of an inlet on the outside of a cylinder, a filter in a ring around the middle of the cylinder and an outlet connected to the center of the cylinder. The top view of panel B illustrates folding of the filter to increase filter surface area. Panel C shows a monoclonal antibody based CTC-trap, where the filter is replaced by a cylinder of open-cell foam coated with anti-EpCAM.

CTC-apheresis may result in high recovery of CTC and a limited number of white blood cells (10^8), which would need to be reduced to below 10^6 cells to make imaging or the sample practical. However, if a wide range of densities needs to be captured, 10^{10} white blood cells will also be captured, probably inhibiting completion of any enrichment procedure before the sample has degraded. Reduction of the number of white blood cells could be achieved by immunomagnetic depletion of white blood cells [6], or by placement of a CTC selective filter on the CTC-outlet of the apheresis device. A technique employing a density floater [7] could help determine the density of CTC before methods are developed that deplete 10^8 white blood cells.

Separation based on size, CTC-Filtration, would require a large area filter, in the order of 1 dm^2. Such size filters with optimal properties (chapter 9) can be fabricated using currently available techniques, and if needed, could be packaged in a small module very similar to a fuel filter in a car. A solution will be needed for the loss of CTC over time (chapter 8), which may be consist of a multi layered filter module or intermittent flow. Once filtration is complete, the filtrate is expected to contain ≈20–50% of CTC (chapter 9) together with $6 \cdot 10^6$ white blood cells. This can be removed from the trap by washing the filter(s). For efficient washing, the material of the filter should prevent adhesion of cells to the surface, for example polycarbonate filters [8]. Techniques for enrichment of CTC from this number of white blood cells are already available (chapter 2).

Separation based on antibody expression, CTC-Mab trap, is possible with EpCAM coated open pore foam. A similar extracorporeal circuit in which the trap is coated with CD95 (anti-FAS) for FAS induced neutrophil inactivation at a blood flow of 300 mL/min has been demonstrated [9]. Additional advantages of the antibody approach are the availability of an extensively validated CTC detection platform for comparison of the device performance as well as the availability of cell lines with known antibody expression relative to CTC [10]. Recovery of CTC from the trap could be done by releasing the bonds between the CTC and the foam, or by digesting the foam. Releasing bonds between CTC and foam could be achieved by washing with a vast molar excess of EpCAM or by digesting the linker between the anti-EpCAM and the foam. For any of these strategies to

[6] Alix-Panabieres, C., et al., Detection of circulating prostate-specific antigen-secreting cells in prostate cancer patients. Clinical Chemistry, 2005. 51(8): p. 1538-41.

[7] Rarecyte, www.rarecyte.com.

[8] Track etched poly carbonate filters have low adhesion, www.whatman.com.

[9] Extracorporeal immune therapy with immobilized agonistic anti-Fas antibodies leads to transient reduction of circulating neutrophil numbers and limits tissue damage after hemorrhagic shock/resuscitation in a porcine model, Lögters et al., Journal of Inflammation 2010, 7:18.

[10] Rao, C.G., et al., Expression of epithelial cell adhesion molecule in carcinoma cells present in blood and primary and metastatic tumors. Int J Oncol, 2005. 27(1): p. 49-57.

work, there should be no a-specific adhesion of cells to the foam (chapter 3). An a-specific adhesion insensitive approach would be digestion of the foam, requiring a foam which can be digested within ≈24 hours without dramatically altering the pH or osmolarity inside the CTC-Mab trap.

Regardless of the trap design, enumeration of CTC should be done by detecting the presence of EpCAM, CK, DNA and the absence of CD45 and/or other hematopoietic markers. With the knowledge we have now, antibody mediated enrichment of CTC from a large volume is the most feasible approach.

Publications

1. Attard G., Swennenhuis J.F., Olmos D., Reid A.H., Vickers E., A'Hern R., Levink R., Coumans F.A.W., Moreira J., Riisnaes R., Oommen N.B., Hawche G., Jameson C., Thompson E., Sipkema R., Carden C.P., Parker C., Dearnaley D., Kaye S.B., Cooper C.S., Molina A., Cox M.E., Terstappen L.W.W.M., de Bono J.S. Characterization of ERG, AR and PTEN gene status in circulating tumor cells from patients with castration-resistant prostate cancer. Cancer Res 69(7): 2912-8, 2009.

2. Coumans F.A.W., Doggen C.J.M., Attard G., de Bono J.S., Terstappen L.W.M.M. All circulating EpCAM+ CD45- CK+ but not EpCAM+ CD45+ CK+ objects predict overall survival in castration-resistant prostate cancer. Ann Oncol 21: 1851-1857, 2010.

3. Rao C., Bui T., Connelly M., Doyle G., Karydis I., Middleton M.R., Clack G., Malone M., Coumans F.A.W., Terstappen L.W.M.M. Circulating melanoma cells and survival in metastatic melanoma. Int. J. Oncology 38: 755-760, 2011.

4. Ligthart S.T., Coumans F.A.W., Attard G., Cassidy A.M., de Bono J.S., Terstappen L.W.M.M. Unbiased and Automated Identification of a Circulating Tumour Cell Definition that Associates with Overall Survival. PLoS ONE 6(11): e27419, doi:10.1371/journal.pone.0027419, 2011.

5. Coumans F.A.W., van der Pol E., Terstappen L.W.M.M. Flat-top illumination profile in an epi-fluorescence microscope by dual micro lens arrays. Cytometry Part A, 81A, p 324–331, doi:10.1002/cyto.a.22029, 2012.

6. Swennenhuis J.F., Foulk B., Coumans F.A.W., Terstappen L.W.M.M. Construction of repeat free Fluorescence In-Situ Hybridization (FISH) probes. Nucleic Acids Research 40 (3): e20, doi:10.1093/nar/gkr1123, 2012.

7. Ligthart S.T., Coumans F.A.W., Terstappen L.W.M.M., Interpretation of changes in Circulating Tumor Cell counts. Translational Oncology, in press, 2012.

8. Coumans F.A.W., Ligthart S.T., Uhr J., Terstappen L.W.M.M. Challenges in the Enumeration and Phenotyping of CTC. Clinical Cancer Research, doi:10.1158/1078-0432.CCR-12-1585, 2012.

9. Coumans F.A.W., Ligthart S.T., Swennenhuis J., Terstappen L.W.M.M. Circulating Tumor Cell - Trapping Devices. In: Biofunctional Surface Engineering in Medicine "Nanobiotechnology" series by Pan Stanford Publishing, in press.

10. Coumans F.A.W., Terstappen L.W.M.M. Detection and characterization of Circulating Tumor Cells by the Cell Search approach. Methods in Molecular Biology, "Circulating Tumour Cells" Humana Press, USA, in press.

11. Sjoerd T. Ligthart, Frank A.W. Coumans, Francois-Clément Bidard, Lieke H.J. Simkens, Cees J.A. Punt, Marco de Groot, Gerhardt Attard, Johann S. de Bono, Jean-Yves Pierga, Leon W.M.M. Terstappen Morphology of circulating tumor cells and survival in breast, colorectal, and prostate cancer. Submitted for publication.

12. Coumans F.A.W., van Dalum G., Beck M., Terstappen L.W.M.M. Filter requirements for circulating tumor cell enrichment and detection. Submitted for publication.

13. Coumans F.A.W., van Dalum G., Beck M., Terstappen L.W.M.M. Factors influencing filtration of tumor cells from whole blood. Submitted for publication.

Conference contributions

1. Coumans F.A.W., Sylvia J., Gross S., Verrant J.V., Greve J., Ymeti A., Terstappen LWMM. An image analysis based effective (immuno) fluorescent cell counter. Abstract 158354. ISAC 2006, Quebec, Canada.

2. Steven Gross, Frank Coumans, John Silvia, Mark Connelly, and Leon W.M.M. Terstappen. Assessment of Cell Viability with a Simple Imaging Device. Abstract 158088. ISAC 2006, Quebec, Canada

3. Dania D. Yaskanin, J. Michael Kelly, Jan F. Keij, Frank. A.W. Coumans, Mark C. Connelly, and Leon W.M.M. Terstappen A Simple Fluorescence Imaging System to Enumerate Residual Leukocytes in Leukodepleted Blood. Abstract 156053 ISAC 2006, Quebec, Canada.

4. Frank Coumans, Leo Grady, Chandra Rao, Jimmy Page, Mark Connely, Leon Terstappen. Counting virally infected cells in nasopharyngeal swabs by image cytometry. ISAC 2008, Budapest, Hungary

5. F. Coumans, C.J.M. Doggen, G. Attard, J.S. de Bono, L.W.M.M. Terstappen. Classification of EpCAM+ CD45- cytokeratin+ objects versus survival in castration resistant prostate cancer. ISMRC 2009, Athens, Greece

6. S.T. Ligthart, F.A.W. Coumans, G. Attard, A. Cassidy, J.S. de Bono, L.W.M.M. Terstappen. Automated identification of circulating tumor cells. Lorentz conference 2011 - Circulating tumor cell isolation and diagnostics, Leiden, The Netherlands.

7. S.T. Ligthart, F.A.W. Coumans, G. Attard, J.S. de Bono2, L.W.M.M. Terstappen. Automated classification of circulating tumor cells optimized using clinical outcome of castration resistant prostate cancer patients. Abstract 4175, AACR 2011, Orlando, FL, USA

8. Guus van Dalum, Frank A.W. Coumans, Markus Beck, Leon W.M.M. Terstappen. Filtration requirements for circulating tumor cell enrichment and detection. ISAC 2012, Leipzig, Germany

9. Guus van Dalum, Frank A.W. Coumans, Markus Beck, Leon W.M.M. Terstappen. Key factors for filtration of tumor cells from whole blood. Abstract 2395, AACR 2012, Chicago, IL, USA

10. Coumans F.A.W., Ligthart S.T., Uhr J., Terstappen L.W.M.M. All patients with metastatic breast, colorectal and prostate carcinoma have circulating tumor cells. Abstract 2391, AACR 2012, Chicago, IL, USA

Patents / patent applications

1. Method and algorithms for cell enumeration in low-cost cytometer.Inventors: Coumans F.A.W., Greve J., Modica F., Terstappen L.W.M.M., Tibbe A., Verrant J. United States Patent No: 7,764,821 B2, July 27, 2010.

2. High sensitivity multiparameter method for rare event analysis in a biological sample. M.C. Connelly, F.A.W. Coumans, S. Gross, M. Kelly. Publication date: 01/29/2009 , Patent application number: 20090029378

Biography

Frank A.W. Coumans, born in The Netherlands, 1978, graduated high school with honors and left his parental home to study applied Physics at the University of Twente. During his studies he completed a year long solo trip around the world, visiting 5 continents. With many cultural experiences as well as his future wife in the pocket, he continued his studies in Enschede, only to leave again for an internship at the University of Buenos Aires, Argentina. Where Frank successfully constructed a 3D two-photon microscope. When he returned to Holland he decided to specialize in biophysics and wrote his Masters thesis on super-resolution Raman microscopy. He received his Master of Science degree in applied physics with honours, with a minor in "Philosophy and Ethics of a Technological Society".

Frank continued his career in the USA. As Principal Systems Engineer at Immunicon Corporation he dedicated himself to rare cell detection, with an initial focus on circulating tumor cells. Frank developed the CellTracks EasyCount platform, a cost efficient, easy to use cytometer for a wide range of applications including basic live/dead cell counts and detection of influenza infected cells in nasopharyngeal swabs. He also developed the CellTracks Analyzer II system, an automated cytometer for imaging magnetically enriched circulating tumor cells from blood samples.

CellTracks Analyzer II won the "Medical Design Excellence Award 2006" and the CellSearch System was recognized with the prestigious "Prix Galien USA 2009". From January 1st 2009 Frank has been developing the next generation circulating tumor cell assay in the Medical Cell BioPhysics group of Prof. Dr. Leon Terstappen (University of Twente, The Netherlands).

Acknowledgements

Welcome to the most read section of this thesis! When I started my work in Enschede my goal was to improve my scientific and writing skills. I would develop a method to enrich circulating tumor cells from several liters of blood and all would be merry. Reality proved to be disobedient; the research evolved in a different direction. Nevertheless, I'm quite satisfied with this thesis. After 3.5 years, 100,000 kilometers by train, 50 liters of blood and innumerable cups of coffee of assorted qualities, I finally get to acknowledge the people who made it possible.

Professor Leon Terstappen has been my mentor for the past nine years, and I am grateful to him for his unconditional support. I thank Guus van Dalum and Sjoerd Ligthart for our collaboration on several projects in this thesis, and for introducing me to some of the weirder things the internet has generated. I admire their patience and persistance. I appreciate Joost Swennenhuis, Markus Beck, and Edwin van Der Pol for generously donating their time to discuss ideas or to work on a manuscript. I'm indebted to Carine Doggen for teaching me biostatistics and to Sabine Siesling for having faith in me to start a project together before knowing where it would go.

Of my coauthors, I'm especially obliged to Gerhardt Attard, Johann de Bono, and Jonathan Uhr, who are all excellent writers, medical doctors and thoughtful scientists. Of the thousands of scientists at the AACR 2012 conference, Gerhardt asked me the most difficult (and inspiring) question. I'm very curious to what he will ask at the defense.

I thank Hans Vrielink, Dirk de Korte, Ineke Slaper-Cortenbach, and Jennita Slomp for their help with obtaining buffy coat and apheresis samples and/or for suggestions on how to remove the aggregates in these samples.

I'm grateful to Veridex, especially Bob Mc Cormick and Mark Conelly, for the generous funding of my research and for providing the clinical data that underpins four chapters in this thesis. I would probably not have started working on this thesis without the good work done by the team at Immunicon/Veridex, of whom especially Jan Keij, Chandra Rao, David Chianese, Steve Gross, Mike Kagan, John Verrant, Arthur Marlin, Bryan

Mosko, Ronald Sipkema, Teresa Bendele, Robin Levy, Madeline Repollet, and Craig Miller have made valuable contributions. I also thank several of them for help with work in this thesis.

I owe many pages to a long list of students including χ^2 Andree, Joep van Bortel, Ana Barbosa Pereira, Arthur Bentlage, Joris Bokkes, Jorick Geessink, Mathijs van Gorkum, Jan Hendriks, Robert Landheer, Jordi van der Linde, Roben Scholten, Bob Steenhuis, Michiel Stevens, and Niels van der Velde. The work by Jordi and Arthur was especially remarkable.

Every PhD program has its tough moments and I am indebted to Jan Greve, and Ingrid Svennsson for helping me through these times. Jan calls em as he sees em, which I appreciate very much. Moral support was also plentiful from the "Drinking-Green-Tea-Ain't-Gay mens night", the Enschede division of "Het vriendenweekend", YoSoFine, and of course my family. Vincent Kappers was kind enough to provide me with a roof for the nights I stayed in Enschede.

Last but not least I thank my wife Jasmijn for experiencing life together with me, it's more worthwhile when you're around.

Frank Coumans

CHAPTER 12

De bloederige ontmaskering van de circulerende tumor cel

Jasmijn Coumans-Rijcken and Frank Coumans
Laymans' explanation of the work in this thesis, in Dutch

Snap je er de ballen van en heb je er zeker geen kaas van gegeten? Dit hoofdstuk is speciaal voor als je hersenen de pan uit spinnen bij het lezen van de rest van dit boek! Hier leggen we geheel op zijn Janboerenfluitjes uit wat de doelen, strategieën en uitdagingen van dit onderzoek zijn. Kind kan de was doen! Hup daar ga je al:

12.1 Het Doel

Circulerende tumor cellen zijn kankercellen die een tumor hebben verlaten en nu in het bloed rond cirkelen. Deze cellen verspreiden de kanker door het lichaam, het zijn deze cellen die uitzaaiingen veroorzaken. Het doel van dit onderzoek is het leren *opsporen en tellen* van deze cellen in bloed, zodat kanker patiënten met uitzaaiingen effectiever behandeld kunnen worden, en zo de kans op genezing groter is. Hoe zit dat dan? Welnu, na constatering van kanker bij een patiënt heeft de arts veel informatie nodig voor het bepalen van de behandeling.
Informatie in een grote tumor vinden is al lang mogelijk en kan gelukkig nauwkeurig gebeuren. Echter, als na verloop van tijd de kanker door het lichaam is uitgezaaid, is het vinden van de correcte informatie en daarmee

de juiste behandelmethode erg moeilijk: vrijwel alle cellen zijn klein en op moeilijk bereikbare plekken in het lichaam. Momenteel tast een arts bij een uitgezaaide tumor behoorlijk in het duister: de kans op genezing is klein. Gelukkig is er hoop. We denken namelijk dat we de juiste behandelmethode toch kunnen vinden als het ons lukt om zo precies mogelijk te weten hoeveel en welke soort tumor cellen er in het bloed van een patiënt zitten. Daarom is het doel van dit onderzoek het opsporen en tellen van circulerende tumor cellen!

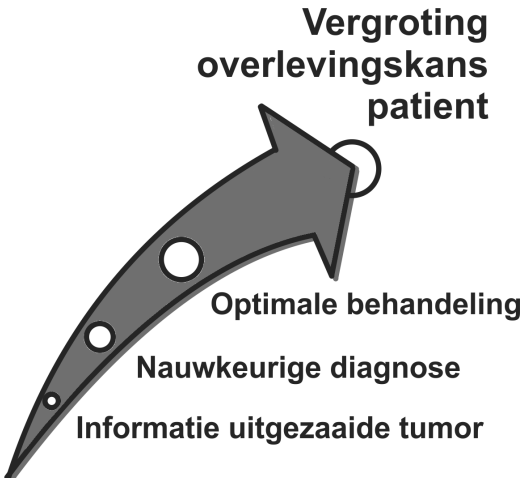

12.2 Het probleem

Het is ontzettend ingewikkeld om op een betrouwbare manier de hoeveelheid circulerende tumor cellen bij een persoon vast te stellen. Het tellen is pas betrouwbaar als het keer op keer hetzelfde resultaat geeft. Er zijn twee enorme obstakels die het tellen van tumor cellen extreem complex maken: ten eerste zijn de cellen heel erg schaars en ten tweede zijn de cellen ook nog eens vreselijk moeilijk te herkennen.

12.2.1 Tumor cellen zijn schaars

Een buisje bloed bevat slechts enkele tumor cellen in een gigantische hoeveelheid, meer dan 40 miljard, overige cellen. Zie die paar tumor cellen maar eens uit die massa te filteren. Hoe doe je dat? Het is alsof je één afwijkende klinker moet opsporen in een klinker-weg met een lengte van Nederland helemaal tot aan Iran. Daar komt nog eens bij dat haast is geboden, we kunnen geen weken zoeken. Kortom: het is zoeken naar een speld in een grote hooiberg. En de tijd tikt. Ai.

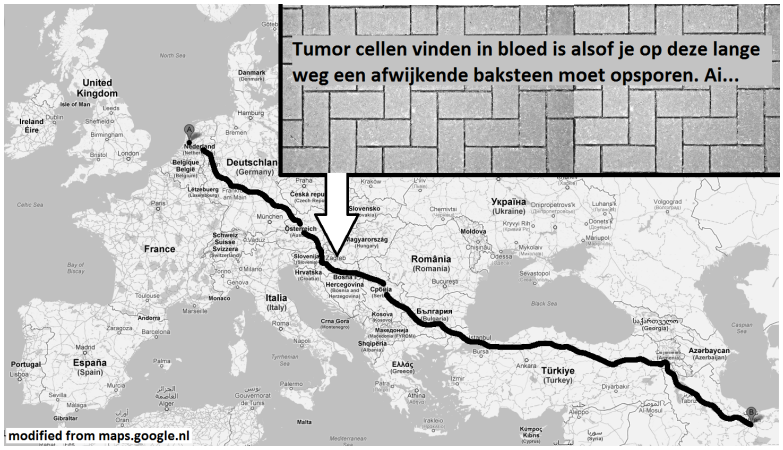

12.2.2 Tumor cellen zijn slecht herkenbaar

We weten nog niet precies wat de eigenschappen zijn van circulerende tumor cellen, waar je hen aan herkent. We zijn dus op zoek naar iets, maar weten niet precies naar wat. Veel cellen lijken op elkaar als twee druppels bloed. Kortom: we speuren naar een speld in een hooiberg, die vermomd is als . . . : hooi!
In dit onderzoek laten we zien dat het weliswaar moeilijk is om de tumor cellen op te sporen maar niet onmogelijk. Hieronder beschrijven we de basismethoden die zijn toegepast om - ondanks de 2 obstakels - tòch de tumorcellen uit iemands bloed te kunnen filteren en tellen.

12.3 De oplossing

12.3.1 Schaarse cellen opsporen

Bloed bestaat uit verschillende componenten, de voornaamste zijn:

Bloedcellen, rode en witte	5.005.000.000.000	per liter bloed
Tumor cellen	±1000	per liter bloed

Je ziet het al: wat een boel bloedcellen! Het is zaak zo snel mogelijk de grote aantallen cellen kwijt te raken, een voorselectie te doen. Als we dat niet doen dan duurt het tellen eindeloos; het onderzoek zou veel te lang duren en niet haalbaar zijn.

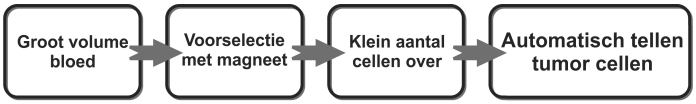

Om een voorselectie te kunnen doen is "CellSearch" ontwikkeld: . CellSearch is een systeem dat cellen uit bloed trekt, het werkt met behulp van een magneet. Hiervoor mengen we eerst ijzer in het bloed. Door met de magneet van CellSearch over het bloed te gaan, trek je de cellen, waar ijzer aan zit, eruit. Dit ijzer is behandeld om het een bijzondere eigenschap te geven; het hecht zich niet zomaar aan alle cellen. Nee. Het hecht zich zelfs bijzonder slecht aan rode en witte bloedcellen maar juist erg goed aan tumor cellen. De cellen die met de magneet uit het bloed worden getrokken, zijn dus in verhouding veel meer tumor cellen. Je kunt een groot deel van het bloed, dat wat niet door de magneet wordt opgepikt, gewoon weggooien want je weet dat er vrijwel geen tumor cellen bij zitten.
En zo hou je dus een veel kleinere groep over. Ha, dat lucht op. Hierdoor kun je de cellen nauwkeuriger bekijken en zijn verdere metingen betrouwbaarder. En betrouwbaarheid maakt in kankeronderzoek het verschil tussen relevante en niet relevante informatie en dus vaak het verschil tussen leven en dood.

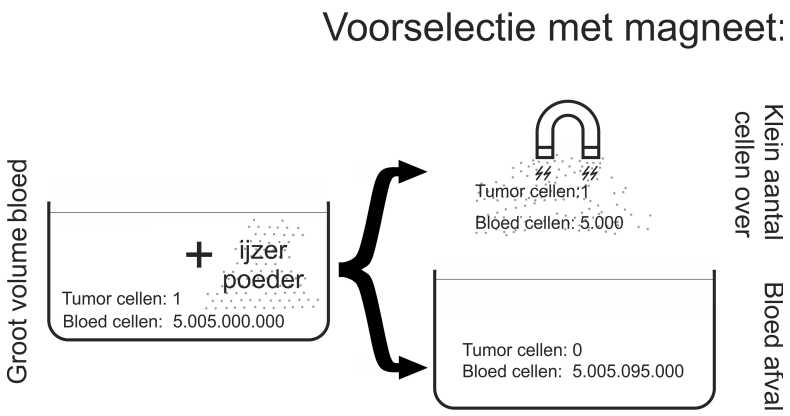

Oké, het grote aantal cellen is dus geëlimineerd en de nullen uit de grote getallen bloedcellen zijn geschrapt. Het grove werk is gedaan. We hebben een kleinere groep cellen overgehouden die we nu aandachtig kunnen bekijken. Mooi! Echter, dan zijn we er nog niet. We moeten nog veel meer cellen laten afvallen om uiteindelijk de tumor cellen over te houden. Tja, dat is niet eenvoudig. Kunnen we de eliminatie verder doorvoeren zonder iedere cel afzonderlijk te moeten oppakken en bestuderen? Ja, dat kan. En wel met een computer!

12.3.2 Vermomde cellen ontmaskeren

Er is nu een veel kleiner aantal cellen over, waar ook onze kanker cellen tussen verstopt zitten. We gebruiken een computer om die cellen automatisch te selecteren en te tellen. De computer moet dan wel weten welke

cellen van de tumor komen, hij moet ze kunnen identificeren als zijnde tumor cellen anders kan hij ze niet filteren. We moeten hem dus een instructie mee geven, een beschrijving van de tumor cel; zo een beschrijving noemen we een fenotype.

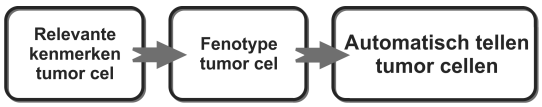

Een fenotype is een abstracte beschrijving van meetbare kenmerken van een organisme. Bijvoorbeeld een fenotype van een vrouw zou kunnen zijn; “rechtopstaand zoogdier met borsten en twee benen”. Kortom, een beschrijving waaraan de computer ziet: “hee dat móet wel een vrouw zijn!”. Door het fenotype uit dit voorbeeld zou de computer in een groep mensen de vrouwen moeten kunnen onderscheiden. Maar kan hij dat met dit fenotype wel nauwkeurig? Sommige eigenschappen van de vrouw blijken relevanter dan anderen. “Borsten” zijn in dit geval bijvoorbeeld relevanter dan “twee benen”. De meeste mannen hebben immers ook twee benen. Voor een goed fenotype ben je dus op zoek naar eigenschappen die zo uniek mogelijk zijn. Zelfs met het fenotype “borsten” blijkt niet helemaal uniek, er bestaan immers ook vrouwen zonder borsten en enkele dikke mannen mèt borsten. Zou er nog een nauwkeuriger fenotype voor de vrouw te maken zijn?
We dwalen af, snel terug naar de cellen: voor ons onderzoek hebben we dus een fenotype van de tumor cel nodig. Het maken van dit fenotype is extreem moeilijk; eigenschappen van tumor cellen kunnen enorm veel van elkaar variëren. Het is bijna onmogelijk om een fenotype te maken dat precies àlle tumor cellen vindt. Dat dus geen enkele tumor cel over slaat maar ook geen andere cellen per ongeluk oppakt (die toevallig een beetje op tumor cellen lijken).
De technische termen voor het mislopen van sommige tumor cellen heet een “te lage gevoeligheid” en voor het oppakken van cellen die je helemaal niet wilde hebben heet een “te lage specificiteit”. Wat is belangrijker? Kies je ervoor om in ieder geval alles te vinden en neem je de verkeerde cellen die er per ongeluk bij zitten op de koop toe, of wil je zo’n puur mogelijk resultaat hebben en neem je een lagere opbrengst tumor cellen voor lief? Waar je voor kiest hangt van je doel af. Ons doel is nog steeds het verschaffen van nauwkeurige informatie aan de arts zodat hij de overlevingskans van de kanker patiënt kan verbeteren. In dit onderzoek hebben we daarom op basis van onze kennis allerlei mogelijke eigenschappen van de tumor cel omschreven. We hebben allerlei fenotypen uitgeprobeerd en uitvoerig getest welke het beste is in het voorspellen van overlevingskansen (hoe? zie “een fruitig voorbeeld”).
Uiteindelijk hebben al die metingen verschillende nuttige eigenschappen van de tumor cel aan het licht gebracht. De computer kan ze goed filteren

doordat we nu op een verantwoorde manier het fenotype voor circulerende tumor cellen maken en ze zo nauwkeurig opsporen en tellen. Een doorbraak!

Fruitig voorbeeld van overlevings analyse. *We willen weten welke eigenschap van een banaan veel invloed heeft op hoe snel hij rot. Daarom ontwerpen we een experiment. We testen nu de eigenschap "vorm". Zouden rechte bananen eerder rotten dan kromme? En maakt de lengte uit? We gaan het uitzoeken zodat we weten met welke eigenschappen we rekening moeten houden als we straks een fenotype willen maken. Zo doen we dat: We nemen 100 mooie gele bananen en volgen ze op de voet. Oh nee! Per ongeluk hebben we er 29 opgegeten tijdens ons onderzoek! We kunnen deze nu niet meer verder meten. We zouden ze uit ons experiment kunnen schrappen, maar dan zou de betrouwbaarheid van ons experiment achteruit gaan want:*

1. *Hoe kleiner je hoeveelheid, hoe minder betrouwbaar je resultaat.*
2. *We hebben alleen gele bananen opgegeten, die totdat we ze opaten niet bruin waren geworden. Als we ze weglaten krijgen we een scheef beeld van de werkelijkheid.*

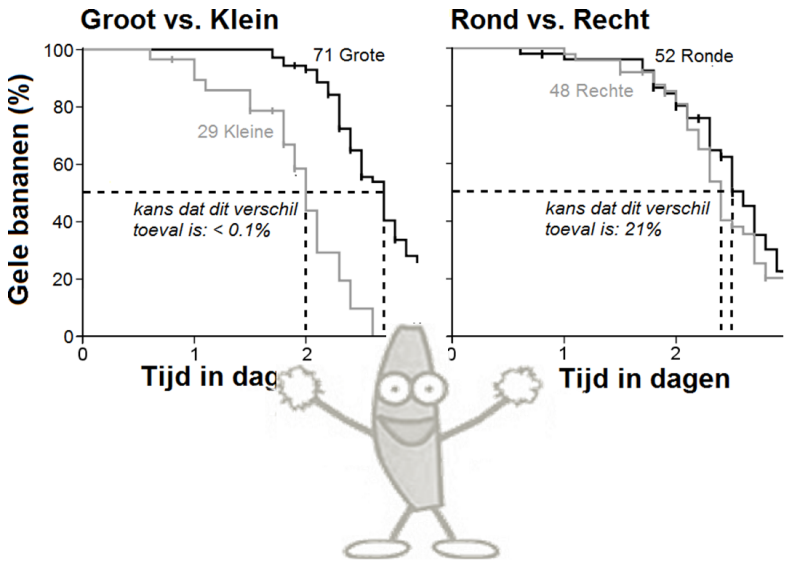

We nemen ze dus toch mee in ons experiment en verwerken ze in een overlevings curve volgens de Kaplan Meier Overlevings Analyse. Nu hebben we een meetbaar verschil tussen kromme en rechte bananen en tussen grote en kleine bananen en zo kunnen we een goede inschatting maken of de vorm uitmaakt de ja of de nee. Kijk zo ziet de curve eruit. De horizontale stippellijn is de mediaan (50%). En wat zien we? De grootte maakt uit! De kromheid maakt juist helemaal niet uit! Fijn om te weten.

12.4 Resultaten

Zo, nu hebben we gezien hoe we een groot deel cellen uit het bloed elimineren met een magneet, hoe we daarna de overgebleven cellen nauwkeurig bekijken en automatisch filteren met behulp van een fenotype, en hoe we een zo betrouwbaar mogelijk fenotype maken met behulp van de overleving analyse. Dit alles om goede informatie te kunnen verschaffen over een uitgezaaide tumor zodat de arts een juiste behandelmethode kan bepalen en hij de patiënt kan genezen.
Met dit onderzoek zijn we weer een klein stapje verder gekomen op de weg naar genezing van een uitgezaaide kanker. Hier houdt het zeker niet op. Verder onderzoek is nodig. Maar de resultaten bieden hoop voor de toekomst.

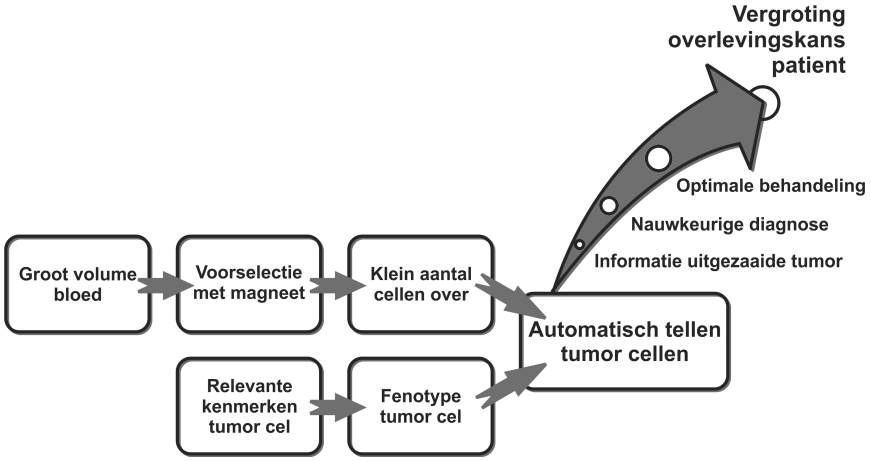

Nog even de resultaten van dit onderzoek op een rijtje. Ze zijn zo mooi dat we er uitroeptekens achter zetten:

1. *Het is gelukt om tumor cellen te tellen!*
2. *We laten zien wat het aantal tumor cellen betekent voor het uitzaaien van een tumor!*
3. *Er zijn twee getallen nodig om te kunnen zeggen hoe agressief een tumor is. De ene kan je bepalen door het aantal tumor cellen te tellen, de andere door die tumor cellen nog beter te bestuderen!*
4. *We tonen aan welke fenotypen het beste werken!*
5. *We laten zien welke hoeveelheid bloed nodig is om tumor cellen te vinden in alle patiënten. Er is voor een betrouwbaar resultaat 5 liter bloed nodig!*

6. *Er zijn mogelijkheden onderzocht om zo'n grote hoeveelheid bloed te verwerken: via een soort nierdialyse. We hebben gevonden dat voor een betrouwbaar resultaat vers bloed nodig is!*

Natuurlijk is in dit hoofdstuk slechts een vereenvoudigd mini tipje van de sluier opgelicht. Er gaan jaren onderzoek achter schuil. Dus als je echt alle ins en outs over de vele uren zwoegen rekenen en experimenteren wilt weten . . .